ENGINEERING THE PHASE BEHAVIOUR OF HIGH PERFORMANCE INKJET COLORANTS

A thesis submitted to the University of Manchester for the degree of Doctor of Engineering in the Faculty of Engineering and Physical Sciences

2011

Marina Sintyureva

School of Chemical Engineering and Analytical Sciences

Contents

Final Word Count: 47794

List of Figures

4

8

List of Equations

List of Tables

The University of Manchester

Marina Sintyureva

Doctor of Engineering

Engineering the Phase Behaviour of High Performance Inkjet Volorants

2011

Abstract

Dyes for inkjet printing are typically of the chromonic type. Chromonic mesophases have gained considerable attention as a well-defined group of lyotropic mesogens with different properties from conventional amphiphiles. While extensive research has been dedicated to the field of surfactant liquid crystals, structural and aggregation studies of chromonics have only emerged as a topic of interest within the last few years.

The liquid crystalline structures in aqueous solutions of commercial Cu - phthalocyanine and black dyes have been examined using a combination of optical microscopy, UV-vis spectroscopy, nuclear magnetic resonance, wide- and small-angle X-ray diffraction and electronic paramagnetic resonance with a view to examining the phase behaviour of the chromonic mesophases formed over a broad range of concentrations and temperatures. These studies were performed in order to resolve outstanding problems concerning structural properties of these systems.

Optical microscopy allowed us to identify the liquid crystalline phases and to construct the phase diagram. The observations show that both of these dyes form nematic mesophase above 15% wt / wt% dye. The small-angle diffraction data confirmed that the nematic phase for the black dye is maintained throughout the 16-25% composition range. A further increase in concentration leads to the formation of the hexagonal phase. The Cu – phthalocyanine dye also formed a nematic phase at low concentrations, with the aggregates undergoing a phase transition to an orientationally ordered chromonic liquid crystal phase at high dye concentration. These studies showed that this ordered phase possessed hexagonal symmetry. The wide-angle X-ray results demonstrated that aggregation involved π-π stacking of the molecules into columns. An additional reflection at ca. 6.8Å was observed for the black dye, which is believed to arise from "head – to – tail" packing of the molecules within the aggregates (a similar phenomenon observed in other azo dyes, e.g. Edicol Sunset Yellow).

The densities of both dyes were measured over the studied range of concentrations. This enabled us to calculate the parameters of the aggregates within the hexagonal mesophase. A comparison between the area of the molecule and the cross-section of the aggregates showed that the aggregates of both dyes were the unimolecular stacks.

Declaration

No portion of the work referred to in this thesis has been submitted in support of an application for another degree or qualification of this or any other university or institute of learning.

"The most fundamental and lasting objective of synthesis is not production of new compounds, but production of new properties."

George Hammond (1921 – 2005)

Acknowledgements

This thesis is dedicated to my parents. Thank you for bringing me up in faith and love.

CHAPTER ONE

1. Introduction

1.1 Business Context of Problem, Aim and Objectives

Colour vision incorporates a variety of physical, chemical, physiological and psychological process. It is mainly based on the capacity of the human eye to perceive all colours occurring in nature by the addition of only three basic colours such as blue, green and red, in such the proportions that, as far as possible, they reproduce the colours of the original image.

Colorants are characterised by their ability to absorb visible light, which lies in the range of wavelengths between 400 and 700 nm, which is the main reason they appeared to be coloured. Natural inorganic and organic colorants have been known and used by humans since prehistoric times. However, the era of commercial manufacturing of the dyes started only with the accidental discovery of Mauveine by the English chemist W.H. Perkin in 1856. Since that time an enormous amount of coloured chemical compounds have been synthesised with about 10000 of them having been manufactured on an industrial scale.

In modern days the colorants have been divided into two distinct groups, which are *dyes* and *pigments*. Pigments are largely insoluble in the medium in which they are applied. They are attached to substrates by additional compounds, for example a polymer in case of a paint. Dyes, on the other hand, are soluble in water or other solvents. They thus lose their particular crystalline structure during application process. The chemical structures of dyes and pigments are often the same. However, the insolubility of the pigments is often achieved by synthesising structures without solubilising groups or by producing insoluble organic molecules. The important industrial application properties of pigments include their tinctorial strength, migration, recrystallisation, heat stability and fastness properties, which are governed by that part of the pigment molecule soluble to a minor degree in the medium to which it is applied. The performance of a commercial pigment is then classified by the way it interacts with the application medium under the conditions determined by its application [1]. Dye prints typically have strong colours and wide gamuts, good ability to penetrate into the media and good transparency. They thus produce attractive prints but they typically have far lower permanence than pigment prints [2]. The chemical structures of the dyes are not reflected in this traditional classification. Additionally dyes are divided into two groups

known as *azo* and *non–azo*. Azo dyes are synthetic colorants that contain an azo group - N = N – as a part of their structure. In theory, azo dyes can supply a complete rainbow of colours, but yellow/red dyes are more common compared to blue/brown dyes. Phthalocyanines represent a group of non – azo dyes and are used mostly for obtaining the cyan colour.

The modern dyeing industry emphasises the optimisation of the manufacturing process and more economic methods of application rather than the development of new structures. It is inclined towards dye stabilisation in the form of a high-strength dye-liquid. This is mainly due to the reason that the manufacturer prefers to give dyes to its customers in the form of aqueous concentrates. This avoids possible difficulties for the customers in dispersing the solid dye into water, it removes the risk of potential dust hazards and finally it enables the consistent formulation of aqueous concentrates. The customers usually prefer to receive the product in the form of concentrated liquids as they can be simply diluted down to the required concentration with minimum transportation costs, since more dye and less water is being transported. The problems with highly concentrated dye solutions appear in the form of their stabilisation and high viscosity. The high strength dye liquids exist in the liquid crystalline state with high viscosity and the possibility of crystallisation taking place in some cases. The use of the additives such as salt helps to formulate these aqueous concentrates so that the customers receive the product of the required quality.

The aggregation behaviour of two chromonic dye systems was investigated. Under certain circumstances these dyes form chromonic lyotropic liquid crystalline mesophases when dissolved in water. However, the structures and the aggregation properties of these mesophases are poorly understood. There is still a lack of knowledge about the general colloid and chemical properties of chromonic dispersed systems. There is also no reliable way of predicting the behaviour and performance of the dye in terms of its molecular structure. This project aims to fill the gap by seeking the dominant factors affecting the formation of the chromonic liquid crystal phases, i.e. structure-property relations for the dye molecules. One dye is a sulphonated derivative of phthalocyanine (cyan) and the other poly-azo (black) dye. Knowledge of the general properties of these systems, i.e. the nature and size of the aggregates and the structure of the mesophases, is of great importance for solving the major handling problems associated with chromonics during different stages of manufacture (from synthesis and purification of the dyes, through shipping of aqueous concentrates or inks to customers to finally the formulation of aqueous concentrates into inkjet inks). This knowledge is also important for the optimisation of the print performance of the dyes.

In order to achieve these aims the following tasks had to be undertaken:

- To determine the concentration and temperature boundaries within which the liquid crystalline mesophases exist and are stable;

- To evaluate the parameters of aggregates formed in aqueous solutions of the studied dye systems;

- To determine the structures of the mesophases formed by the dyes in aqueous solution of the studied systems with the help of small – angle X-ray diffraction in conjunction with other physical methods.

The project was set up in collaboration between the University of Manchester and Fujifilm Imaging Colorants (FFIC). The testing methods and understanding developed will be applied to specific long term problems associated with both novel colorant research and the manufacture and processing of intermediates and final products.

1.2 Fujifilm Imaging Colorants (FFIC) – Industrial Sponsor

A company can be seen and examined from various angles and perspectives. Some people associate the company with its graphical image while others link it with its product range. The pressure on companies to stand out constantly increases due to ever-increasing competition. However, companies that successfully manage their brand can expect benefits such as advantages of market entry and differentiation over their competitors [3]. Fujifilm Imaging Colorants (FFIC) stands out from the number of the companies working in the same area as it can provide a business with several benefits both externally and internally: sophisticated product development, quality manufacture, extensive intellectual property. These generate consumer confidence and loyalty, they create employee motivation, attract new employees and stimulate investments. FFIC is a global leader in the introduction, development and production of innovative, high performance inkjet colorants. Highly experienced scientists within the company with core competencies in the field of organic chemistry, resin/polymer chemistry and application science work towards technological developments in the home/office print market. The company's business is tailored towards the needs of the customers in order to provide the flexibility, speed of response and high quality manufacturing standards [4]. There are three major sites FFIC operates on with more than 350 people working towards the success of the business. The Research and Development facilities are located in Blackley, Manchester; however, the manufacturing activities are performed in Grangemouth, UK and New Castle, Delaware, USA.

CHAPTER TWO

2. Literature Review

2.1 Liquid Crystals

The state of matter, characterised by an arrangement of constituent molecules that possesses structural properties intermediate between those of a solid crystal and an isotropic liquid, is known as liquid crystalline (LC) state. The liquid crystalline state comprises a variety of condensed matter phases differing in the type and degree of orientational and positional order. The liquid crystalline phases are also known as mesophases (where the Greek prefix "*meso*" stands for middle or mid), whilst substances forming liquid crystals are frequently referred to as mesogens. It is a thermodynamically stable state of matter resembling a liquid in its rheological properties. Thus, it looks like a fluid, forms drops and takes up the shape of the container. However, it also possesses a number of crystalline properties, such as the presence of long-range orientational order and the anisotropy of optical, electrical, magnetic, mechanical and other properties [5, 6].

Individual molecules do not show these liquid crystalline properties, but they possess the ability to form partially ordered structures when aggregating with other molecules due to their anisotropic nature. This ability (mesogeneity) is the main property of the liquid crystalline materials and plastic crystals, and the study of the relationship between the molecular structure and their mesogeneity is the basis of liquid crystalline chemistry.

Different mesophase morphologies are characterised by the extent of orientational and positional order. It is mainly determined by the fact that the molecules of liquid crystals possess the orientation of the long (or short) axes, which is characterised by the vector ***n*** or a director. There can be one, two or three such the spatial orientations, and some liquid crystalline materials in addition might even have some partial translational order.

Despite the fact that liquid crystalline materials are the objects of the interest of many scientists, the nature of this state of matter is not completely understood. The postulates on the nature of the liquid crystalline state are based on the relationship with the anisotropy of intermolecular interactions forces, depending on dipole-dipole, dispersive and donor-acceptor interactions. Orientational ordering of the molecules of liquid crystals and relatively weak

nature of their intermolecular interactions represent the physical base of crystal defectoscopy with the use of liquid crystals.

Thermotropic liquid crystals were first discovered by an Austrian botanist F. Reinitzer in 1888, who determined 2 melting points for cholesterol benzoate [7]. Since then the area of liquid crystalline science has been developing rapidly by the studies of many chemists, biologists and physicists. Lots of fundamental questions have not yet been answered, which can be explained by the wide phase variety of this state, non-universality of its properties and the complication of the molecular structure.

2.2 Classification of Liquid Crystals

The first classification of liquid crystals was developed by the French physicist G. Friedel [8], according to which the classification of liquid crystals includes nematic, smectic and cholesteric types of liquid crystalline materials. These structural types belong to *thermotropic* liquid crystals, which are formed through the process of heating a crystals or cooling an isotropic liquid. Thus, their existence is limited to a range of temperatures and pressures.

Smectics exhibit the properties mostly related to crystalline materials. The molecules in these types of liquid crystals are located in layers with the molecular centres of gravity being mobile within the smectic plane (in two dimensions). Orthogonal smectics (SmA) with the long axes of molecules arranged in perpendicular to the layer's plane differ from tilted smectics (SmC) with the long molecular axes located under an angle to the layer's plane as shown in Figure 2.1.

<p style="text-align:center;">a   b</p>
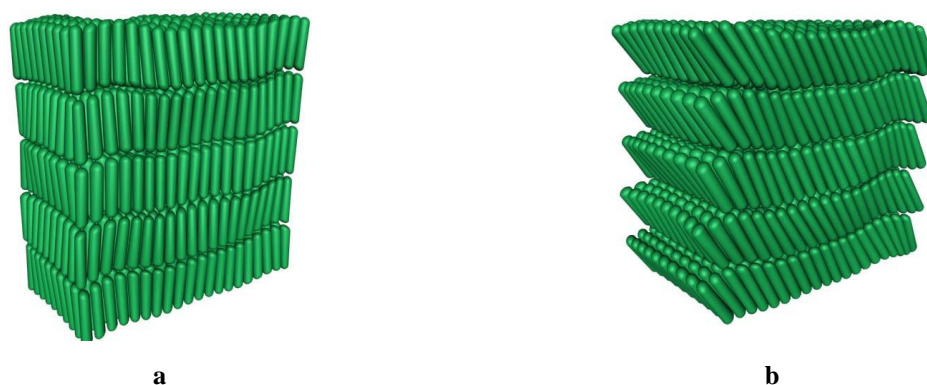
Figure 2.1   **Main types of smectic liquid crystals: orthogonal smectics (SmA) (a), tilted smectics (SmC) (b) [9].**

Nematics only exhibit one-dimensional orientational order of long (calamitics) or short (discotics) molecular axes (Figure 2.2). The molecular centres of gravity in nematic liquid crystalline materials are located chaotically in space.

<p style="text-align:center;">a   b</p>

Figure 2.2   **Main types of nematic liquid crystals: calamitics (a) [10], discotics (b) [11].**

Cholesteric type of liquid crystals is formed from the chiral (optically active) molecules with an asymmetric carbon atom (compared to symmetric nematic molecules). The mesophases formed by such the molecules were firstly observed for cholesterol derivatives, which originated the name for this type of liquid crystalline materials. Cholesterics in many ways are similar to nematics, where the translational order is attained; they are formed with the addition of small quantities of chiral substances (mole %) to nematics [12]. In this case additional spiral twist of molecules is present, which is the reason why cholesteric liquid crystals are often called "twisted nematics" (Figure 2.3).
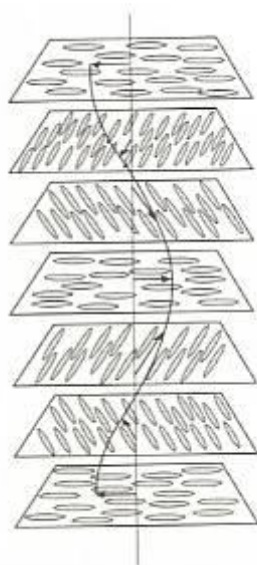
Figure 2.3   **Structure of the cholesteric liquid crystalline phase [9].**

Lyotropic liquid crystals are formed through the process of dissolving a range of diphilic substances in various solvents and usually have more complicated molecular structure than thermotropic liquid crystals [13]. Lyotropic liquid crystals are composed of self associated aggregates and possess a variety of ordering transitions with changes in concentration and temperature [14]. Such the compounds are association colloids with two distinct parts, which combine the hydrophobic and hydrophilic regions (Figure 2.4) – features explaining the thermodynamical favourability for being more concentrated in interfacial regions rather than in bulk phases.

Hydrophilic ionic (polar) group   **Hydrophobic non-ionic (non-polar) group**

Figure 2.4   **An amphiphile [15].**

The thermodynamical properties of amphiphilic molecules in solution are controlled by the affinity of the hydrophilic region to the water molecules and the tendency of the solvent to avoid the contact with the hydrophobic region. The hydrocarbon region of an

amphiphile molecule is insoluble in water. However, the introduction of an ionic (polar) group changes this situation as the solvent – head group interactions become strong compared to hydrocarbon – water interactions, the hydrophobicity of an apolar solute is reduced and the solubility is achieved. An increase in surfactant concentration leads to the association of these molecules into *micelles*. It happens at a certain solution concentration - the critical micelle concentration (CMC) and above the certain temperature – the Krafft temperature. When forming such micelles in a polar solvent (water), the hydrocarbon chains of surfactant molecules gather in the hydrocarbon nucleus, and the hydrophilic polar groups facing the water region form the hydrophilic shell. Because of this hydrophilic shell shielding the hydrocarbon nucleus from the contact with water, the surface tension on the micelle-water interface is decreased, permitting the thermodynamical stability of micellar systems. Such micellar systems represent the structural elements from which the liquid crystals are made of, forming, for example, lamellar or cylindrical forms.

Between the end of 1960s and the middle of the 1970s, two main lyomesophases were known for lyotropic liquid crystalline materials: a lamellar phase with its layered structure and a middle phase with its hexagonal packing of cylindrical micelles. At low amphiphile concentration the formation of an isotropic micellar solution containing spherical micelles precedes the formation of both of these phases. At high amphiphile concentration a solid phase is formed.

The facts mentioned above along with the analogy with the thermotropic liquid crystals led to the idea that some intermediate phases with an ordered arrangement of separate structural units had to exist between isotropic micellar solutions and highly ordered mesophases. These phases in accordance with terminology were called "nematic". As a micellar solution is the initial phase corresponding to a thermotropic isotropic phase, the structural elements in the nematic phase are anisotropic (cylindrical or discotic) micelles.

The existence of such micelles was supported by a number of facts. First of all, the theory of micelle formation forecasted that the shape of micelles can be changed from spherical to more asymmetric structures [5]. Experimental proof of the existence of asymmetric micelles in a large number of micellar solutions formed by a number of amphiphilic compounds were obtained by light scattering [16, 17], small-angle X-ray diffraction [18] and optical microscopy [19].

At present there are two main types of lyotropic nematics (in analogy with thermotropic nematics). In the first, the mesophase is composed of cylindrical micelles and is

called calamitic. Nematic micelles of the second type have the shape of discs, which gives them the name of "discotics".

Along with the surfactant materials there are two more classes of lyotropic liquid crystals, which form ordered structures at high concentrations. These are *polymeric* (semi-rigid or rigid surfactant polymers), and *chromonic* (a range of dyes, drugs, nucleic acids, antibiotics, carcinogens and anticancer agents [20].

Polymeric liquid crystals are made of the low-molecular weight monomers (rod- or disc-like) linked together in the form of polymers. The amphiphiles can be attached to each other by either their hydrocarbon regions or the polar head groups and the polymers themselves can be joined by the use of cross-links. The appearance of the mesophases formed depends mostly on the polymeric backbone and monomer nature. Nematic, cholesteric and smectic types of mesophases are very common for rod-like polymers, and the new types of mesophases are formed when disc-like molecules take part in the formation of the polymers.

Chromonic liquid crystals form a well-defined group of lyotropic liquid crystalline phases with the behaviour different from those systems described above, which primarily is because of the differences in the structure of mesogens and the mesophases formed. Dyes for inkjet printing are typically of the chromonic type of lyotropic liquid crystalline material.

2.3 Chromonic Liquid Crystals

2.3.1 Historical Overview

Inkjet dyes exhibit lyotropic liquid crystalline behaviour called *chromonic,* after the antiasthmatic drug disodium chromoglycate, which is a typical representative of this class of lyotropic liquid crystals. Chromonic mesophases make one of the subgroups of lyotropic discotic liquid crystals, which are characterised by a columnar packing of the planar molecules [21-24].

Chromonics were first observed in the beginning of the 20th century, when in 1915 Sandquist reported the first observation of the mesogenic properties of dyes when he detected "nematic threads" in an aqueous solution of 10-bromo(-chloro)-phenanthrene-3(-6)-sulphonic acid (Figure 2.5) under the optical microscope [25, 26].

Almost at the same time the antitrypanosomiasis drug Bayer 205 was produced by the Bayer Company, which drew the attention of Balaban and King. They investigated the properties of naphthylamine disulphonic acid and its derivatives in aqueous solution, and studied the mesogenic properties of this drug by optical microscopy [27].

Ten years later Gaubert reported several phase transitions (through nematic and smectic) by tartrazine (Figure 2.6) on slow cooling [28].
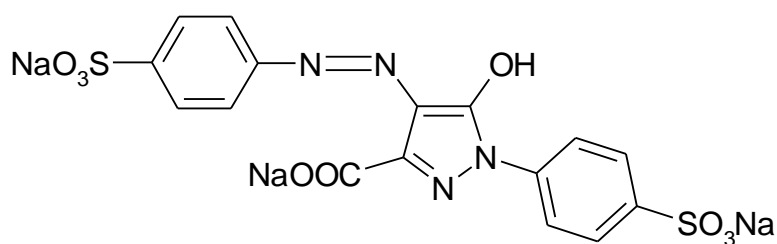
Almost at the same time Scheibe and Jelley independently conducted research on the cationic pseudo – isocyanine dye 1:1'-diethyl-cyanine chloride. Scheibe [29] on the basis of viscosity measurements, reported that the narrow absorption and fluorescence bands exhibited by the studied dye in aqueous solution were due to reversible polymerisation. He proposed the model of molecular packing into aggregates and suggested that the polymer aggregates were stacks of piled-up planar molecules with the inductive forces of the π-electrons holding the molecules in juxtaposition. Two-dimensional ladder and staircase arrangements were proposed for the molecules adsorbed on surfaces, with one-dimensional analogues for the arrangements in solution. Independent research carried out by Jelley [30] on an aqueous solution of 1:1'-diethyl-cyanine chloride (Figure 2.7) revealed a phase with the appearance of

birefringent nematic threads on "ageing". He proposed this mesophase possessed one-dimensional order and was analogous to the nematic phase reported at that time for thermotropic liquid crystals. It was suggested that the viscosity abnormalities of this system could be attributed to the formation of nematic aggregates of dye molecules in solution.

Figure 2.7   Molecular structure of 1:1'-diethyl-cyanine chloride (commonly referred to as PIC).

All these attempts to approach the nature of chromonic liquid crystals were prior to the extensive work carried out on disodium chromoglycate (DSCG) (Figure 2.8). Following the research work of Althounyan [31] it was marketed by Fisons as an antiasthmatic drug and was better known under its trade name "Intal" (from "interfere with allergy" [32]) and "Chromolyn" in the USA.
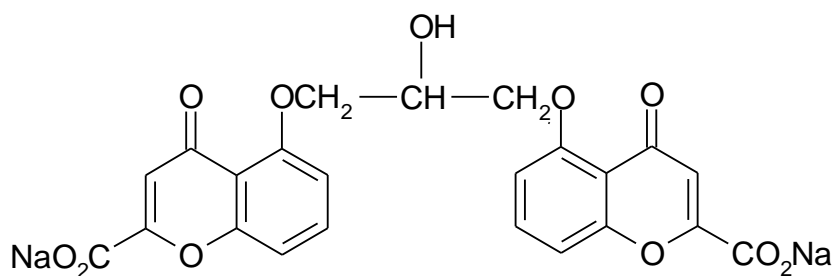
Figure 2.8   Molecular structure of Disodium Chromoglycate (Intal).

Cox, Woodard and McCrone [33] at the McCrone Research Institute in London investigated means to improve the dosage formulation for this inhalant. They identified two mesophases and constructed the phase diagram of the peritectic type, which is now

28

considered to be characteristic for chromonic materials. At the lower concentrations the nematic (N) phase appeared under polarised light in the form of a twisted threadlike texture. At higher concentrations the middle (M) phase was identified by its herringbone texture. X-ray diffraction revealed a series of sharp small-angle diffraction peaks in the ratio 1:1/√3:1/√4 for the middle phase suggesting that the phase consisted of a hexagonal array of rods. Another sharp reflection between 3.42–3.48 Å was also observed in the wide-angle region and was independent of concentration. A year later Hartshorne and Woodland [34] carried out a more detailed optical and X-ray analysis and proposed a model for the nematic and middle phases. The aggregate parameters were calculated based on a model in which the drug and water were completely separated, as in a classical amphiphilic hexagonal phase. The column diameter was determined to be approximately 16 Å. This value was consistent with a formation of a column of cross-sectional area equivalent to a single molecule. It was proposed that the drug molecules were planar and the two ring systems were rotated 90° with respect to each other on the formation of an aggregate. The transition from the middle to nematic phase was thought to be caused by the aggregates falling apart due to transitions and rotations of the planar Intal molecules.

Ten years later J. Lydon and T. Atwood [35] investigated DSCG/water system experimentally and proposed new models for the nematic and middle mesophases. These models described the DSCG rods as square cylinders with a cavity in the centre occupied by water as well as surrounding the rods. Also they described the transition from the middle to the nematic phase by the increase in water concentration, thus, resulting in the increase of rods separation and loss of hexagonal symmetry. This model also gave an explanation for the appearance of wide-angle reflection at 3.4 Å for both mesophases. It was the first of several papers which, with Attwood and Turner, led to the most significant advances in the area of this group of lyotropic liquid crystals.

Later, after the extensive research of Goldfarb, Luz, Spielberg and Zimmermann [36] the structural feature responsible for 3.4 Å was revealed as it was in a perpendicular position to those producing the low-angle reflections They concluded it to be due to the periodical distance of the aromatic molecules stuck together along the rod axis, whilst the small-angle reflection was due to the periodicity of the rods themselves.

The behaviour of DSCG was considered to be unique with no other examples of such behaviour in drug / water systems being reported. Attwood, Lydon and Jones extended the study of chromonic mesophases by reporting the formation of two lyomesophases by the dyes Sirius Supra Brown and Acid Red. A dye Sirius Supra Brown with the molecular structure

shown on Figure 2.9 formed a lyotropic mesophase at room temperature and 16% wt / wt% concentration [37]. The analysis of X-ray diffraction patterns revealed that the separation between the dye molecules in a stack is 3.4 Å (the precise thickness of an aromatic molecule), along with the small-angle X-ray diffraction patterns in ratio of $1:1/\sqrt{3}$ indicating hexagonal packing.
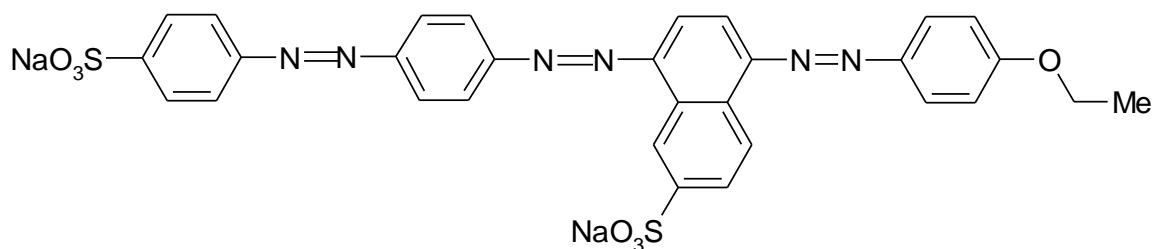
Figure 2.9   Molecular structure of Sirius Supra Brown.

The model of such the hexagonal packing of aggregates is shown on Figure 2.10 and was built with the consideration of the real rectangular structure of dye molecules.
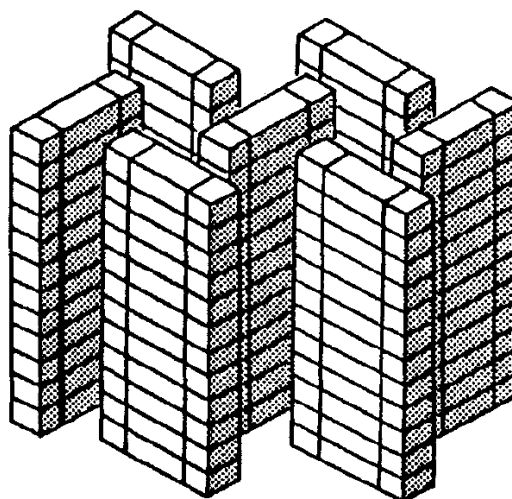
Figure 2.10   Model of hexagonal packing of the middle (M) chromonic phase [38, 39].

Some dyes exhibited a more complicated phase behaviour. As an example, Acid Red (Figure 2.11) went through four different phase transitions, thus, exhibiting four different textures on heating according to Attwood and Lydon [37].
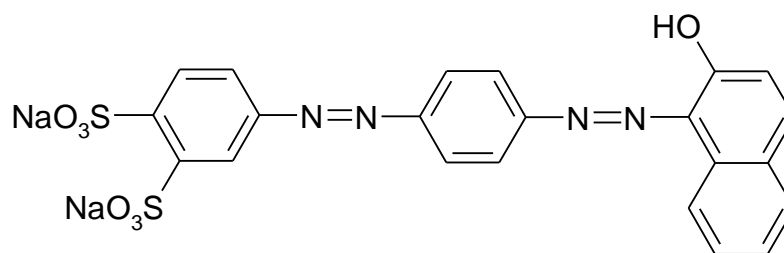
Figure 2.11   **Molecular Structure of Acid Red Dye.**

The ordinary middle (M) phase was formed at the room temperature and 14% wt/wt% dye concentration in aqueous solution. However, on heating the sample up to 50°C lenticular regions started being observed under the optical microscope [37]. On further heating the lenticular regions merged together to form an islet texture. At temperatures higher than 90°C the lenticular regions started appearing again in a reticulated form. While the nematic phase exhibited the characteristic nematic schlieren texture, the middle phase appeared grainy and ill-defined under the optical microscope. This texture was reproduced in the middle phase of DSCG by the addition of electrolyte. It was suggested that the repulsive forces between the aggregates in the middle phase were reduced by the presence of salt impurities in the commercial sample resulting in the contraction of the middle phase into a gel and hence the appearance of the grainy texture. These results were considered to be satisfactory evidence for the lyomesophases formed by the dyes to be structurally analogous to the chromonic nematic and middle phases.

Knowledge about chromonic liquid crystals became more widespread after the research carried out by Turner and Lydon [40], which proved that a large number of dyes exhibited behaviour similar to the chromonic ones observed previously. Peripheral evaporation scans of the studied dye solutions showed a sharp boundary between nematic and hexagonal phases. However, a number of dyes exhibited a boundary, which was difficult to detect, thus, indicating a gradual transition from nematic to a hexagonal phase. This new chromonic phase was called the P phase. This behaviour was explained in terms of the lack of rotational correlation between the constituent columns as they possessed circular cross-sections leading to a gradual packing of stacks on the nematic / middle phase transition. At the same time the phase called the O phase was reported in which the hexagonal symmetry of the middle phase was reduced to orthorhombic symmetry through the loss of the rotational freedom of the aggregates. All these lyotropic columnar systems were thought to be

31

analogous to the thermotropic discotic phases, thus, suggesting the existence of the new chromonic phases at lower temperatures and higher concentrations than the M phase [41].

Many questions remained open, including the understanding of the reasons governing the formation of these lyotropic liquid crystals. The following rules were formulated during the studies of how the liquid crystalline properties are affected by the molecular structure [38]. If a hydrocarbon part of a dye molecule was planar and all hydrophilic groups were located around the periphery of the molecule, so that the planar part of the molecule was hydrophobic, the molecules could freely slide on the surfaces of each other without any steric obstacles in their way. The liquid crystalline phases were readily affected by conditions including the range of pH, ionic strength, temperature and concentration, in which dyes were present in aqueous solution of the electrolyte. The necessary requirement was thought to be that the adsorption of electrolyte ions should not break the conditions described above. These conditions were common and justified themselves for the search of new chromonic systems. Further investigations by Attwood and Lydon revealed similar patterns for a number of other antiasthmatic and antiallergic drugs, which formed chromonic lyotropic liquid crystals [39]. There was now no doubt that this type of lyotropic liquid crystalline behaviour was distinct from that of amphiphilic systems.

Research on the miscibility of chromonic and amphiphilic hexagonal phases was carried out and the results were published in 1990 [39]. The outcome was that the hexagonal phases of these two types of lyotropic liquid crystalline materials were immiscible, though opposite results were obtained for the isotropic solutions. The immiscibility of these liquid crystalline phases was explained by the incompatibility of the mesophase structures, and not the chemical nature of the components. All these facts together led to a suggestion that this type of liquid crystal behaviour was novel and it was decided to call these systems *chromonic,* from the bis-chromone structure of disodium chromoglycate.

The studies performed by Mateer, Tiddy and Harrison on water soluble cyanine dyes (Figure 2.12) revealed that these particular dyes form a lamellar phase at low dye concentration [14]. The phase behaviour was characterised by optical microscopy and NMR spectroscopy along with the wide- and small – angle X-ray diffraction studies.
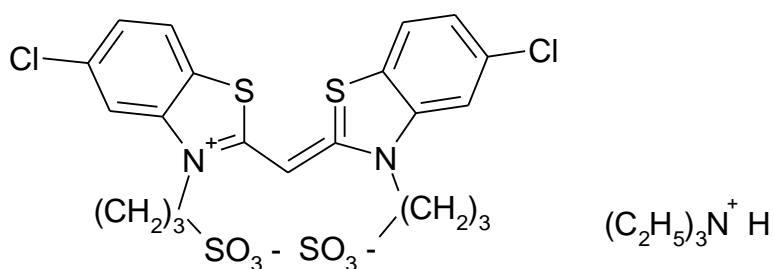
Figure 2.12   A typical cyanine – based dye.

A series of orders were produced by small – angle XRD in a ratio corresponding to the formation of a simple one-dimensional lamellar lyomesophase. A layer structure similar to open lattice brickwork was proposed. Considering the similarity of the cyanine dyes to the previously studied chromonic systems as opposed to amphiphiles, it became possible to conclude that this type of dye formed a new category of chromonic mesogens, thus, leading to a conclusion about the existence of the two distinct types of chromonic liquid crystalline materials based on the way they aggregate. The first one is characterised by a layered structure of aggregate packing, whilst the second one exhibits columnar assembly of aggregates with its classic nematic and hexagonal mesophases along with the more complicated and yet unknown mechanisms of mesophase formation.

The area of chromonic liquid crystals was further widened by the research carried out by Ormerod and Tiddy [42]. The lyomesomorphic behaviours of the two water soluble dyes, Edicol Sunset Yellow and Nylomine Red A-2B were characterised by optical microscopy and multi-nuclear NMR methods. These dyes exhibited two contrasting types of columnar chromonic behaviour by displaying N/M and P phase respectively. Edicol Sunset Yellow (Figure 2.13) formed the nematic phase at 30% wt/wt% dye. A two-phase N/M region was observed by optical microscopy and ^{2}H NMR. The N to M transition was found to be accompanied by a significant change in aggregate order parameter.
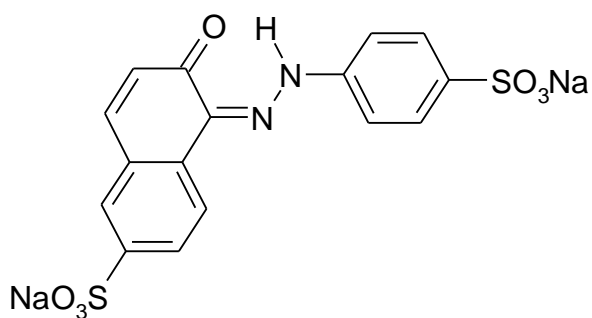
Figure 2.13   Molecular structure of Edicol Sunset Yellow.

The stability of the nematic phase with respect to concentration and temperature was achieved by adding salt as opposed to the addition of urea causing disaggregation proven by ^{2}H NMR. It suggested the strong binding of the urea to the dye aggregates. The dye Nylomine Red (Figure 2.14) formed the P phase at very low dye concentrations ($\approx$0.25% wt/wt% dye).
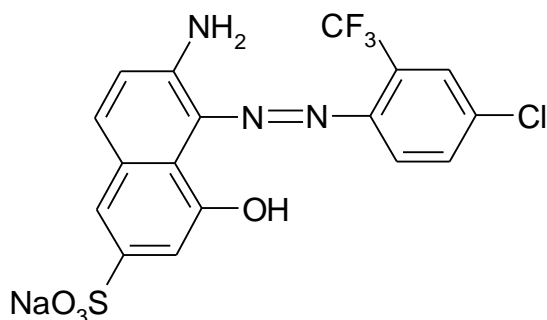
Figure 2.14   Molecular structure of Nylomine Red A-2B.

The studies performed by ^{23}Na NMR reveal that the order parameter of the counter ion was of higher magnitude in Nylomine Red compared to that in Edicol Sunset Yellow. With the addition of salt to the lower concentrations of Nylomine the P phase became unstable and precipitated in a form of solid crystals. However, the phase diagram of the Nylomine dye in aqueous solution changed drastically when salt solution with a concentration lower than 1M was added. These changes indicated Nylomine was more sensitive to the effects of electrolytes than Edicol. The empirical data revealed many differences in the behaviour of these dyes, both in solution and in the presence of additives, and led to the suggestion that these differences were caused by contrasting mesomorphic properties of these dyes [43].

34

Comparison of the aggregate cross-sectional areas for these dyes revealed that the aggregate formed by Nylomine had a much greater value than that of Edicol, thus, suggesting the formation of a multi-molecular stack with a ring arrangement proposed for the aggregate forming a hollow cylinder [42]. Later the study on Edicol Sunset Yellow was extended by our group at the University of Manchester and Fujifilm Imaging Colorants [44]. The main objective of our research was to explore the molecular structure within the aggregates of the Edicol Sunset Yellow dye. Multiple techniques, such as optical microscopy, multi-nuclear NMR (^{1}H, ^{2}H, ^{13}C, [23]Na) and X-ray diffraction were used in order to examine the solution and liquid crystalline phases. We also wished to determine the tautomeric form present in both dilute and concentrated solutions. We measured and analysed ^{13}C NMR spectra showing that the compound existed predominantly in the hydrazone form. ^{1}H NMR helped to study the state of aggregation of the dye in solution with respect to variable concentration. The decrease in the chemical shift of the protons was observed as a result of raising the concentration, indicating the extent to which aggregation occurred over the range of compositions and providing evidence of the involvement of the whole dye molecules into the stacks. Remarkably, from proton NMR of the mesophases it was possible to obtain molecular order parameters using direct proton dipolar splittings. Optical microscopy allowed us to identify the liquid crystalline phases and to construct the phase diagram. X-ray diffraction data proved packing of the molecules into single molecule columnar aggregates. An unusual feature of the X-ray diffraction pattern of the mesophases occurred in the form of diffuse off-axis reflections at ca. 6.8 Å. It was proposed that these arise from "head-to-tail" molecular packing within the stacks, a result also predicted by recent computer simulation studies [45].

2.3.2 Fundamental Properties of Chromonic Materials

Chromonic lyotropic liquid crystals are a distinct class of self – assembled systems. They are remarkable in that their building blocks are stacks of plank-like aromatic molecules with the multiple ring structures often derived from drugs, dyes and nucleic acids. These units self-assemble in aqueous solution primarily due to $\pi - \pi$ interactions and Van der Waals forces, and, subsequently, as stacks or groups of stacks, form orientationally ordered liquid crystalline phases. The average size of the aggregates and their organisation in solution strongly depends on concentration, temperature and ionic additives. There are generally two accepted phases formed by chromonics. The orientationally ordered nematic (N) phase is characterised by the schlieren texture and nematic arrangement of the stacks (N_{col} abbreviation will be used in the subsequent chapters). The positionally ordered middle (M) phase exhibits the columnar packing of chromonic molecules in a regular two-dimensional hexagonal arrangement and can be characterised by its grainy or herringbone textures (Col_h will be used in the following chapters of this thesis).

Dye molecules assemble either in a parallel or in a head-to-tail fashion within the aggregates. When molecules aggregate face-to-face forming the ladder like structures, they are referred as the H – aggregates. The molecules assembling in heat-to-tail fashion are called J-aggregates. However, these are two extreme situations as the actual difference between H- and J- aggregates is determined by the slippage angle α since it can vary from 0 to 90°. The formation of H – aggregates occurs when this angle is greater than 32° (Figure 2.15) [46].
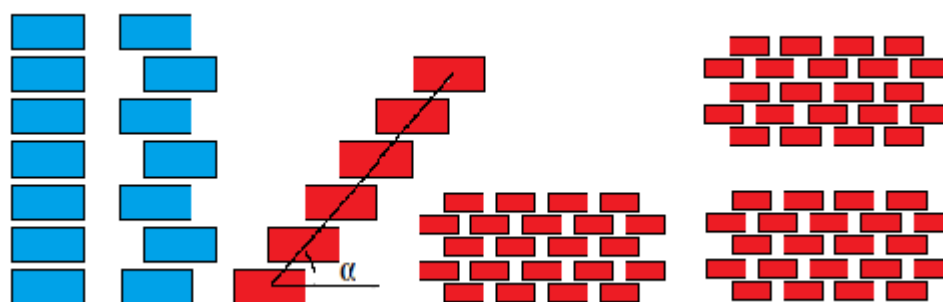
Figure 2.15   Schematic representations of chromonic columnar aggregates, H –   aggregates (blue) and J – aggregates (red) in the form of brickwork structure [46].

These systems exhibit characteristic phase diagrams, optical textures and XRD results. They do not possess any critical micelle concentration (CMC) and there is no Krafft temperature as it is observed for the lyotropic liquid crystals formed by amphiphilic molecules [46, 47]. In comparison with surfactant micelles, the structural elements of lyotropic chromonic liquid crystals do not have well-defined size (length) as there is no geometrical limitation to the addition of any subsequent molecules to an already existing stack or aggregate. This behaviour was first noticed during the studies of nucleic acids and nucleosides and was called isodesmic [41, 46, 48, 49]. The standard Gibbs energy increment of aggregation for each additional molecule is nearly constant, irrespective of the column length. This mechanism leads to an exponential distribution of the number of molecules in a stack (or on their length) [48]. Subsequently, these systems exhibit the multi - peritectictic phase diagrams due to the progressive way the columns form.

There are plenty of dyes known presently that exhibit chromonic behaviour when diluted in water. Liquid crystalline dyes embrace several groups including cyanine, anthraquinone, azo dyes. They are usually represented in water-soluble forms as salts and acids. The aggregation characteristics of the dyes have a major influence on their liquid crystalline behaviour and the factors which have been suggested as the primary reasons for the dye aggregation are described in the following chapter.

CHAPTER THREE

3. Formation of Aggregates and Their Stability

Long-range orientational order in solutions of liquid crystalline materials results from interactions of the mesogens. Amphiphiles self-associate in water to form aggregates due to the hydrophobic interactions between the surfactants, which are considered to be driven by the entropic effects involving water molecules and the hydrophilic parts of the amphiphile molecules [50]. However, the forces driving the aggregation of chromonic liquid crystalline materials are radically different. Several factors have been proposed, which include π-π interactions, van der Waals forces, electrostatic effects, hydrophobic interactions, hydrogen bonds, planarity and tautomerism [42].

3.1 Hydrophobic Effect

The hydrophobic effect is a driving force for the self-association of molecules with low polarities in aqueous solutions. At low concentrations a large fraction of the molecules are un-aggregated in which the hydrophobic parts are exposed to water. At a particular concentration (critical micelle concentration (CMC)) micelles begin to form. In a micelle, the hydrophobic groups come together and have little exposure to water. The driving force is believed to be the entropic gain obtained by the release of water molecules previously hydrating the free hydrophobic groups [51]. However, it is difficult to see how the same effect can drive the aggregation of chromonic materials. One reason is that chromonics do not possess distinct hydrophobic and hydrophilic regions. They are composed of poly-aromatic rather than aliphatic molecules with some solubilising groups located around the peripheries and not attached to the ends [20]. The aromatic cores of the chromonic molecules are insoluble in water, thus, as the stacks grow, the area of aromatic rings exposed to aqueous solution decreases. In terms of hydrophobicity, if a dye molecule is considered to equivalent to an amphiphile, thus the aromatic centre is equivalent to the surfactant hydrocarbon chain. However, the values for the enthalpy, entropy and free energy changes on the transfer of an aromatic hydrocarbon from a non-polar environment to an aqueous medium appear to be considerably different from those exhibited by aliphatic hydrocarbons [52]. The aromatic hydrocarbons exhibit much smaller changes in free energy indicating a lesser degree of

hydrophobicity compared to aliphatic ones. At the same time, there is no particular boundary when the free energy reaches its minimum on aggregation, no signs of a CMC and no structure resembling a micelle. The aggregation of dyes is considered to be an exothermic, enthalpy-driven process.

It is believed that the hydrophobic interactions affect the formation of the dye aggregates to some extent, but they are not the dominant driving force.

3.2 Hydrogen Bonding

Hydrogen bonding was another factor considered to be important for dye aggregate stability. The first suggestion was that the dye molecules were bound together in the form of a sandwich with water molecules trapped in the middle, the separation distance being around 4 Å [37, 53, 54]. In this model, hydrogen bonding (either dye – dye or dye – water) could be a significant factor. It is well-known that the inter-molecular distance within the stack appears at 3.4 - 3.7 Å for chromonic mesophases [14, 42, 55]. This separation distance would vary if different dye/water systems produced different hydrogen bonding interactions. These data thus signify that water cannot be trapped inbetween the dye molecules and hydrogen bonds do not govern the dye aggregates stability in aqueous solutions. Subsequently, it was proposed that the driving force for dye aggregation includes a significant contribution from π-π interactions between the dye molecules. Earlier concepts about the formation of aggregates involved the delocalised electrons of cyanine chromophore [29, 56], associating the aggregation into dimers and higher aggregates with the strong dispersion forces and the high polarisability of the chromophore [56].

3.3 π-π Interactions

The chromonic stack is determined by the planar structure of the aromatic core comprised of chromonic molecules and by the unique conjugation with them. π-π interactions are strong forces, which are caused by the attractive electronic interactions between the π-electrons and σ-framework of the aromatic molecular regions. Chromonic molecules possess carbon atoms which are sp^2-hybridised. The neighbouring atoms become bonded due the formation of the σ bonds caused by the end – to – end overlapping of these hybridised sp^2-

orbitals. However, each carbon also possess an unhybridised *p* orbital with one electron that extends above and below the molecular plane. The overlap of these *p* orbitals creates two rings of electron density, one above and one below the plane of the aromatic core. When two molecules with large aromatic regions approach each other, the π - clouds of each molecule force the molecular planes to lie approximately parallel to each other. The interaction force occurring between these π-clouds is known as π - π interaction. Hunter and Sanders [57] worked out a model explaining this type of interactions based on the experimental work carried out on a porphyrin and suggested this molecule could be considered as a positively charged σ-framework located between two negatively charged π-regions (Figure 3.1). The key feature of this model is that the σ-framework is considered to be separate from the π-electron clouds, thus, suggesting that π-π interactions result from the predominant π-σ attractions overcoming the π-π repulsion. This produces an offset or slipped geometry within the stack. Wide – angle X-ray diffraction performed on the chromonic liquid crystals reveals that the smallest intermolecular non-binding distance between pairs of atoms on adjacent dye molecules does not differ to a great extent from 3.4 Å. The magnitude of this value is equivalent to the distance between two adjacent aromatic molecules in a chromonic stack. Therefore, the phenomenon of a 3.4 Å spacing reported for most aggregating chromonic systems studied up to date indicates that π – π interactions play a major role in dye aggregation. However, it should not be considered the only major force for dye aggregation given that van der Waals forces are a significant factor with respect to the aggregation of dyes and chromonic materials in general.
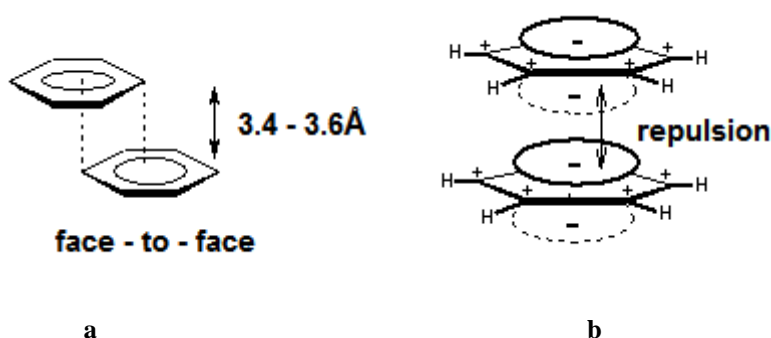
Figure 3.1   The face – to – face type of π- π interactions (a) with the charge distribution of two face – two – face π – systems (b) [58].

3.4 Van der Waals Forces

The mechanism of aggregation of dye molecules in water is affected by various factors among which attractive van der Waals interactions have often played a significant role. The energy of interactions generally consider the energy of association of two molecules and displacement of solvent, energies of which are both strongly associated with van der Waals interactions. There are three well-defined types of interactions contributing to the total long-range interaction between polar molecules - *orientation*, *induction* and *dispersion* forces [59, 60]. The *orientation* or Keesom interaction is the Boltzmann-averaged interaction between two permanent dipoles. The induction effect is due to electric field deforming the electronic clouds of a neighbouring molecule and creating the appearance of a polar molecule. A permanent dipole on one molecule induces another dipole in non-polar molecule by the field of the polar molecule. However, the attraction between two molecules is usually explained by the dispersion or London forces. For non-polar systems, a temporary dipole in one molecule induces opposite dipoles in surrounding molecules. It occurs due to the fact that the negative / positive charge in a portion of a molecule distorts the electron cloud of an adjacent portion of another molecule, causing an opposite charge to develop there. As a result the fluctuating dipoles appear in an atom. This type of interactions is universal as it arises between any particles irrespective of their charge and dipole presence. The energy of dispersion interactions is much lower than that of orientation and induction interactions. However, the dispersion forces between two molecules become stronger when the number of atoms in the molecule increases. The interaction can then be long ranged (2 – 100 Å). In addition, these forces also affect molecular orientations. Aromatic molecules have the largest dispersion forces when the molecules are parallel, i.e. the planes of the aromatic rings are in parallel to each other with the parallel arrangement of the axes of polarisability.

Dyes generally possess conjugated nitrogen heterocyclic systems. Delocalisation of the positive charge generates these strong molecular interactions that promote dye self-association. The planarity of the molecules arising from their size and aromaticity allows them to pack on the top of each other in a parallel arrangement maximising the dispersion forces.

3.5 Electrostatic Repulsive Forces

Chromonic liquid crystals are formed through the process of dissolving a range of diphilic materials in aqueous media. The process of dissolving dye molecules in water is usually accompanied by the hydrogen bonding of water to the ionic parts of the solute molecules. This condition was first mentioned by T. Attwood and J. Lydon on their studies of lyotropic liquid crystal behaviour of anti-asthmatic drugs [61].

Chromonic molecules have rigid aromatic cores with the solubilising groups arranged around the periphery of the molecules. Consequently, there are the significant electrostatic repulsive forces occurring between the similarly charged groups. The role of water in favouring aggregation in aqueous solution results from its high dielectric constant, and, hence, its ability to reduce the repulsive forces operating between the charges of these groups. As a result the ionic moieties pack in such a way so that the electrostatic repulsive forces are minimised. In addition, the size of these solubilising groups and steric interactions have an effect on the stability of the dye aggregates in aqueous solution. Hence, the variation of electrostatic and steric interactions caused by changes in the number and positions of the ionic solubilising groups will result in stacking of dye molecules in alternative ways.

The properties of a solvent in which the dyes are dissolved, therefore, are of the paramount importance due to the presence of impurities (electrolytes) and additives (a consequence of the manufacturing process), which can greatly influence the ionic strength, dielectric constant and, hence, the aggregation properties of the dyes.

3.6 Planarity and Tautomerism

The planar structure of chromonic molecules plays a very important role in formation of aggregates. It allows the molecules to stack relatively easily in columns. It also allows the π-π interactions along with van der Waals forces to be maximised. The non-coplanarity of an aromatic system reduces the overlap of π – electrons. In case of phthalocyanine molecules, as the aromatic system departs from planarity, its stability diminishes [62].

It is difficult to state that the tautomeric form has a significant effect on dye aggregation as not much attention has been paid to this phenomenon. There is also inconsistent data in the literature. Although it is likely that the different tautomeric forms

predominant in aqueous solutions could affect the process of aggregation, the understanding of its precise role is limited.

CHAPTER FOUR

4. Materials and Methods

One of the main aims of this thesis is to perform the structural and aggregation studies in order to understand the phase behaviour of several chromonic systems in aqueous solution. The aggregation properties of the selected dyes were therefore studied to build a comprehensive understanding of the liquid crystalline behaviour within the structures formed. The techniques used in these studies included optical microscopy, X-ray diffraction (XRD), ultra-violet and visible absorption spectroscopy along with proton nuclear magnetic resonance spectroscopy (NMR) and electron paramagnetic resonance technique. This chapter describes the methods used and their potential for study of the liquid crystalline behaviour of the chromonic dyes.

4.1 Materials and Preparation

The dye samples were supplied by Fujifilm Imaging Colorants and were used as received (without any purification). The aqueous dye samples were prepared gravimetrically using distilled water or deuterium oxide (99.9 atom % D) obtained from Aldrich Chemical Co. Ltd. The samples were prepared in the glass vials. Starting mixtures containing different compositions of the dyes and water were accurately weighted to $\pm$ 1mg with the solvent added drop by drop until the required concentration was reached. The pH was adjusted to 7-9 with the 2M NaOH. In order to obtain homogeneous solutions, the samples were agitated in the ultra-sonic bath, sealed and left at ambient temperature on the bench for a week for equilibration.

4.2 Optical Microscopy

Polarising optical microscopy is one of the most practical techniques for studying liquid crystals, identifying the particular mesophases, observing phase transitions and, thus, constructing phase diagrams [63-68].

Most crystalline materials possess the property of permitting the light to pass through them. The light waves are considered to be transverse electromagnetic waves as followed from the electromagnetic theory [69]. The asymmetry is characteristic for the transverse electromagnetic waves and can be experimentally studied by the use of the asymmetric (*anisotropic*) system, e.g. a crystal, where the atoms are located in the lattice in a way that the properties of this crystal in different directions are different. Such materials are characterised by 2 indices of refraction and often referred to as *double-refracting* or *birefringent* materials. There is also another type of crystals which allows the light of a given colour to pass through them with the same velocity in all directions. This type of medium is called *isotropic* and has a single index of refraction.

The main difference in these two media is the phenomenon of the double refraction determined by the different velocities of light in a crystal for two light waves polarised in mutually perpendicular planes. This fact determines the difference in propagation velocities of light at different directions in crystals, i.e. *optical anisotropy* of a crystalline medium. Usually, if the medium is anisotropic in relation to one particular property, it's anisotropic to all others. Anisotropy is determined by the character of special arrangements of atoms and molecules, which can be the anisotropic systems by themselves, i.e. their properties might be dependent on the light propagation direction inside an atom or molecule. Usually the anisotropic molecules oriented in a certain way possess the anisotropy for the whole medium [70] .

The majority of liquid crystalline phases are anisotropic, and, hence the velocity of light is not the same in all directions. There are two indices of refraction, thus, referring to as *double*-refracting or *birefringent* materials. Due to this, mesophases can be studied by optical microscopy. When light is passed through the sample with the crossed polars, the vibration of the light from the polarisers is resolved by the medium into two components which travel with different velocities corresponding to two angles of refraction.

These two rays are polarised in mutually perpendicular directions. One of them is called the *ordinary* (0) ray and is usually characterised by an index of refraction n_0, which is the same in all directions. Another one is called the *extraordinary* (E) ray, which travels with the different speed and in different direction. It is usually characterised by an index of refraction n_E, which varies with the direction of propagation. By measuring experimentally the values of the rays' velocities in all directions through the crystal, it is possible to build a surface, which will be reached by light at the time t from any point of the crystal. This ray surface will have quite a complicating shape, although resembling an ellipsoid (Figure 17c).

When two circular cross-sections of this ellipsoid coincide with each other, it represents a uniaxial crystal. In this case this ellipsoid is called the ellipsoid of revolution with the rotation axis determining the direction of the crystal optic axis and coinciding with one of the main directions of the crystal.

For a uniaxial crystal the angle between the optic axes equals zero and two joined axes determine the direction along which a wave propagates in the crystal with only one certain velocity. According to it the wave surface looks like two contiguous surfaces: one represented by a sphere (for the ordinary ray) (Figure 4.1a) and an ellipsoid of revolution (for an extraordinary ray) (Figure 4.1b). The points of contiguity of these surfaces lie on the optic axis.
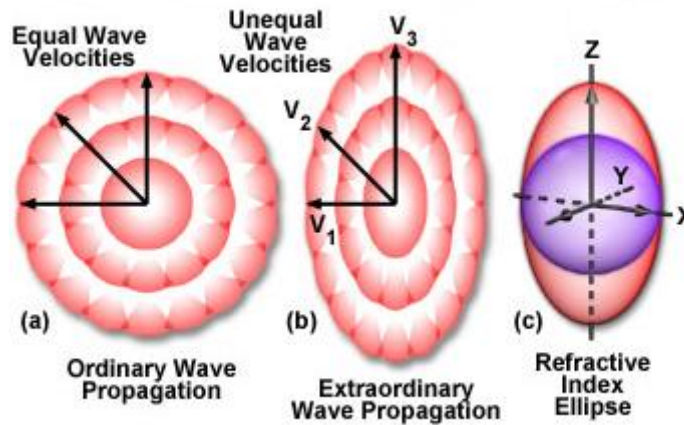
Figure 4.1   The behaviour of an ordinary light ray in a birefringent crystal: the propagation through an isotropic crystal (a), through an anisotropic medium with refractive index varying as a function of direction (b), refractive index ellipse (c) [71] Figures (a) and (b) are perpendicular views.

The differences between the behaviour of the ordinary and extraordinary rays inside the crystals correspond to the differences in the directions of the electric vector in relation to the optic axis. For the ordinary ray this vector is always perpendicular to the optic axis. That is why with the ordinary vector oriented in any directions, the electric vector is oriented always in the same way to the optic axis and its velocity is not dependent on its direction. The electric vector of the extraordinary ray always lies in the same plane with the optic axis and its direction forms an angle with the axis (from $0°$ to $90°$) depending on the ray direction.

The difference between these refractive indices of an anisotropic system is called the birefringence and means that the two analyser components are in phase resulting in the interference colours being observed (Figure 4.2). These interference colours are dependent upon the orientation of the sample and its thickness (colour more intense when sample is thin). The anisotropic system can appear dark though due to the four possible orientations at $90^{\circ}C$ to each other, which arise as a result of the light being parallel to the polarisers. Therefore, in order to obtain the brightest colours the vibration directions of light should be at $45^{\circ}C$ to the polarisers [72].
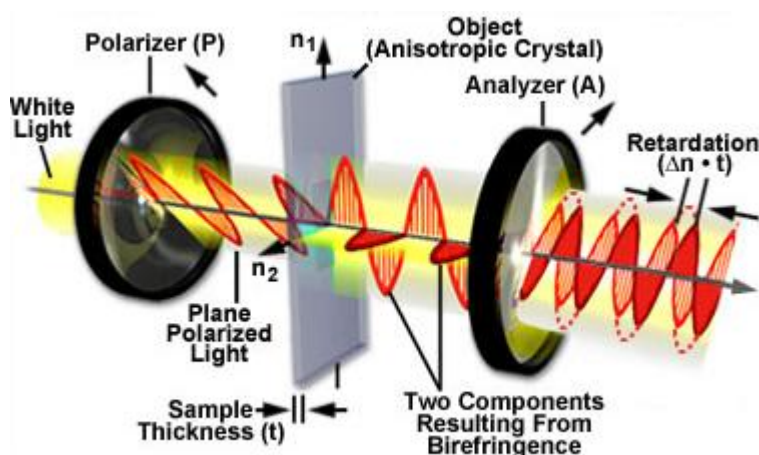
Figure 4.2   Light travelling through birefringent material under crossed polars [71].

Where there is no difference between these refractive indices emerging from the sample, the components along the analyser direction will be equal and opposite in phase. The indicatrix for the isotropic media will look like a sphere. As a result the darkness appears under the polarising microscope since the plane of polarisation is unaltered by the sample [73].

Optical microscopy comes as a very useful tool for obtaining the information related to mesophase structure of a liquid crystalline sample. Various distinctive optical textures arise for birefringent mesophases resulting from both phase structure and disclinations or defects within the phase. These optical textures are used for characterisation of liquid crystalline phase present.

Isotropic phases are identical along any three orthogonal directions in space; however, anisotropic structures are not. Cubic phases are optically isotropic making them difficult to distinguish one from another under the microscope, although their high viscosity helps to identify them along with their position in the phase sequence. Each anisotropic mesophase

exhibits at least one characteristic type of optical texture. Nematic phase can be recognised by its schlieren texture, which consists of numerous mobile lines. These lines result from the discontinuities within the phase and are mobile due to the low viscosity of the nematic phase. The presence of oily streaks or Maltese cross textures suggests the appearance of a lamellar mesophase whereas the hexagonal phase possesses its characteristic fan-like texture due to the growth of small fan-like units on cooling. An irregular boundary is formed when the initial units get together. The fine patterns characteristic of a fan-like texture indicate that hexagonal texture is composed of narrow focal conic domains [66].

The P phase is usually recognised by its striated, tiger-skin texture, which formation is due to the circular cross-sections of the aggregates composed of the dye stacks connected locally, but not completely coalesced clusters. These columnar bundles are able to lie above one another and any disclinations appearing within the phase occur in the form tiger-skin optical texture.

4.2.1 Optical Microscopy – Experimental

Optical Microscopy was used to examine the optical textures of the dye samples. The experiments were carried out on a BX41 (Olympus) and a Carl Zeiss Axioplan-2 polarised optical microscope connected to a JVC-TK 1280E CCD (charged coupled device) digital camera and a THMS600 hot stage (Linkam) with an accuracy of $\pm 1°C$. The analysis of the images was performed using the software provided by the microscope manufactures, which was Olympus Image Pro Plus and Carl Zeiss Linksys, Version 2.41. Calibration of the microscopes and lens was performed once every 3 months through the year.   The experimental work always started with the evaporation scan, which was used for the observation of the phase changes on solvent evaporation. A range of phases was observed as separate concentric stretches along the edge of the sample. The experiment was run at room temperature. In order to build phase diagrams each of the dye solutions was investigated under the microscope in 3 heating and cooling cycles, when the temperature was altered in steps, using alternatively a hot stage and liquid nitrogen (as a coolant). A small amount of the sample was placed onto a microscope slide and covered with a cover slip. Using the hot stage the sample was heated up to $90°C$ and cooled down to $2°C$ at a rate of $2°C$ per minute. The phases observed were recorded as a phase diagram.

4.3 X-ray Diffraction

X-ray diffraction is a powerful method for studying the microscopic properties of chromonic liquid crystalline phases. Properties of X-rays include their ability to penetrate into the bulk of the materials along with the high spatial resolving power determined by their wavelength being similar to the interatomic and intermolecular distances.

X-rays were first discovered by the German physicist W.C. Röntgen in 1895 and the wave nature and wavelength range confirmed in 1912 by M. von Laue [74]. The X-ray region is normally considered to be that part of the electromagnetic spectrum lying between 0.1 and 100 Å (1 Å = 10^{-10} m), being bounded by the γ-ray region to the short-wavelength side and the vacuum ultraviolet region to the long wavelength side (Figure 4.3). X-rays are relatively short-wavelength, high-energy beams of electromagnetic radiation.
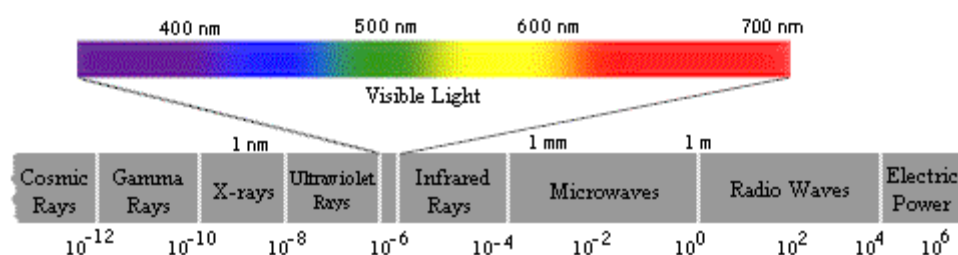
Figure 4.3   Electromagnetic spectrum [75].

Early attempts to confirm the dual nature of X-rays, i.e., their particle and wave character were frustrated by experimental difficulties involved with the handling of the very short wavelengths in question. However, not until the classical work of Max von Laue in 1912 was the wave character confirmed by diffraction experiments from a single crystal. From this single experiment has developed the field of X-ray crystallography, of which X-ray powder diffractometry is the important part. X-ray crystallography, using single crystals or powder, is mainly concerned with structural analysis. A crystal has a great many three-dimensional periodic relationships between the atoms that compose it. Thus, a crystal may diffract a monochromatic X-ray wave in a number of different directions in three-dimensional space. The angles of diffraction will depend on the various periodic relationships between the atoms making up the crystal.

49

W.H. Bragg with his son W.L. Bragg in 1913 described an imaginary crystal lattice plane grid system from which X-rays could be reflected. They also demonstrated that diffraction only occurred when the path difference between scattered waves from adjacent parallel planes was equal to an integral multiple of the wavelength (λ), resulting in constructive interference (Figure 4.4). This leads to the elucidation of the Bragg's law given in Equation 4.1,

$$2\,d_{hkl}\,\sin\theta_{hkl} = n\lambda$$

Equation 4.1

where the path difference is inherently described by the use of the Miller indices (*h, k, l*). The inter-planer spacing is denoted by *d* and the angle of incident radiation by *θ*. If the scattering centers are progressively misaligned, then destructive interference occurs and no diffraction is observed.
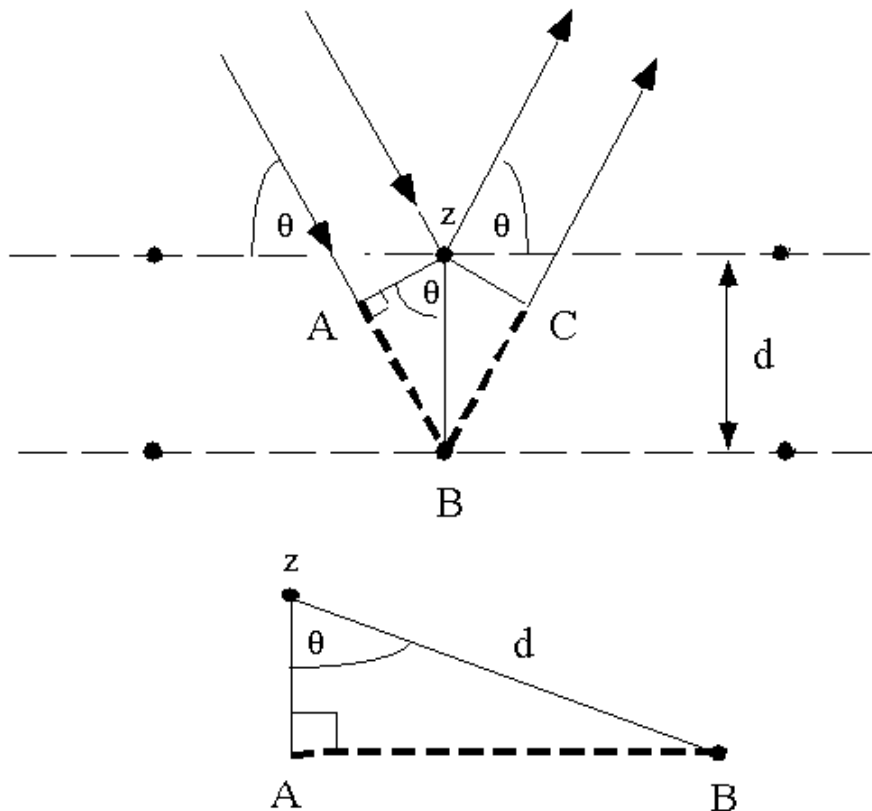
Figure 4.4   **Schematic representation of X-ray diffraction [76].**

X-ray radiation is most commonly generated in diffractometers using an X-ray tube. In an X-ray tube electrons are accelerated towards a positively-biased target, the most common being copper and molybdenum. The accelerated electrons cause the ejection of core electrons from the metal target and the relaxation of electrons from higher energy orbitals. This relaxation causes photons of a wavelength in the X-ray region to be emitted. In the case of a copper target, electrons from either the $2p$ or $3p$ orbitals relax into the $1s$ orbital generating what is known as k_α or k_β radiation respectively. The X-rays are then passed through a monochromator, or a filter, to select a single wavelength. Initially the diffracted radiation was detected using the darkening of photographic film, but more recently scintillation or ionisation movable detectors are used. Cu k_α radiation has a wavelength of 1.5418 Å, and Cu k_β wavelength is equal to 1.3922 Å. These are similar in magnitude to the interatomic distances in crystals. X-rays are scattered by the electrons that surround the nucleus of an atom, therefore the amount of beam scattered depends on the number of electrons present, i.e. the atomic number.

4.3.1 Synchrotron Sources of X-ray Radiation

The theory of the XRD method incorporates different areas of physics including atomic physics, electrodynamics, wave and geometric optics with crystallography, physics and solid state chemistry, which are all closely connected by complicated mathematics.. This method is well developed, although it still continues to grow, especially with the development of the new sources of radiation, which include the synchrotron sources. The main differences between synchrotron radiation and that generated by X-ray tubes are:

- the wide continuum spectrum
- polarised light;
- generated by short pulses;
- highly collimated;
- highly intense (10^{20} higher) [77].

This powerful and unique method is advantageous primarily due to a highly increased speed of X-ray structural and spectral measurements, which allow measurements that could not be done in the laboratory. These include the determination of the molecular structure as well as the investigation of process dynamics of formation and any changes of conformation

of molecules and clusters, and even the processes of breakage and formation of chemical bonds. It helps to carry out research into such complicated phenomena as magnetic and structural ordering near the phase transition regions in condensed systems including amorphous and liquid phases [78].

Synchrotron radiation is a type of electromagnetic radiation emitted by relativistic charged particles when a constant magnetic field makes them move in circular orbits. This method was founded by the English physicist J.A. Schott, who attempted to explain in 1912 the polarizing properties and the angular distribution of the electromagnetic radiation of an electron on a circular orbit [79].

A synchrotron is the cyclic accelerator of charged particles. It is an electrovacuum unit with an approximately circular vacuum chamber where the particles (electrons or positrons) are pushed by impulses of the electric field to accelerate to a velocity close to the speed of light. Powerful electromagnets direct the particles' motion on periodic trajectory. The synchrotron radiation can be generated by any relativistic charged particles: electrons, positrons, protons and so on. There is much more energy required for the acceleration of protons up to the relativistic velocities than for electrons. This is due to the differences in mass for these particles making it much easier to accelerate the light particles such as electrons and positrons as their velocities approach the speed of light in the beginning of the acceleration process and later their speed can be considered constant. Each time they pass through the field of the magnet, the relativistic particles receive a centripetal acceleration and generate synchrotron radiation.

The X-ray scattering studies were conducted at the EPSRC Synchrotron Radiation Source (SRS) in Daresbury. It is considered to belong to the second generation of synchrotron radiation sources. In order to produce powerful beams of synchrotron radiation the storage rings are used as the main units for the optimization of storage and long-term retention of the beam of accelerated particles. It aims to produce powerful radiation of photons with high stability and homogeneity. These synchrotrons were designed for the accumulation of the high electron current in a beam, its high collimation and stability at energies $1.5 - 2.5$ GeV for the periods of time longer than 10 hours. The SRS is a 2 GeV electron storage ring with a lifetime longer than 24 hours. The storage ring is the main source for the synchrotron radiation and is the third step in the process of acceleration. In the first two steps, the particles (electrons, positrons) are generated and accelerated in the linear accelerator up to energies of tens of MeV and are then injected into the preliminary acceleration or the buster. The electrons flying through the intervals of the acceleration

stations millions of times in the synchrotron regime accelerate up to the energies equal of hundreds of MeV or some GeV. Then these ultrarelativistic particles are injected to the storage ring by the use of the special deflected channel (the magnetic path called an inflector of a storage ring) on the trajectories close to the trajectory of the storage accumulator. The accelerating stations in the process of injection keep the energy of electrons approximately equal to the energy in the booster and accumulate the electric current. After the accumulation of the required number of electrons, i.e. reaching the required current of the beam, the injection is stopped and the energy of the accumulated electrons is raised by the accelerating stations of the storage up to the working energy levels, which vary from 2 to 8 GeV dependent on the size of the storage ring. Various stations are located around this storage ring. Stations 2.1 for the small-angle XRD and 14.1 for the wide-angle XRD were used in these particular studies.

Station 2.1 provides a time resolved small angle scattering where the distances from 40 to 500 Å can be examined at a fixed wavelength of 1.54 Å. The camera length between the detector and the sample was between 1 and 1.5 m – these distances were required due to the small diffraction angles involved.

Station 14.1 provides a wide-angle scattering for the studies where the distances as small as 2 Å up to 50 Å can be measured. It provides X-ray beam with high energy resolution at the wavelength of 1.488 Å.

4.3.2 X-ray Diffraction by Liquid Crystals

X-ray powder diffraction is one of the most valuable and reliable techniques for elucidating liquid crystalline phase structures. The diffraction patterns obtained by X-ray analysis consist of sets of reflections which are characteristic of specific liquid crystal phases. XRD is not the best method for studying the orientational order in liquid crystalline materials; however, the translational order can be easily examined with the aid of X-rays. The diffraction peaks arising at the θ angle positions are reciprocally related to the separation distances between the molecules or the groups of molecules. The quality of separation over large distances is easily reflected by the sharpness of the peaks. The ratio of the small angle peak positions is related to the long-range organisation of the phase and is summarised in Table 4.1 for each individual type of the mesophase. The wide angle peak positions reveal the translational order over short distances or for the liquid crystalline materials with short periodicities.

Table 4.1 Diffraction patterns of liquid crystalline phases.

Liquid Crystal Phase	Characteristic X-ray patterns	
Isotropic (I)	Two diffuse rings in small-angle and wide-angle experiments.	
Nematic (N)	Field aligned: - one pair of diffuse spots at small angle due to molecular length; - one pair of semi-circular spots at wide angle due to molecular lateral direction. Field unaligned: diffuse ring similar to that observed for isotropic phase.	
Hexagonal Columnar (Col$_h$)	XRD reflections in the ratio d: $d/\sqrt{3}$: $d/\sqrt{4}$: $d/\sqrt{7}$... in small-angle experiments corresponding to spacing between the planes in a hexagonal lattice. The hexagonal array of small angle reflections occurs when the X-ray beam is incident along the column axis.	

The isotropic phase does not exhibit any long range positional or orientational order. This phase is in all regards similar to a liquid. The anisotropic (calamitic) molecules constituting the isotropic phase show a diffraction pattern in the form of the two diffuse concentric rings. The small angle diffraction pattern corresponds to the effective molecular length with the wide-angle pattern originated from the average width of the constituting molecules. These peaks are weak and broad [80]. The nematic phase is characterised by long-

range orientational order. The diffraction pattern of an unaligned nematic phase is similar to the one observed for the isotropic phase. However, cooling the isotropic sample in the presence of an external magnetic field changes the appearance of the diffraction patterns. The two diffuse rings change to two semi-circular reflections when the incident beam is perpendicular to the field. The small angle reflections are parallel to the direction of the magnetic field and the wide-angle reflections are concentrated in perpendicular direction.

Considering chromonic liquid crystalline materials to be different from all other types of lyotropic liquid crystals, the attention should be focused on the special X-ray patterns characteristic for chromonic compounds. There is at least one sharp diffraction peak observed in the wide angle region at the distances of $3.4 - 3.8$ Å, which arises due to the stacking of aromatic rings and indicates the molecular packing into columns. This diffraction pattern is characteristic for all mesophases formed by chromonics and is independent of the concentration of the sample.

Small angle X-ray diffraction for nematic phases reveals the appearance of a diffuse peak corresponding to the continuous range of column-to-column distances. The patterns for the hexagonal phase give the series of peaks in the ratio of $1: 1/\sqrt{3} : 1/\sqrt{4} : 1/\sqrt{7} : 1/\sqrt{9}$, which correspond to the patterns observed for the hexagonal phases of the conventional amphiphilic systems. The spacings for the hexagonal phases may vary for different mesogens, but they are inversely proportional to the square root of the concentration.

4.3.3 X-ray Diffraction – Experimental

A small amount of the sample was carefully placed in a 1.0 mm glass Lindemann capillary tube in such a way as to provide at least a 10 mm length of the sample through which the X-ray beam passed. The tube was then sealed in order to prevent the loss of the solvent and mounted horizontally into an adapted Linkam hot-stage and equipped with a Linkam TMS 90 temperature control system.

4.3.3.1 Small-angle X-ray Scattering (SAXS)

The X-ray diffraction studies of the samples were performed at the EPSRC Synchrotron Radiation Source (SRS), Daresbury Laboratories, Warrington and Elettra Synchrotron Radiation Source in Trieste, Italy. Station 2.1 of Daresbury Laboratories was

used for the small angle scattering (SAXS) at a fixed wavelength of 1.54 Å. The detector used was the RAPID 2-D detector system. All experiments were performed at a distance (between the detector and the sample) of 1 m and 1.5 m respectively providing a special resolution up to 150 Å. Variable temperature measurements were taken on the selected samples at $10°C$ intervals over the temperature range 5 - $85°C$ on one heating and cooling cycle. Heating and cooling was carried out using a Linkam hot-stage made specifically to fit capillaries. Temperatures were obtained with an accuracy of 0.2°C. All sample peak positions were calibrated by running samples of wet rat tail collagen, which has specific orders of reflection and corresponding *d*-spacings. The orders of reflection are shown in Figure 4.5 and summarised in Table 4.2.
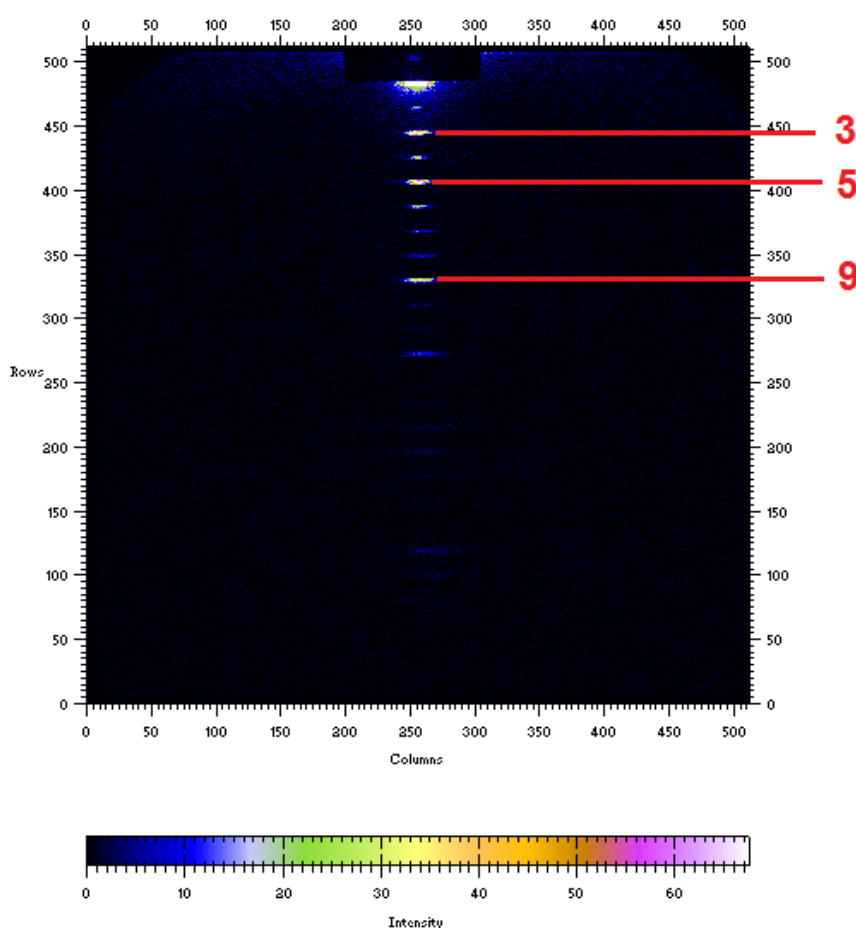
Figure 4.5   **Small-angle X-ray diffraction pattern for wet rat tail collagen taken at Station 2.1, SRS, Daresbury, UK. 9, 5 and 3 label specific orders of reflection. Other orders observed and corresponding *d* spacings can be found in Table 4.2. Image is from 2-D binary data file consisting of 512 vertical (columns) and 512 horizontal (rows) channels created from data collected on 2-D multi-wire area detector.**

Table 4.2   Orders of reflection and *d* spacings observed for wet tail collagen observed in Figure 4.5, where *q* corresponds to a scattering vector.

Order	*d* (Å)	$q(\text{Å}^{-1})$
3	223	0.028
4	167.5	0.038
5	134	0.047
6	116	0.05
7	96	0.065
8	84	0.075
9	74	0.08
10	67	0.094
11	61	0.103
12	56	0.11
13	51.5	0.12
15	44.6	0.14
20	33.5	0.18
21	32	0.196

The small angle X-ray diffraction studies were also performed at Elettra Synchrotron Radiation Source, Trieste, Italy. Station 5.2 was used for these studies. The experimental station was equipped with the 165 mm CCD detector. Our attention was focused on the phase transition from hexagonal to nematic on heating, which was investigated over the temperature range 5 - 21°C at 0.5°C intervals on heating only. Samples were kept in heat sealed Lindemann tubes to prevent water loss. Heating was carried out using a Linkam hot-stage made specifically to fit capillaries. Temperatures were obtained with an accuracy of 0.2°C. All sample peak positions were calibrated by running samples of wet rat tail collagen.

4.3.3.2 Wide-angle X-ray Scattering (SAXS)

Wide-angle X-ray diffraction was carried out on station 14.1 at the Synchrotron Radiation Source (SRS), Daresbury Laboratories, Warrington. Temperature control was obtained as for SAXS in section above. The detector used was an ADSC Quantum 4R CCD with an active area of 180 mm^2 and a readout time of 3 s [81]. The wavelength of the X-rays was 1.488 Å. The distance between the detector and a sample was 200 mm, which allowed a range of short *d*-spacings to be observed. All sample data and peak positions were calibrated using beeswax at a distance of 200 mm whose 2 specific peak positions are well known and shown in Figure 4.6.
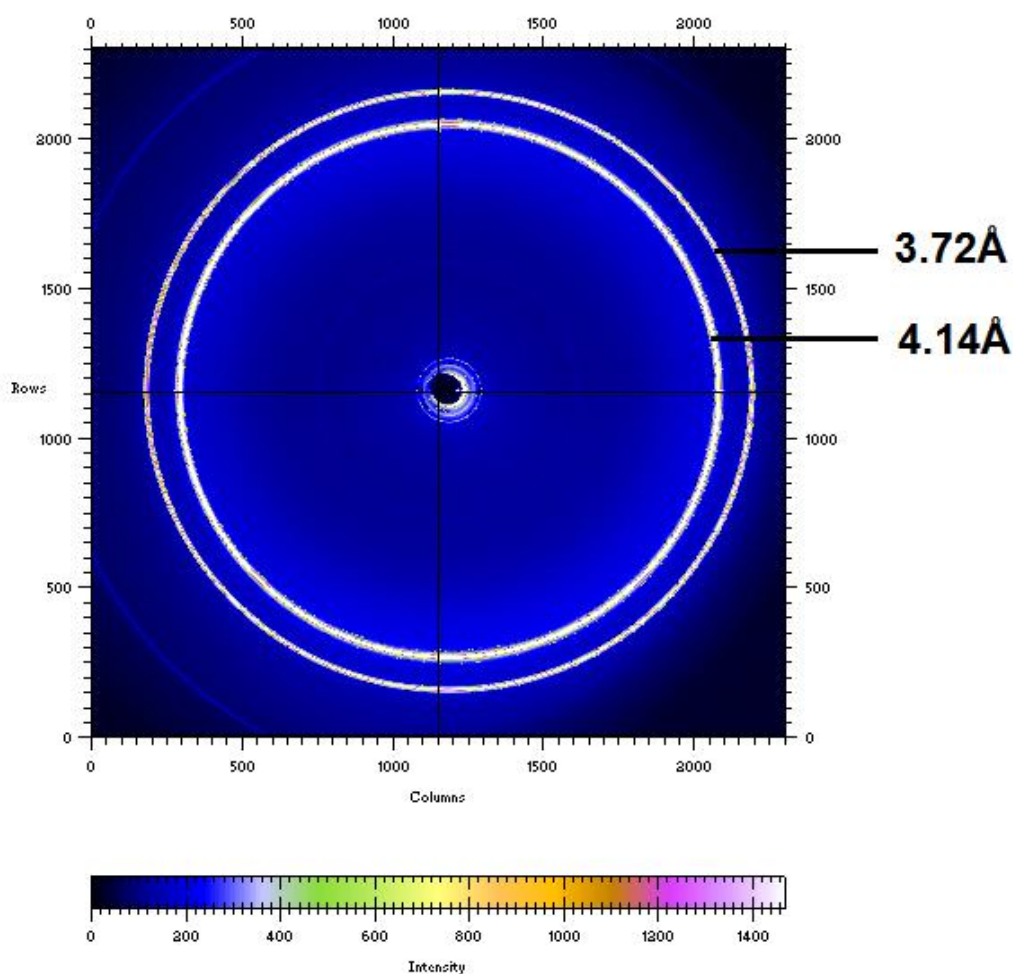
Figure 4.6   **Wide – angle X-ray diffraction pattern for beeswax taken at Station 14.1, Synchrotron Radiation Source (SRS), Daresbury, UK. The experiment was performed at 25°C Image is from 2-D binary data file consisting of 512 vertical (columns) and 512 horizontal (rows) channels created from data collected on 2-D multi-wire area detector.**

Rat tail collagen and beeswax are commonly used to calibrate SAXS and WAXS data since their *d* spacings are well known and documented. Two clear rings are observed for beeswax on the small angle system at 3.72 Å and 4.14 Å. The lines on the wet rat tail collagen diffraction pattern represent the orders tabulated in Table 4.2. The *d* spacings and relative intensities are well known hence one can calibrate SAXS data using one or more of the peaks seen. The differences in diffraction patterns (rings for beeswax and spots for rat tail collagen) are related to orientation within the samples. The beeswax is effectively 'powder' like and contains many domains of varying orientation hence the pattern observed is an average of these and is thus displayed as a ring. Rat tail collagen on the other hand is highly orientated hence spots are observed.

The data analysis was carried out using the program Fit2D [82]. The calibration protocol calculated the sample – to – detector distance, beam centre and the two tilt angles to specify the detector with respect to the beam. The XRD patterns in a form of Debye - Scherrer rings recorded by a 2D detector were then converted into 1D format providing a plot of conventional intensity versus channel number. The position and width of the peaks after background subtraction give the values of d-spacings necessary to characterise the studied systems. The results and conclusions drawn from the data are discussed in the following chapters.

4.4 UV – vis Spectroscopy

The electronic spectra of molecules are found for wavelengths in the range 100 – 800 nm of the electromagnetic spectrum. The human eye is sensitive to the visible region ranging in wavelengths between 400 – 800 nm. The ultra – violet (UV –vis) region includes two spectral regions corresponding to near ultra – violet (200 – 400 nm) and far or vacuum ultra – violet (< 200 nm). The Greek letter λ is used for denoting a wavelength in UV-visible absorption spectroscopy and is measured in nanometres (nm) along with the arising absorption bands, which are characterised by the molar absorptivities ε measured in mol^{-1} cm^{-1} at maximum absorption. A molecule can exist in a number of energy states [83]. The lowest energy level is the ground state where both electrons are in the bonding molecular orbital. When a sample M is irradiated with a continuous spectrum of light, UV or visible radiation is absorbed [70] resulting in electronic excitation. This increase in energy is equal to the energy of a photon and this process can be represented by Equation 4.2,

$$M + h\nu \rightarrow M^{*}$$
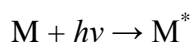
Equation 4.2

where $h\nu$ represents the energy of a photon and M^{*} stands for the electronically excited molecule. This electronic excitation involves a movement of an electron from a bonding molecular orbital to an anti – bonding molecular orbital. This electronic transition is generally also accompanied by changes in vibrational and rotational energy levels (Figure 4.1).
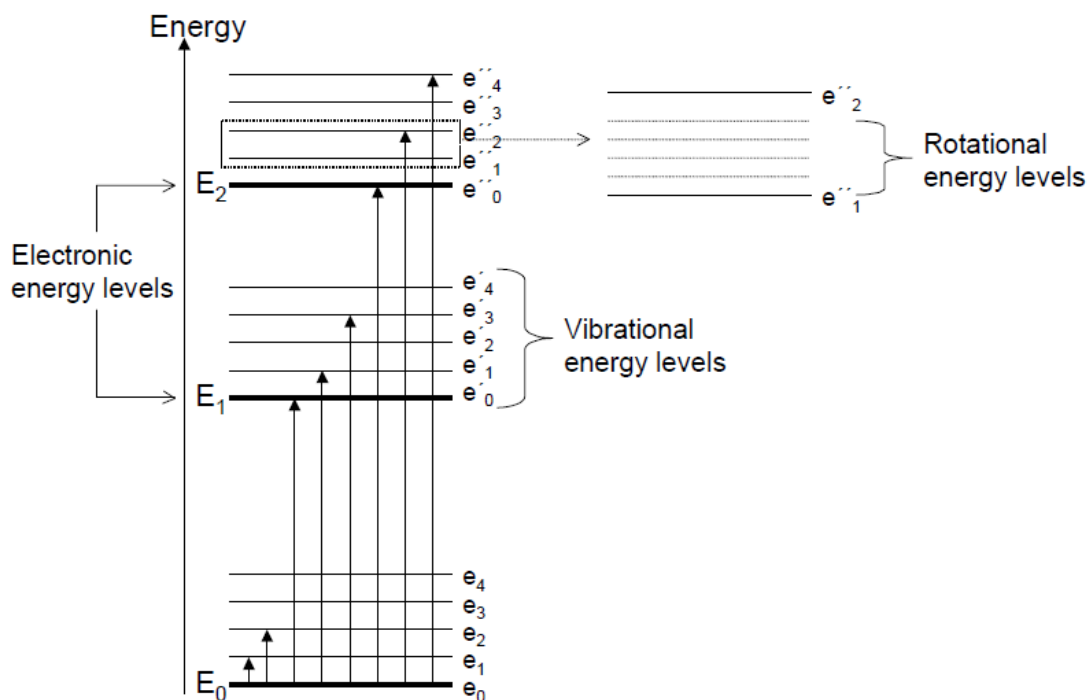
Figure 4.7   **Energy level diagram showing the changes in energy in the electronic, vibrational or rotational energy of the molecule.**

The excited state exists for a very short period of time (10^{-8} – 10^{-9} s) after which the molecule returns to its ground state via a relaxation process. The energy produced by the relaxation process is converted to either heat or fluorescent radiation; however, the amount of thermal energy produced is negligible and does not have a major effect on the behaviour of the studied system, i.e. the temperature barely changes.

Colour arises due to the presence of one or more unsaturated linkages or groups in the molecules. These are called *chromophores*. Typical examples of chromophores are C = C, C = O, N = N etc. There are also some groups which increase the colouring potential of the chromophores but do not confer colour on their own. These are called *auxochromes* and typical examples would include C – Br, C – OH, C – NH_2 etc. Saturated molecules do not show any signs of absorption in the near ultra – violet and visible regions. However, when an auxochrome is introduced in a saturated system, the absorption maximum is likely to shift to a longer wavelength. Furthermore, when a chromophore is present it causes absorption in the near ultra – violet and visible regions. The wavelength of absorption maximum (λ_{max}) is used to identify the presence of chromophoric systems and this varies for different chromophores [84].

Substitution or structural changes in the studied system lead to changes in the wavelength and intensity of absorption bands. When the absorption peak shifts to the longer wavelength these changes are known as bathochromic shifts, but changes to shorter wavelengths are called hypsochromic shifts. When the intensity of the absorption band is increased, it is known as a hyperchromic effect; a decrease is called a hypochromic effect. The factors influencing the structural character and the position of absorption bands include the nature of the solvent, pH and the temperature. The polarity of the solvent is known to modify the electronic environment of the absorbing chromophore [85]. Polar solvents tend to move the position of the absorption bands and decrease the vibrational structure of the bands.

Cu-Phthalocyanine dyes have a tendency to associate in aqueous solution. At extremely low dye concentrations the dye molecules exist in monomeric form. As the dye concentration is increased the dye molecules begin to aggregate into dimers and higher aggregates (Section 6.2, Figure 6.15). These changes in the absorption spectra with increasing dye concentration allow changes in the aggregated state of the dye to be monitored and correlated with the phase behaviour of the dye.

4.4.1   UV-vis Spectroscopy – Experimental

Extremely dilute samples were required for the UV – visible analysis of the dye, so samples were prepared by volumetric dilution. A dye stock solution of Cu – phthalocyanine dye (2.5% wt/wt%) was prepared as described above and was used to make subsequent dilutions using deionised water as the diluent. All dilutions were made using the Eppendorf pipettes. The samples were placed in a sonic bath to ensure homogeneity of the solution prior to the experimental work. UV – vis spectra were recorded on an Agilent 8453 spectrometer using quartz cuvettes with path lengths in the range of 10 µm to 1 cm. The concentration range studied was from 2.5% to 0.0012% wt/wt% dye (2.1×10^{-4} M – 6.9×10^{-8} M).

4.5 Nuclear Magnetic Resonance Spectroscopy

The basis of NMR rests on the interaction of the nuclear magnetic moment with the applied magnetic field (B_0). As described by the Zeeman splitting, nuclei with spin $I \neq 0$, when placed into a magnetic field, will populate a number of distinct energy levels given by $2I +1$ due to their magnetic moment μ. Therefore, ^{1}H, ^{13}C, ^{15}N, ^{19}F, ^{31}P with spin of ½ will populate one of two energy levels. The relative populations (η) of these quantised energy levels are described as Boltzmann distribution [86].

$$\frac{\eta_{upper}}{\eta_{lower}} = e^{\Delta E / kT}$$

Equation 4.3

where $\Delta E << \kappa T$ where κ is the Boltzmann constant and T is the absolute temperature.

The splitting of these energy levels is specific to each NMR active isotope due to each having its own specific gyromagnetic ratio (γ), making the NMR technique element specific. When the nuclei are then irradiated at a unique frequency called the Larmor frequency, they will resonate between the upper and lower energy levels, distributing the Boltzman equilibrium. The energy of both emission and absorption is the same, therefore, when irradiated a single peak corresponding to the splitting of the energy levels is recorded depending upon their population difference. The difference in energy is quite small and corresponds to the frequencies of electromagnetic radiation in the radio frequency range (up to 1 GHz) with present magnet technology. This means that NMR technique is non-destructive. However, it is also one of the least sensitive analytical methods because the probability of observing a spectroscopic transition depends on the existence of a difference in population between two states. By increasing the applied magnetic field this population difference is increased and, thus, the sensitivity of the technique.

Since the peak intensity corresponds to the population, it is directly representative of the number of nuclei in a certain electronic environment. The electronic environment is determined by the interaction of the electrons of the observed nuclei, with the electrons of surrounding nuclei, and changes to this environment affect the degree to which the discrete energy levels are split. Therefore, different electronic environments will cause the nuclei to

resonate at different frequencies, giving characteristic signals (chemical shifts or shielding differences). Indirect spin-spin splitting occurs between nuclei when one nucleus is located near another non-equivalent one. This is transmitted through the electrons in the chemical bonds and results in the splitting of the resonance peaks into doublets, triplets etc with the coupling constant (Δv) of a few hertz [87].

Dipole - dipole interactions often occur between the nuclei, which results in much broader (up to 10kHz) splittings. The interaction and, hence, the magnitude of the splittings, is proportional to ($3\cos^2\theta$-1), where θ stands for the angle between the liquid crystal director and the vector joining the two interacting nuclei.

Chromonic molecules are different from the conventional amphiphile molecules by having an aromatic rather than an aliphatic structures [41]. Protons in the neighbourhood of the aromatic rings exhibit higher chemical shifts compared to those in the vicinity of the aliphatic regions [88]. The values of the chemical shifts change proportionally with the number of aromatic rings near a proton [89, 90]. The theory behind it considers the chemical shifts incorporating the diamagnetic and paramagnetic contributions of the electrons associated with a particular nucleus, the total contributions from the other atoms and the ones caused by the mobile π-electrons [91]. The diamagnetic and paramagnetic contributions are considered to be similar for benzene and ethylene, thus, making the two other contributions responsible for the observed differences in chemical shifts. The last contribution is assumed to have the largest effect on the values of the chemical shifts and is termed a "ring-current effect".

The ring-current effect is caused by the non-local currents in the π-electron systems and the aromaticity of any ring is generally defined as the ability to sustain these ring currents [92]. It is generally assumed that there is a freedom for the circulation of the six π-electrons around the circle formed by the σ-framework when the electromagnetic field is induced (produced when the external magnetic field B_0 is turned on). The secondary field resulting from this current can then be approximated by the field of a dipole opposed to B_0 and located in the centre of the ring. It results in large average deshielding of the protons in the molecular plane and outside the ring since the average secondary magnetic field, which is opposite the applied magnetic field and centred inside the ring. And conversely, protons in the region above or below the plane of the ring are strongly shielded as the ring current is added to the external field. The induction of the ring current is only possible when the external magnetic field B_0 is perpendicular to the benzene ring.

Another effect influencing the chemical shifts is the induced magnetic moments of neighbouring atoms and bonds. The situation for Hydrogen is quite clear as its nucleus is shielded by its 1S electron density, which is much smaller compared with the shielding of nuclei of heavier atoms with the filled inner shells. As a result, the magnetic dipoles at the neighbouring atoms and groups will have an effect on the local magnetic field and it will be much more significant in determining the shifts of the proton resonance than for the heavier atoms.

It is also very important to mention the occurrence of the chemical exchange, which implies the movement of a nucleus from one environment to another [93, 94]. It readily occurs for isomers or aggregating systems. Exchange processes are classified by their rate relative to the NMR timescale. The slow exchange is defined by the presence of the individual signals on the spectra, which are produced by the characteristic individual sites of the molecule. The fast exchange regime yields a spectrum time – averaged over the different environments [95] and only one peak for all of the chemical environments is involved in the exchange process. Exchange can cause line broadening without the resonance into more than one peak. The line width of the peaks defined as the full – width of a resonance line, depends on the T_2 relaxation time of the molecules. The small and the large molecules have extremely long T_1 relaxation time, however, the T_2 relaxation time relevant for the line width remains low for large molecules [96] and resulting in broad peaks in the spectra. At higher concentrations and lower temperatures the lines get broader as a result of larger aggregates, which are characterised by shorter relaxation times, thus, producing the broader peaks in the NMR spectra.

4.5.1 NMR Spectroscopy – Experimental

The samples were prepared in deuterium oxide solvent. ^{1}H (499.96 MHz) spectra were recorded at 25°C on a Bruker AV500 NMR spectrometer equipped with a 5 mm z-gradient autotune broadband probe. The ^{1}H chemical shifts were referred to internal TMS (δ = 4.8).

4.6 Density Measurements – Experimental

The density of the samples was measured using an Anton Paar model DMA-5000 oscillating U-tube densimeter, provided with automatic viscosity correction, two integrated platinum thermometers and a stated accuracy of 5×10^{-6} g cm^{-3}. The temperature in the cell was regulated to a precision (i.e. repeatability, standard deviation) of ± 0.001 C° with a solid-state thermostat. The in-cell thermometer was calibrated to an uncertainty of 0.01 ºC. The apparatus was calibrated every time before each experiment with dry air and distilled water. The temperature profile used for the chromonic systems involves one heat/cool cycle between 5 to 85ºC. Density measurements were taken at increments of 5ºC.

The measured density is the sum of a dye and water densities. Therefore, the density of water as a function of temperature between 5 and 85ºC was measured and then the water density contribution was subtracted from the measured value.

4.7 EPR Spectroscopy – Experimental

EPR spectra were measured with a Bruker ER300D spectrometer fitted with a dual-mode cavity (type ER4116DM). Perpendicular-mode spectra were obtained at 9.7 GHz. The instrument was interfaced to a ESP1600 computer (Bruker Analytische Messtechnik GmBH, Silberstreifen, W-7512, Rheinstetten 4, Germany) and equipped with a variable temperature cryostat and liquid helium transfer line (Oxford Instruments, Osney Mead, Oxford , England).

CHAPTER FIVE

5. Copper Phthalocyanine Dye

5.1 Phthalocyanines

In the beginning of the twentieth century commercially available Blue pigments consisted mainly of Ultramarine Blue, Prussian Blue, Indigo derivatives and some azo derivatives. However, most of these colorants had poor chemical resistance and insufficient light and ozone fastness, hence, none of these colorants exhibited the desired properties demanded by the dye industry. A cheap and durable pigment that could fill the bluish region of the colour space was required. The discovery of copper phthalocyanine dyes provided with a satisfactory solution to this problem.

The word *phthalocyanine* originates from the combination of the Greek words, which perfectly describe the colourful properties of this compound: "na*phtha*" (rock oil) and "*cyanide*" (dark blue). The first observation of the compound later called phthalocyanine (Pc) was made as a highly coloured blue by-product in the chemical reaction of *ortho* − (1,2) − disubstituted benzene derivatives. During the preparation of *ortho* − cyanobenzamide from phthalimide and acetic acid Braun and Tcherniac in 1907 from the South Metropolitan Gas Company in London observed a dark coloured material insoluble in water. Later on de Diesbach and von den Weid from Fribourg University in 1927 produced a 23% yield of a stable blue material during the reaction of *ortho*-dibromobenzene with copper cyanide in refluxing pyridine. These coloured products belonging to new class evolved as metal-free and Cu (II) phthalocyanines [97].

The next important step in the history of this interesting material took place in 1928, when Dandridge A.G. from Grangemouth plant of Scottish Dyes Ltd obtained a blue-greenish material by accident followed by a patent covering the preparation and properties of the substance in 1929 [98]. A sample was sent to Professor Jocelyn F. Thorpe at Imperial College in London for structure elucidation. The investigation was carried out by a newly appointed lecturer Reginald P. Linstead. Collaboration between Linstead and ICI resulted in the publications of a series of papers where the structure of phthalocyanine compound along with the synthesis of its metal derivatives were described [99] [99-102]. These colorants were not

only the pigments interesting from an academic point of view, but were also of high practical value. ICI started manufacturing copper phthalocyanine pigment under the name of Monastral Blue in 1935 [103].

The phthalocyanine colorants have fascinating functional characteristics and present very interesting properties, which make them an excellent example to illustrate the advantageous properties of an organic material in the field of chemical engineering. Phthalocyanines are easily sublimed and can be crystallised with exceptional purity. They are highly stable and do not degrade up to temperatures of 400°C. They are not affected by strong acids or bases [104]. Copper Phthalocyanine molecules are non-polar, polycyclic, planar molecules, which show very interesting optical properties. The conjugated π-system, containing 18 electrons in the macrocyclic ring, is the reason of the intense absorption in the near-infrared region and the compounds have a wide variety of current and potential applications in various fields of organic semi-conductor lasers, non-linear optical materials, charge generating materials for photocopiers, photodynamic therapy of tumours, catalysts for the photo oxidation, optical recording materials and gas sensors [105]. Enormous efforts have been made to develop new phthalocyanine molecular materials and to seek further applications. The latest emphasis in both academic research and industrial field has been focused on the design and synthesis of novel phthalocyanine species, structure – property relationships, self-assembly properties and in the areas of molecular electronics, optoelectronics and dye-sensitised solar cells.

The aim of this research is to optimise the behaviour of a copper phthalocyanine dye by controlling its aggregation. Altering the peripheral substitution of the macrocyclic ring is one way of tailoring the solubility properties of this dye. Aggregation has great importance on the optical properties of phthalocyanine compounds. Since most of applications are developed from the optical properties of phthalocyanines, an understanding and control of aggregation are of practical significance as well as being of scientific interest.

5.1.1 Performance

Operations management is concerned with creating the products and services, which are the important reason for any organisation's existence. Each operation requires a tightly defined set of objectives that relate specifically to the company's basic task of satisfying customer requirements. The five basic performance objectives, which apply to all types of operations, are quality, speed, dependability, flexibility and cost [106]. Manufacturing copper phthalocyanine dyes should comply with all these objectives, which is the reason why there is a need for phthalocyanine dyes and ink compositions having desirable performance characteristics. In particular, the dye is strongly required to have a good cyan colour, a high resistance to light, humidity, heat and, when printed on paper to be resistant against oxidative gases in the environment. Copper phthalocyanine dyes used at present show good performance in light fastness compared with the magenta and yellow dyes [107]. However, phthalocyanine dyes are liable to problems associated with the solubility of the dye. The dissolution failure, which can occur during the manufacturing process, causes insoluble products to precipitate during storage or throughout the use of the product. As a result the precipitation of the dye cause clogging of the printing head or ejection failure, which results in serious deterioration of the printed image [108]. Hence, it is desired by both the manufacturer and the customers for the dyes to be stable in the form of a high-strength dye solution. The customers prefer to deal with the dyes in form of concentrated liquid because it eliminates the complexity in dispersing the solid dye into water and enables consistently formulated liquids to be used along with removing the potential risk hazards. Another problem arising throughout the formulation of the dyes is the transportation cost: a more concentrated dye solution can be produced and shipped to the customers with lower transportation costs, since more dye and less water is being transported. Therefore, two more problems arise with high strength dye solutions for the manufacturers of the dyes in the form of stability and viscosity. The highly concentrated dye solutions exist in a liquid crystalline form possessing a high viscosity. Crystallisation can readily occur at the higher dye concentrations. The conditions for the dye to be stable in liquid crystalline phases also vary on geographical location. Therefore, it is important to know the boundaries within which the dye is stable in the liquid-crystalline phase allowing the manufacturer to formulate more "user-friendly" product for the customers populating the lands from the extreme cold regions to the tropical climates. In this matter, the importance of aggregation and the knowledge of

conditions in which the product exists in the form of stable high concentrated dye solution become important for obtaining the product with the enhanced performance characteristics.

5.1.2 Fastness

Fastness of the dye is influenced by the structure of the dye along with the external environmental parameters such as oxygen, moisture, temperature, air contaminants (sulphur and nitrogen oxides from pollution), light and concentration of the dyes [109, 110]. The surface properties, the chemical and physical structure of the substrate, residual solvent within the substrate and porosity also have a significant influence on the fastness of the printed image [111].

One of the most important indicators of the dye's performance is light fastness, which is a measure of how resistant the dye is to fading when exposed to light. When dyes fade, they undergo a photochemical reaction which starts with the absorption of visible or ultraviolet light. Absorption of a photon by an organic molecule leads to formation of electronically excited state, which is the starting point for subsequent reaction steps [112]. Photochemical process of degradation of the dyes may follow different pathways, and a wide range of different products may result.

The light fastness comes as an important issue for industry for the reasons of finding the ways of quenching the fading of dyes without increasing the costs of production.

Another very important property is ozone fastness, as prints may be exposed to low level ozone that can arise from such things as photocopiers and general air pollution. Ozone fastness is generally referred to as the resistance against oxidative atmospheres. The destructive agents include the air contaminants such as nitrogen oxide present in the exhaust fumes from automobiles; sulphur oxides contained in the exhaust fumes generated by the thermal power stations, factories or plants; ozone generated from these gases by a photochemical radical chain reaction with the solar light, photochemical smog rich in oxygen – nitrogen or oxygen – hydrogen radicals; and hydrogen peroxide radicals produced by chemical plants using specific chemicals. All these chemicals can cause degradation of the dye in the form of discoloration to a greenish hue and a reduction in the printing density. Therefore, if the printed image is widely used and being exposed to light or active gases in the environment, a dye and ink composition having light fastness and excellent resistance against active gases in the environment are more strongly demanded. It is difficult to find a

phthalocyanine dye satisfying these requirements at a high level. However, it has been suggested that when the copper phthalocyanine dye is used in aggregated form, the stability against light, heat and oxidative gases is remarkably improved as compared with the dye in the monomeric dispersion state. Furthermore, by the formation of aggregates, the spectral properties including the cyan hue are greatly improved. The conditions to which the dye is exposed to may be changed, but the differences in the dye performance are expected to be negligible due to the formation of the firm aggregates. For example, the good light fastness exhibited by the aggregates could be due to the fact that aggregates can dissipate the energy from the light by vibrations within the dimer or larger aggregates, which is not possible with monomers.

5.1.3 Bronzing

One of the problems associated with the quality of a printed image with a high optical density is a so-called bronze phenomenon. The dye crystals deposit on the surface of the paper when the image dries reflecting the light to cause metallic gloss. This phenomenon is considered to arise when the dye solubility in aqueous solution is decreased. In general, the phthalocyanine dyes are produced by a process of sulphonation. In this case, sulphonation takes place at any site of the phthalocyanine core and the number of sites sulphonated is difficult to control. Accordingly, when a sulpho group is introduced under such reaction conditions the site and the number of sulpho groups introduced into the product cannot be specified, which results in a mixture of dyes with different numbers of substituents in different substitution site. In this mixture a component having low solubility, for example, a component where the number of sulphonated sites on the phthalocyanine core is 0 or 1, is mixed and the solubility is likely to be insufficient for use as a water-soluble dye. The generation of bronze phenomenon is not only associated with the decrease in the optical density of the printed image, but also causes the differences in the quality of the colour of the printed image. Therefore, preventing the bronze phenomenon is one of the important tasks for the dyer manufacturer.

One method known so far and often used in industry for preventing the bronzing phenomenon is to add specific nitrogen – containing compounds or specific titanium compounds. However, these additives are known to decrease various performance characteristics of copper phthalocyanine inks, thus, affecting the quality of the printing

image. Addition of the small amount of alkanolamine prevents bronzing, but it is known to increase the pH of the ink to 11 or more, which affects the printer's nozzles, create problems with safety and causes a decrease in the water resistance of the printed image.

Another method for preventing clogging and, hence, improving the solubility is via the addition of an alkali metal compound. It is known to prevent the formation of aggregates and to decrease the viscosity of ink formulations. This method works well for phthalocyanines dyes with a short storage period, but leads to changes in physical properties and the deposition of solid components in dye solutions on long time storage. As such, additives have both positive and negative effects on the performance of dyes. Accordingly, a method for inhibiting bronze phenomenon not relying on additives is preferred. In this situation, control of the aggregation appears to be an important issue along with controlling the size of the aggregates for optimising the copper phthalocyanine dye performance. Too large aggregates favour crystallisation of the dye and, thus, leave the dye deposits on the paper when the image is completely dry.

Hence, the aggregates present in the final product should be of the intermediate size in order to exhibit the good cyan colour, stability against light, humidity heat and oxidative gases in the environment.

5.2 Structure of Copper Phthalocyanine Dye

Crude copper phthalocyanine dye is manufactured by the phthalodinitrile process, which starts with the reaction between substituted phthalodinitrile and a copper salt. In this reaction the dye is produced by reacting three parts of 4-R_1- phthalonitrile (substance A) with R_1 representing the hydrophilic group, one part of 4-R_2-phthalonitrile (substance B) part with R_2 representing the hydrophobic group, copper containing inorganic salt and the suitable organic solvent. Two phthalonitrile materials (A and B) are required for the manufacturing process resulting in production of several compounds along with the structural isomers forming the final product. The probability of each compound formed during the final stage of the manufacturing process and being present in aqueous solution can be determined utilising the principles of binomial expansion and are presented in Table 5.1 .

Table 5.1 Calculated distribution of final product yields.

Type of Isomer Formed	Probability (%)
AAAA	31.6%
AAAB	42%
AABB	21%
ABBB	4.7%
BBBB	0.7%

The chemical with the highest yield of the final product (42%) is the one having 3 hydrophilic and one hydrophobic group located around the periphery of the copper phthalocyanine core. Therefore, the copper phthalocyanine dye's structure can be represented by the formula shown in Figure 5.1
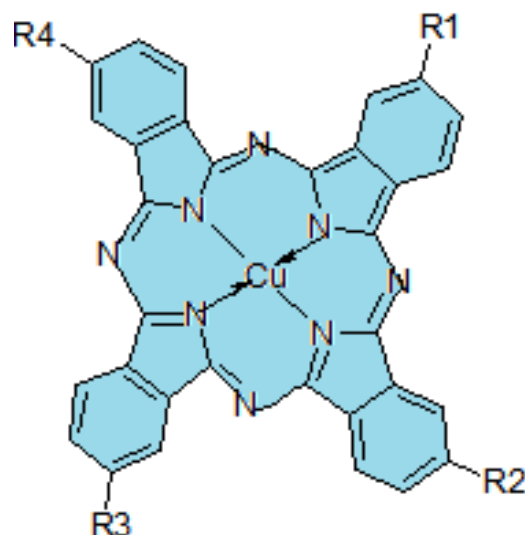
Figure 5.1   **Molecular structure for copper phthalocyanine dye.**

where three of each R_1, R_2, R_3 and R_4 representing a hydrophilic group $-SO_2-(CH_2)_3SO_3^+$ with the Na^+ counter ion; and one of the groups attached to the periphery of the molecule being of the hydrophobic nature. The analysis and explanation of the empirical data along with calculations based on the results were carried out using the chemical structure of this compound.

Due to the presence of hydrophilic groups within the molecule, this dye exhibits good solubility and dispersibility in aqueous solution.

The molecular weight of the studied copper phthalocyanine dye molecule is 1444 including the molecular weights of three sodium counter ions.

CHAPTER SIX

6. Copper Phthalocyanine Dye Phase Behaviour

6.1 Optical Microscopy

A polarising optical microscopy study was carried out in order to determine the mesophase formation on the basis of birefringent optical textures. A peripheral evaporation scan was used as a preliminary way of studying the chromonic phase behaviour of Cu-phthalocyanine dye. In this experiment, a small amount of isotropic dye solution was put on a microscope slide and the solvent was allowed to evaporate bringing about gradual appearance of birefringent droplets in the isotropic bulk. This initially resulted in the formation of the nematic phase on the edge of the cover slip, with progression towards the centre of the microscopic slide the solution gradually became isotropic (Figure 6.1a). This was caused by the concentration gradient due to evaporation of water. Upon further evaporation of solvent, an outer band consisting of the more concentrated hexagonal phase started to develop around the still progressing nematic phase on the edge of the cover slip (Figure 6.1b). No sharp boundary was seen between these two phases. Solid dye eventually started to form at the edge of the cover slip, though not before significant proportions of the nematic and middle phases had become stable.

a   b
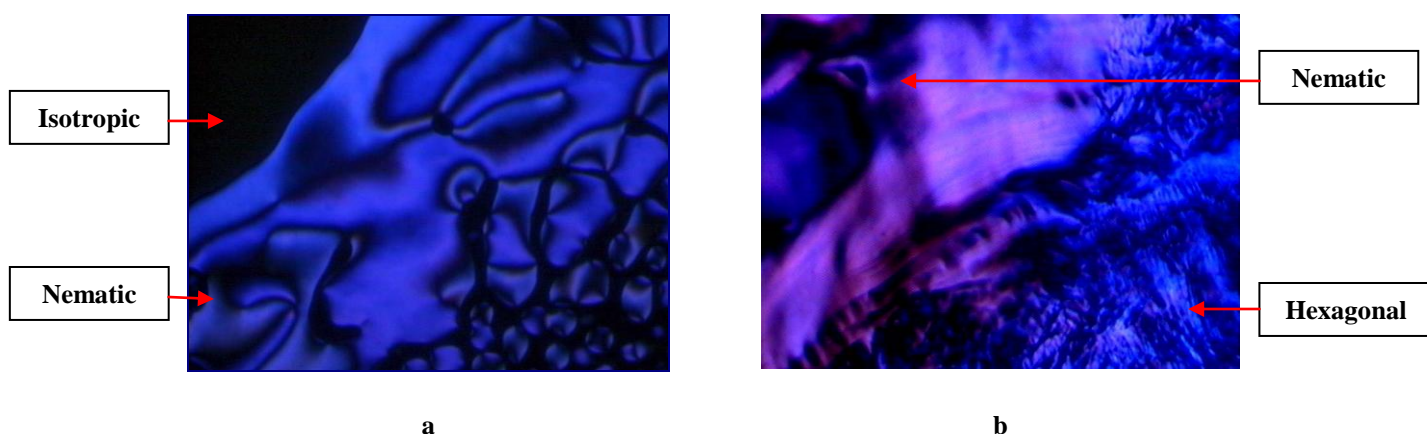
Figure 6.1   **Peripheral evaporation of an isotropic solution of Cu-phthalocyanine dye, formation of nematic (N_{col}) phase (magnification $\times$ ca. 200) (a), formation of hexagonal (Col_h) phase (magnification $\times$ ca. 100) (b).**

The phase diagram of Cu-phthalocyanine dye / water is shown in Figure 6.2. The samples of dye solutions were heated to 90°C and then subsequently cooled to 3°C at a rate of 2°C / min on a microscope slide to observe phase transitions during 3 heat / cool cycles. The sequence of phases and temperature changes is similar to those previously observed for other chromonic systems and gives a clear indication of the overall peritectic form of the temperature / composition phase diagram as shown in Figure 6.2.
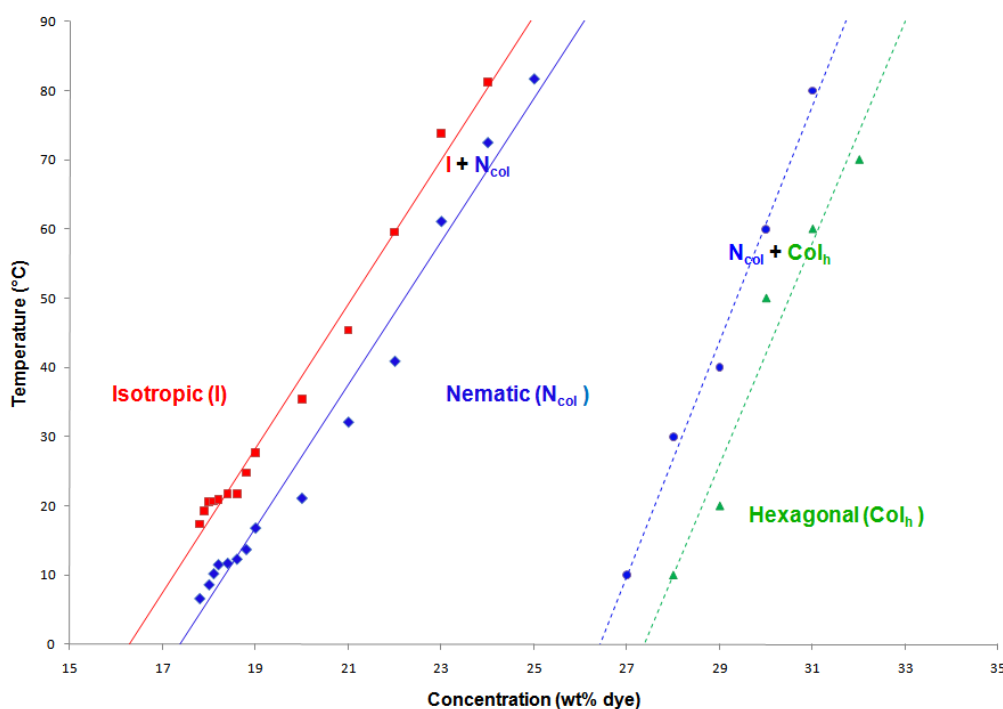
Figure 6.2   **Phase diagram of Cu-phthalocyanine dye in aqueous solution (the boundaries for isotropic (I) and nematic (N_{col}) phases obtained by optical microscopy, and the boundary between nematic (N_{col}) and hexagonal (Col_h) obtained by SAXS (the features at the bottom of the I/N_{col} are not regarded as significant and produced by errors in preparation of the samples).**

Aqueous solutions below 17.8 wt% dye at room temperature were observed to be isotropic (I), having no birefringence, and appeared black when examined between crossed polarisers of an optical microscope. In order to check the presence of a homeotropically aligned mesophase, a simple rheology test was carried out by applying a gentle pressure to the coverslip. The appearance still remained non-birefringent, and there was no mesophase present. The formation of a mesophase was observed at 17.4°C in the form of small

birefringent droplets gradually appearing in the isotropic bulk on cooling the sample of 17.8 wt% Cu-phthalocyanine dye at a rate of 2°C/min (Figure 6.3a). These droplets coalesced at 6.7°C and formed a bulk liquid-crystalline phase. The schlieren texture indicated the formation of a chromonic nematic (N_{col}) phase (Figure 6.3b). The sample started to freeze at approximately 0°C due to the significant ratio of water to dye in the solution.
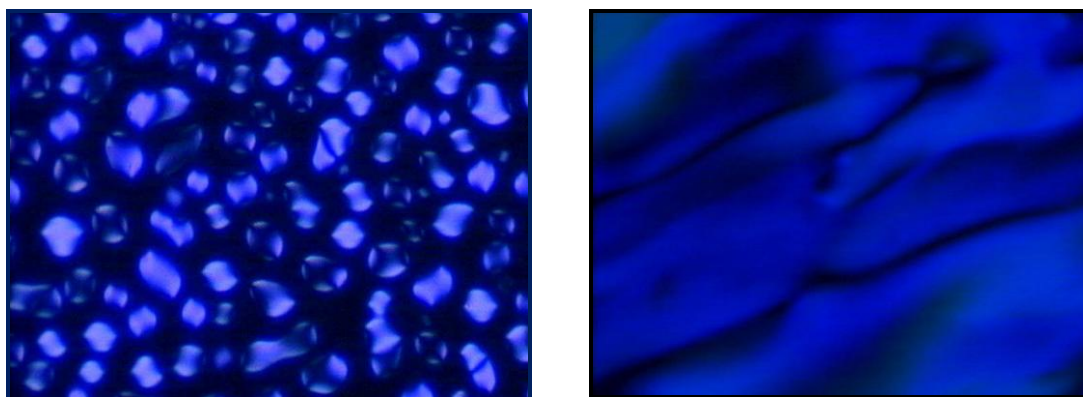
Figure 6.3   **Formation of the nematic phase observed for 17.8% wt/wt% Cu-phthalocyanine dye; birefringent droplets at 15°C (magnification × ca. 200) (a), schlieren texture formed by the nematic phase observed at 6°C (magnification x ca. 200) (b).**

The temperature stability of the nematic phase clearly increased as the concentration was raised. An increase in the concentration of the nematic phase resulted in the development of the fan-shaped optical texture. This typical texture is shown in Figure 6.4 and is characteristic of the hexagonal phase (Col_h). Once the transition from nematic to hexagonal phase was complete, there was no significant texture change upon further cooling. The fan texture persisted unchanged for all concentrations exhibiting hexagonal phase through cooling the samples down to 0°C.

Figure 6.4 The optical fan-like texture of the hexagonal phase observed for 31% wt/ wt% Cu-phthalocyanine dye at 23.4ºC temperature (magnification x ca. 200).

Heating the hexagonal phase resulted in disintegration of the fan-like texture with nematic regions starting to form around the fan-like domains (Figure 6.5).
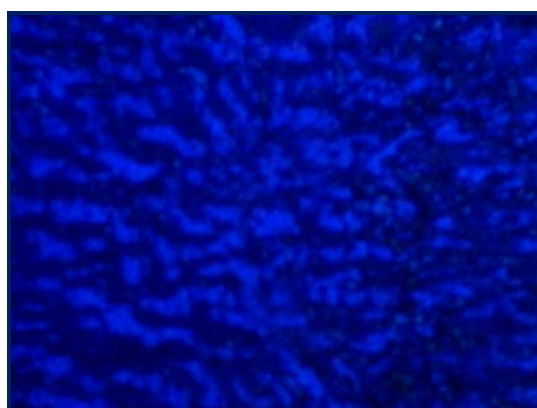
Figure 6.5   Disintegration of the fan-like texture on heating the hexagonal sample of 31% wt/wt% Cu-phthalocyanine dye at 19°C (magnification × ca. 100).

Prior to the complete disappearance of the hexagonal phase the sample of 31% wt/wt% dye entered the two phase ($Col_h + N_{col}$) region. The transition temperatures were not exactly the same during heating and cooling due to equilibration and hysteresis (2 - 3°C) across the phase transition between the isotropic − nematic and the nematic − hexagonal phases. Repeated heating and cooling was found to increase this transition range along with the transition temperatures. The average of transition temperatures during heating and cooling were used for constructing the phase diagram.

Cooling the nematic phase shows a gradual and continual change with increasing graininess of the texture as the N_{col} / Col_h transition is approached (Figure 6.6).
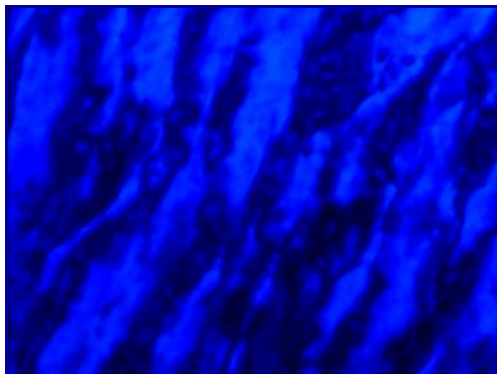
Figure 6.6   **Microscopic texture observed on cooling the nematic (N_{col}) phase near the N_{col} – Col_h transition (29% wt/wt%, 5°C), (magnification × ca. 200) .**

The textural change in the nematic phase was also observed on reheating the sample at a slightly higher temperature. This transition is initially very subtle and thus it is difficult to obtain accurately the temperature at which the transition occurs (Figure 6.7). Due to this the small angle X-ray diffraction results were used to construct the boundary for the nematic – hexagonal transition on the present phase diagram (Figure 6.2).

A possible explanation for this phenomenon is that the continuing formation of the more ordered phase is comparable to that of condensation of the less ordered optical domains on cooling and increasing the concentration. The aggregates do not rearrange distinctly on formation of the hexagonal phase, furthermore suggesting a weak first-order N_{col}-Col_h phase transition.
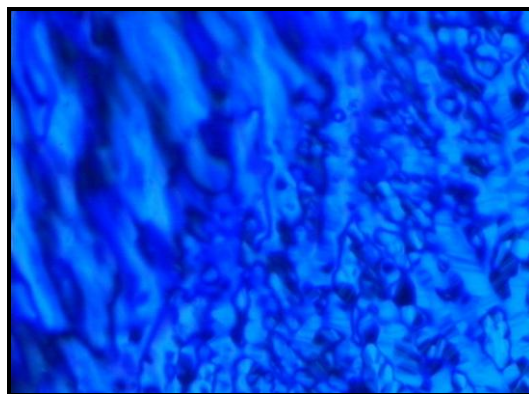
Figure 6.7   The nematic (N_{col}) to hexagonal (Col_h) transition observed for Cu-phthalocyanine dye on peripheral evaporation scan at 23.4ºC temperature. The boundary region is very vague (magnification $\times$ ca. 200).

At higher temperatures the nematic phase starts melting leading to the development of the distinctive reticulated texture (Figure 6.8) with islands of isotropic solution held within a continuous network of the nematic phase. This texture is characteristic of the two-phase (N_{col} + I) region. This two-phase region of (N_{col} + I) exists for about 10 ºC before the system is completely optically isotropic.
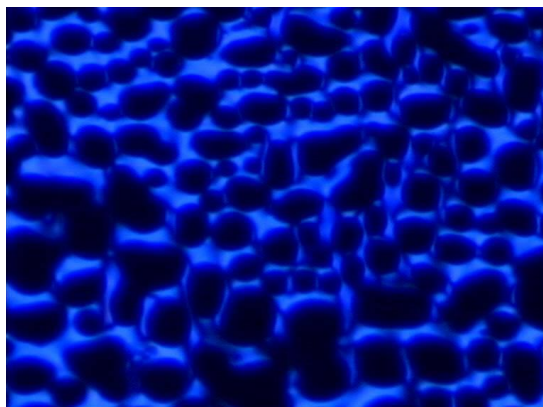
Figure 6.8   Two-phase (N_{col} + I) region observed for 19 wt% Cu-phthalocyanine dye at 22.3 ºC (magnification x ca. 100).

On cooling, the phase sequence is completely reversed, with birefringent droplets of nematic phase starting to appear in the isotropic continuum until the nematic phase is formed. On

further decrease of temperature the two-phase region (N_{col} + Col_h) starts developing with the domains of the hexagonal phase growing and congregating within the nematic phase until the hexagonal only remains.

The phase behaviour results are highly correlated with the viscosity observed by shear experiments, with an upward shift in the phase boundary correlating with an increase in solution viscosity and vice versa. The isotropic phase has a very low viscosity being similar to that of water. The nematic phase appears quite fluid, having the viscosity similar to writing inks. However, the hexagonal phase exhibits quite high viscosity, so it does not flow and can hardly be agitated by vigorous shaking. It results from the fact that as the hexagonal phase develops, the columns are packing closer and growing in length, hence, the mobility of the aggregates is reduced.

In summary, the Cu-phthalocyanine dye exhibits the sequence of phase transitions as shown in Figure 6.9. According to the phase diagram (Figure 6.2) there is no single composition that can show the entire phase sequence shown here.
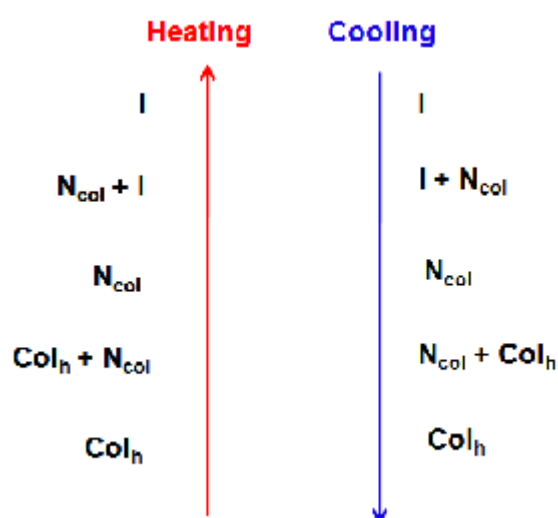
Figure 6.9   **Sequence of phase transitions on heating the hexagonal phase (red arrow) and on cooling from isotropic phase (blue arrow).**

In this chapter the bulk properties of the mesophases exhibited by the copper phthalocyanine dye are described. These include the composition and temperature dependence, the behaviour

during phase transitions and also the relative viscosities of the phases. The solution behaviour of the Cu-phthalocyanine dye naturally influences its liquid crystalline properties at higher compositions. Consequently, UV-vis spectroscopy was used to study the state of aggregation of this dye in solution, with respect to the concentration.

6.2 UV-vis Spectroscopy

UV-visible spectroscopy has been widely used to determine the onset of self-association of dyestuff molecules in aqueous solution, as the extensively conjugated aromatic chromophoric systems of Cu-phthalocyanines often go through the electronic transitions generating intense bands in their absorption spectra. The form of the spectra is similar to those which have been observed for other Cu-phthalocyanine dyes with the same chromophoric system [113, 114]. The absorption spectra in the range 300 nm $\leq \lambda \leq$ 750 nm for aqueous solutions of studied Cu-phthalocyanine dye with concentrations in the range 0.0010% - 3% are shown on Figure 6.10.
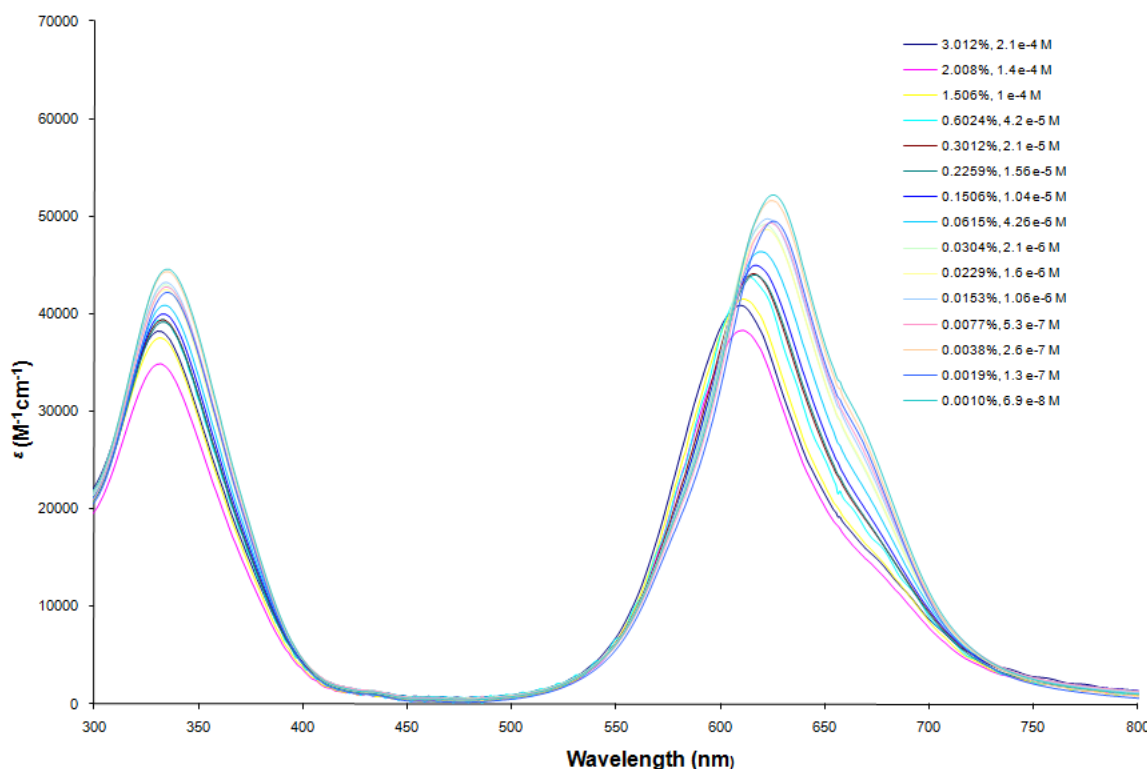
Figure 6.10   Absorption spectra of Cu-phthalocyanine dye aqueous solutions in the range of concentrations 0.0010% - 3% at 22.8 ºC [115].

The spectrum of an aqueous solution of Cu-phthalocyanine dye displays three characteristic absorption bands. The first one occurs in the ultra-violet (UV) region at the wavelength of about 340 nm and is called the B or Soret band. It is usually used as a "marker" band as it does not depend on aggregation over the wide range of concentrations and conditions [113]. This band arises due to an electronic $^1A_{1g} \rightarrow {}^1E'_u$ transition to the highest-energy vacant π^* orbital [62]. The second one appears in the visible region at the range of wavelengths between 609 nm – 625 nm. This is the Q-band, which is the strongest and often well-resolved absorption band in a vast number of phthalocyanines. The Q band absorption is of the π - π^* origin. It is caused by the transition from the highest occupied molecular orbital of $^1A_{1u}$ symmetry, to the lowest unoccupied molecular orbital of E_g symmetry [116], which results in a doubly degenerate first excited state of ^1E_u symmetry. The high molar absorptivity of $\sim 10^5$ L mol^{-1} cm^{-1} of this band is an indication of the higher purity and depth of colour of this phthalocyanine dye [117]. This band is usually attributed to those molecules within the aggregates. A shoulder on the Q-band is apparent at all compositions studied. It is thought to be associated with the forbidden transition to the higher excited energy level.

The third band arises at the wavelength of about 665 nm and corresponds to the dye monomer. The difficulty arises with observing this band for highly aggregating systems as quite often it is overlapped with the Q-band.

The shape of the absorption curve exhibits the steep slope with the small width, and it does not change distinctly on the increase of concentration. However, the peaks are slightly broadening and the intensity of the bands is observed to be increased with the peaks shifting slightly to the lower wavelength region (i.e. both hyperchromic and hypsochromic shifts) as the concentration is increased. Table 6.1 represents absorption maxima for the Q-band for the range concentrations studied. These values are subject to errors arising from absorption / aggregation of the dye on the glass slides used as a sample cell, and inaccuracies introduced by the gravimetric dilution process.

Table 6.1   **Absorption maxima for the Q-band for Cu-phthalocyanine dye at 22.8°C.**

c (%)	c (M)	log c	λ (nm)	ε (M^{-1} cm^{-1})
0.0010	6.9×10^{-8}	-7.16	625	52197
0.0019	1.3×10^{-7}	- 6.89	625	49513
0.0038	2.6×10^{-7}	- 6.59	624	51631
0.0077	5.3×10^{-7}	- 6.28	623	49397
0.0153	1.06×10^{-6}	- 5.97	622	49695
0.0229	1.6×10^{-6}	- 5.8	621	48660
0.0304	2.1×10^{-6}	- 5.68	621	47165
0.0615	4.26×10^{-6}	- 5.37	619	46664
0.1506	1.04×10^{-5}	- 4.98	617	45006
0.2259	1.56×10^{-5}	- 4.8	616	44054
0.3012	2.1×10^{-5}	- 4.68	615	44078
0.6024	4.2×10^{-5}	- 4.38	613	43937
1.5060	1×10^{-4}	- 3.98	611	41550
2.0080	1.4×10^{-4}	- 3.86	610	38356
3.0120	2.1×10^{-4}	- 3.68	609	40917

Monitoring the molar absorption coefficients as the function of dye concentration can be used to study the nature and extent of aggregation. The decrease in the absorption coefficient (Figure 6.13) and shift in the wavelength of the absorption maximum (Figure

6.14) can be explained by utilising the exciton coupling theory as the absorption spectra of dye aggregates usually show great differences when compared to the individual molecules [118-121]. This method qualitatively explains the spectral properties of dye aggregation and is built on the assumption that there is negligible overlap of respective molecular orbitals, therefore preserving the individual characteristics of chromophores in the aggregates. Furthermore, the location of the transition moment of the electronic transition is presumed to be in the centre of the chromophore with its polarisation axis lying in parallel to the long axis of the chromophore. Interaction of the excited states of the chromophores in the aggregate is directly proportional to the magnitude of the transition dipole moments located within the Cu-phthalocyanine ring and is inversely proportional to the cube of their separation. Furthermore, if two adjacent CuPc molecules of D_{4h} symmetry are lying in the face-to-face arrangement, the exciton coupling produces a splitting of the ^1E_u excited state into two energy levels Q_+ and Q_- (Figure 6.11). The energy level which will produce the light absorption is usually determined by the relative orientation of the transition dipole moments.

Dye molecules can aggregate either in a parallel (H-aggregation) or in a head-to-tail (J-aggregation) way. In case of formation of H-aggregates the transition dipoles can only be aligned in two ways (Figure 6.11). The first one describes the parallel way of cofacial stacking of two molecules, which normally produces an excited state that is higher in energy than the one in the monomer. It usually happens due to electrostatic repulsion between the transition dipole moments. If the transition dipole moments are oriented in an antiparallel way, then a decrease in the excited state energy occurs. Considering the transition moment of the aggregate to be given by the vector sum of both components, transitions from the ground state to the lower excited energy level are forbidden. Therefore, the lower energy exciton interaction produces no net dipole change and, hence, no light absorption. Transitions to the higher energy levels for cofacial dimers are very intense (allowed). Figure 6.15 shows clearly that the absorption band caused by the dimers of the dye molecules aggregated in a parallel way is expected to be blue-shifted (hypsochromic) relative to its position in the isolated molecular spectrum.
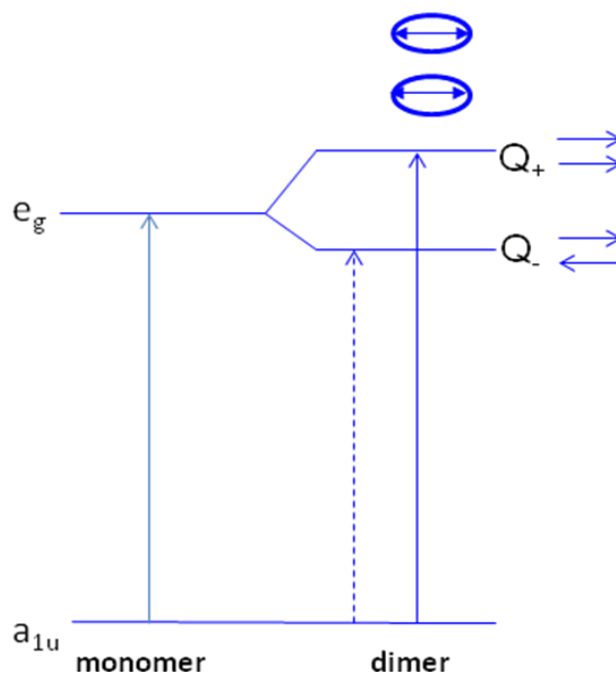
Figure 6.11   Exciton splitting of the Q-band between two molecules of Cu-Phthalocyanines in cofacial arrangement (H-aggregates) (a simplified model). [122].

By contrast if the dye molecules stack in the end to end manner, the transition dipoles are in a head-to-tail orientation. The in-phase arrangement of transition dipoles results in electrostatic attraction, which further results in occurrence of a lower energy level (Figure 6.12). At the same time out-of-phase arrangement of transition dipoles leads to repulsion resulting in the higher energy level. The corresponding transition from the ground state to the low energy level leads to a red shift of the transition in the dimers within J-aggregates compared to that of the monomeric spectrum.
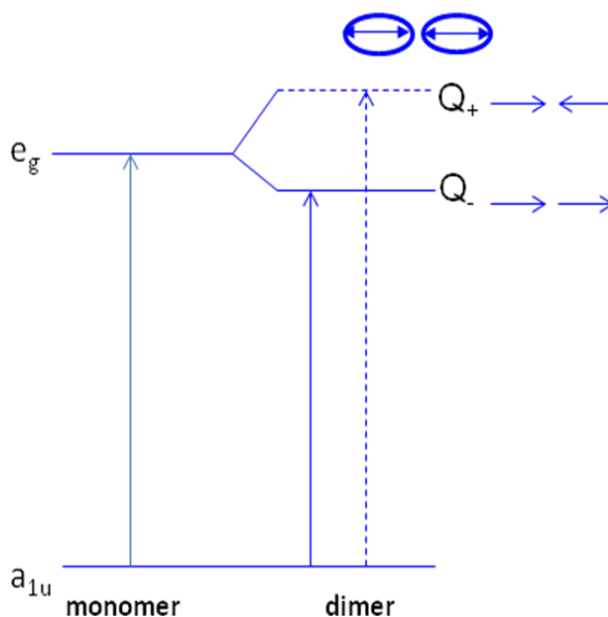
Figure 6.12   **Exciton splitting of the exciton splitting of the excited state of dye aggregates in head-to-tail arrangement (J-aggregates) (a simplified model). [122]**

In order to explain the electronic absorption spectra obtained for Cu-phthalocyanine dye aggregates in solution, the dimeric exciton coupling model can be extended [123, 124]. For the molecules lying in a face-to face manner within the aggregates the blue-shifted Q-band is an indication owing to the exciton coupling and increasing the energy level of the excited state. The hypsochromic changes of the Q-band with the increase of concentration are very consistent, implying that the dye is present almost entirely in an associated form over the experimental range of concentrations, hence suggesting the formation of H-aggregates in water.
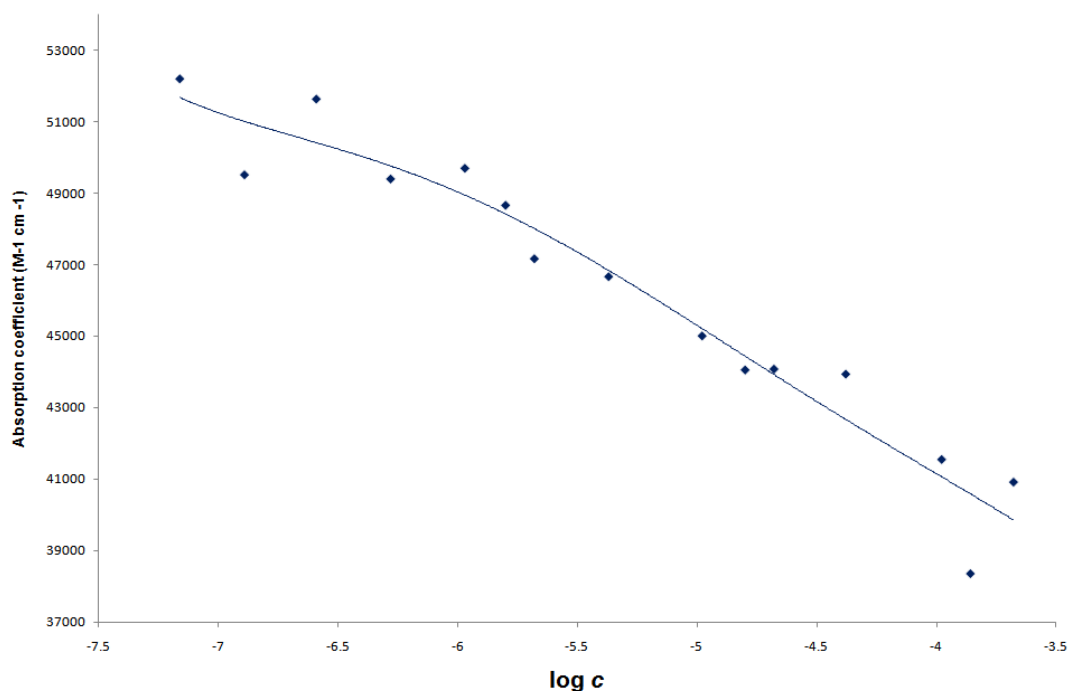
Figure 6.13   The variation of ε with concentration of Cu-phthalocyanine dye.

The changes in absorption coefficient for all spectra at the wavelength corresponding to λ_{max} are illustrated in Figure 6.13. The clear decrease in ε value can be observed with the increase of concentration, which suggests that aggregation is occurring. At any particular wavelength, the total absorbance A_T can be found using Equation 6.1

$$A_T = \sum_{n=1}^{\infty} \varepsilon_n c_n l$$

Equation 6.1

where ε_n is the molar absorptivity of the *n*-mer, c_n is the concentration of the *n*-mer and l is the path length. If aggregation is not occurring within the studied range of concentrations, then the absorption coefficient should have approximately the same value due to the presence of only one type of species in the solution. As the absorption coefficients at higher concentrations appear to be much lower compared to those at lower concentrations, therefore, the graph shows the decreasing trend (Figure 6.13) signalling that the aggregation is occurring with the increase of concentration.

87
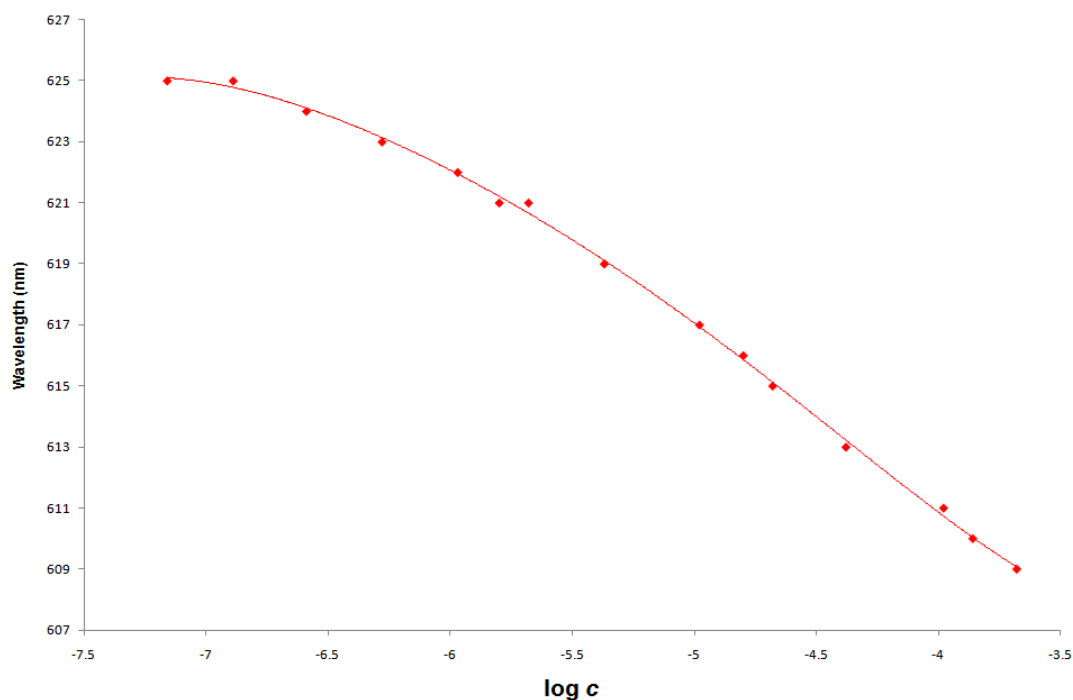
Figure 6.14   **The variation of λ_{max} with concentration of Cu-phthalocyanine dye.**

The change in wavelength (λ_{max}) is shown in Figure 6.14. It can be clearly seen that there is a significant decrease in the value of λ_{max} with increasing concentration. It is important to note that a liquid crystalline phase was not observed by optical microscopy within the range of concentrations in which the UV - vis experiment was conducted, thus, occurring in isotropic phase. The nematic phase only started to appear at ~ 18% wt / wt% dye concentration in aqueous solution at room temperature. Therefore, this reduction in λ_{max} must be signalling about a significant increase in the aggregation of dye molecules even within the isotropic phase upon raising the dye concentration.
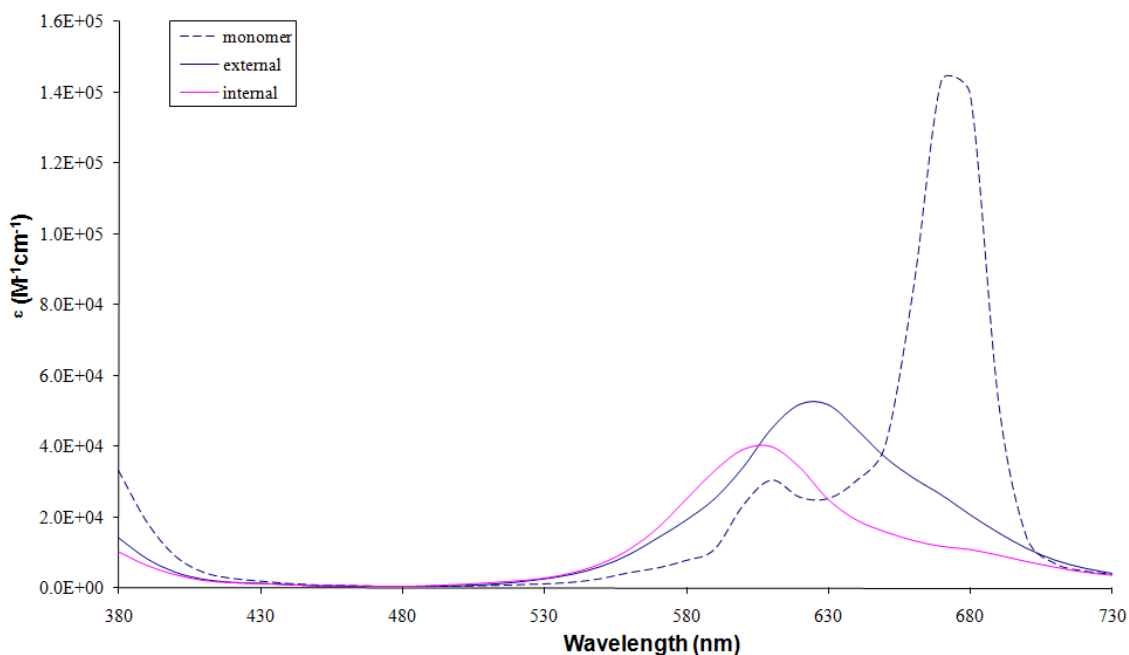
Figure 6.15   **Fitted molar absorption coefficients of monomer, dimer and aggregated molecules of Cu-phthalocyanine dye in aqueous solution.**

The graph above shows how the absorption spectrum varies for the studied dye with three different absorbing species present in the aqueous solution. Two absorption bands dominate the absorption spectrum of monomeric Cu-phthalocyanine. These bands are the intense Q band with λ_{max} value of approximately 670 nm, and a weak satellite band, which is observed near 610 nm (dotted blue spectrum, Figure 6.15). As the solution concentration is increased, the shape of the spectrum changes, appearing now in the form of a single long-wave band and resulting from broadening of the region accommodating the π electrons of a chromophore. λ_{max} value is shifted hypsocromically to a value of approximately 610 nm (blue spectrum). The absorption coefficient appears to be different to that containing the monomeric species, therefore, suggesting a mixture of monomeric and dimeric species present in the solution. As more molecules are accumulated in the associate, the band broadens up subsequently and the λ_{max} shifts further to the blue region signalling about the increase in aggregation and suggesting the presence of a mixture of monomers, dimers and higher oligomers.

Different mathematical models have been developed for the quantitative description of $\pi - \pi$ aggregation. Theoretical model of Israelachvili describes the systems undergoing self-association in aqueous solution along with the equilibrium between N individual molecules and the aggregates formed by these molecules as shown in Figure 6.16 [60].
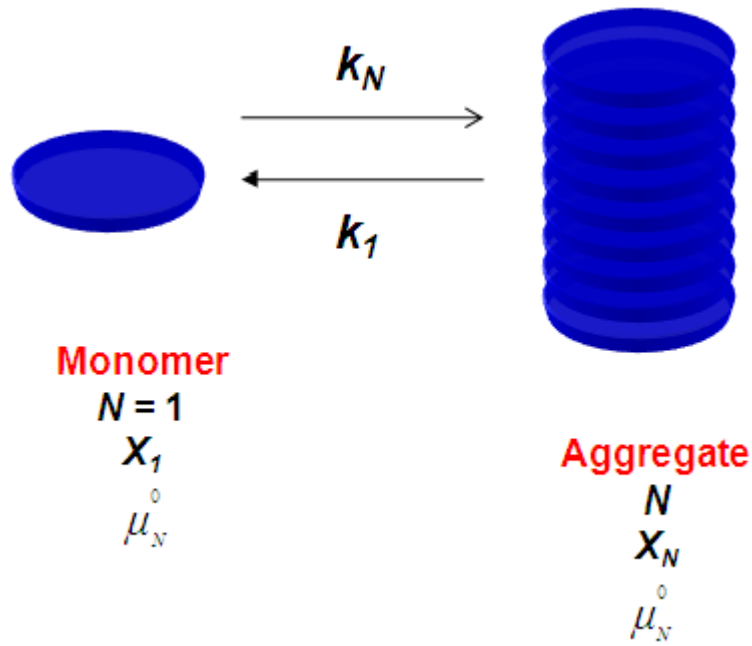
Figure 6.16 **Aggregation of *N* monomers in Cu-phthalocyanine dye according to Israelachvili theory [60].**

The equilibrium constant is the ratio of two reaction rates with

$$\text{rate of aggregation} = k_1 X_1{}^N$$

$$\text{rate of disaggregation} = k_N (X_N / N),$$

$$\text{thus, } k = k_1 / k_N = \exp [- N (\mu_N^0 - \mu_1^0) / k_B T]$$

Equation 6.2 [60]

If X_N corresponds to a molecular volume fraction in an aggregate of *N* molecules and μ_N^0 is the mean interaction free energy per molecule in aggregates of aggregation number *N*, then X_N can be written in terms of the volume fraction of an isolated molecule, X_1, to give Equation 6.3,

$$X_N = N\{X_I \exp\left[(\mu_1^0 - \mu_N^0)/k_BT\right]\}^N$$

Equation 6.3

where k_B is the Boltzmann constant and T is the absolute temperature.

The important condition for the formation of large aggregates is that there should be a difference in energies between the molecules in aggregated and monomeric states due to the molecules within different species experiencing different interactions with their surroundings, thus making $\mu_N^0 < \mu_1^0$ along with μ_N^0 decreasing with N.

The mean interaction free energy per molecule for the formation of one-dimensional aggregates can then be found by

$$\mu_N^0 = -\frac{N-1}{N}\alpha\kappa_BT$$

Equation 6.4

assuming that the molecule – molecule bond energy, of the the order αk_BT, *with α* remaining constant for each of the $(N-1)$ bonds in an aggregate of N molecules.

The volume fraction of molecules in an aggregate of N molecules can then be found by

$$X_N = N[X_1e^\alpha]^N e^\alpha$$

Equation 6.5

Considering the total volume fraction of dye molecules in the solution φ, then

$$\phi = \sum_{N=1}^{\infty} X_n = \sum_{N=1}^{\infty} N[X_1e^\alpha]^N e^{-\alpha}$$

$$= X_1/(1-X_1e^\alpha)^2$$

Equation 6.6

Thus,

$$X_1 = \frac{(1 + 2\phi\, e^\alpha) - \sqrt{1 + 4\phi\, e^\alpha}}{2\phi\, e^{2\alpha}}$$

Equation 6.7

This theory is widely used for establishing the relationship between aggregate size distribution and volume fraction (ϕ), the association energy (α) and temperature.

The isodesmic model proposed by J. R. Henderson [48] is another model for the description of extended dye aggregates. In this model the aggregates are assumed to be of one-dimensional character. For isodesmic behaviour, the addition of each molecule to the columnar aggregate is accompanied by a constant change in the equilibrium constant. Thus, the isodesmic chemical equilibria, based on the law of mass action, can be described as

$$M + M \leftrightarrow M_2 \qquad\qquad c_2 = k_2 c_1^2$$

$$M_2 + M \leftrightarrow M_3 \qquad\qquad c_3 = k_3 c_2 c_1 = k_2 k_3 c_1^3$$

$$....$$

$$M_{n-1} + M \leftrightarrow M_n \qquad\qquad c_n = k_n c_{n-1} c_1 = k_2 k_3 \ldots k_{n-1} k_n c_1^n$$

Equation 6.8

where c_1, c_2, c_3 ... c_n are the corresponding molar concentrations of monomeric, dimeric, trimeric and n-meric species; k_2, k_3, k_n are the equilibrium constants for an addition of a monomer to another monomer, dimer, trimer, (n-1)-mer.

According to the isodesmic model

$$k = k_2 = k_3 = \ldots = k_n$$

Equation 6.9

therefore, the concentration of n-mer c_n along with the total solute concentration c_t can be determined by

$$c_n = k^{n-1}c_1^n$$

Equation 6.10

$$c_t = (c_1 + 2kc_1^2 + 3k^2c_1^3 + \ldots + nk^{n-1}c_1^n)$$

Equation 6.11

Growth of an aggregate algebraically can be expressed as the series of expansion

$$1 + 2a + 3a^2 + \ldots + na^{n-1} = 1 / (1 - a)^2$$

Equation 6.12

with the condition that $0 < a < 1$, thus,

$$c_t = c_1 / (1 - kc_1)^2$$

Equation 6.13

Solving Equation 6.13 leads to

$$c_1 = \frac{2kc_t + 1 - \sqrt{4kc_t + 1}}{2k^2c_t}$$

Equation 6.14

Furthermore, in order to obtain the fraction of aggregated molecules within the larger stacks the following relationship between the concentration of monomers and the total concentration of molecules should be considered

$$\chi_m = \frac{c_1}{c_t}$$

Equation 6.15

with χ_m corresponding to the fraction of monomeric species.

Therefore, the fraction of aggregated molecules within the large stacks can be found by using Equation 6.16

$$\chi_a = 1 - \frac{2kc_t + 1 - \sqrt{4kc_t + 1}}{2k^2 c_t^2}$$

Equation 6.16

There have been many studies of aggregation in solutions of phthalocyanine compounds [125-128] and most of them applied the monomer – dimer equilibrium model in order to attempt a quantitative description of $\pi - \pi$ aggregation. One of the shortcomings of such models appears in the form of limited approach to the process of aggregation by having only one fitted equilibrium constant. P.J Camp recently proposed a simple model in which the process of aggregation is not restricted to the presence of monomeric, dimeric and trimeric species [123] in aqueous solution, but the formation of larger aggregates is also accounted for.

The aggregation of Cu-phthalocyanine molecules is associated with the stacking of the planar molecular aromatic cores into the columns ranging in size from monomers to the aggregates of the infinite size, thus, the issue of polydispersity should not be ignored. Camp has developed the model, which takes into account the full equilibrium distribution of clusters formed by such columnar aggregates of molecules. His approach is built on the assumption that there are two different conditions the molecules with the stack are exposed to. First one corresponds to the condition describing the molecules located at the ends of the columns, hence, neighbouring with only one molecule (Figure 6.17b). Second one describes the molecules sitting inside the columns, thus sandwiched between two neighbouring molecules (Figure 6.17c).

The model was developed using statistical mechanics principles, although the results come in excellent agreement with those obtained from thermodynamics [114]. Therefore,

Camp described aggregation process occurring in two stages, which include the familiar monomer – dimer equilibrium followed by further equilibrium for inclusions of additional monomers.

$$\text{Monomer} \leftrightarrow \text{Dimer} \qquad\qquad \nu_{ex}$$

$$n - \text{mer} + \text{Monomer} \leftrightarrow (n + 1) \text{ mer, where} \quad (n \geq 2) \qquad \nu_{in}$$
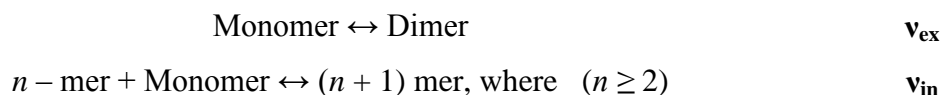
where ν_{ex} and ν_{in} are single molecule parameters describing molecular confinement by neighbouring molecules.

ε_{mon} $\qquad\qquad\qquad\qquad$ ε_{ext} $\qquad\qquad\qquad\qquad$ ε_{int}

a $\qquad\qquad\qquad\qquad\qquad$ b $\qquad\qquad\qquad\qquad\qquad$ c
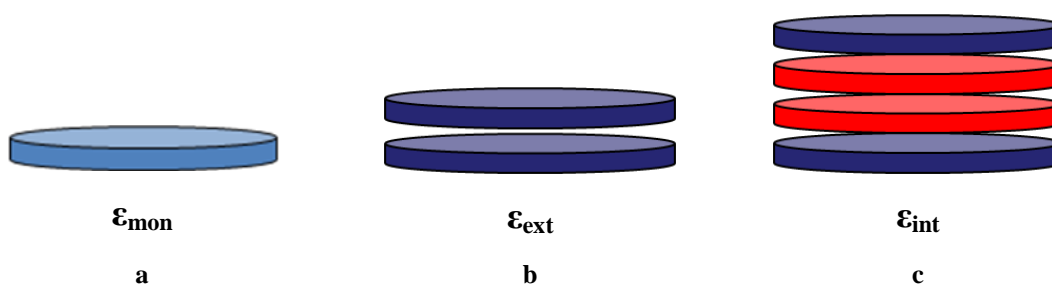
Figure 6.17 **Schematic representation of the Cu-phthalocyanine aggregation with three absorbing species present: the monomer (a), the dimer (b) and the larger aggregate (c) with navy discs representing external molecules and red discs representing internal molecules.**

Thus, the aggregation process of Cu-phthalocyanine dye can be studied by considering that there are only three absorbing species present in the solution at a given concentration.

Consider a system with N solute molecules in a volume V and at a temperature T which contains N_1 free monomers, N_2 dimers and N_n n-mers. At equilibrium, the concentration of n-mers can be found using Equation 6.17

$$c_n = N_n / V$$

Equation 6.17

with the total concentration of monomers being related to c_n by Equation 6.18

$$c_1 = \sum_{n=1}^{\infty} nc_n$$

Equation 6.18

Furthermore, the relationship between c_n and c_1 can be expressed by Equation 6.19

$$c_n = v_{ex} v_{in}^{n-2} c_1^n$$

Equation 6.19

assuming the solution of aggregates is sufficiently dilute and any interactions between the aggregates can be ignored, thus, considering solution to be ideal. Equation 6.19 can be used for showing that the equilibrium constants for two separate steps of aggregation are equal to v_{ex} (for monomer – dimer equilibrium) and v_{in} (for further equilibrium with higher aggregates).

Combining Equations 6.17 and 6.19 gives the following equation for c_1

$$c = c_1 + \frac{v_{ex} c_1^2 (2 - v_{in} c_1)}{(1 - v_{in} c_1)^2}$$

Equation 6.20

In order to incorporate the experimental data into the theoretical model and analyse the effective molar absorption coefficients, the estimation of the mole fractions of molecules exposed to different environments is required (Equation 6.15). Based on the assumption that there are two molecules located at the ends of an aggregate, and combining Equations 6.15 and 6.19, the values for χ_1, χ_{in} and χ_{ex} can be found by

$$1 = \chi_1 + \frac{v_{ex} c \chi_1^2 (2 - v_{in} c \chi_1)}{(1 - v_{in} c \chi_1)^2}$$

Equation 6.21

96

$$\chi_{ex} = 2\sum_{n=2}^{\infty} \frac{c_n}{c} = \frac{2v_{ex}c\chi_1^2}{(1-v_{in}c\chi_1)}$$

Equation 6.22

$$\chi_{in} = 1 - \chi_1 - \chi_{ex} > 0$$

Equation 6.23

The first limitation of this model arises when $v_{in} = v_{ex}$ and in this case the equilibria on both stages of aggregation are governed by only one equilibrium constant. In this case the mole fraction are then given by

$$\chi_1 = \frac{1}{v_{ex}c} + \frac{(1-\sqrt{1+4v_{ex}c})}{2(v_{ex}c)^2}$$

Equation 6.24

$$\chi_{ex} = \frac{2v_{ex}c\chi_1^2}{(1-v_{ex}c\chi_1)}$$

Equation 6.25

$$\chi_{in} = 1 - \chi_1 - \chi_{ex} > 0$$

Equation 6.26

Another limitation of this model arises when the equilibrium is of the monomer – dimer type, hence, $\nu_{in} = 0$. Therefore, the composition of the solution can be given by

$$\chi_1 = \frac{-1 + \sqrt{1 + 8\nu_{ex}c}}{4\nu_{ex}c}$$

Equation 6.27

$$\chi_{ex} = 2\nu_{ex}c\chi_1^2$$

Equation 6.28

$$\chi_{in} = 1 - \chi_1 - \chi_{ex} = 0$$

Equation 6.29

For the analysis of the experimental data five parameters are required: the two equilibrium constants and the three extinction coefficients, which can be assigned to single molecules ε_1 (λ), external molecules ε_{ex} (λ) and internal molecules ε_{in} (λ) (Figure 6.17). Thus, at any particular wavelength, λ, the total absorption coefficient can be found by

$$\varepsilon(\lambda) = \chi_1\varepsilon_1(\lambda) + \chi_{ex}\varepsilon_{ex}(\lambda) + \chi_{in}\varepsilon_{in}(\lambda)$$

Equation 6.30

The experimental data were fitted using equations 6.21 – 6.29 for three different species present in aqueous solution. The best set of consistent parameters was found by employing an iterative process. Firstly it was assumed that the three extinction coefficients

(ε_I, ε_{in} and ε_{ex}) were the same for each concentration. The estimate of the monomer spectrum ε_I (λ) was derived from the spectrum of Cu-phthalocyanine dye measured experimentally in disaggregating solvent dimethyl sulfoxide (DMSO). The estimate of the aggregated spectrum ε_{in} (λ) was made by measuring the spectrum of the dye at high dye concentrations in aqueous solution in a very short path length cell (5 μm). The individual spectrum of the dimeric species present in a solution could not be obtained experimentally due to the formation of higher order aggregates. Therefore, the dimer spectrum estimation was based upon the averaged absorption coefficient values found within the experimental monomer and aggregated spectra. The equilibrium constants were then obtained at λ_{max} with the approximate values equal to

$$k_{ex} \sim 2.9 \times 10^8$$
$$k_{in} \sim 8.75 \times 10^5 \qquad k_{in} > k_{ex} > 0$$

The equilibrium constants (k_{in}, k_{ex}) were then fit at λ_{max} corresponding to the monomer spectrum.

The next stage of the analysis is to calculate the spectra by permitting the parameters (ε_I (λ), ε_{ext} (λ), ε_{in} (λ), k_I and k_{in}) to be variable across all wavelengths through the fitting process. In order to reduce the discrepancies exhibited between the experimental and calculated spectra, the curves were adjusted with the help of simplex minimisation to obtain the best possible fit of calculated spectra within the empirical data. Figure 6.15 displays the fitted molar absorption coefficients ε_I (λ), ε_{ext} (λ), ε_{in} (λ) in the range of 380 nm $\leq \lambda \leq$ 730 nm for monomer, dimer and aggregated molecules of Cu-phthalocyanine dye in aqueous solution.

Furthermore, it becomes possible to plot the distribution of aggregate sizes as a function of concentration. The variation of the calculated number average size of aggregates in water according to Camp's model is illustrated in Figure 6.18.
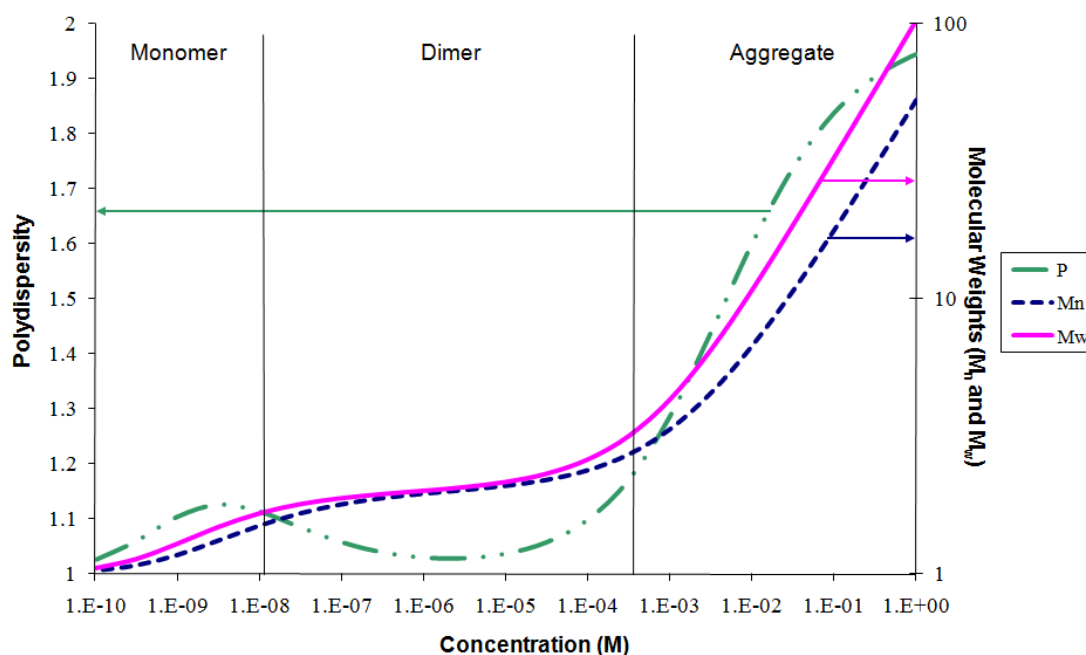
Figure 6.18   Calculated number average size of aggregates for Cu-phthalocyanine dye in aqueous solution.

The model shows that at low dye concentrations ($c < 10^{-8}$ M), the dye exists mainly in monomeric form. At intermediate concentration ($10^{-8} \leq c \geq 10^{-4}$) the dye molecules are present predominantly in dimeric form. The formation of trimers and higher oligomers occurs above $c \approx 10^{-4}$. It can be inferred from Figure 6.18 there are distinguishable levels of higher aggregates even at very low concentrations as a result of the distribution of aggregate sizes.

In this chapter the aggregation properties of Cu-phthalocyanine dye were investigated by UV-vis absorption spectroscopy and equilibrium statistical mechanics for a wide range of concentrations. The experimental data confirm the H type aggregation process with its parallel arrangement of the dye molecules forming a nearly vertical stack. The impact of changes in dye concentration upon the equilibrium cluster distribution was obtained by utilising the sensitivity of the peak intensities at the absorption maxima.

The next logical step in building a comprehensive understanding of the studied system would be to investigate the behaviour of Cu-phthalocyanine dye at higher concentrations on formation of mesophases. The primary objective is to attain the inter- and intra-aggregate ordering by X-ray diffraction, thus allowing the phases to be clearly identified in addition to the examination of the nature of the aggregates. The results obtained by X-ray diffraction are described in the next section.

6.3 Electron Paramagnetic Resonance (EPR)

Electron Paramagnetic resonance is a valuable method for gaining detailed structural information about the studied copper phthalocyanine dye [129]. There was no planning for EPR experimental measurements at the beginning of the project. At the later stages of the work a collaboration with the labs of Dr V. S. Oganesyan and Dr M.R. Cheesman from the University of East Anglia (UEA) has been established which allowed me to travel to UEA and participate in performing low temperature Continuous Wave (CW) EPR experiments on the copper phthalocyanine dye.

Electron Paramagnetic Resonance (EPR) has been used to study the process of molecular self-association of copper phthalocyanine dye in aqueous solutions. In general, EPR measurements can be employed as a useful source of information about the nature of the surrounding of a paramagnetic Cu^{2+} ion [130].

Copper phthalocyanine materials having Cu^{2+} as a central atom are $S = \frac{1}{2}$ systems. If two such phthalocyanines are close enough that the metals interact, the bimetallic system will have a singlet ($S = 0$) and triplet ($S = 1$) states. If the rate of electron exchange between the metals is fast compared to the resonance frequency (9.5 GHz as in X-band EPR spectrometer), then each electron experiences nuclear spin equal to the total nuclear spin of the two metal atoms ($I = 3$ for Cu_2^{2+}). It results in the hyperfine splitting (hfs), which is half that for a related mononuclear $S = \frac{1}{2}$ system. The EPR transitions will be further split by the zero field splitting, D, which is originates from the electron − electron dipolar interaction [131]. The superhyperfine (shfs) structure is also characteristic of copper phthalocyanine substances and is derived from the interactions of the $3d^0$ electron configuration of copper atom with four equivalent nitrogen ($I = 1$) atoms of the isoindole groups.

Figure 6.19 shows typical EPR spectrum obtained for the copper phthalocyanine dye in aqueous solution at room temperature. All studied copper phthalocyanine dye solutions (with the lowest concentration equal to 1.4×10^{-7} M) show a single relatively broad and weakly asymmetric singlet in the EPR spectrum as shown in Figure 6.19, and it does not resolve (give) any hyperfine patterns attributed to copper (four-line multiplet) and superhyperfine ones corresponding to nitrogen (nine-line multiplet). These patterns can be explained as the sum of the contributions from all orientations of the molecule relative to magnetic field, wherein the hyperfine structures are obscured by the magnetic electron spin − electron spin dipolar interactions between the neighbouring copper phthalocyanine molecules. UV-vis absorption spectroscopy has already proved the high tendency of this dye

to aggregate in aqueous solutions. If the dye molecules were indeed in monomeric form at 1.4×10^{-7} M concentration, the average copper – copper interaction distance would be at least several hundred angstroms, giving rise to an EPR spectrum characterised by well delineated copper hfs and nitrogen shfs structure. Empirical data obtained by XRD reveals that the molecules pile on the top of each other within the stacking period of 3.5 Å (± 0.05 Å), thus making the individual contributions from each individual Cu^{2+} beyond the limits of the detector and any hyperfine and superhyperfine contributions impossible to see. The conditions of the experiment were being changed (1×10^{-4} M $\geq$ c $\geq$ 1×10^{-7} M), although the spectrum still remains the same in the form of a strong broad singlet.
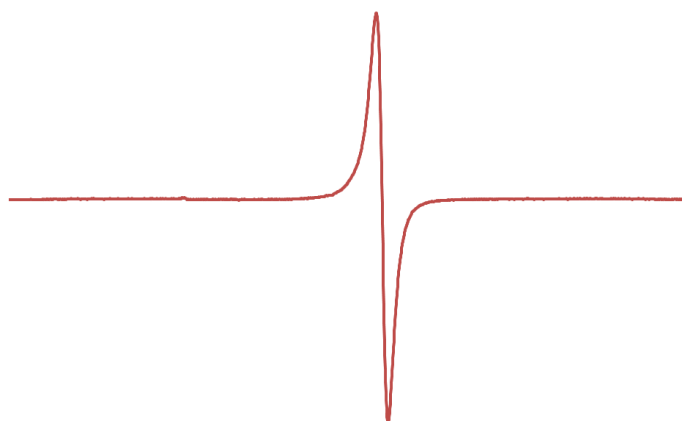
Figure 6.19   **EPR spectra of copper phthalocyanine dye at 1.4×10^{-7} M concentration at 55K (-218 °C).**

CW EPR is a powerful method for gaining the valuable information about the kinetics of aggregation along with the magnetic properties of the dye in monomeric, dimeric and aggregated forms. Given that the gross features of the EPR spectrum indicate molecular aggregation, it is also possible to determine the relative degree of aggregation of the phthalocyanine dye in aqueous solution from the corresponding EPR line shape. To accomplish this it is necessary first to understand the kind of EPR line shape that would be expected to arise from a random distribution of isolated microscopic copper phthalocyanine complexes and second to understand the changes in spectra which occur at higher concentrations of these complexes as the perturbing influence of intermolecular spin – spin interactions increases. At very high magnetic concentration the shape of the composite or EPR spectrum is essentially dominated by the effects of intermolecular spin exchange coupling. In order to obtain the spectra for isolated molecules the copper phthalocyanine dye

can be diluted with the copper free phthalocyanine complex, which would give the spectra with the hfs and shfs attributed to copper and nitrogen respectively. By diluting the copper phthalocyanine one would be able to increase the resolution of the hfs and shfs in the spectra. [129, 132].

CHAPTER SEVEN

7. Structural Studies of Copper Phthalocyanine Dye

7.1 X-ray Diffraction

Based on the results found using the optical microscopy and UV visible spectroscopy measurements, it was felt pertinent to investigate the structure of the Cu-Phthalocyanine dye aggregates using Synchrotron X-ray scattering experiments. The aggregate structure was investigated using both small angle and wide angle X-ray scattering (SAXS and WAXS, respectively). The important results are presented below in Figures 7.1, 7.2 for the wide-angle diffraction, and in Figures 7.3 – 7.25 for the changes in the higher order spacings of phthalocyanine dye with temperature and concentration.

7.1.1 Wide – angle X-ray Diffraction (WAXS)

The internal structure of the columns was found experimentally by wide-angle X-ray diffraction carried out on station 2.1 at the Synchrotron Radiation Source (SRS), Daresbury Laboratories. A sample was placed in to a Lindemann tube and heated to 85°C at 10°C per minute. A scan was taken every 10°C (for clarity only certain scans are discussed here). The diffraction pattern at 5°C and integrated plots obtained as a function of temperature over the heating run are shown in Figures 7.1 and 7.2. The diffraction patterns for most of the concentrations studied contain one strong sharp diffraction peak observed in the wide angle region at a distance of 3.5 Å (± 0.05 Å) along the axial direction (Figure 7.1). This observed stacking period corresponds precisely both to the thickness of the aromatic cores and to the well-known piling distance of aromatic layers in general [133]. Therefore, the plain phthalocyanine cores are not only superposed in close contact with each other, but also are lying in perpendicular to the column axis (Figure 7.1). An unusual feature of the X-ray diffraction pattern of the mesophases in the form of diffuse off-axis reflections at ≈ 6.8 Å was not observed for this dye.
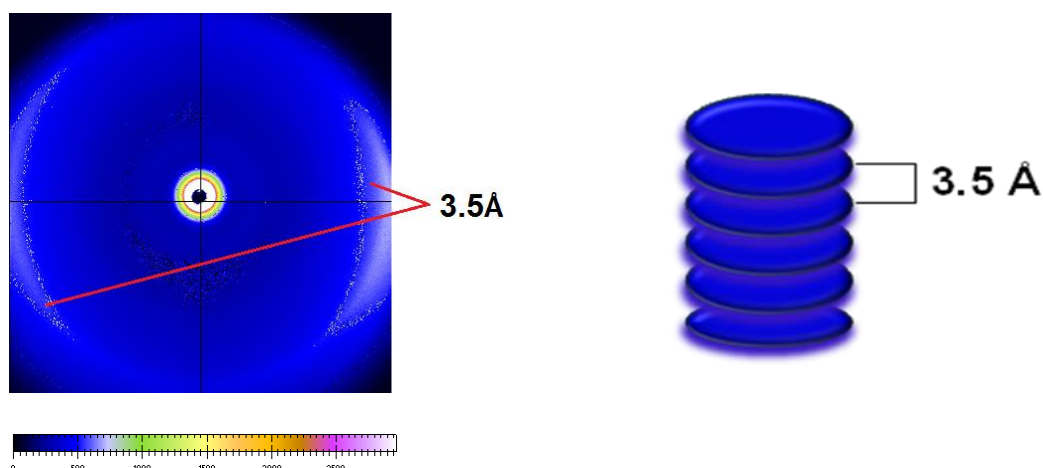
Figure 7.1 Wide – angle XRD patterns for Cu-phthalocyanine dye, 21% wt/wt% at 25°C (isotropic phase). 3.5 Å *d*-spacing correlating to the distance between adjacent molecules in a stack in the N_{col} phase.

There is no appreciable variation in the separation between Cu-phthalocyanine molecules within a stack on temperature (Figure 7.2), which also supports the assumption that $\pi - \pi$ interactions play the dominant role in holding the molecules together to form the aggregates [20, 35, 134, 135].
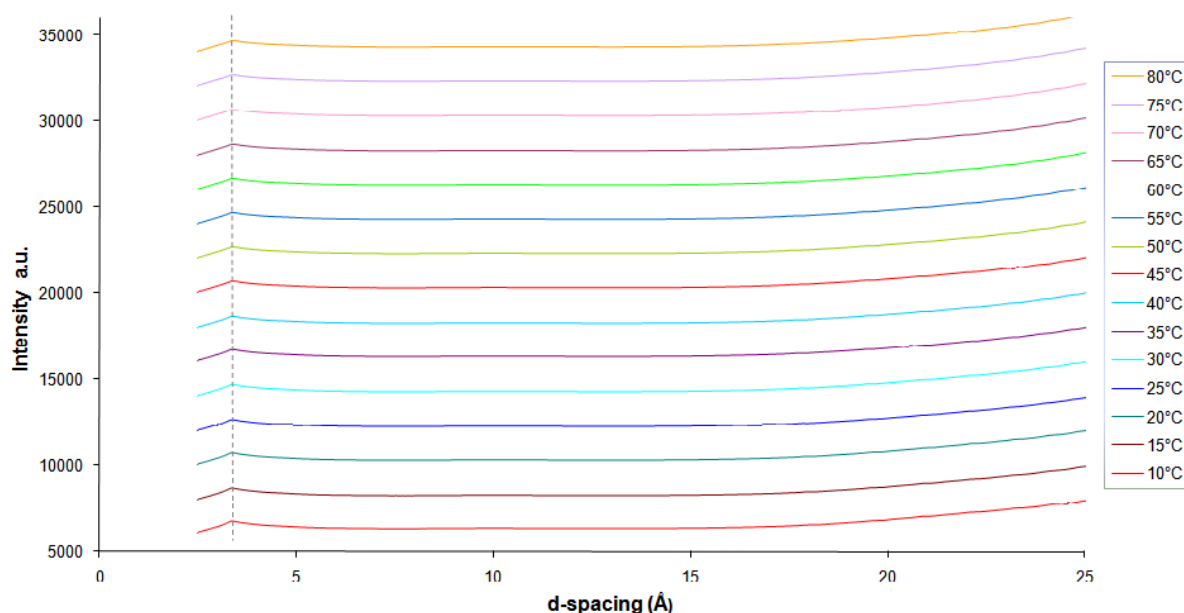
Figure 7.2 Wide-angle X-ray diffraction patterns for Cu-phthalocyanine dye 21% wt/wt% (isotropic phase) as a function of temperature over the heating run. A dashed line marks the peak observed at 3.5 Å, which is always present over the studied range of temperatures and concentrations. (a.u. = arbitrary units).

7.1.2 Small – angle X-ray Diffraction (SAXS)

The extensive study by small-angle X-ray diffraction over a wide range of temperatures and concentrations was performed on Cu-phthalocyanine dye / water system. These studies were carried out on station 2.1 at the Synchrotron Radiation Source (SRS), Daresbury Laboratories as described in section 4.3.3.1. This dye exhibited concentration dependent small-angle X-ray diffraction patterns. The *d* spacings over the temperature range 5 - 85°C at 5°C intervals on heating and cooling are shown at the end of this section in Table 7.2. In general the number of reflections observed was dependent on the mesophase with more reflections occurring in the Col_h phase than in the N_{col} phase (Figures 7.3, 7.4). At high dye concentration (> 28% wt/wt% for the Cu-phthalocyanine dye), the diffraction ring corresponding to d_0 in the Col_h phase approaches the wide-angle limit of detection under the conditions employed, therefore, the higher orders are not observed. Below this concentration the diffraction patterns were composed of concentric rings of Bragg reflections from poorly aligned domains of mesophase. The sharpness and high intensity of the diffraction peaks are related to the extent to which the separations extend periodically over large distances, therefore indicating a high degree of order at high dye concentrations (Figures 7.5, 7.6).

| a | b | c |
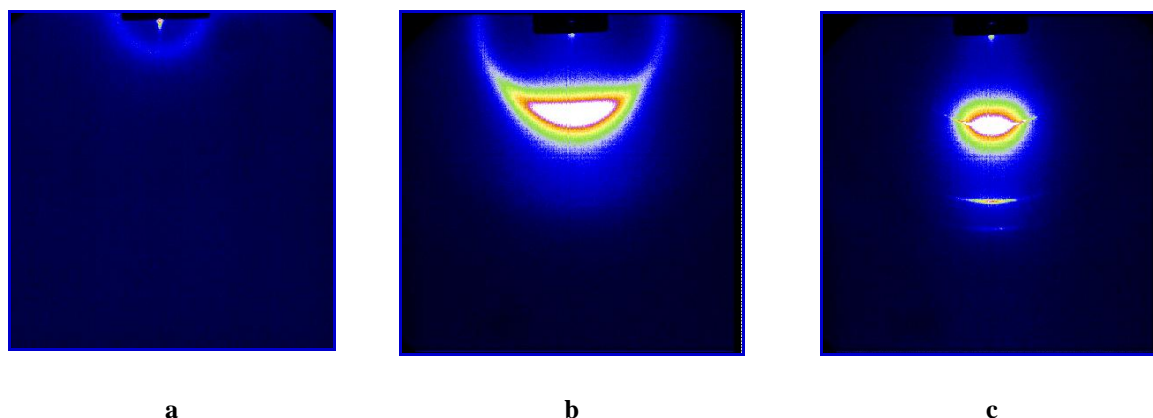
Figure 7.3   Small - angle diffraction patterns shown by Cu-phthalocyanine dye for isotropic phase at 16% wt/wt%, 25°C (a), N_{col} phase at 27% wt/wt%, 25°C (b) and three distinct features for Col_h phase at 31% wt/wt%, 25°C (c).
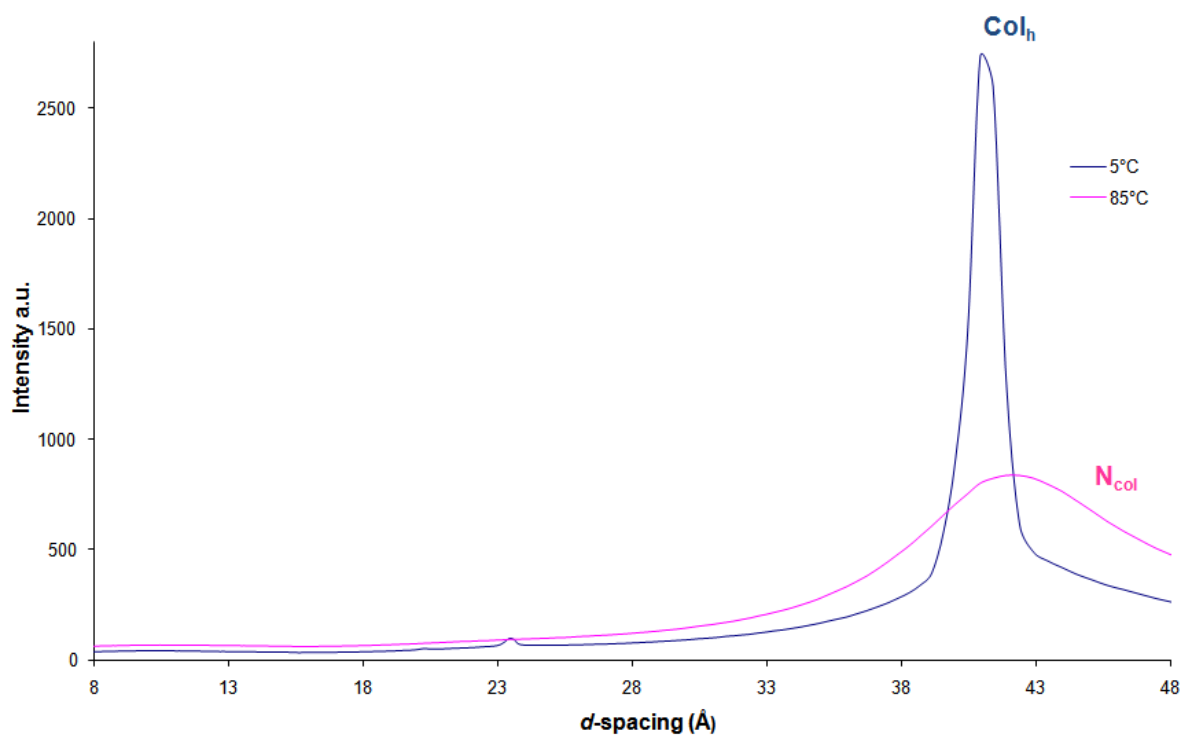
Figure 7.4   The small-angle X-ray diffraction patterns for 31% wt/wt% of Cu-phthalocyanine dye showing the difference in spectral patterns for Col_h phase (blue) and N_{col} phase (pink).

$d_0 = 39.7\text{Å} (\pm 0.2\text{Å})$

$d_0/\sqrt{3} = 23.0\text{Å} (\pm 0.2\text{Å})$

$d_0/\sqrt{4} = 19.9\text{Å} (\pm 0.2\text{Å})$
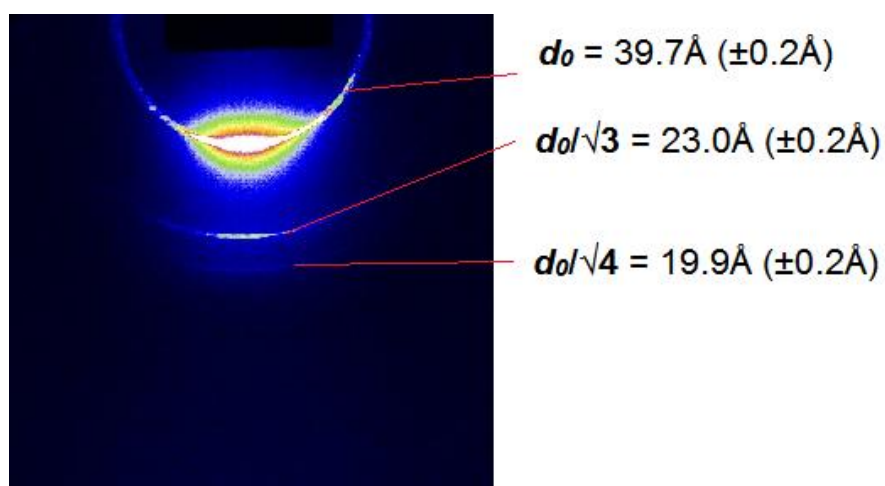
Figure 7.5   The diffraction patterns of Cu-phthalocyanine dye Col_h phase (32% wt/wt%, 5°C), showing three distinct features.
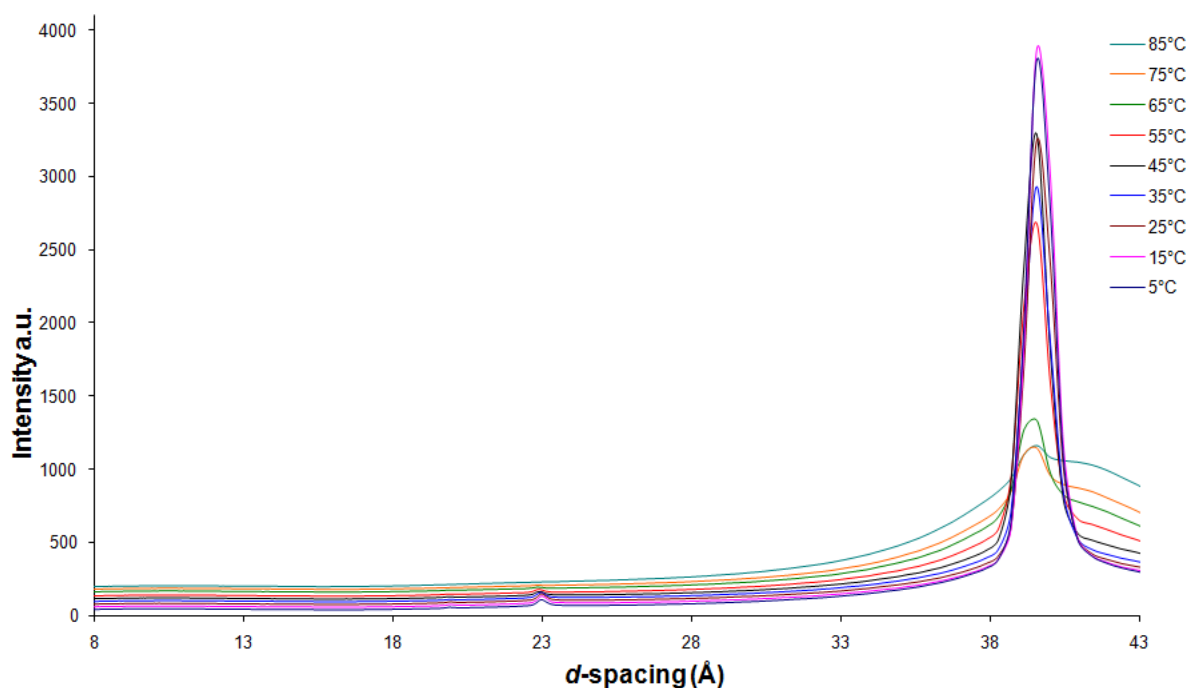
Figure 7.6   **Small-angle X-ray diffraction patterns for 32% wt/wt% of Cu-phthalocyanine dye in the Col$_h$ phase (5 - 65°C) and Col$_h$ + N$_{col}$ coexisting region (75 - 85°C).**

Figure 7.5 shows a degree of alignment, induced initially by centrifuging the samples into Lindemann X-ray tubes. The samples became aligned with the tube walls on 3 – 4 days storage. The director of the liquid crystalline phases aligned along the long axis of the capillary. The wide angle diffraction is concentrated along the long axis of the capillary tube and the small angle diffraction along the direction perpendicular to the long axis of the tube. At low dye concentrations some disorder was apparent from the low intensity, diffuse nature of the reflections and a decrease in the number of orders observed (Figure 7.7). These observations indicate the presence of either nematic or isotropic phase.

<center>a</center>

<center>b</center>

Figure 7.7   **The small angle diffraction patterns of the nematic phase shown by Cu-phthalocyanine dye for 26% wt/wt% at 25°C (a) and 21% wt/wt% at 25°C (b).**

The information obtained from the small angle X-ray diffraction for nematic phases with the nature of orientationally-ordered fluid reveals the appearance of a diffuse peak (Figure 7.9) corresponding to the continuous range of column-to-column distances. The peaks are diffuse because these positional correlations only extend over short distances. Such correlations also exist in the isotropic phase. A clear difference between the scattering from the isotropic and the nematic phases can be observed if the samples are aligned in the magnetic field producing a uniform alignment of the magnetic director n. The diffraction pattern for the isotropic phase remains unaltered while the one for the nematic phase becoming concentrated along the meridional direction. The magnetic field was not applied to the samples under consideration, hence making it difficult to judge whether the phase is isotropic or nematic on the XRD results alone and requiring combination with the data obtained by optical microscopy (Figure 7.8).
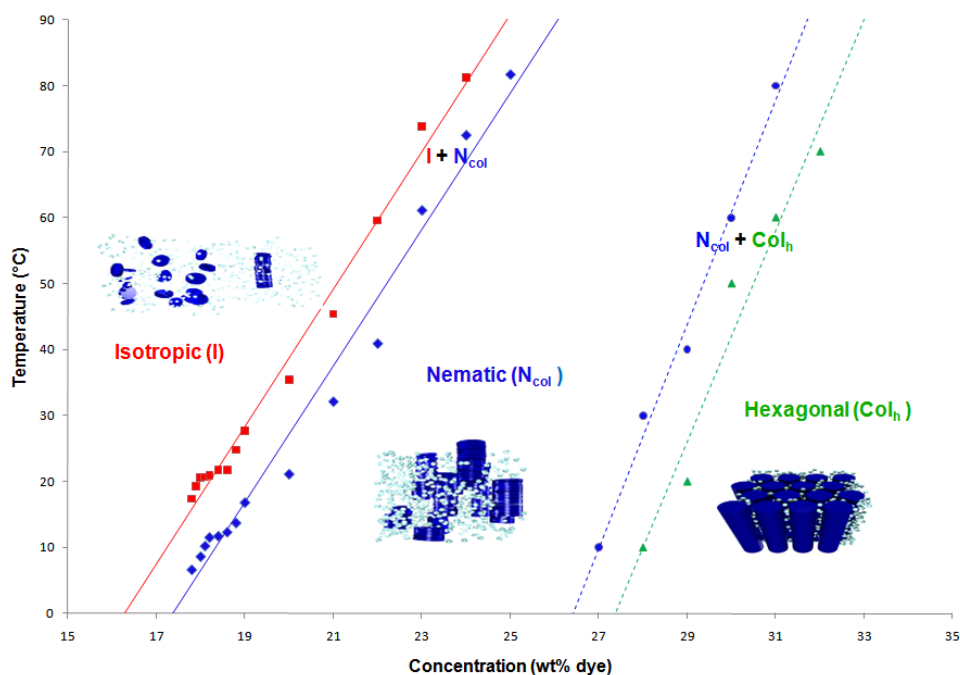
Figure 7.8 **Phase diagram of the Cu-Phthalocyanine dye showing the boundaries for isotropic (I) and nematic (N_{col}) phases obtained by optical microscopy, and the boundary between nematic (N_{col}) and hexagonal (Col_h) obtained by SAXS.**

It is important to note that the meridional arc corresponding to the spacing between the planes in the nematic phase appears at 90° to the equatorial arcs produced by the inter-aggregate repeat (Figure 7.1, Figure 7.7). This indicates that the intra- and inter-aggregate repeats are perpendicular to one another in the nematic phase.
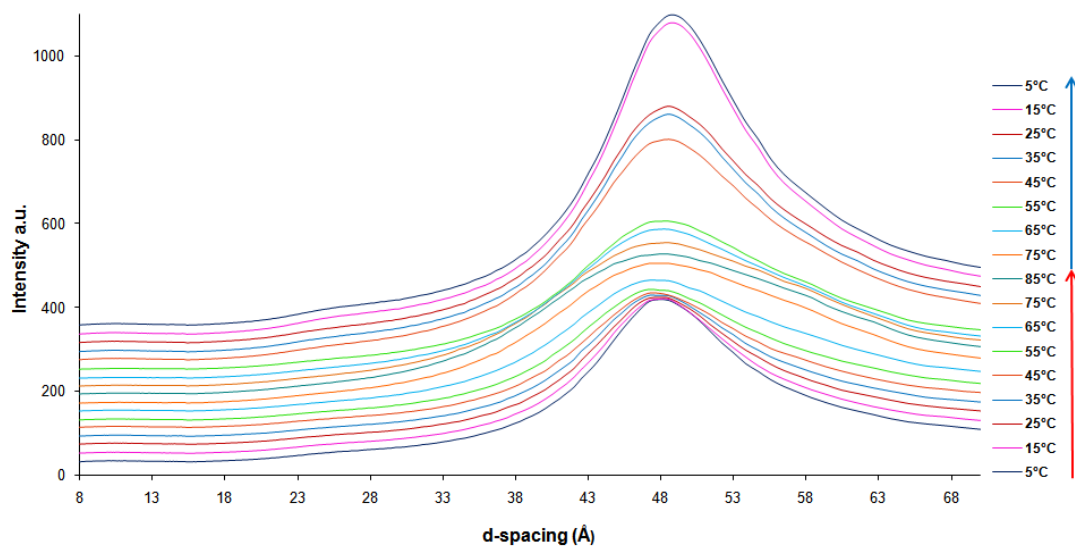
Figure 7.9   The small angle peak spacings as a function of temperature over one temperature cycle for Cu-phthalocyanine dye solution 25% wt/wt%. A diffuse peak is related to the inter-columnar distances within the nematic phase.

The N_{col} phase exhibited a small decrease of d_0 with the increase of temperature (Figure 7.10).
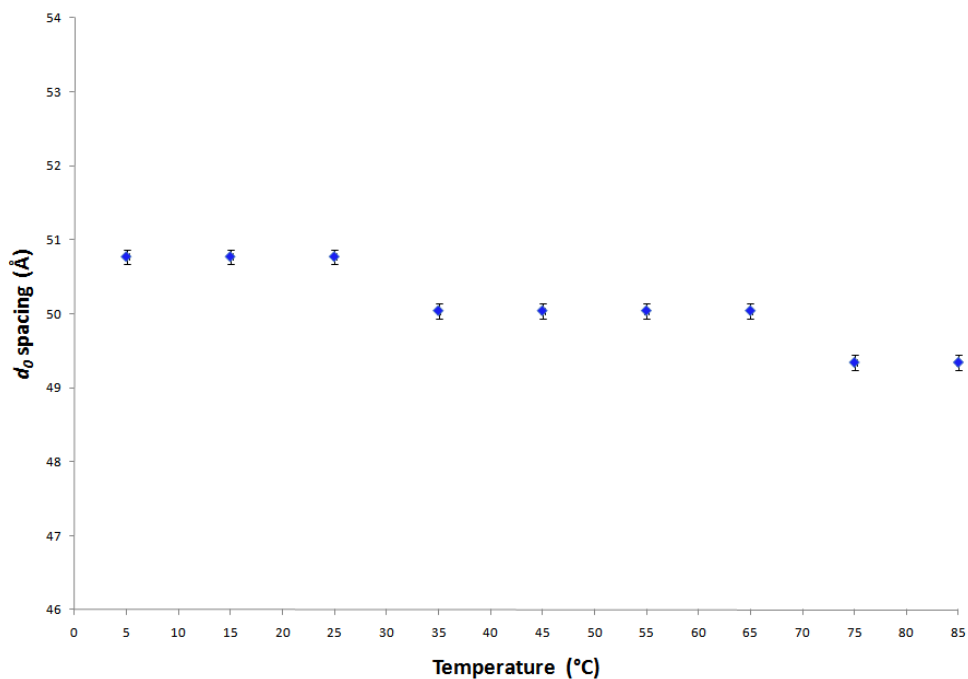
Figure 7.10   Variation of inter-stacking separation ($d \pm 0.2 \text{Å}$) as a function of temperature exhibited by Cu-phthalocyanine dye for 22% wt/wt%. N_{col} phase was stable over the studied range of temperatures (5°C - 85°C).

111

Similar thermal behaviour was observed for the Disodium Chromoglycate DSCG [136] and C.I. Direct Blue 67 [137]. On heating, the stacks are expected to fall apart, thus, reducing d_0 and increasing the diameter of the ring of the diffraction pattern (Figure 7.11). The d_0 values do not change by a large amount on heating (within the bounds of each concentration exhibiting nematic phase). These X-ray diffraction results therefore suggest that although the correlation lengths of the stacks are reduced on heating, the aggregates of Cu-phthalocyanine dye still remain large at higher temperatures due to the dye molecules being bound very strongly within the stacks.

| a | b |

Figure 7.11   **The small angle diffraction patterns of the nematic phase shown by Cu-phthalocyanine dye for 26% wt/wt% at 5°C (a) and 75°C (b).**

Furthermore, the observation of the isotropic phase at higher temperatures by optical microscopy suggests a complete loss in orientational / positional order of the phthalocyanine dye system. However, the wide-angle reflection at 3.5 Å for the concentrations lower than 17% dye wt/wt% indicates that the molecules are still in columnar aggregates. The loss of order might be affected by a decrease in the stack size assuming the loss of orientational order of the nematic phase. These variable temperature X-ray diffraction studies confirm a very high stability of the aggregates with respect to heating; thus, implying the binding between the molecules is strong.

A decrease of d_0 within the nematic phase was observed as the concentration of the dye in aqueous solution was increased (Figure 7.12).
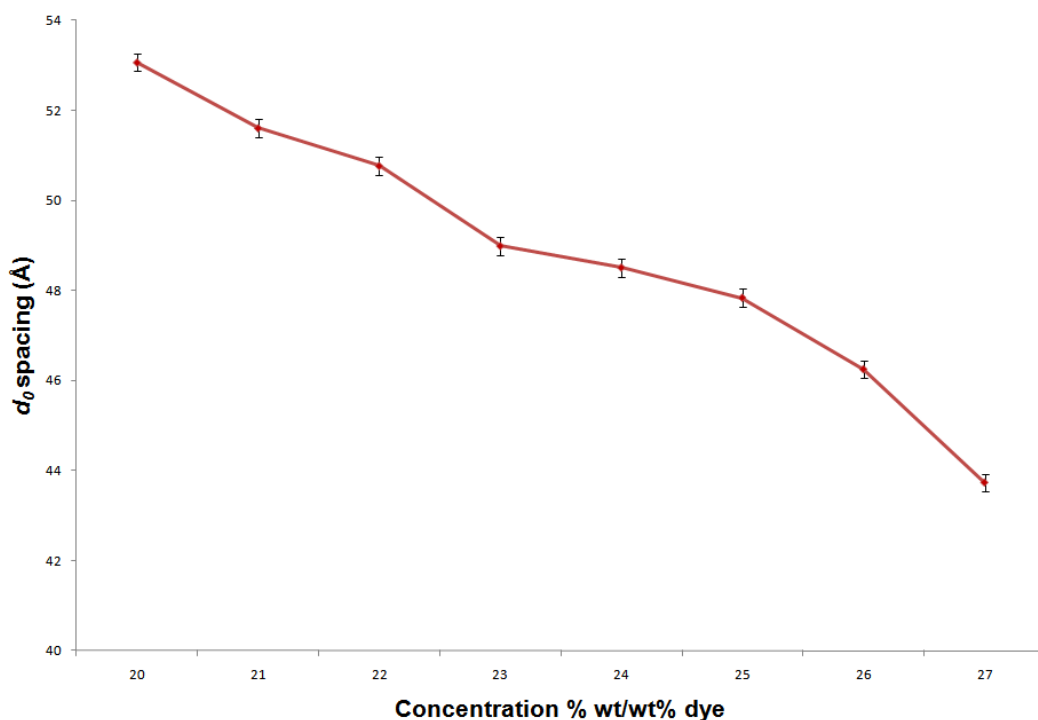
Figure 7.12   **Variation of inter-stacking separation ($d \pm 0.2\text{Å}$) as a function of concentration at 25°C exhibited by Cu-phthalocyanine dye within the N_{col} phase.**

This can be explained by the fact that as the amount of dye in water is increased, the dye columns take more space within the volume unit, getting tighter to each other, thus, decreasing the distance between the aggregates and resulting in higher ordering of the phase. On the other hand, the steep increase of full width at half-maximum (FWHM) was observed with the decrease of concentration (Figure 7.13). The increase of FWHM of the XRD peaks could be ascribed to the fragmentation and disordering of the aggregates [138].
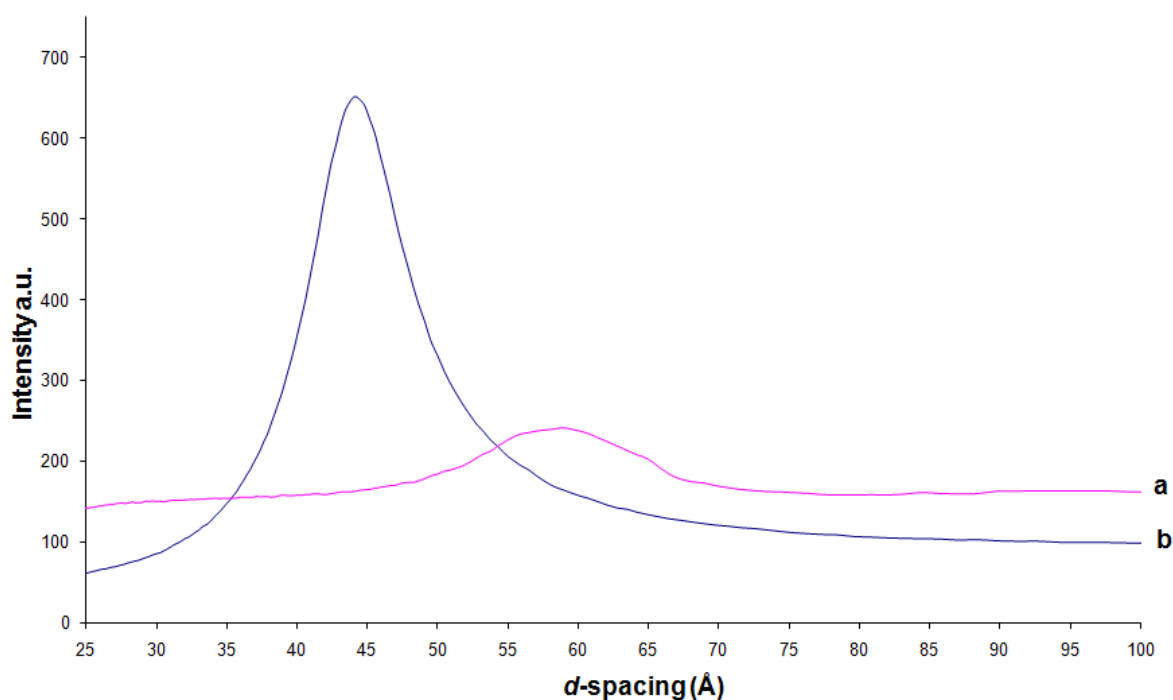
Figure 7.13 **The small angle XRD diffraction patterns showing the difference in FWHM for the samples of Cu-phthalocyanine dye within the N_{col} phase: a) 20% dye wt/wt% at 5°C; b) 27% dye wt/wt% at 5°C.**

From the X-ray diffraction patterns observed for Cu-phthalocyanine dye for concentrations higher than 28% wt/wt% at small scattering angles, the mesophase formed was identified as hexagonal Col_h. The dye forms a hexagonal mesophase showing sharp, intense Bragg reflections at low q values which correspond to the patterns observed for the hexagonal phases of conventional amphiphilic systems [39, 139-141]. These reflections are characteristic of a mesophase possessing 2-dimensional hexagonal periodicity i.e. in the ratio d_0: $d_0/\sqrt{3}$: $d_0/\sqrt{4}$ etc. indicative of a highly ordered columnar mesophase. From simple geometry it becomes clear that the primary reflection from the hexagonal structure will be a, corresponding to (200), as seen in Figure 7.14, and then the other ones will be due to layer spacings of $a/\sqrt{3}$ (020), and $a/\sqrt{4}$ (220) or (400).
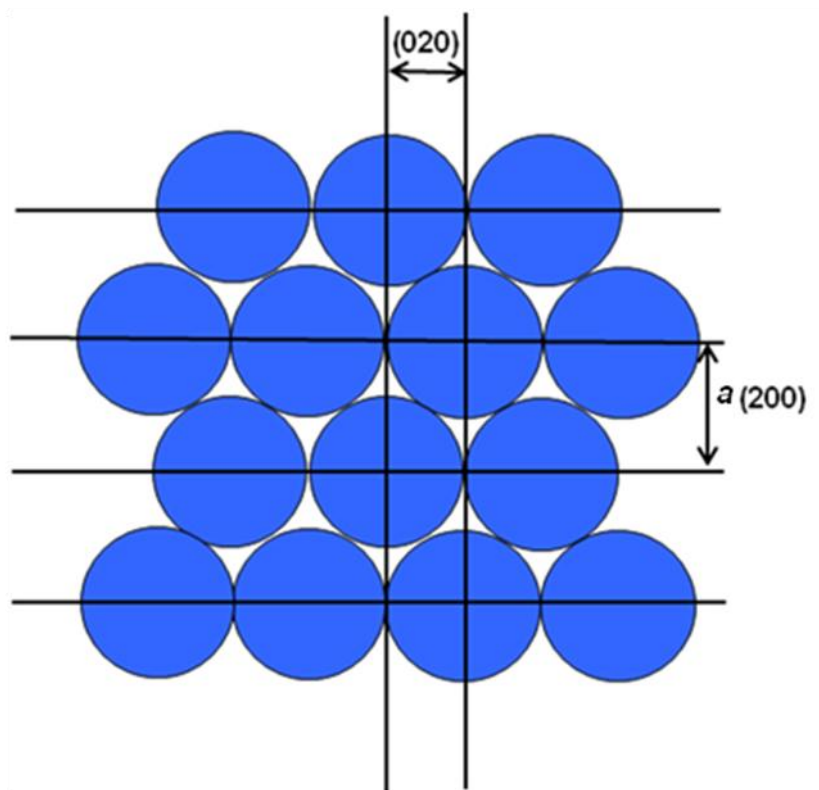
Figure 7.14   **Diffraction spacings from columns of discs positioned on a hexagonal lattice.**

The most concentrated sample studied (33% wt/wt%) displayed sharp first (d_0) and second (d_1) diffraction peaks at the temperatures up to 75 °C (Figures 7.15, 7.16). The third diffraction peak (d_2) was observed at the temperatures up to 65 °C (Figure 7.16). The d_0 / d_1 / d_2 ratio for these peaks is equal to d_0 / $\sqrt{3}$ / $\sqrt{4}$, thus indicating that the hexagonal symmetry over the temperature range 5 > 75 °C is preserved for this concentration.
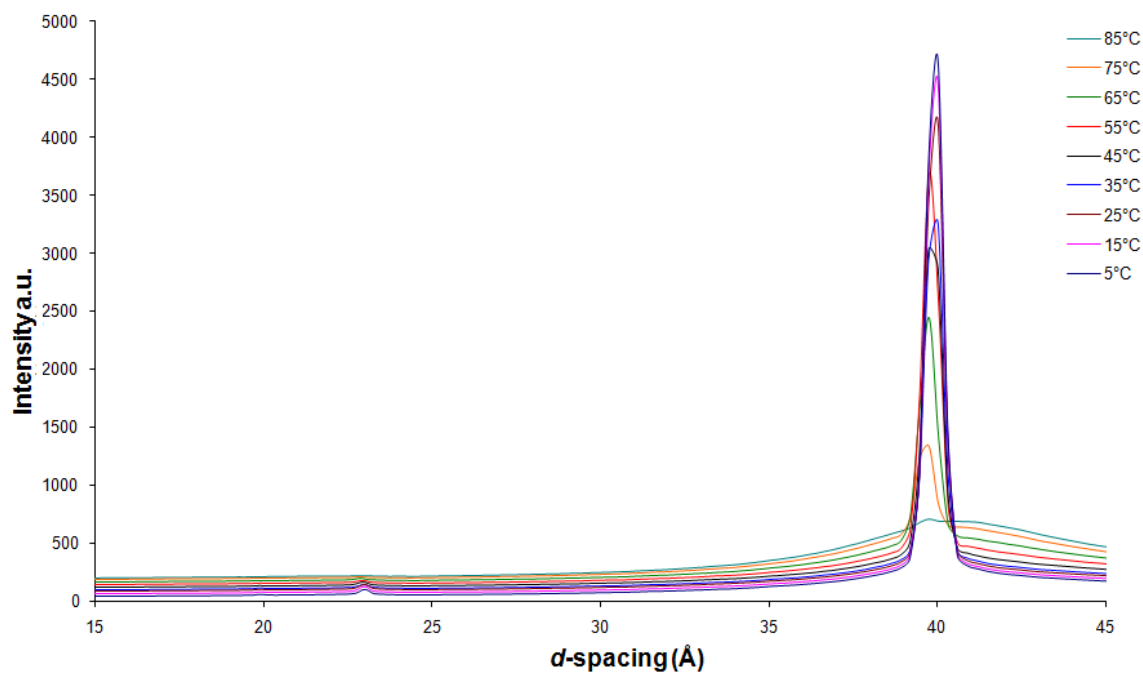
Figure 7.15   The small-angle data plotted as a function of temperature over one heating cycle for 33% wt/wt% Cu-phthalocyanine dye. The intense peak corresponding to d_0 spacing shows a decrease in the sharpness and intensity on heating.
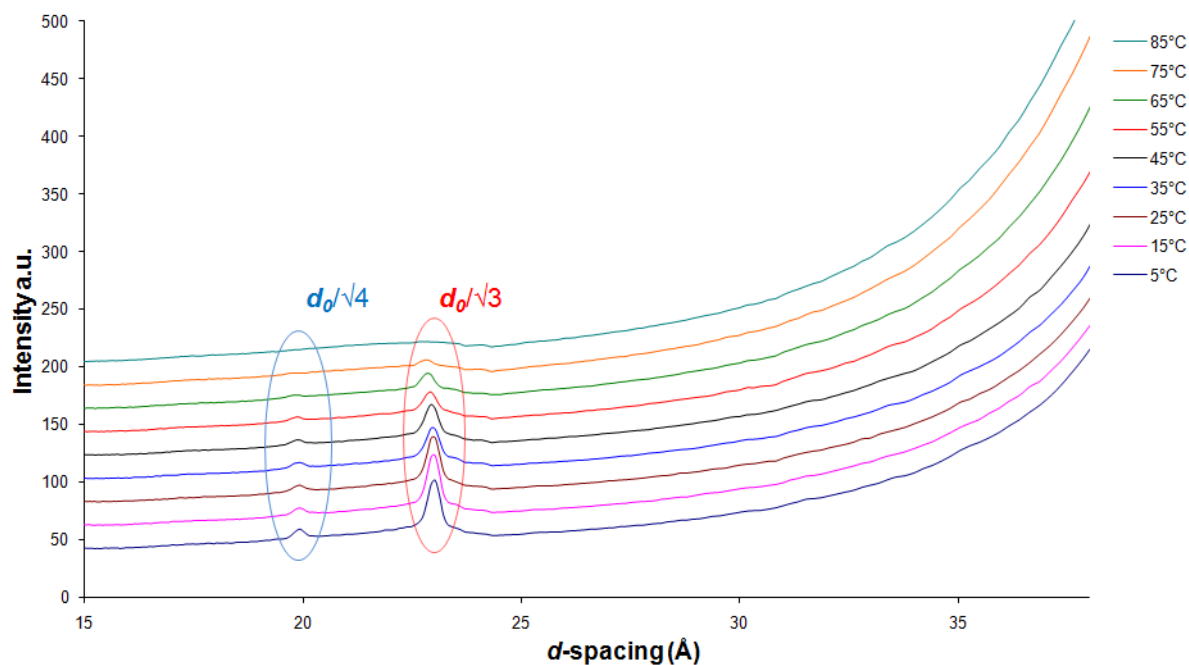
Figure 7.16   Fragment of the small-angle X-ray diffraction patterns plotted as a function of temperature over one heating cycle for 33% wt/wt% Cu-phthalocyanine dye. Highlighted areas show the changes in the second and the third order diffraction peaks on heating respectively.

116

As the concentration of the dye in the solution is decreased, then the existence of hexagonal symmetry seems to be vanishing away gradually. So for 32% dye concentration the second order peak arising at 75 °C is becoming less intense compared to the one observed for 33% dye concentration (Figure 7.17).
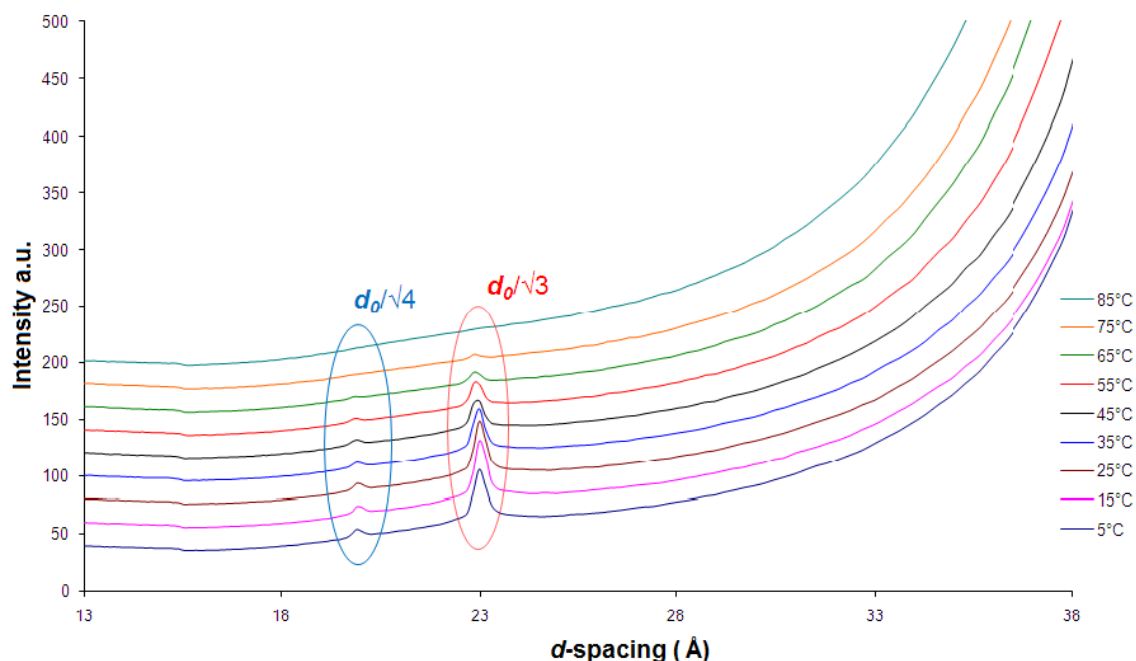
Figure 7.17   **Fragment of the small-angle X-ray diffraction patterns plotted as a function of temperature over one heating cycle for 32% wt/wt% Cu-phthalocyanine dye. Highlighted areas show the changes in the second and the third order diffraction peaks on heating respectively.**

However, for 30% dye concentration at 65°C the first order diffraction peak loses its sharpness and becomes broad with the second order peak becoming less distinct and the third order peak disappearing altogether. These differences in the diffraction pattern at 65°C compared to 55°C imply that a phase transition has occurred along with the loss of the hexagonal symmetry (Figures 7.18, 7.19).
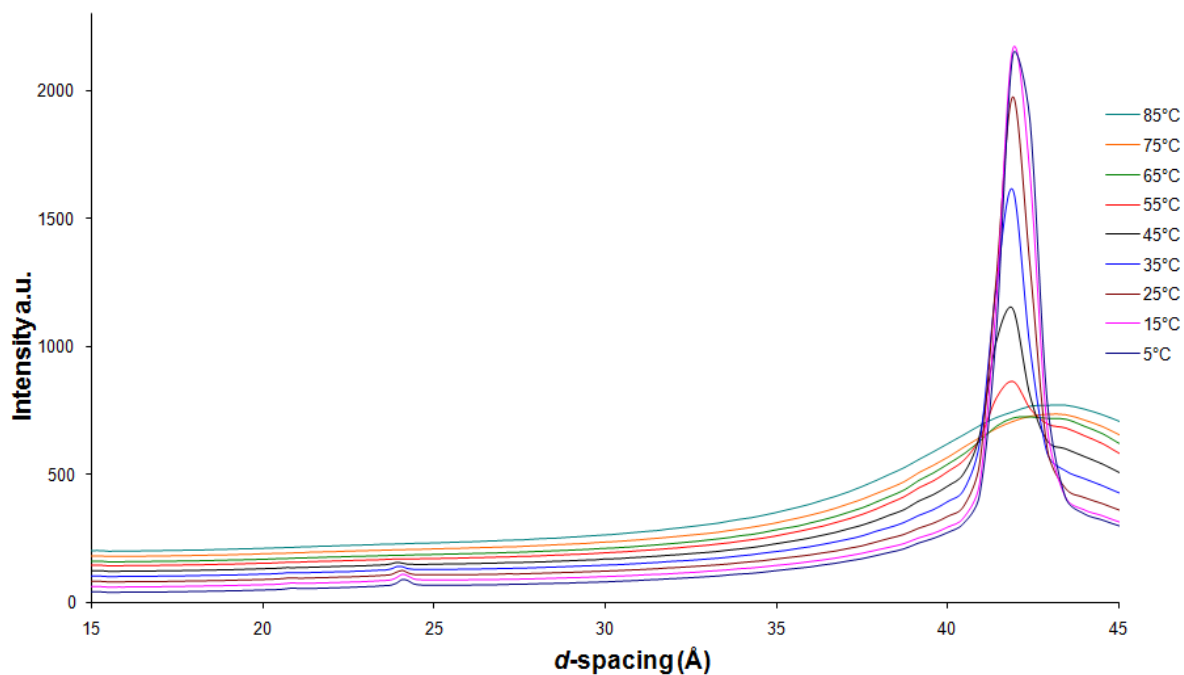
Figure 7.18   The small-angle data plotted as a function of temperature over one heating cycle for 30% wt/wt% Cu-phthalocyanine dye. The initial intensity of the hexagonal phase is lost with the first order diffraction peak becoming broad at 65°C.
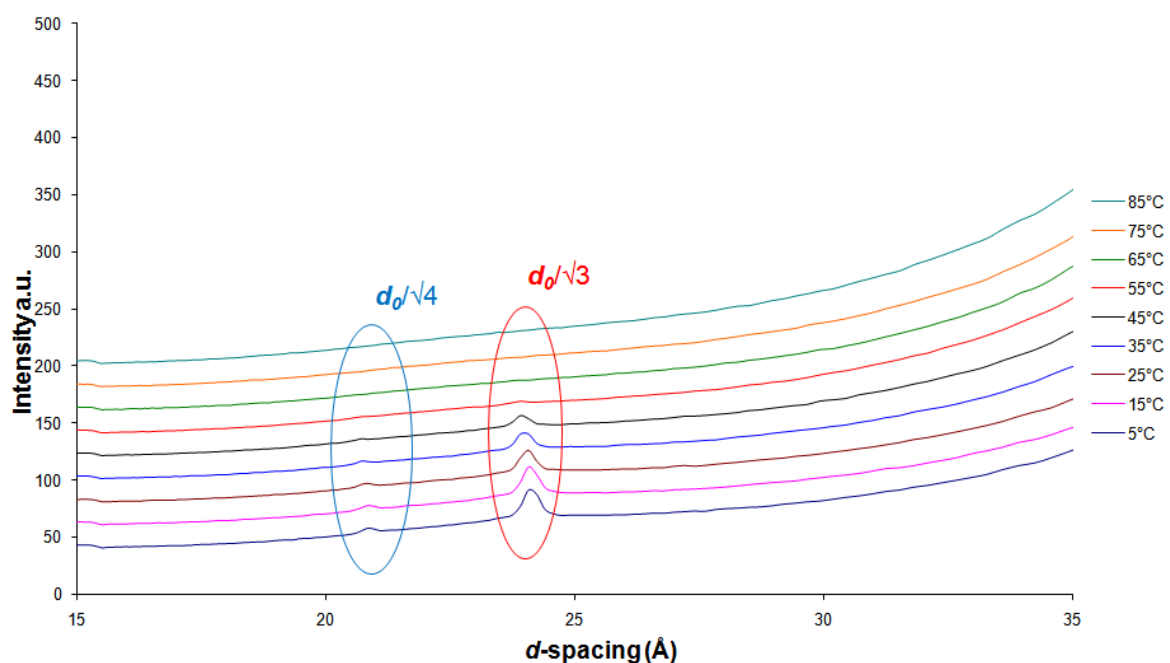
Figure 7.19   Fragment of the small-angle X-ray diffraction patterns plotted as a function of temperature over one heating cycle for 30% wt/wt% Cu-phthalocyanine dye. Highlighted areas show the changes in the second and the third order diffraction peaks on heating respectively.

118

The hexagonal phase was observed for samples with concentrations as low as 28%, where the ratio of $d_0 : d_0/\sqrt{3}$ still can be detected.

The interesting observation is that the sharpness of the first order reflection gradually changes as the temperature is raised, which might be an indication of the gradual transition from hexagonal to nematic phase, i.e. weak first or second order rather than strongly first order. The nematic – isotropic transition has been a focus of enormous attention, although the nematic – hexagonal transition still remains one of the interesting phenomena drawing lots of attention nowadays. X-ray results also confirm the observations made with the help of polarising optical microscopy by peripheral evaporation scan, revealing the gradual transition from the more to a less ordered mesophase. The 29% wt/wt% sample was studied in more details by small-angle X-ray diffraction. The experiment was conducted at the Elettra Synchrotron Radiation Source, where the phase transition from hexagonal to nematic was investigated over the temperature range 5 - 21°C at 0.5°C intervals on heating. The d spacings observed at each temperature are summarised in Table 7.1.

The sample at the lowest temperature (5°C) displayed a sharp and intense first order diffraction peak with the second order being clearly discernible (Figure 7.20). At temperatures up to 12°C the ratio of the position of the higher order peak compared to that of the first order diffraction peak is in excellent agreement with the ratio of $1:\sqrt{3}$ which is characteristic of a hexagonal lattice. By contrast, above 12.5°C the second order peak disappears, which is indicative of the presence of hexagonal phase below this temperature. Only one order is observed at the 12.5 – 14°C range of temperatures (Figures 7.22, 7.23); however the sharpness of the peak implies that the phase still remains hexagonal. The d_0 spacing decreases slightly within the temperature range at which hexagonal phase exists. It might be due to the reduction in the size of the aggregates, therefore the stacks are becoming smaller and getting closer to one another, thus, reducing d_0.

Table 7.1 The variation of the *d* spacings (± 0.1Å) of Cu-phthalocyanine dye / water 29% wt/wt% with temperature.

T°C	d_0 (Å)	d_1 (Å)	T°C	d_0 (Å)	d_1 (Å)	T°C	d_0 (Å)	d_1 (Å)
5.0°C	41.2	23.8	10.5°C	41.0	23.8	16.0°C	41.6	-
5.5°C	41.2	23.8	11.0°C	41.0	23.8	16.5°C	41.6	-
6.0°C	41.2	23.8	11.5°C	41.0	23.8	17.0°C	41.6	-
6.5°C	41.2	23.8	12.0°C	40.9	23.8	17.5°C	41.6	-
7.0°C	41.0	23.8	12.5°C	40.9	-	18.0°C	41.6	-
7.5°C	41.0	23.8	13.0°C	40.9	-	18.5°C	41.6	-
8.0°C	41.0	23.8	13.5°C	40.9	-	19.0°C	41.6	-
8.5°C	41.0	23.8	14.0°C	40.9	-	19.5°C	41.8	-
9.0°C	41.0	23.8	14.5°C	40.9	-	20.0°C	41.8	-
9.5°C	41.0	23.8	15.0°C	41.4	-	20.5°C	41.8	-
10.0°C	41.0	23.8	15.5°C	41.6	-	-	-	-
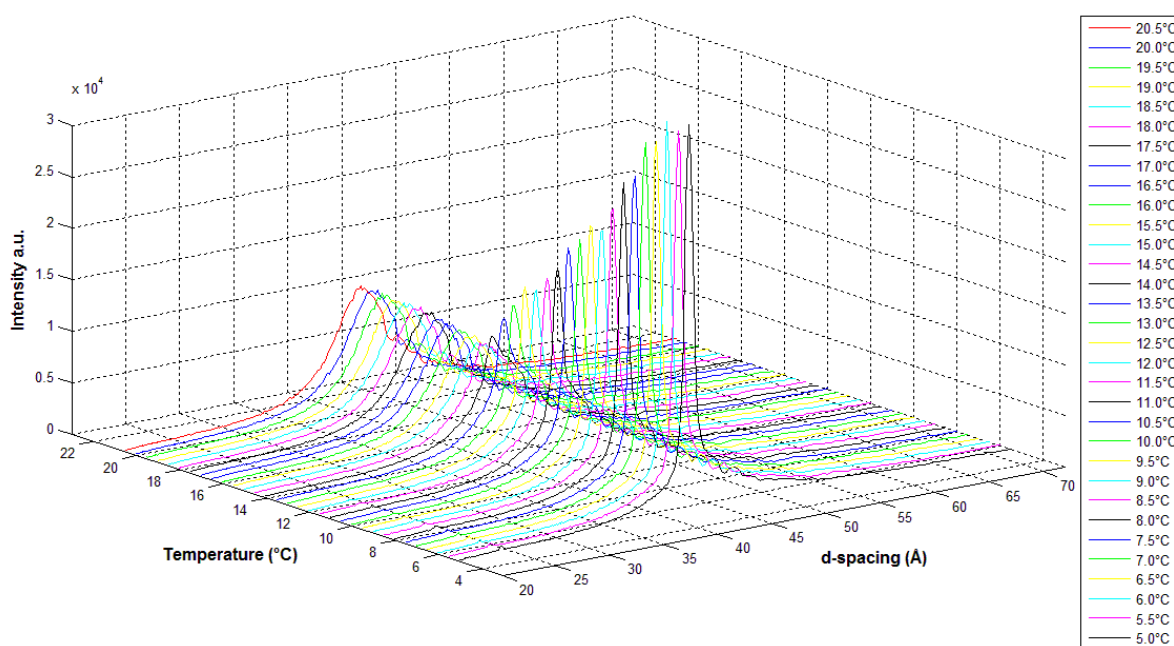
Figure 7.20   3D small-angle X-ray diffraction patterns for Cu-phthalocyanine dye 29% wt/wt% at the range of temperatures 5 – 20.5°C at 0.5°C intervals.
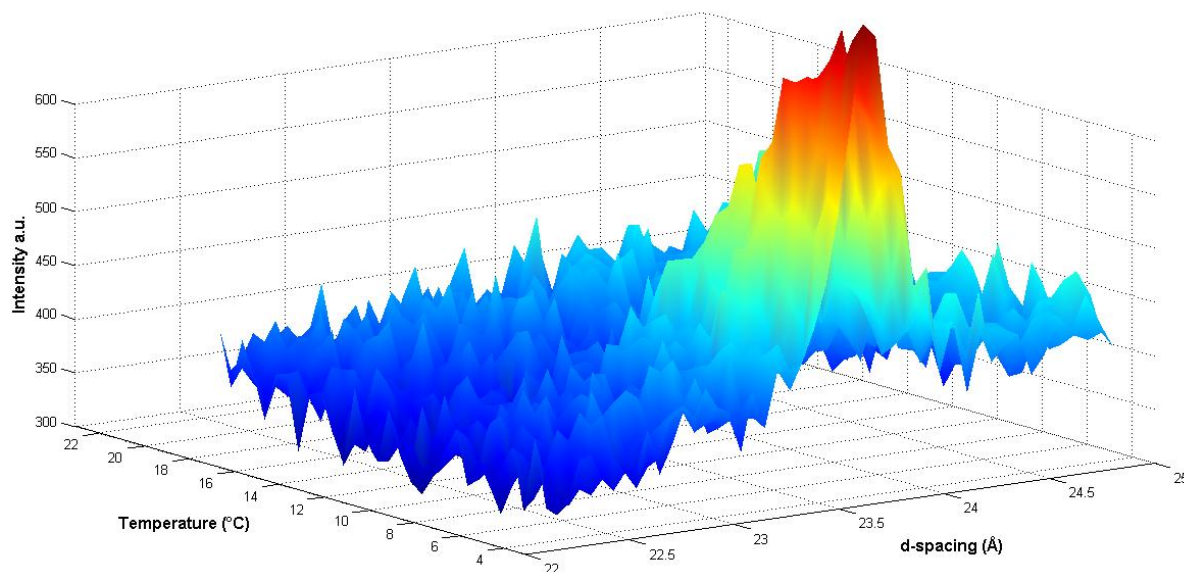
Figure 7.21 3D fragment of the small-angle X-ray diffraction patterns for Cu-phthalocyanine dye 29% wt/wt% at the 5 – 20.5°C range of temperatures, showing the gradual reduction in intensity of the second order peak.

As the temperature is increased even further, the d_0 spacing slightly increases at the temperature of 15°C, while the first order peak becomes completely broad (Figures 7.22, 7.23). These differences imply that the phase transition has occurred. The presence of a broad first order peak and lack of any other well-defined orders implies that the phase formed is nematic-like in nature at the temperatures higher than 15°C. The way the broadening of the first peak occurred suggests that the transition from hexagonal to nematic is gradual. The values of d_0 on further increase of temperature (15 – 20.5°C) did not change by large amount (Table 7.1), which supports the suggestion about the higher stability of aggregates.

A possible explanation for the observed phenomenon could be accounted for by the transition from hexagonal to nematic in a sequence of at least two subsequent steps via a transitional phase. This intermediate phase occurs as pretransitional phenomenon at the hexagonal – nematic transition on heating, and is composed of the dye stacks connected locally, but not completely coalesced clusters [142]. Therefore, the nematic phase on hexagonal – nematic transition can be seen as fragmented hexagonal phases with long range nematic order of congregates with local hexagonal order, which results in a continuous structural transition from the hexagonal phase at lower temperatures to a nematic phase at higher temperature.

121
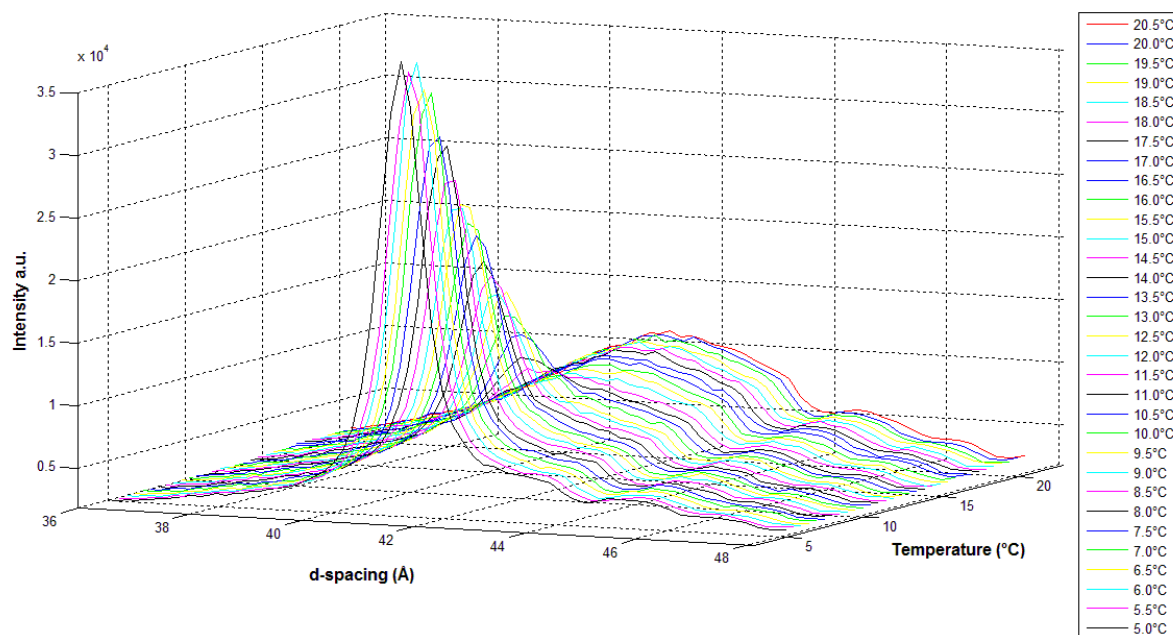
Figure 7.22   3D fragment of the small-angle X-ray diffraction patterns for Cu-phthalocyanine dye 29% wt/wt% at the 5 – 20.5°C range of temperatures, showing the gradual broadening of the first order peak indicative of gradual hexagonal – nematic phase transition.
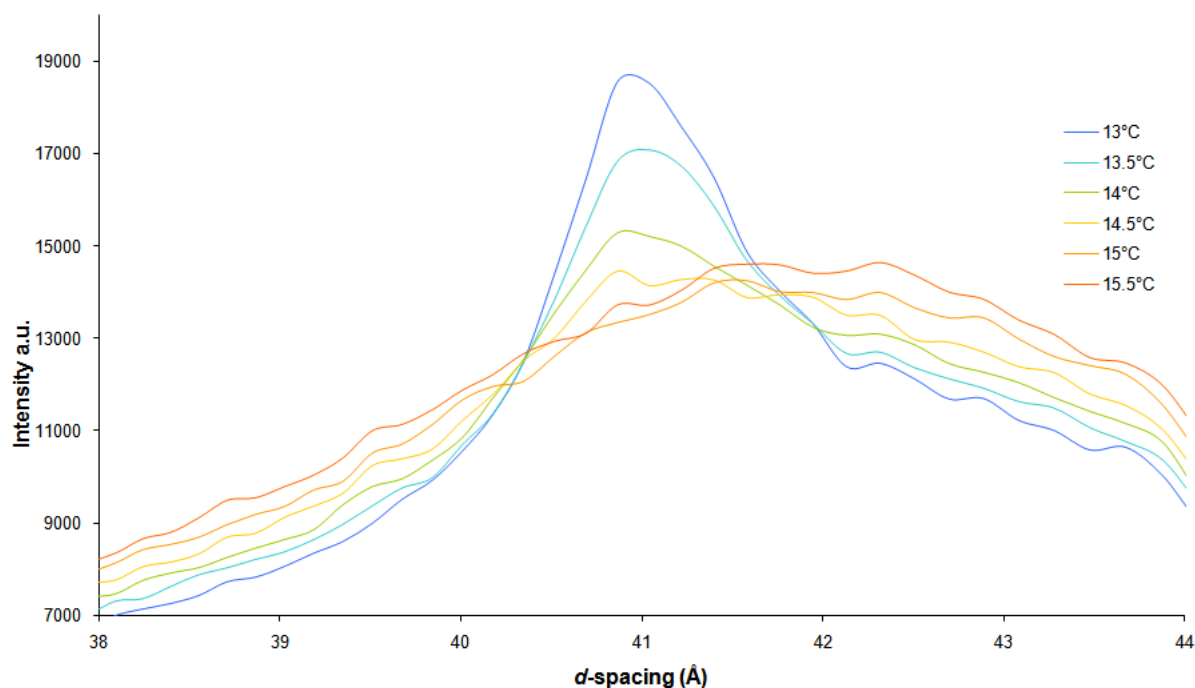
Figure 7.23   2D fragment of the small-angle X-ray diffraction patterns for Cu-phthalocyanine dye 29% wt/wt% on the phase transition (13 – 15.5°C), showing the gradual broadening of the first order peak indicative of gradual hexagonal – nematic phase transition.

On cooling, the hexagonal symmetry appeared again, but with a slight delay. For 30% dye concentration the hexagonal symmetry is lost in a temperature interval between 55°C and 65°C on heating (Figure 7.24), though reappears in the temperature interval of 35 – 45 °C as the temperature is decreased (Figure 7.25). Hence, on cooling the system is slow to re-order back into the hexagonal lattice from the nematic – like array, which might be due to slow aggregation kinetics, i.e. the changes in demixing of aggregates. It obviously takes longer time for the aggregates to arrange into hexagonal lattice on cooling rather than lose the hexagonal symmetry on heating, thus indicating that the transition has a certain level of hysteresis present.
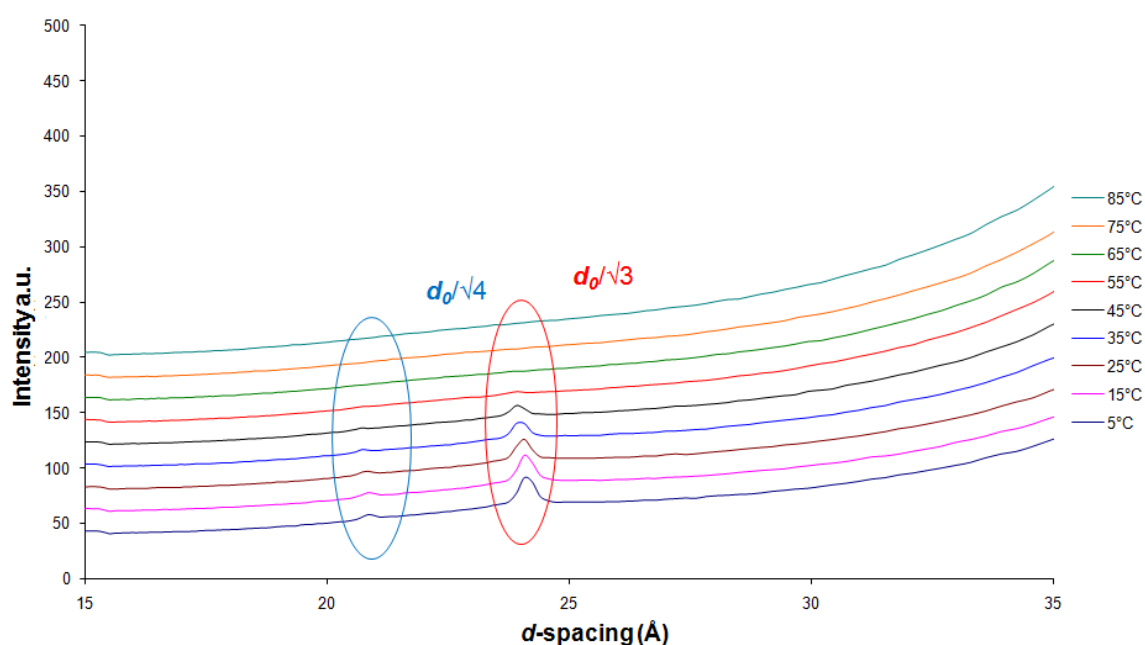
Figure 7.24   **Fragment of the small-angle X-ray diffraction patterns plotted as a function of temperature over one heating cycle for 30% wt/wt% Cu-phthalocyanine dye. Highlighted areas show the changes in the second and the third order diffraction peaks on heating respectively.**
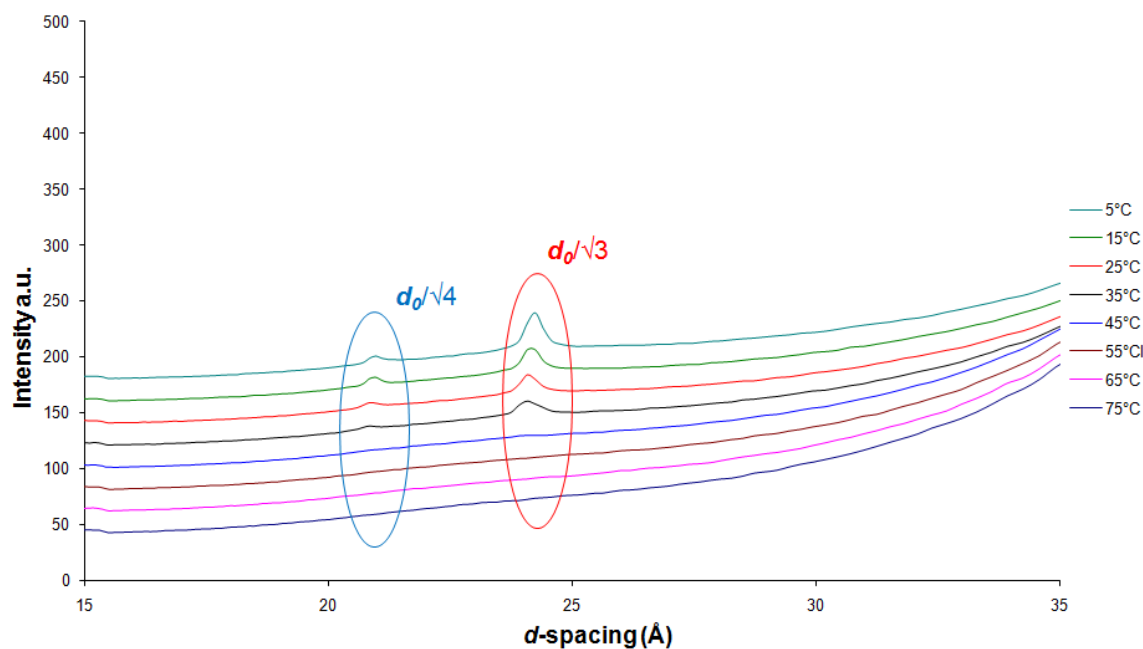
Figure 7.25   **Fragment of the small-angle X-ray diffraction patterns plotted as a function of temperature over one cooling cycle for 30% wt/wt% Cu-phthalocyanine dye. Highlighted areas show the changes in the second and the third order diffraction peaks on cooling respectively.**

These X-ray diffraction studies enable the nematic and hexagonal phases to be identified. Utilising the data obtained by X-ray diffraction it was possible to determine the number of mesophases formed and their composition. In addition, the dimensions of the mesophase aggregates are calculated and reported in the next section.

Table 7.2 Inter-aggregate parameters ($d \pm 0.2$Å) for Cu-phthalocyanine dye for various concentrations and temperatures. Data derived from SAXS XRD.

T°C	33% wt% CuPc				32% wt% CuPc				31% wt% CuPc			
	{00l} orders	d_0	$d_0/\sqrt{3}$	$d_0/\sqrt{4}$	{00l} orders	d_0	$d_0/\sqrt{3}$	$d_0/\sqrt{4}$	{00l} orders	d_0	$d_0/\sqrt{3}$	$d_0/\sqrt{4}$
5°C	3	39.7	23.0	19.8	3	39.7	23.0	19.9	3	40.9	23.4	20.2
15°C	3	39.7	23.0	19.8	3	39.7	23.0	19.9	3	40.9	23.4	20.2
25°C	3	39.7	22.9	19.8	3	39.7	23.0	19.9	3	40.9	23.4	20.2
35°C	3	39.7	22.9	19.8	3	39.7	23.0	19.9	3	40.9	23.4	20.1
45°C	3	39.7	22.9	19.8	3	39.7	23.0	19.9	3	40.9	23.3	20.1
55°C	3	39.7	22.9	19.8	2	39.7	22.8	19.8	3	40.5	23.3	20.1
65°C	3	39.7	22.8	19.8	2	39.7	22.8	19.8	3	40.5	23.3	20.1
75°C	2	39.7	22.8	-	2	39.7	22.8	-	2	40.9	23.3	-
85°C	1	39.7	-	-	1	39.7	-	-	1	41.9	-	-
75°C	2	39.7	22.8	-	2	39.7	22.8	-	1	40.9	-	-
65°C	3	39.7	22.8	19.8	2	39.7	22.8	-	3	40.5	23.3	20.0
55°C	3	39.7	22.9	19.8	3	39.7	22.8	19.9	3	40.5	23.1	20.0
45°C	3	39.7	23.0	19.8	3	39.7	22.8	19.9	3	40.5	23.1	20.0
35°C	3	39.7	23.0	19.8	3	39.7	23.0	19.9	3	40.5	23.1	20.0
25°C	3	39.7	23.0	19.8	3	39.7	23.0	19.9	3	40.5	23.1	20.0
15°C	3	39.7	23.0	19.8	3	39.7	23.0	19.9	3	40.5	23.1	20.0
5°C	3	40.0	23.0	19.9	3	39.7	23.0	19.9	3	40.5	23.1	20.0

T°C	30% wt% CuPc				29% wt% CuPc				28% wt% CuPc			
	{00l} orders	d_0	$d_0/\sqrt{3}$	$d_0/\sqrt{4}$	{00l} orders	d_0	$d_0/\sqrt{3}$	comments	{00l} orders	d_0	$d_0/\sqrt{3}$	comments
5°C	3	41.9	24.1	20.7	2	42.7	24.5	peak	2	43.8	24.8	peak
15°C	3	41.9	24.1	20.7	2	42.7	24.5	peak	2	43.2	24.8	peak
25°C	3	41.9	24.1	20.7	2	42.7	24.5	peak	2	43.2	24.8	peak
35°C	3	41.4	23.9	20.7	1	43.8	-	diffuse peak	1	43.2	-	peak
45°C	3	41.4	23.9	20.6	1	43.8	-	diffuse peak	1	43.2	-	peak
55°C	2	41.4	23.7	-	1	43.8	-	diffuse peak	1	43.2	-	peak
65°C	1	41.4	-	-	1	43.8	-	diffuse peak	1	44.3	-	diffuse peak
75°C	1	42.4	-	-	1	43.8	-	diffuse peak	1	44.3	-	diffuse peak
85°C	1	42.9	-	-	1	43.8	-	diffuse peak	1	44.3	-	diffuse peak
75°C	1	42.9	-	-	1	43.8	-	diffuse peak	1	44.3	-	diffuse peak
65°C	1	42.9	-	-	1	43.8	-	diffuse peak	1	44.3	-	diffuse peak
55°C	1	42.4	-	-	1	43.8	-	diffuse peak	1	44.3	-	diffuse peak
45°C	1	41.9	-	-	1	43.8	-	diffuse peak	1	44.3	-	diffuse peak
35°C	3	41.9	24.1	20.7	1	43.8	-	diffuse peak	1	43.2	-	peak
25°C	3	41.9	24.1	20.7	2	42.7	24.5	peak	2	43.2	24.7	peak
15°C	3	41.9	24.1	20.8	2	43.2	24.5	peak	2	43.2	24.8	peak
5°C	3	41.9	24.2	20.8	2	43.2	24.5	peak	2	43.2	24.8	peak

T°C	27% wt% CuPc {00*l*} orders	*d₀*	26% wt% CuPc {00*l*} orders	*d₀*	25% wt% CuPc {00*l*} orders	*d₀*	24% wt% CuPc {00*l*} orders	*d₀*	23% wt% CuPc {00*l*} orders	*d₀*	22% wt% CuPc {00*l*} orders	*d₀*
5°C	1	44.1	1	46.2	1	47.8	1	48.5	1	50.2	1	50.8
15°C	1	44.1	1	46.2	1	47.8	1	48.5	1	48.8	1	50.8
25°C	1	43.7	1	46.2	1	47.8	1	48.5	1	48.8	1	50.8
35°C	1	43.7	1	46.2	1	47.2	1	48.5	1	48.8	1	50.0
45°C	1	43.7	1	46.2	1	47.2	1	48.5	1	48.8	1	50.0
55°C	1	43.7	1	46.2	1	47.2	1	48.5	1	48.8	1	50.0
65°C	1	43.7	1	46.2	1	47.2	1	48.5	1	48.8	1	50.0
75°C	1	43.7	1	45.7	1	47.8	1	47.8	1	48.8	1	49.3
85°C	1	43.7	-	-	1	47.8	1	47.8	-	-	1	49.3
75°C	1	44.1	-	-	1	47.8	1	48.5	-	-	1	49.3
65°C	1	44.1	1	46.2	1	47.8	1	48.5	1	48.8	1	50.0
55°C	1	44.1	1	46.2	1	47.8	1	48.5	1	48.8	1	50.0
45°C	1	44.1	1	46.2	1	47.8	1	49.2	1	49.5	1	50.0
35°C	1	44.1	1	46.2	1	48.5	1	49.2	1	49.5	1	50.0
25°C	1	44.1	1	46.2	1	48.5	1	49.2	1	49.5	1	50.0
15°C	1	44.1	1	46.2	1	48.5	1	49.2	1	50.2	1	50.0
5°C	1	44.1	1	46.2	1	48.5	1	49.9	1	50.2	1	50.8

T°C	21% wt% CuPc {00*l*} orders	*d₀*	20% wt% CuPc {00*l*} orders	*d₀*	19% wt% CuPc {00*l*} orders	*d₀*	18% wt% CuPc {00*l*} orders	*d₀*	17% wt% CuPc {00*l*} orders	*d₀*	16% wt% CuPc {00*l*} orders	*d₀*
5°C	1	52.4	1	55.6	1	55.6	1	58.4	1	58.4	1	60.4
15°C	1	51.6	1	54.7	1	55.6	1	57.4	1	58.4	1	58.4
25°C	1	51.6	1	53.1	1	54.7	1	57.4	1	58.4	1	58.4
35°C	1	51.6	1	51.5	1	53.9	1	55.6	1	58.4	1	58.4
45°C	1	50.9	1	51.5	1	51.5	1	51.5	1	57.4	1	58.4
55°C	1	50.9	1	51.5	1	51.5	1	51.5	1	56.5	1	57.4
65°C	1	50.9	1	51.5	1	51.5	1	51.5	1	53.9	1	55.6
75°C	1	50.9	1	50.8	1	50.8	1	51.5	1	51.5	1	53.9
85°C	-	-	1	51.5	1	50.8	1	50.8	1	51.5	1	54.7
75°C	-	-	1	50.8	1	50.8	1	50.8	1	57.4	1	53.9
65°C	1	50.9	1	50.8	1	50.8	1	51.5	1	57.4	1	54.7
55°C	1	51.6	1	50.8	1	50.8	1	51.5	1	58.4	1	58.4
45°C	1	51.6	1	50.8	1	51.5	1	55.6	1	58.4	1	58.4
35°C	1	52.4	1	51.5	1	52.3	1	55.6	1	58.4	1	58.4
25°C	1	52.4	1	51.5	1	54.7	1	57.4	1	58.4	1	59.4
15°C	1	51.6	1	52.3	1	55.6	1	57.4	1	58.4	1	60.4
5°C	1	52.4	1	54.7	1	55.6	1	57.4	1	58.4	1	60.4

15% wt% CuPc		
T˚C	{00*l*} orders	d_0
5˚C	1	62.5
15˚C	1	62.5
25˚C	1	61.4
35˚C	1	60.4
45˚C	1	58.4
55˚C	1	58.4
65˚C	1	60.4
75˚C	1	58.4
85˚C	1	54.7
75˚C	1	58.4
65˚C	1	60.4
55˚C	1	59.4
45˚C	1	60.4
35˚C	1	60.4
25˚C	1	60.4
15˚C	1	62.5
5˚C	1	62.5

7.2 Intra- and Inter-Aggregate Arrangements

Based on the results found using the density and X-ray diffraction measurements, it becomes possible to determine the structure and packing of the Cu-phthalocyanine dye in aqueous solution. The chromonic mesophase formed by the Cu-phthalocyanine dye at high concentrations has been identified as columnar hexagonal with the structure corresponding to the stacking of the aromatic cores in columns laterally assembled according to a two dimensional hexagonal lattice. From simple geometry, the columnar structure can be characterised by two parameters, such as the intercolumnar distance, a, and the intracolumnar stacking period of the molecules along the columnar axis. Considering that the hexagonal lateral ordering of the stacks is developed over the long distances, it is possible to determine the intercolumnar parameters of the aggregates by small-angle X-ray diffraction. The internal structure of the columns was found experimentally by wide-angle X-ray diffraction and described as regular distance with a period of only 3.5 Å.

Given the values of intracolumnar distance, it is important to understand how the columns are packed within the long-range order of the hexagonal mesophase. Therefore, the approach of Luzzati [143] to the characterisation of amphiphilic systems, has been applied here in the study of lyotropic chromonic dye mesophases. The lattice type and symmetry relating to the long-range translational order of a specific mesophase may be determined by analysis of its small-angle Bragg reflections, whose reciprocal spacings (s_{hkl}) are in characteristic ratios. The dye was studied over a wide range of compositions (Table 7.3) and the hexagonal columnar phase was observed at the $28 - 33\%$ wt/wt% dye concentration range in aqueous solution.

In order to proceed further with the structural analysis and to elucidate the dimensions of the composite mesophase aggregates, several assumptions have to be considered. The first is that the hexagonal phase is composed of infinitely long and cylinders. The second implies that only the hydrophobic regions of the molecule make up the cylinder while all other parts, such as hydrophilic groups, counter-ions and water, are segregated out from the hydrophobic regions of the molecule and from calculations of the phase dimensions. The columns formed are rigid and infinitely long with all pairs of neighbouring axes located at constant distance and in parallel arrangement to each other, therefore corresponding to hexagonal packing of discs in a plane. The projection on the plane perpendicular to the column axis defines a two-dimensional lattice, the symmetry of which is determined by Equation 7.1 with which all the observed spacings agree.

$$d*^2_{hkl} = a*^2 (h^2 + k^2 + hk)$$

Equation 7.1

where $d*_{hkl}$ is defined as a reciprocal spacing (Å^{-1}) of the reflection with characteristic h, k and l Miller indices; and $a*$ is the dimension of the reciprocal unit cell of the hexagonal phase.

The small-angle diffraction patterns for Cu-phthalocyanine exhibited up to 3 sharp reflections corresponding to the lattice spacings d_0, $d_0 / \sqrt{3}$, $d_0 / \sqrt{4}$. These spacings are characteristic of the (hk0) reflections similarly exhibited by the amphiphilic systems forming the smectic S_B phase with its hexagonal symmetry. The number of reflections observed was dependent on the unit cell spacings of the mesophase. The unit cell is a parallelogram with the edges equal to the lattice spacing a (Figure 7.26) and the angles equal 120º and 60º respectively.
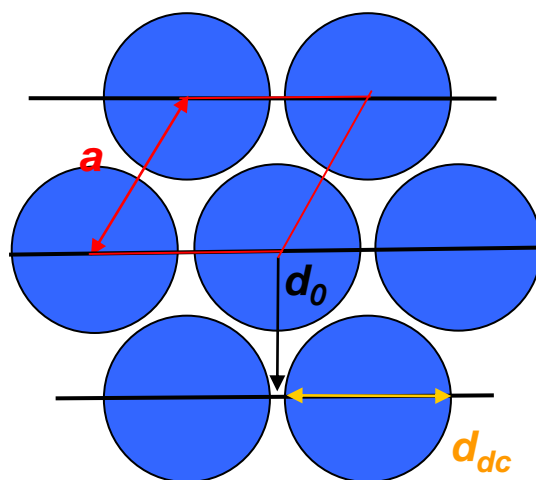
Figure 7.26   **Schematic representation of the chromonic hexagonal mesophase.**
The aggregate parameters are correlated to the data in Table 7.3.

This hexagonal lattice parameter a can be obtained from the primary reflection with the spacing d_0 in accordance with Equation 7.2,

$$a = 2d_0 / \sqrt{3}$$

Equation 7.2

Geometrical relations provide the relationship between the effective diameter of the columns, d_{dc} the lattice parameter, a, and volume fraction φ of Cu-phthalocyanine dye using Luzzati's equation for hexagonal packing of rods (Equation 7.3),

$$d_{dc} = a \left[(2\sqrt{3} / \pi) \, \varphi_d \right]^{1/2}$$

Equation 7.3

where d_{dc} is a column diameter (Å), a is a column separation (Å), φ_d is the volume fraction of dye, which is the ratio of the volume of Cu-phthalocyanine dye to the volume of the solution of the dye. The volume fraction of dye can then be estimated by Equation 7.4,

$$\varphi_d = \left[1 + \{ v_w (1 - c) / (v_d \, c) \} \right]^{-1}$$

Equation 7.4

where v_w, v_d are the partial specific volumes of dye and water ($cm^3 g^{-1}$) and c is the dye weight concentration (Equation 7.5) of the hydrophobic dye region, thus excluding sulphonic acid parts, counterions and water.

$$c = \frac{wt_{dye}}{wt_{dye} + wt_{water}}$$

Equation 7.5

In order to subtract these ionic moieties the actual dye concentration was multiplied by 0.56 which was calculated using Equation 7.6,

$$wt_{\text{hydrophobic region}} = \frac{M_{r\,\text{dye}} - M_{r\,\text{hydrophilic region}}}{M_{r\,\text{dye}}}$$

Equation 7.6

The changes in interplanar distances as a function of volume fraction provide information about the way the aggregates are distributed in space, i.e. about the lattice type. Considering the shape of aggregates and a type of lattice corresponding to the aggregates packing, it becomes possible to obtain this relationship in analytical form. The spacings for the hexagonal phases may vary for different mesogens, but they are inversely proportional to the square root of the concentration.. It is significant for our understanding that the structure is growing only in two-dimensions, thus, making the column length infinitely large. A plot of the *d* spacing, log *d_0*, against the reciprocal volume fraction of dye, log (1/*φ_{dc}*), is shown in Figure 7.27.
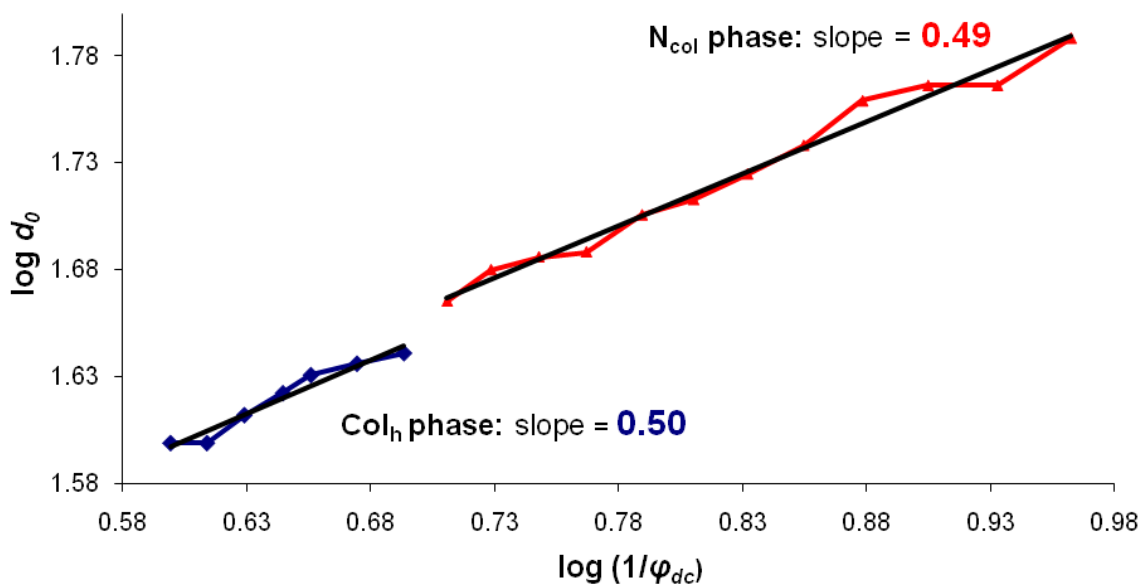
Figure 7.27   **Log *d_0* against log (1/φ_{dc}) for Cu-phthalocyanine dye (Cross-sectional area of an aggregate was calculated for the Col$_h$ phase only).**

It has been employed in order to illustrate the swelling behaviour of the columnar mesophases over the large range of concentrations. The two lines on the graph represent best-fit lines for the hexagonal (blue line) and nematic (red line) phase samples. The slight

discontinuity in the two lines is an indication of the phase transition. The gradient of the best fit line for the hexagonal phase samples is 0.5, which is the expected value for the phase being periodic in two dimensions and, hence, undergoing 2-D swelling. However, for the nematic samples the gradient is similar (0.49), which suggests that even in the relatively disordered nematic phase the aggregates pack together locally in an approximately hexagonal manner. The addition of water to the system periodic in one dimension only, i.e. an amphiphilic lamellar phase, results in one-dimensional swelling of the layered phase on dilution and giving a gradient of 1.

In addition to these calculations, the number of dye molecules per unit cell can be determined if the concentration, the density and the molecular weight of the dye are known. The density of the solution was measured experimentally for each studied concentration in the range of 5°C - 85°C temperatures on heating and cooling. The density of the pure dye then was calculated using Equation 7.7,

$$\rho_{dye} = (\rho_{solution} - (wt\%_{water} \times \rho_{water})) / wt\%_{dye}$$

Equation 7.7

where ρ_{sol} is the density of the dye solution measured experimentally and ρ_w is the density of water.

The area per molecule at the dye / water interface for hexagonal symmetry is then can be derived using equation 7.8,

$$S_{dc} = (4M_d \, v_d \, 10^{24}) / d_{dc} \, N$$

Equation 7.8

The column diameters and the areas for the hexagonal columnar phase samples are presented in Table 7.3.

The calculations show that the theoretical cross-sectional area of the phthalocyanine core is around 170 Å^2, which was determined using the bond lengths and van der Waals radii as shown in Figure 7.28.
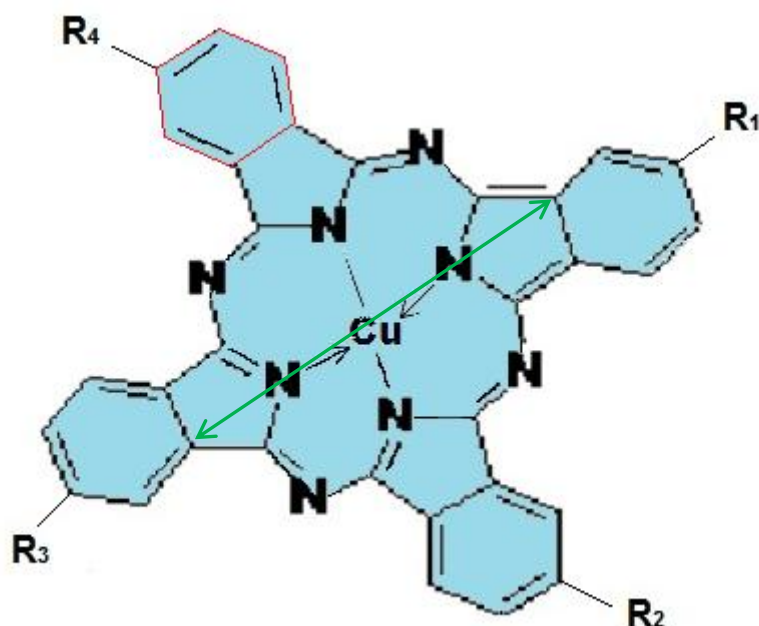
Figure 7.28   **Schematic representation of the way the theoretical cross-sectional area of Cu-phthalocyanine dye molecule was calculated.**

1. **Porphyrine** molecular length ≈**12.3 Å**; $S_{porphyrine} \approx$ **150 Å^2**
2. $S_{benzene\ ring} \approx$ **5.09 Å^2**
3. S_{dc} = **170 Å^2**

The calculated area shows the cross section of the aromatic core of the column excluding the hydrophobic region attached to the periphery of the phthalocyanine core. The comparison of the calculated and experimental molecular areas reveals that the experimental value for cross-sectional area appears to be slightly larger. With the molecules oriented normal to the column axis, the experimental value represents the surface of the phthalocyanine molecule, enlarged to include the cross-sectional area of one peripheral hydrophobic group in a liquid-like state. Consequently, it is reasonable to conclude that the column is comprised of unimolecular dye stacking.

From the value of cross-sectional area and intra-columnar period it is possible to calculate the volume of the hydrophobic part of one Cu-phthalocyanine dye molecule in the columnar aggregate. It can be derived using Equation 7.9,

$$V = 3.5 \times S_{dc}$$

Equation 7.9

The volume of one molecule gives the approximate value of 650 $\AA^3$, which is in good agreement with crystallographic volume equal to 587 $\AA^3$ of non-substituted phthalocyanine at room temperature [144], enlarged by adding for the peripheral hydrophobic moiety a rough 60 $\AA^3$.

$$V = 3.5 \times S_{dc}$$

Table 7.3 Inter-aggregate parameters for Cu-phthalocyanine dye for various concentrations and temperatures. Data derived from SAXS XRD.

T˚C	{00l} orders	d_0	$d_0/\sqrt{3}$	$d_0/\sqrt{4}$	log d_0	a	ρ_{sol} (g/cm^3)	ρ_d (g/cm^3)	v_d	φ_{dc}	d_{dc}	S_{dc} (Å^2)
						33% wt% CuPc						
5˚C	3	39.7	23.0	19.8	1.60	45.9	1.156438	1.841222	0.543118	0.11	16.0	183.8
15˚C	3	39.7	23.0	19.8	1.60	45.9	1.154321	1.833626	0.545368	0.11	16.0	184.3
25˚C	3	39.7	22.9	19.8	1.60	45.9	1.150437	1.821742	0.548925	0.11	16.1	185.2
35˚C	3	39.7	22.9	19.8	1.60	45.9	1.146661	1.814631	0.551076	0.11	16.1	185.8
45˚C	3	39.7	22.9	19.8	1.60	45.9	1.142324	1.808036	0.553086	0.11	16.1	186.5
55˚C	3	39.7	22.9	19.8	1.60	45.9	1.137247	1.800521	0.555395	0.11	16.1	187.3
65˚C	3	39.7	22.8	19.8	1.60	45.9	1.130761	1.788154	0.559236	0.11	16.1	188.5
75˚C	2	39.7	22.8	-	1.60	45.9	1.120049	1.755542	0.569625	0.11	16.2	190.9
85˚C	1	39.7	-	-	1.60	-	1.100939	1.680074	0.595212	0.12	-	-
75˚C	2	39.7	22.8	-	1.60	45.9	1.114337	1.724833	0.579766	0.11	16.3	192.8
65˚C	3	39.7	22.8	19.8	1.60	45.9	1.123732	1.750363	0.57131	0.11	16.2	190.7
55˚C	3	39.7	22.9	19.8	1.60	45.9	1.131162	1.767806	0.565673	0.11	16.2	189.3
45˚C	3	39.7	23.0	19.8	1.60	45.9	1.136719	1.777902	0.562461	0.11	16.2	188.3
35˚C	3	39.7	23.0	19.8	1.60	45.9	1.142353	1.79147	0.558201	0.11	16.2	187.2
25˚C	3	39.7	23.0	19.8	1.60	45.9	1.147328	1.805027	0.554008	0.11	16.1	186.1
15˚C	3	39.7	23.0	19.8	1.60	45.9	1.150254	1.81176	0.551949	0.11	16.1	185.6
5˚C	3	40.0	23.0	19.9	1.60	46.2	1.154532	1.830975	0.546157	0.11	16.0	184.4
						32% wt% CuPc						
5˚C	3	39.7	23.0	19.9	1.60	45.9	1.15124	1.836668	0.544464	0.11	15.8	187.0
15˚C	3	39.7	23.0	19.9	1.60	45.9	1.149034	1.828386	0.546931	0.11	15.8	187.5
25˚C	3	39.7	23.0	19.9	1.60	45.9	1.145425	1.81774	0.550134	0.11	15.8	188.3
35˚C	3	39.7	23.0	19.9	1.60	45.9	1.141654	1.810539	0.552322	0.11	15.8	189.0
45˚C	3	39.7	23.0	19.9	1.60	45.9	1.137305	1.803798	0.554386	0.11	15.8	189.7
55˚C	2	39.7	22.8	19.8	1.60	45.9	1.132286	1.796518	0.556632	0.11	15.8	190.5
65˚C	2	39.7	22.8	19.8	1.60	45.9	1.126064	1.785402	0.560098	0.11	15.8	191.6
75˚C	2	39.7	22.8	-	1.60	45.9	1.116391	1.757764	0.568905	0.11	15.9	193.8
85˚C	1	39.7	-	-	1.60	-	1.098692	1.688108	0.592379	0.11	-	-
75˚C	2	39.7	22.8	-	1.60	45.9	1.109846	1.721564	0.580867	0.11	16.1	196.0
65˚C	2	39.7	22.8	-	1.60	45.9	1.118818	1.745325	0.572959	0.11	16.0	194.0
55˚C	3	39.7	22.8	19.9	1.60	45.9	1.126068	1.762126	0.567496	0.11	16.0	192.5
45˚C	3	39.7	22.8	19.9	1.60	45.9	1.131915	1.773986	0.563702	0.11	15.9	191.4
35˚C	3	39.7	23.0	19.9	1.60	45.9	1.137421	1.787126	0.559558	0.11	15.9	190.3
25˚C	3	39.7	23.0	19.9	1.60	45.9	1.142242	1.800135	0.555514	0.11	15.9	189.3
15˚C	3	39.7	23.0	19.9	1.60	45.9	1.145573	1.809243	0.552717	0.11	15.9	188.6
5˚C	3	39.7	23.0	19.9	1.60	45.9	1.149418	1.82659	0.547468	0.11	15.8	187.5

31% wt% CuPc												
T˚C	**{00*l*} orders**	**d_0**	**$d_0/\sqrt{3}$**	**$d_0/\sqrt{4}$**	**log d_0**	**a**	**ρ_{sol} (g/cm³)**	**ρ_d (g/cm³)**	**v_d**	**φ_{dc}**	**d_{dc}**	**S_{dc} (Å²)**
5˚C	3	40.9	23.4	20.2	1.61	47.3	1.146042	1.834695	0.54505	0.10	16.0	184.8
15˚C	3	40.9	23.4	20.2	1.61	47.3	1.143747	1.825659	0.547747	0.10	16.0	185.4
25˚C	3	40.9	23.4	20.2	1.61	47.3	1.140413	1.8163	0.55057	0.10	16.0	186.1
35˚C	3	40.9	23.4	20.1	1.61	47.3	1.136647	1.808989	0.552795	0.10	16.0	186.7
45˚C	3	40.9	23.3	20.1	1.61	47.3	1.132286	1.802082	0.554914	0.10	16.0	187.4
55˚C	3	40.5	23.3	20.1	1.61	46.7	1.127325	1.795042	0.55709	0.10	15.8	190.4
65˚C	3	40.5	23.3	20.1	1.61	46.7	1.121367	1.785237	0.56015	0.10	15.9	191.4
75˚C	2	40.9	23.3	-	1.61	47.3	1.112733	1.762809	0.567276	0.10	16.1	191.1
85˚C	1	41.9	-	-	1.62	-	1.096445	1.699115	0.588542	0.11	-	-
75˚C	1	40.9	-	-	1.61	-	1.105355	1.720649	0.581176	0.11	-	-
65˚C	3	40.5	23.3	20.0	1.61	46.7	1.113904	1.742592	0.573858	0.11	16.0	194.0
55˚C	3	40.5	23.1	20.0	1.61	46.7	1.120974	1.758751	0.568585	0.11	16.0	192.5
45˚C	3	40.5	23.1	20.0	1.61	46.7	1.127111	1.772511	0.564171	0.11	16.0	191.3
35˚C	3	40.5	23.1	20.0	1.61	46.7	1.132489	1.785229	0.560152	0.11	16.0	190.2
25˚C	3	40.5	23.1	20.0	1.61	46.7	1.137156	1.797689	0.55627	0.11	15.9	189.2
15˚C	3	40.5	23.1	20.0	1.61	46.7	1.140892	1.809345	0.552686	0.10	15.9	188.4
5˚C	3	40.5	23.1	20.0	1.61	46.7	1.144304	1.824764	0.548016	0.10	15.8	187.4

30% wt% CuPc												
T˚C	**{00*l*} orders**	**d_0**	**$d_0/\sqrt{3}$**	**$d_0/\sqrt{4}$**	**log d_0**	**a**	**ρ_{sol} (g/cm³)**	**ρ_d (g/cm³)**	**v_d**	**φ_{dc}**	**d_{dc}**	**S_{dc} (Å²)**
5˚C	3	41.9	24.1	20.7	1.62	48.4	1.140844	1.831114	0.546116	0.10	16.1	183.9
15˚C	3	41.9	24.1	20.7	1.62	48.4	1.138460	1.821288	0.549062	0.10	16.1	184.5
25˚C	3	41.9	24.1	20.7	1.62	48.4	1.135401	1.813314	0.551476	0.10	16.1	185.1
35˚C	3	41.4	23.9	20.7	1.62	48.4	1.131640	1.805893	0.553743	0.10	16.1	185.8
45˚C	3	41.4	23.9	20.6	1.62	47.8	1.127267	1.798816	0.555921	0.10	16.0	188.7
55˚C	2	41.4	23.7	-	1.62	47.8	1.122364	1.792036	0.558024	0.10	16.0	189.5
65˚C	1	41.4	-	-	1.62	-	1.116670	1.783637	0.560652	0.10	-	-
75˚C	1	42.4	-	-	1.63	-	1.109075	1.766797	0.565996	0.10	-	-
85˚C	1	42.9	-	-	1.63	-	1.094198	1.709562	0.584945	0.10	-	-
75˚C	1	42.9	-	-	1.63	-	1.100864	1.718354	0.581952	0.10	-	-
65˚C	1	42.9	-	-	1.63	-	1.108990	1.738328	0.575266	0.10	-	-
55˚C	1	42.4	-	-	1.63	-	1.115880	1.753782	0.570196	0.10	-	-
45˚C	1	41.9	-	-	1.62	-	1.122307	1.769553	0.565114	0.10	-	-
35˚C	3	41.9	24.1	20.7	1.62	48.4	1.127557	1.781805	0.561229	0.10	16.2	187.1
25˚C	3	41.9	24.1	20.7	1.62	48.4	1.132070	1.793662	0.557518	0.10	16.2	186.2
15˚C	3	41.9	24.1	20.8	1.62	48.4	1.136211	1.808019	0.553091	0.10	16.2	185.2
5˚C	3	41.9	24.2	20.8	1.62	48.4	1.139190	1.821356	0.549041	0.10	16.1	184.4

					29% wt% CuPc							
T˚C	**{00l} orders**	d_0	$d_0/\sqrt{3}$	*comments*	**log d_0**	a	ρ_{sol} (g/cm³)	ρ_d (g/cm³)	v_d	φ_{dc}	d_{dc}	S_{dc} (Å²)
5˚C	2	42.7	24.5	peak	1.63	49.3	1.129779	1.792002	0.558035	0.10	16.3	185.8
15˚C	2	42.7	24.5	peak	1.63	49.3	1.127633	1.783321	0.560752	0.10	16.3	186.4
25˚C	2	42.7	24.5	peak	1.63	49.3	1.124629	1.775481	0.563228	0.10	16.3	187.0
35˚C	1	43.8	-	diffuse peak	1.64	-	1.120920	1.768227	0.565538	0.10	-	-
45˚C	1	43.8	-	diffuse peak	1.64	-	1.116586	1.761276	0.56777	0.10	-	-
55˚C	1	43.8	-	diffuse peak	1.64	-	1.111636	1.754132	0.570082	0.10	-	-
65˚C	1	43.8	-	diffuse peak	1.64	-	1.105836	1.744976	0.573074	0.10	-	-
75˚C	1	43.8	-	diffuse peak	1.64	-	1.097906	1.72571	0.579471	0.10	-	-
85˚C	1	43.8	-	diffuse peak	1.64	-	1.084085	1.673176	0.597666	0.10	-	-
75˚C	1	43.8	-	diffuse peak	1.64	-	1.092328	1.691678	0.591129	0.10	-	-
65˚C	1	43.8	-	diffuse peak	1.64	-	1.099604	1.706952	0.585839	0.10	-	-
55˚C	1	43.8	-	diffuse peak	1.64	-	1.106091	1.720301	0.581294	0.10	-	-
45˚C	1	43.8	-	diffuse peak	1.64	-	1.111846	1.732356	0.577249	0.10	-	-
35˚C	1	43.8	-	diffuse peak	1.64	-	1.116981	1.744194	0.573331	0.10	-	-
25˚C	2	42.7	24.5	peak	1.63	49.3	1.121389	1.755713	0.569569	0.10	16.4	188.2
15˚C	2	43.2	24.5	peak	1.64	49.9	1.125032	1.767452	0.565786	0.10	16.6	185.1
5˚C	2	43.2	24.5	peak	1.64	49.9	1.127942	1.780794	0.561547	0.10	16.5	184.2

					28% wt% CuPc							
T˚C	**{00l} orders**	d_0	$d_0/\sqrt{3}$	*comments*	**log d_0**	a	ρ_{sol} (g/cm³)	ρ_d (g/cm³)	v_d	φ_{dc}	d_{dc}	S_{dc} (Å²)
5˚C	2	43.8	24.8	peak	1.64	50.6	1.127487	1.76623	0.566178	0.10	16.5	186.3
15˚C	2	43.2	24.8	peak	1.64	50.0	1.125350	1.757359	0.569036	0.10	16.3	189.2
25˚C	2	43.2	24.8	peak	1.64	50.0	1.122362	1.749493	0.571594	0.10	16.3	189.8
35˚C	1	43.2	-	peak	1.64	-	1.118693	1.742459	0.573902	0.10	-	-
45˚C	1	43.2	-	peak	1.64	-	1.114360	1.735554	0.576185	0.10	-	-
55˚C	1	43.2	-	peak	1.64	-	1.109161	1.726922	0.579065	0.10	-	-
65˚C	1	44.3	-	diffuse peak	1.65	-	1.103139	1.716422	0.582607	0.10	-	-
75˚C	1	44.3	-	diffuse peak	1.65	-	1.094206	1.690556	0.591522	0.10	-	-
85˚C	1	44.3	-	diffuse peak	1.65	-	1.079889	1.633466	0.612195	0.10	-	-
75˚C	1	44.3	-	diffuse peak	1.65	-	1.087226	1.646434	0.607373	0.10	-	-
65˚C	1	44.3	-	diffuse peak	1.65	-	1.094868	1.66414	0.600911	0.10	-	-
55˚C	1	44.3	-	diffuse peak	1.65	-	1.101671	1.679577	0.595388	0.10	-	-
45˚C	1	44.3	-	diffuse peak	1.65	-	1.107724	1.693607	0.590456	0.10	-	-
35˚C	1	43.2	-	peak	1.64	-	1.113133	1.707314	0.585715	0.10	-	-
25˚C	2	43.2	24.7	peak	1.64	50.0	1.117673	1.719854	0.581445	0.10	16.4	191.6
15˚C	2	43.2	24.8	peak	1.64	50.0	1.121444	1.732668	0.577144	0.10	16.4	190.7
5˚C	2	43.2	24.8	peak	1.64	50.0	1.124637	1.748214	0.572012	0.10	16.3	189.7

27% wt% CuPc							
T°C	{00*l*} orders	d_0	log d_0	ρ_{sol} (g/cm³)	ρ_d (g/cm³)	v_d	φ_{dc}
5°C	1	44.1	1.64	1.124762	1.817775	0.550123	0.09
15°C	1	44.1	1.64	1.122694	1.809027	0.552783	0.09
25°C	1	43.7	1.64	1.119730	1.801021	0.555241	0.09
35°C	1	43.7	1.64	1.116067	1.793754	0.55749	0.09
45°C	1	43.7	1.64	1.111741	1.786623	0.559715	0.09
55°C	1	43.7	1.64	1.106816	1.779449	0.561972	0.09
65°C	1	43.7	1.64	1.100964	1.769655	0.565082	0.09
75°C	1	43.7	1.64	1.093201	1.75048	0.571272	0.09
85°C	1	43.7	1.64	1.081192	1.706391	0.586032	0.09
75°C	1	44.1	1.64	1.090710	1.734156	0.576649	0.09
65°C	1	44.1	1.64	1.097245	1.745284	0.572973	0.09
55°C	1	44.1	1.64	1.103098	1.755085	0.569773	0.09
45°C	1	44.1	1.64	1.108429	1.76492	0.566598	0.09
35°C	1	44.1	1.64	1.113166	1.774743	0.563462	0.09
25°C	1	44.1	1.64	1.117249	1.784763	0.560299	0.09
15°C	1	44.1	1.64	1.120596	1.795279	0.557017	0.09
5°C	1	44.1	1.64	1.123182	1.807421	0.553274	0.09

26% wt% CuPc							
T°C	{00*l*} orders	d_0	log d_0	ρ_{sol} (g/cm³)	ρ_d (g/cm³)	v_d	φ_{dc}
5°C	1	46.2	1.67	1.119771	1.815532	0.550803	0.09
15°C	1	46.2	1.67	1.117725	1.806628	0.553517	0.09
25°C	1	46.2	1.67	1.114791	1.798595	0.55599	0.09
35°C	1	46.2	1.67	1.111139	1.791238	0.558273	0.09
45°C	1	46.2	1.67	1.106654	1.782897	0.560885	0.09
55°C	1	46.2	1.67	1.101685	1.77532	0.563279	0.09
65°C	1	46.2	1.67	1.095186	1.760941	0.567878	0.09
75°C	1	45.7	1.66	1.087627	1.742632	0.573844	0.09
85°C	-	-	-	-	-	-	-
75°C	-	-	-	1.082001	1.704334	0.586739	0.09
65°C	1	46.2	1.67	1.090051	1.725985	0.579379	0.09
55°C	1	46.2	1.67	1.096546	1.740337	0.574601	0.09
45°C	1	46.2	1.67	1.101766	1.749623	0.571552	0.09
35°C	1	46.2	1.67	1.106571	1.760142	0.568136	0.09
25°C	1	46.2	1.67	1.110773	1.771243	0.564575	0.09
15°C	1	46.2	1.67	1.114241	1.782911	0.56088	0.09
5°C	1	46.2	1.67	1.116917	1.796104	0.556761	0.09

				25% wt% CuPc			
T°C	{00l} orders	d_0	log d_0	ρ_{sol} (g/cm^3)	ρ_d (g/cm^3)	v_d	φ_{dc}
5°C	1	47.8	1.68	1.114233	1.808662	0.552895	0.08
15°C	1	47.8	1.68	1.112244	1.799842	0.555604	0.08
25°C	1	47.8	1.68	1.109360	1.791926	0.558059	0.08
35°C	1	47.2	1.67	1.105745	1.784659	0.560331	0.08
45°C	1	47.2	1.67	1.101455	1.777519	0.562582	0.08
55°C	1	47.2	1.67	1.096570	1.770416	0.564839	0.08
65°C	1	47.2	1.67	1.090878	1.761381	0.567736	0.08
75°C	1	47.8	1.68	1.084687	1.752255	0.570693	0.08
85°C	1	47.8	1.68	1.077721	1.740828	0.574439	0.08
75°C	1	47.8	1.68	1.083815	1.746084	0.57271	0.08
65°C	1	47.8	1.68	1.089546	1.751954	0.570791	0.08
55°C	1	47.8	1.68	1.094898	1.758583	0.56864	0.08
45°C	1	47.8	1.68	1.099809	1.76587	0.566293	0.08
35°C	1	48.5	1.69	1.104214	1.773824	0.563754	0.08
25°C	1	48.5	1.69	1.108027	1.782492	0.561012	0.08
15°C	1	48.5	1.69	1.111135	1.791994	0.558038	0.08
5°C	1	48.5	1.69	1.113447	1.803099	0.554601	0.08

				24% wt% CuPc			
T°C	{00l} orders	d_0	log d_0	ρ_{sol} (g/cm^3)	ρ_d (g/cm^3)	v_d	φ_{dc}
5°C	1	48.5	1.69	1.109978	1.811277	0.552097	0.08
15°C	1	48.5	1.69	1.107903	1.801488	0.555097	0.08
25°C	1	48.5	1.69	1.104982	1.793053	0.557708	0.08
35°C	1	48.5	1.69	1.101223	1.784545	0.560367	0.08
45°C	1	48.5	1.69	1.096654	1.775208	0.563314	0.08
55°C	1	48.5	1.69	1.091139	1.76335	0.567102	0.08
65°C	1	48.5	1.69	1.083443	1.739373	0.57492	0.08
75°C	1	47.8	1.68	1.069057	1.669668	0.598921	0.08
85°C	1	47.8	1.68	-	-	-	-
75°C	1	48.5	1.69	1.065504	1.643466	0.60847	0.09
65°C	1	48.5	1.69	1.076951	1.691497	0.591192	0.08
55°C	1	48.5	1.69	1.084593	1.715076	0.583065	0.08
45°C	1	49.2	1.69	1.090751	1.731676	0.577475	0.08
35°C	1	49.2	1.69	1.096127	1.746964	0.572422	0.08
25°C	1	49.2	1.69	1.100563	1.760465	0.568032	0.08
15°C	1	49.2	1.69	1.104170	1.773959	0.563711	0.08
5°C	1	49.9	1.70	1.107260	1.791232	0.558275	0.08

				23% wt% CuPc			
T˚C	**{00*l*} orders**	**d_0**	**log d_0**	**ρ_{sol} (g/cm^3)**	**ρ_d (g/cm^3)**	**v_d**	**φ_{dc}**
5˚C	1	50.2	1.70	1.104721	1.805787	0.553775	0.08
15˚C	1	48.8	1.69	1.102749	1.796407	0.556667	0.08
25˚C	1	48.8	1.69	1.099766	1.78722	0.559528	0.08
35˚C	1	48.8	1.69	1.095962	1.778129	0.562389	0.08
45˚C	1	48.8	1.69	1.091298	1.767823	0.565667	0.08
55˚C	1	48.8	1.69	1.086112	1.75818	0.56877	0.08
65˚C	1	48.8	1.69	1.080127	1.746554	0.572556	0.08
75˚C	1	48.8	1.69	1.072847	1.728753	0.578452	0.08
85˚C	-	-	-	1.059601	1.668568	0.599316	0.08
75˚C	-	-	-	1.070357	1.7096	0.584932	0.08
65˚C	1	48.8	1.69	1.078498	1.734023	0.576694	0.08
55˚C	1	48.8	1.69	1.084717	1.74745	0.572263	0.08
45˚C	1	49.5	1.69	1.089993	1.757785	0.568898	0.08
35˚C	1	49.5	1.69	1.094555	1.767306	0.565833	0.08
25˚C	1	49.5	1.69	1.098444	1.777051	0.56273	0.08
15˚C	1	50.2	1.70	1.101602	1.787584	0.559414	0.08
5˚C	1	50.2	1.70	1.103903	1.799495	0.555712	0.08

				22% wt% CuPc			
T˚C	**{00*l*} orders**	**d_0**	**log d_0**	**ρ_{sol} (g/cm^3)**	**ρ_d (g/cm^3)**	**v_d**	**φ_{dc}**
5˚C	1	50.8	1.71	1.101512	1.816923	0.550381	0.07
15˚C	1	50.8	1.71	1.099594	1.807587	0.553224	0.07
25˚C	1	50.8	1.71	1.096773	1.799376	0.555748	0.07
35˚C	1	50.0	1.70	1.093214	1.791978	0.558043	0.07
45˚C	1	50.0	1.70	1.088959	1.784665	0.560329	0.07
55˚C	1	50.0	1.70	1.084099	1.77741	0.562617	0.07
65˚C	1	50.0	1.70	1.078548	1.768977	0.565298	0.07
75˚C	1	49.3	1.69	1.072878	1.763575	0.56703	0.07
85˚C	1	49.3	1.69	1.064581	1.74073	0.574472	0.07
75˚C	1	49.3	1.69	1.070792	1.746793	0.572478	0.07
65˚C	1	50.0	1.70	1.076595	1.753265	0.570364	0.07
55˚C	1	50.0	1.70	1.082110	1.761408	0.567728	0.07
45˚C	1	50.0	1.70	1.087076	1.769516	0.565126	0.07
35˚C	1	50.0	1.70	1.091457	1.777842	0.56248	0.07
25˚C	1	50.0	1.70	1.095208	1.786786	0.559664	0.07
15˚C	1	50.0	1.70	1.098235	1.796653	0.55659	0.07
5˚C	1	50.8	1.71	1.100556	1.809232	0.552721	0.07

				21% wt% CuPc			
T°C	**{00*l*} orders**	**d_0**	**log d_0**	**ρ_{sol} (g/cm³)**	**ρ_d (g/cm³)**	**v_d**	**φ_{dc}**
5°C	1	52.4	1.72	1.096156	1.810343	0.552381	0.07
15°C	1	51.6	1.71	1.094331	1.80139	0.555127	0.07
25°C	1	51.6	1.71	1.091546	1.793193	0.557664	0.07
35°C	1	51.6	1.71	1.088001	1.785705	0.560003	0.07
45°C	1	50.9	1.71	1.083769	1.778422	0.562296	0.07
55°C	1	50.9	1.71	1.078911	1.771054	0.564635	0.07
65°C	1	50.9	1.71	1.073488	1.763545	0.56704	0.07
75°C	1	50.9	1.71	1.066758	1.749227	0.571681	0.07
85°C	-	-	-	1.054786	1.694638	0.590097	0.07
75°C	-	-	-	1.062740	1.715377	0.582962	0.07
65°C	1	50.9	1.71	1.070261	1.736359	0.575918	0.07
55°C	1	51.6	1.71	1.075884	1.745553	0.572884	0.07
45°C	1	51.6	1.71	1.080960	1.754757	0.569879	0.07
35°C	1	52.4	1.72	1.085486	1.764518	0.566727	0.07
25°C	1	52.4	1.72	1.089324	1.774473	0.563547	0.07
15°C	1	51.6	1.71	1.092427	1.78535	0.560114	0.07
5°C	1	52.4	1.72	1.095530	1.805069	0.553995	0.07

				20% wt% CuPc			
T°C	**{00*l*} orders**	**d_0**	**log d_0**	**ρ_{sol} (g/cm³)**	**ρ_d (g/cm³)**	**v_d**	**φ_{dc}**
5°C	1	55.6	1.75	1.090800	1.803822	0.554378	0.07
15°C	1	54.7	1.74	1.089068	1.795285	0.557015	0.07
25°C	1	53.1	1.72	1.086319	1.787096	0.559567	0.07
35°C	1	51.5	1.71	1.082788	1.779507	0.561953	0.07
45°C	1	51.5	1.71	1.078579	1.772252	0.564254	0.07
55°C	1	51.5	1.71	1.073723	1.764759	0.56665	0.07
65°C	1	51.5	1.71	1.068428	1.758263	0.568743	0.07
75°C	1	50.8	1.71	1.060638	1.73413	0.576658	0.07
85°C	1	51.5	1.71	1.044991	1.644579	0.608058	0.07
75°C	1	50.8	1.71	1.054688	1.681475	0.594716	0.07
65°C	1	50.8	1.71	1.063927	1.718431	0.581926	0.07
55°C	1	50.8	1.71	1.069658	1.728785	0.578441	0.07
45°C	1	50.8	1.71	1.074844	1.739199	0.574977	0.07
35°C	1	51.5	1.71	1.079515	1.750542	0.571252	0.07
25°C	1	51.5	1.71	1.083440	1.761618	0.56766	0.07
15°C	1	52.3	1.72	1.086619	1.773612	0.563821	0.07
5°C	1	54.7	1.74	1.090504	1.801203	0.555185	0.07

				19% wt% CuPc			
T°C	{00*l*} orders	d_0	log d_0	ρ_{sol} (g/cm³)	ρ_d (g/cm³)	v_d	φ_{dc}
5°C	1	55.6	1.75	1.085444	1.795867	0.556834	0.06
15°C	1	55.6	1.75	1.083805	1.787795	0.559348	0.06
25°C	1	54.7	1.74	1.081092	1.779622	0.561917	0.06
35°C	1	53.9	1.73	1.077575	1.771925	0.564358	0.06
45°C	1	51.5	1.71	1.073389	1.764705	0.566667	0.06
55°C	1	51.5	1.71	1.068535	1.757075	0.569128	0.06
65°C	1	51.5	1.71	1.063368	1.751701	0.570874	0.06
75°C	1	50.8	1.71	1.054518	1.716737	0.5825	0.06
85°C	1	50.8	1.71	1.035196	1.588625	0.629475	0.07
75°C	1	50.8	1.71	1.046636	1.643348	0.608514	0.07
65°C	1	50.8	1.71	1.057593	1.69793	0.588953	0.06
55°C	1	50.8	1.71	1.063432	1.709561	0.584945	0.06
45°C	1	51.5	1.71	1.068728	1.721307	0.580954	0.06
35°C	1	52.3	1.72	1.073544	1.734392	0.576571	0.06
25°C	1	54.7	1.74	1.077556	1.746698	0.572509	0.06
15°C	1	55.6	1.75	1.080811	1.759918	0.568208	0.06
5°C	1	55.6	1.75	1.085478	1.796184	0.556736	0.06

				18% wt% CuPc			
T°C	{00*l*} orders	d_0	log d_0	ρ_{sol} (g/cm³)	ρ_d (g/cm³)	v_d	φ_{dc}
5°C	1	58.4	1.77	1.080088	1.787811	0.559343	0.06
15°C	1	57.4	1.76	1.078542	1.780249	0.561719	0.06
25°C	1	57.4	1.76	1.075865	1.772087	0.564306	0.06
35°C	1	55.6	1.75	1.072362	1.764265	0.566808	0.06
45°C	1	51.5	1.71	1.068199	1.757081	0.569126	0.06
55°C	1	51.5	1.71	1.063347	1.749297	0.571658	0.06
65°C	1	51.5	1.71	1.058308	1.745167	0.573011	0.06
75°C	1	51.5	1.71	1.048398	1.698142	0.588879	0.06
85°C	1	50.8	1.71	1.025401	1.527062	0.654852	0.07
75°C	1	50.8	1.71	1.038584	1.601642	0.624359	0.06
65°C	1	51.5	1.71	1.051259	1.675856	0.59671	0.06
55°C	1	51.5	1.71	1.057206	1.688913	0.592097	0.06
45°C	1	55.6	1.75	1.062612	1.702145	0.587494	0.06
35°C	1	55.6	1.75	1.067573	1.717176	0.582352	0.06
25°C	1	57.4	1.76	1.071672	1.730858	0.577748	0.06
15°C	1	57.4	1.76	1.075003	1.745451	0.572918	0.06
5°C	1	57.4	1.76	1.080452	1.79139	0.558226	0.06

				17% wt% CuPc			
T˚C	{00*l*} orders	d_0	log d_0	ρ_{sol} (g/cm^3)	ρ_d (g/cm^3)	v_d	φ_{dc}
5˚C	1	58.4	1.77	1.075887	1.790006	0.558657	0.06
15˚C	1	58.4	1.77	1.074252	1.781128	0.561442	0.06
25˚C	1	58.4	1.77	1.071622	1.773099	0.563984	0.06
35˚C	1	58.4	1.77	1.068172	1.765548	0.566396	0.06
45˚C	1	57.4	1.76	1.063970	1.757763	0.568905	0.06
55˚C	1	56.5	1.75	1.058700	1.745438	0.572922	0.06
65˚C	1	53.9	1.73	1.050781	1.711399	0.584317	0.06
75˚C	1	51.5	1.71	1.042961	1.683714	0.593925	0.06
85˚C	1	51.5	1.71	-	-	-	-
75˚C	1	57.4	1.76	1.041659	1.670166	0.598743	0.06
65˚C	1	57.4	1.76	1.048533	1.688007	0.592415	0.06
55˚C	1	58.4	1.77	1.054011	1.696645	0.589398	0.06
45˚C	1	58.4	1.77	1.059178	1.707898	0.585515	0.06
35˚C	1	58.4	1.77	1.063863	1.72071	0.581156	0.06
25˚C	1	58.4	1.77	1.067882	1.734181	0.576641	0.06
15˚C	1	58.4	1.77	1.071174	1.749099	0.571723	0.06
5˚C	1	58.4	1.77	1.073936	1.769704	0.565066	0.06

				16% wt% CuPc			
T˚C	{00*l*} orders	d_0	log d_0	ρ_{sol} (g/cm^3)	ρ_d (g/cm^3)	v_d	φ_{dc}
5˚C	1	60.4	1.78	1.071686	1.793349	0.557616	0.05
15˚C	1	58.4	1.77	1.069962	1.782982	0.560858	0.05
25˚C	1	58.4	1.77	1.067379	1.775096	0.56335	0.05
35˚C	1	58.4	1.77	1.063982	1.767845	0.56566	0.05
45˚C	1	58.4	1.77	1.059741	1.759378	0.568383	0.05
55˚C	1	57.4	1.76	1.054053	1.741938	0.574073	0.05
65˚C	1	55.6	1.75	1.043254	1.674219	0.597294	0.06
75˚C	1	53.9	1.73	1.037524	1.668267	0.599424	0.05
85˚C	1	54.7	1.74	-	-	-	-
75˚C	1	53.9	1.73	1.044734	1.748024	0.572075	0.05
65˚C	1	54.7	1.74	1.045807	1.70246	0.587385	0.05
55˚C	1	58.4	1.77	1.050816	1.70613	0.586122	0.05
45˚C	1	58.4	1.77	1.055744	1.715164	0.583035	0.05
35˚C	1	58.4	1.77	1.060153	1.725489	0.579546	0.05
25˚C	1	59.4	1.77	1.064092	1.738735	0.575131	0.05
15˚C	1	60.4	1.78	1.067345	1.754033	0.570115	0.05
5˚C	1	60.4	1.78	1.067420	1.746159	0.572686	0.05

15% wt% CuPc						
T˚C	**{00*l*} orders**	**d_0**	**log d_0**	**ρ_{sol} (g/cm³)**	**ρ_d (g/cm³)**	**v_d**	**φ_{dc}**
5˚C	1	62.5	1.80	1.067485	1.796202	0.55673	0.05
15˚C	1	62.5	1.80	1.065672	1.784158	0.560488	0.05
25˚C	1	61.4	1.79	1.063136	1.776442	0.562923	0.05
35˚C	1	60.4	1.78	1.059792	1.769536	0.56512	0.05
45˚C	1	58.4	1.77	1.055512	1.760302	0.568084	0.05
55˚C	1	58.4	1.77	1.049406	1.73708	0.575679	0.05
65˚C	1	60.4	1.78	1.035727	1.631265	0.613021	0.05
75˚C	1	58.4	1.77	1.032087	1.649944	0.606081	0.05
85˚C	1	54.7	1.74	-	-	-	-
75˚C	1	58.4	1.77	1.047809	1.835345	0.544857	0.05
65˚C	1	60.4	1.78	1.043081	1.717987	0.582077	0.05
55˚C	1	59.4	1.77	1.047621	1.71603	0.58274	0.05
45˚C	1	60.4	1.78	1.052310	1.722543	0.580537	0.05
35˚C	1	60.4	1.78	1.056443	1.730043	0.57802	0.05
25˚C	1	60.4	1.78	1.060302	1.743022	0.573716	0.05
15˚C	1	62.5	1.80	1.063516	1.758733	0.568591	0.05
5˚C	1	62.5	1.80	1.060904	1.718596	0.58187	0.05

CHAPTER EIGHT

8. Black Azo Dye

8.1 Structure of Black Azo Dye

The general formula for making an azo dye requires two organic compounds- a coupling component and a diazo component. Since these can be altered considerably, an enormous range of possible dyes are available, especially as the starting molecules are readily available and cheap. Furthermore, the simplicity of the reactions mean that the process can be scaled up or down very easily. Energy requirements for the reaction are low, since most of the chemistry occurs at or below room temperature. The environmental impact is reduced by the fact that all reactions are carried out in water, which is easy and cheap to obtain, clean and dispose of. All these factors make azo dyes very cheap to produce.

The black dye used for the aggregation studies is a typical representative of an azo dye organic molecule. The structure can be schematically represented in the following way,
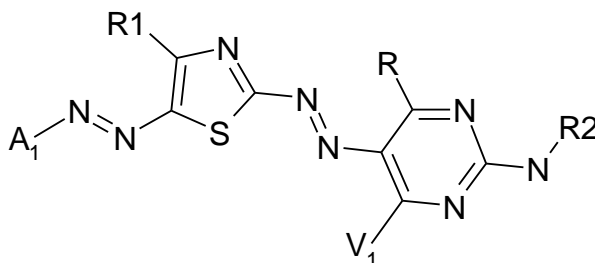
Figure 8.1 **Molecular structure for the black dye.**

where A_1 represents a tri − substituted heterocyclic group; R standing for the aliphatic group, V_1 is the substituted aryl group; R_1 representing a heterocyclic group and R_2 standing for aryl − sulphonated group. This dye has 5 solubilising sulphonic groups attached to periphery of the dye molecule with the counter ion for the ionic hydrophilic groups being a lithium ion. The analysis and explanation of the experimental data along with calculations based on the results were carried out using this chemical structure [145].

The dye is highly soluble in water. The molecular weight used for calculations was 1127 including the molecular weights of 5 solubilising groups arranged around the periphery of the azo dye molecule.

8.2 Optical Microscopy

Optical Microscopy was used in order to investigate the phase behaviour of the black dye in aqueous solution and to build the phase diagram. A 10% wt/wt% dye solution was studied under the optical microscope and was observed to be isotropic at 23.2°C. This sample then was left under the microscope for a peripheral evaporation scan as it allows easy recognition of the phases within the samples of the black dye on slow evaporation of the solvent. The phase behaviour expected for this dye at the nematic - hexagonal transition of the resulting concentration gradient has previously been predicted through the knowledge of the chromonic phase behaviour. A phase evaporation scan for this dye had been completed to see if the phases were as expected. It revealed the appearance of birefringent regions in the isotropic bulk on slow evaporation of solvent, which indicated the formation of a liquid crystalline phase (Figure 8.2a). Further evaporation of water allowed these areas of birefringence to merge together leading to a formation of a bulk nematic phase (Figure 8.2b).

a   b
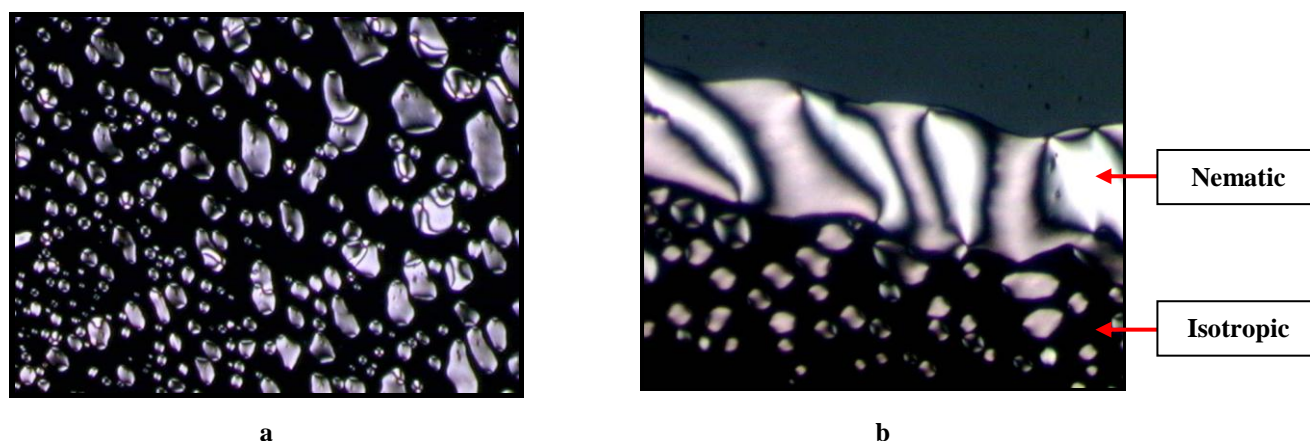
Figure 8.2   **The polarising micrographs of aqueous solution of the black dye on the appearance of the birefringent droplets (a), on the formation of the nematic phase (b) (magnification × ca. 100).**

Further evaporation of solvent caused the development of an outer region around the still progressing nematic phase, which corresponded to the more concentrated hexagonal phase. There was no sharp boundary observed between the nematic and hexagonal phases (Figure 8.3).
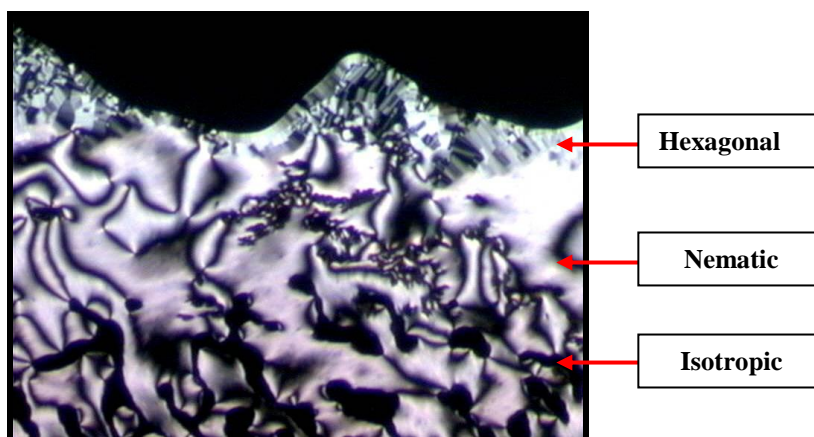
Figure 8.3   **Optical textures for black dye observed on evaporation scan (magnification ×
ca. 100). Labels refer to the liquid crystalline phases formed.**

The phase diagram of black dye / water is shown in Figure 8.4. The samples of dye solutions in the 15 – 29% wt/wt% dye concentration range were heated to 90°C and then subsequently cooled to 2°C at a rate of 2°C / min on a microscope slide to observe phase transitions during 3 heat / cool cycles. The sequence of phases and temperature changes is similar to those previously observed for other chromonic materials and for Cu-phthalocyanine dye in particular, which gives a clear indication of the overall peritectic form of the temperature / concentration phase diagram as shown in Figure 8.4.
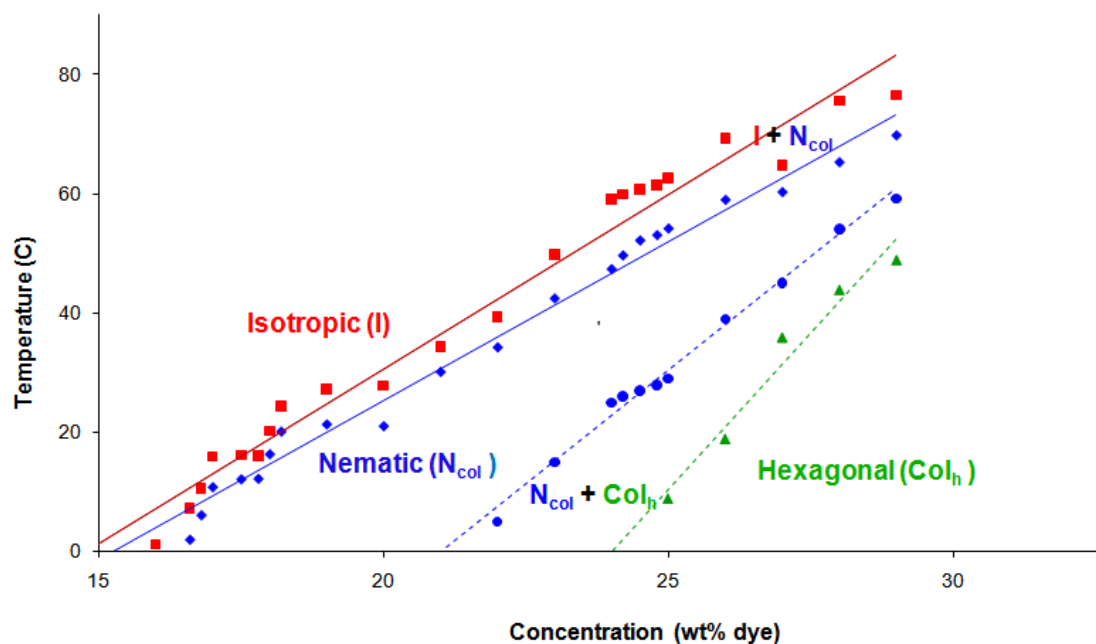
Figure 8.4 **Phase diagram of the black dye in aqueous solution.**

Examination of the solutions at higher concentration showed that nucleation of the liquid crystalline phase started at 15% wt/wt% dye with the small birefringent droplets appearing at 2.9°C and melting with the increase of temperature. When the concentration was increased the observed optical texture of the bulk phase formed had a schlieren appearance, which was characteristic of the chromonic nematic (N_{col}) phase (Figure 8.5). The temperature stability of the nematic phase clearly increased as the concentration was raised.

Figure 8.5 **Nematic phase observed for 21% wt/wt% black dye at 21.8°C (magnification ×
ca. 200).**

By further increasing the concentration the appearance of the nematic phase changed and appeared in the form of the "herringbone texture" (Figure 8.6a), which indicated the formation of the more ordered hexagonal phase (Col$_{h)}$. It is worth noting that the term "herringbone" is used for chromonic mesophases in two different contexts: on a molecular level it illustrates the transversal packing of the stacks in the hexagonal phase (Figure 8.6b), and additionally it describes the striped optical texture of the hexagonal phase (Figure 8.6a) formed on increasing the concentration of the dye within the nematic phase. As the hexagonal phase is developed, the stacks become packed closer to each other and increase in length. The phenomena can be attributed to the fact that it is thermodynamically easier to extend a column than to create a new one [41].

a   b
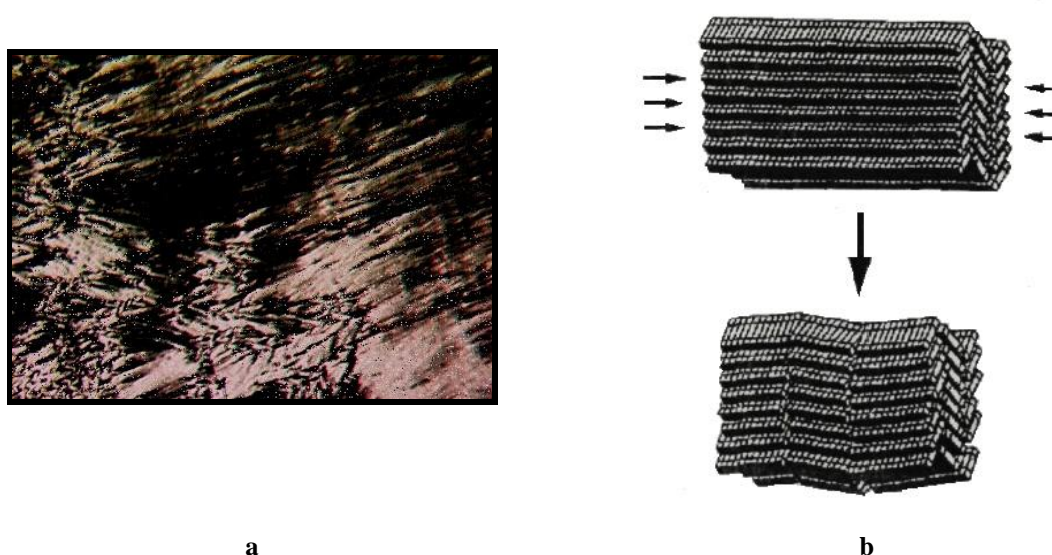
Figure 8.6   **The herringbone texture observed for 28% wt/wt% black dye at 21.5°C**
(magnification × ca.100) (a); and the origin of the herringbone texture of the
hexagonal mesophase [41] (b).

There were no major texture changes observed on cooling once the transition from nematic to hexagonal phase was complete. The herringbone texture remained stable throughout the range of concentrations exhibiting the hexagonal phase on cooling the samples to 0°C.

On heating the hexagonal phase the thin stripes of the herringbone texture became larger, which resulted in the appearance of a texture similar to that of a mosaic one as shown

in Figure 8.7. This texture indicated the presence of the two – phase (Col_h + N_{col}) region, which exists in a 10 - 15°C temperature range.

Figure 8.7   **Mosaic texture appearing on heating the hexagonal sample of 26% wt/wt% black dye at 20°C (magnification × ca.200).**

The transition from hexagonal to a nematic phase was very subtle resulting in difficulties in obtaining accurate temperature measurements at the transition point. Small – angle X-ray diffraction results were used for displaying the boundaries for the nematic – hexagonal transition (Figure 8.4, dotted lines).

When the nematic phase was heated, it passed into the two-phase region where the isotropic regions were surrounded by the nematic threads forming a texture more or less reminiscent of the reticulated one (Figure 8.8).

Figure 8.8   **Melting of the nematic phase observed for 26% wt/wt% black dye at 57°C on heating (magnification × ca. 100).**

On further heating the nematic phase melted and passed into the isotropic region. The N_{col} - I transition temperature depended on dye concentration and increased as the solution got more concentrated. The phase diagram includes a narrow 5-7°C biphasic region where the nematic (N_{col}) and isotropic phases coexist (Figure 8.4).

On the subsequent cooling, the I - N_{col} transition occurred in the form of isolated drops, which grew bigger and merged together indicating the formation of the nematic phase (Figure 8.9).

Figure 8.9   **Formation of the nematic phase on cooling 26% wt/wt% black dye at 55°C (magnification × ca. 100).**

For this dye the phases do not form and melt at the same temperature with heating and cooling. There is a difference of ≈ 1 - 2°C between cycles. For example on heating 24.5% wt/wt% black dye the N_{col} phase melted at 54°C yet formed at 52°C on cooling. This decrease in temperature is attributed to the polydispersity of the dye and resultant non-equilibrium effects. The average of the transition temperatures during heating and cooling were used for the construction of the phase diagram.

In summary, the observed textures and the sequence of phases exhibited by the black dye followed the phase sequence observed for other chromonic systems and the Cu-phthalocyanine dye in particular. The textures observed formed an excellent starting point for the identification of the mesophases formed by the black dye. Further studies of the phase behaviour of the black dye were carried out by wide - and small – angle X-ray diffraction studies.

8.3 X-ray Diffraction

To re-iterate from previous chapters, synchrotron radiation at Daresbury Laboratories, Warrington, UK was used for the X-ray diffraction (XRD) studies for both wide – angle (WAXS) and small – angle X-ray scattering (SAXS). The details of experimental work are covered in sections 4.3.3.1 and 4.3.3.2.

8.3.1 Wide – angle X-ray Diffraction (WAXS)

Wide – angle X-ray diffraction was used in order to obtain the internal parameters of the stacks formed by the black dye. A sample was placed into a Lindemann tube, which then was heated and cooled from 5°C to 95°C at a rate of 10°C per minute. A scan was taken every 10°C (for clarity purposes only the certain scans are discussed in this chapter). A typical wide – angle X-ray diffraction pattern observed for the black dye in aqueous solution is shown in Figure 8.10 and it was composed of 3 features. The first reflection was observed close to the central beam stop and corresponded to the long – range distances within the phase formed.
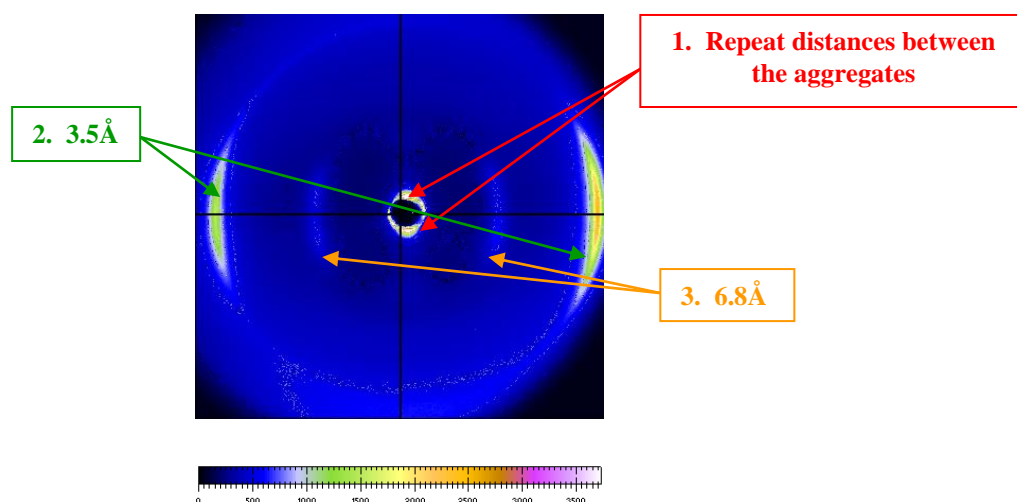
Figure 8.10 **Wide – angle X-ray diffraction pattern of 25% wt/wt% black dye at 45°C.**

The second feature was observed at ca. 3.5 Å and represented the thickness of the aromatic molecule, hence the repeat distance between two adjacent black dye molecules

within the stack. This reflection was observed at the whole range of temperatures and concentrations for the black dye and for other chromonic systems on packing of polycyclic molecules in aggregates [37, 42, 146]. It varied slightly with changes in temperature and concentration in the range of ca.3.5 – 3.6 Å (ca. 3%). It is also worth mentioning that this reflection was also present in the X-ray spectra of the powders of the dried dyes [147]. Interestingly, in addition to the 3.5Å line due to π- π stacking, another wide-angle reflection at 6.8 Å was observed (Figure 8.11), which was very weak and suggested a head-to-tail packing of the molecules within the stacks [44]. The 6.8 Å was not observed for the Cu-phthalocyanine system, which may be due to the circular cross-sectional area of the cyan dye molecules. This reflection did not vary with changes in temperature and concentration. In conclusion these two wide-angle reflections are believed to represent an integral part of the stack.
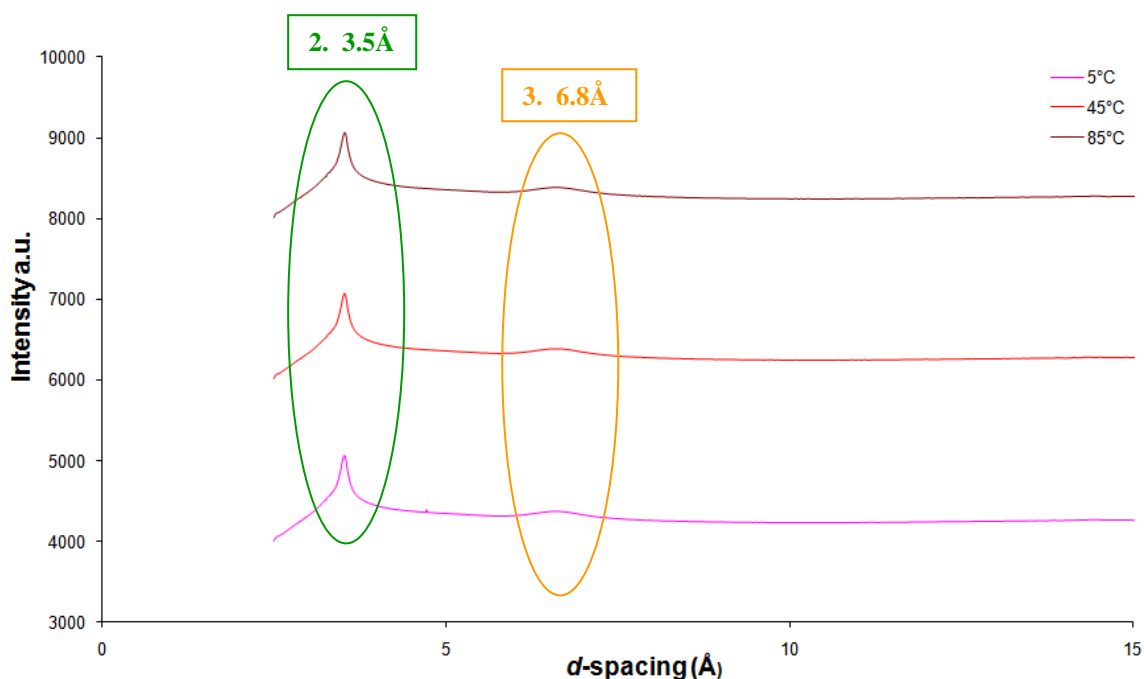
Figure 8.11   **Wide-angle X-ray diffraction patterns for the black dye 25% wt/wt% as a function of temperature over the heating run. Two reflections are always present over the studied range of temperatures and concentrations.**

The first reflection corresponding to the repeat distances between the aggregates appeared in the form of a pair of equatorial arcs and came at 90° to the second and the third axial reflections produced by the intra-aggregate repeat. Therefore, the second and the third

153

wide – angle reflections in relation to the first one confirmed the perpendicular arrangement of the inter- and intra-aggregate spacings.

8.3.2   Small – angle X-ray Diffraction (SAXS)

Small – angle X-ray diffraction (SAXS) was used in order to identify the liquid crystalline phases along with determination of the structure of aggregates. The system was studied over 15 – 29% wt/wt% dye concentration range on heating and cooling. The d spacings were calculated from the experimental spectra parameters measured over the temperature range 5° - 85°C at 10°C intervals are summarised in Table 8.1 at the end of this section. The important results are presented below in Figures 8.12 – 8.22 and describe the changes within the long-range order of the black dye with temperature and concentration.

The small - angle diffraction patterns were composed of concentric rings of Bragg reflections from poorly aligned domains of mesophase. The mesophase alignment with the capillary walls occurred on storage. The samples were prepared and packed into capillaries approximately a week before the data collection in Daresbury. The position of the diffraction arcs show that the aggregates are all oriented with their long axes perpendicular to the length of the Lindemann capillary (Figure 8.12).
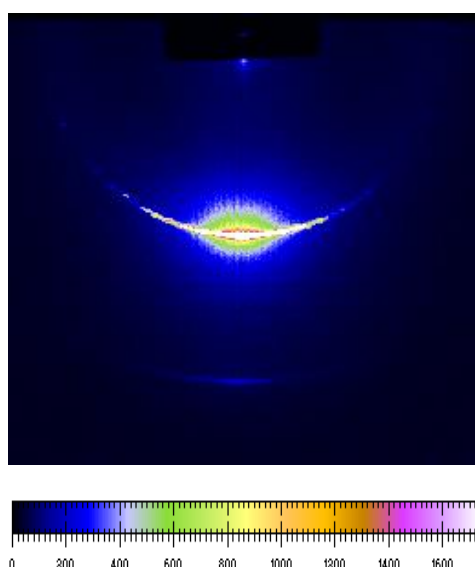
Figure 8.12   **Small – angle X-ray diffraction for 29% wt/wt% black dye at 5°C.**

154

The first and the most intense reflection observed in the small-angle region is the first (d_0) order repeat, which is suggested to be originated from the repeat distances of the lattice accommodating the aggregates in unoriented mesophases. The intensity and sharpness of this peak are associated with the extent of the long range periodical separations within the phase formed (Figure 8.13). The majority of the diffraction patterns for the dye concentrations higher than 25% consisted of two orders of reflection. The ratio of a higher order to a first order diffraction peak is in excellent agreement with the ratio of d_0: d_0/3, which suggests the formation of the hexagonal phase at higher concentrations, although this lattice must be imperfect, which is proved by the small number of the reflections observed [55]. One of the reasons of this crystalline lattice being deficient is the exponential character of aggregates distribution on their size [48]. This distribution is characterised by wide polydispersity and the presence of a large number of aggregates of a small length (along with very long aggregates).

By contrast, below 25% wt/wt% dye the first order peak appears to be broader and less intense with no higher orders observed (Figure 8.13). Low intensity of the peaks along with the diffuse nature of reflections and a decrease in the number of orders observed suggests the occurrence of phase transition with the subsequent disordering of the system. The nematic phase forms at lower concentrations with no positional ordering between the aggregates, therefore, such a lattice must be very irregular with the broad range of repeats within this lattice.
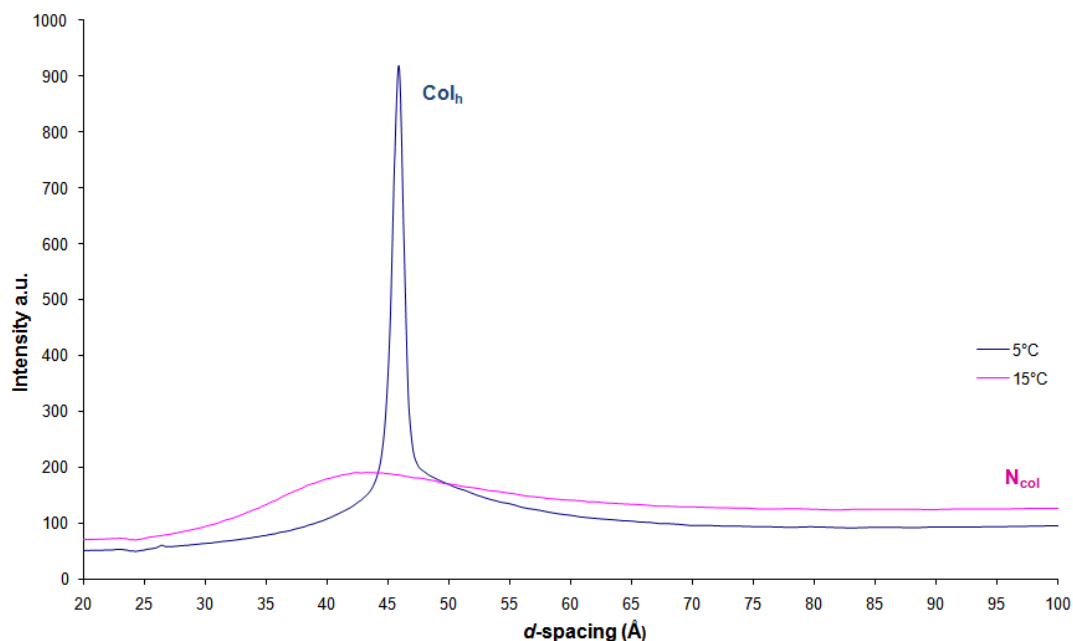
Figure 8.13 **The small-angle X-ray diffraction patterns for 25% wt/wt% black dye showing the difference in spectral patterns for Col$_h$ (blue) and N$_{col}$ (pink).**

The inter-aggregate distances were calculated over the whole range of concentrations and Figure 8.14 clearly displays the decreasing tendency of column – to – column separations with the increase of concentration. At higher concentrations the number of aggregates is expected to be higher, the stacks pack closer to each other resulting in the smaller value of the repeat distance within the hexagonal lattice.
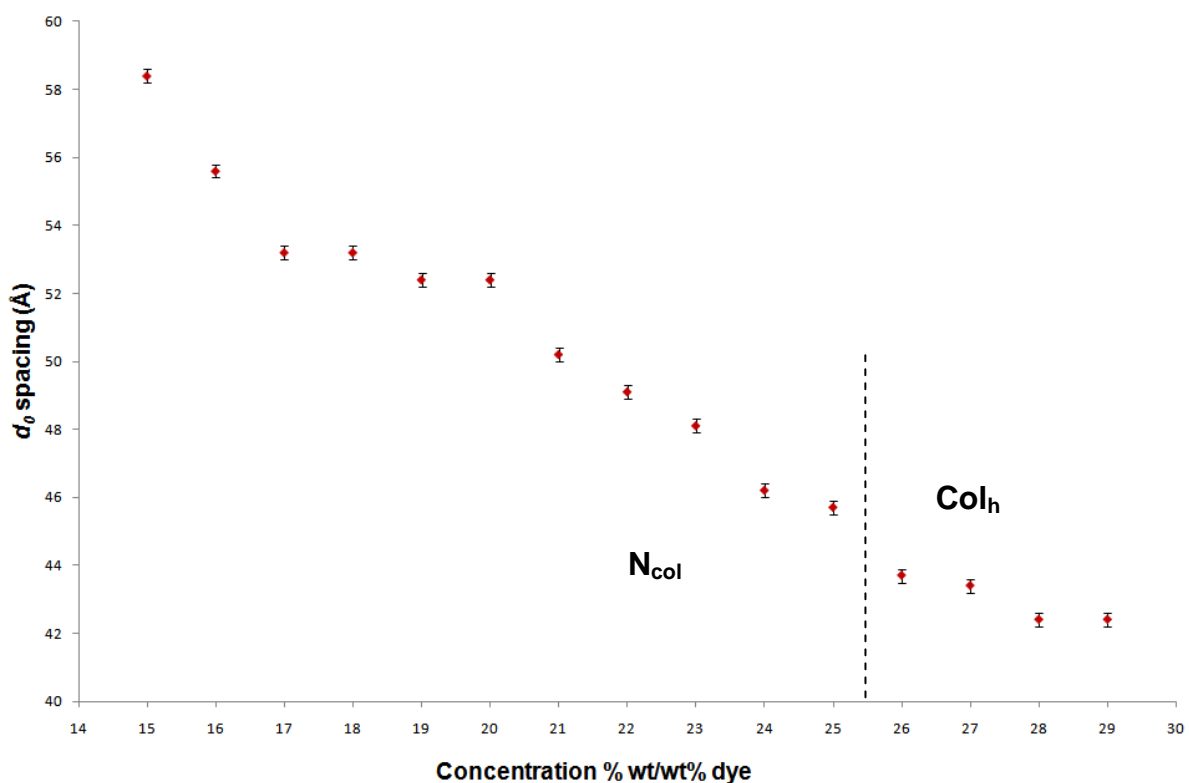
Figure 8.14   **Variation of inter-stacking separation ($d \pm 0.2$Å) as a function of concentration at 25°C exhibited by black dye within the N_{col} and Col_h phase.**

The black dye system was also studied by small-angle X-ray diffraction over a range of temperatures. Calculated values of the inter-stack spacings as a function of temperature are summarised in Table 8.1.

For the highest concentration studied (29% wt/wt% dye) the sharp first and second order diffraction peaks are observed for the temperatures up to 65°C on heating (Figure 8.15). The ratio of d_0 / d_1 is an excellent agreement with the ratio indicating the formation of the hexagonal phase (1:√3). The sharpness of the first order peak along with its intensity gradually decreases on heating and eventually this peak becomes diffuse at 75°C (Figure 8.16 a, b). The sharpness of the first order peak is due to the distances between the aggregates in the hexagonal phase being well-defined and constrained by the lattice. The first order observed within the concentrations exhibiting the hexagonal phase represents the distance between the planes of the aggregates and not the distance between the aggregates.
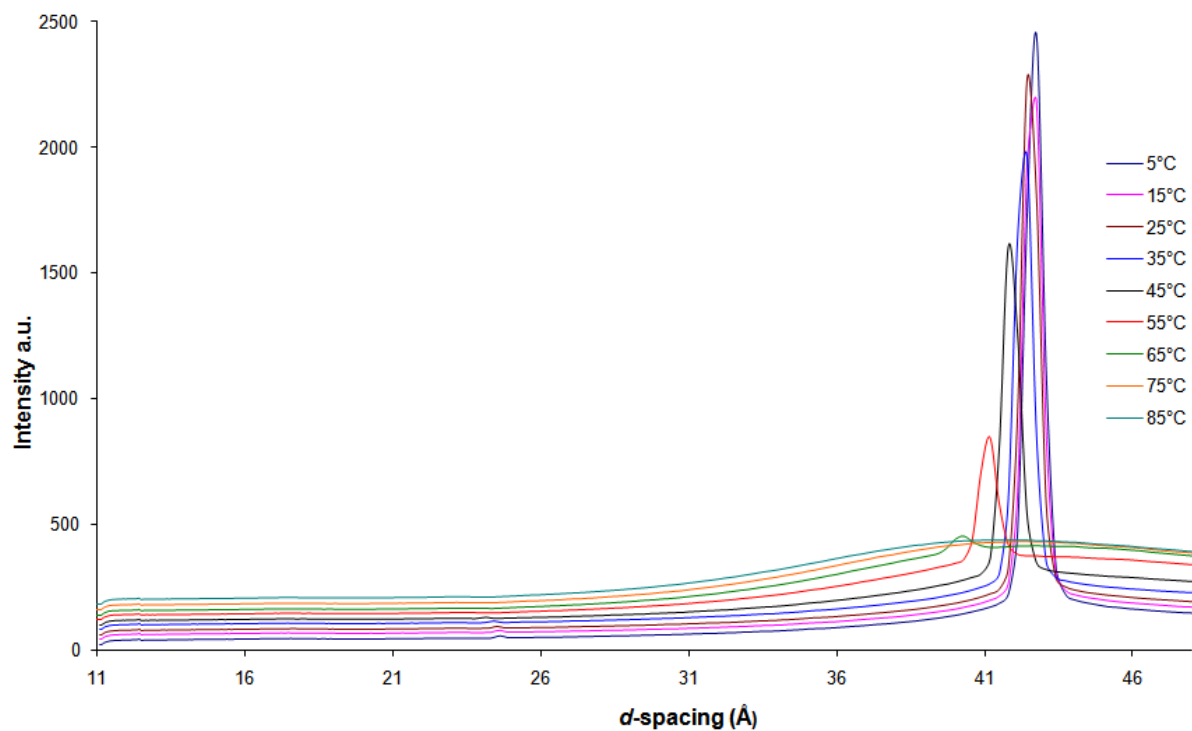
Figure 8.15   Small – angle diffraction patterns for 29% wt/wt% black dye on heating in the Col$_h$ phase (5° - 65°C) and N$_{col}$ phase (75° - 85°C).

.
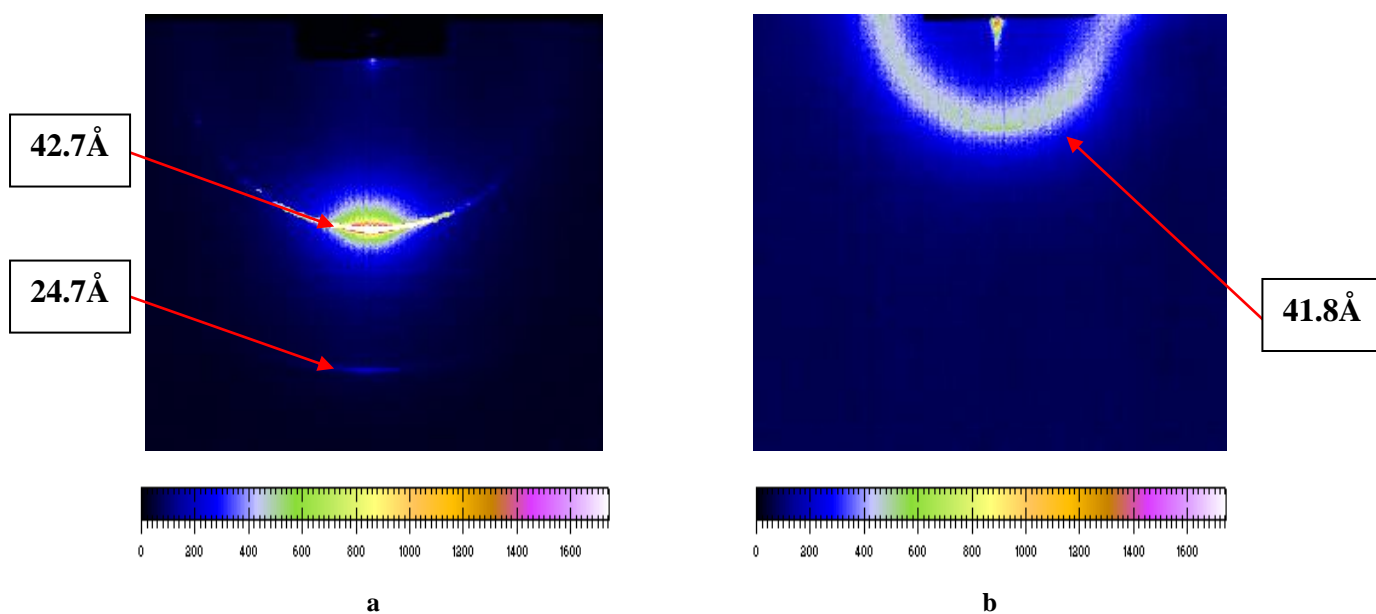
Figure 8.16   Small – angle X-ray diffraction for an unaligned sample of 29% wt/wt% black dye at 5°C (a) and 85°C (b).

The *d*-spacing values become smaller with the increase of temperature within the boundaries of the same phase (Figure 8.17), implying the reduction in the size of the stacks, larger number of stacks and the closer distance between the stacks.
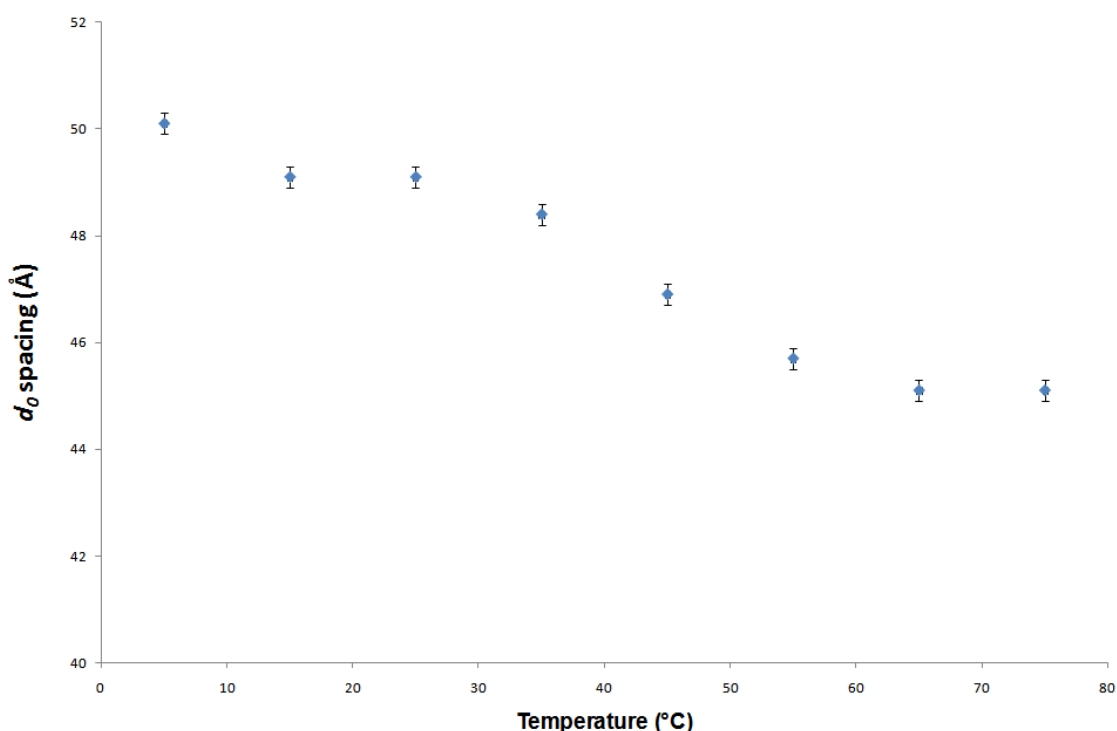
Figure 8.17   **Variation of inter-stacking separation (*d* ±0.2Å) as a function of temperature exhibited by black dye for 22% wt/wt%. N_{col} phase was stable over the studied range of temperatures (5°C - 75°C).**

However, with the changes in diffraction patterns on further heating the *d*-spacing values increase with the first order peak becoming broad along with the lack of any well-defined higher order peaks (Figures 8.18, 8.19). This implies the occurrence of the phase transition with the changes of aggregates packing from hexagonal into a nematic-like array. The *d*-spacing measured by small-angle X-ray diffraction now represents the distances between the separate bundles of the stacks within the nematic phase. Optical microscopy reveals that this transition appears to be gradual. Therefore, to study the nature of this transition in greater details on heating and cooling the small-angle X-ray diffraction measurements should be taken in much smaller temperature steps.
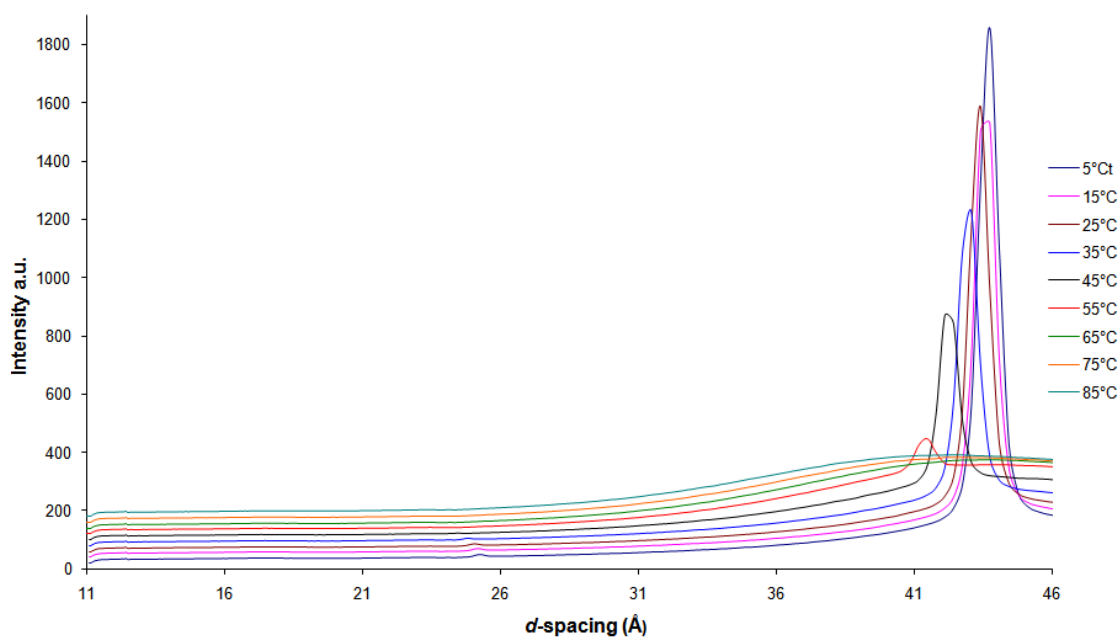
Figure 8.18   Small – angle diffraction patterns for 27% wt/wt% black dye on heating: Col_h phase (5° - 55°C) and N_{col} phase (65° - 85°C).
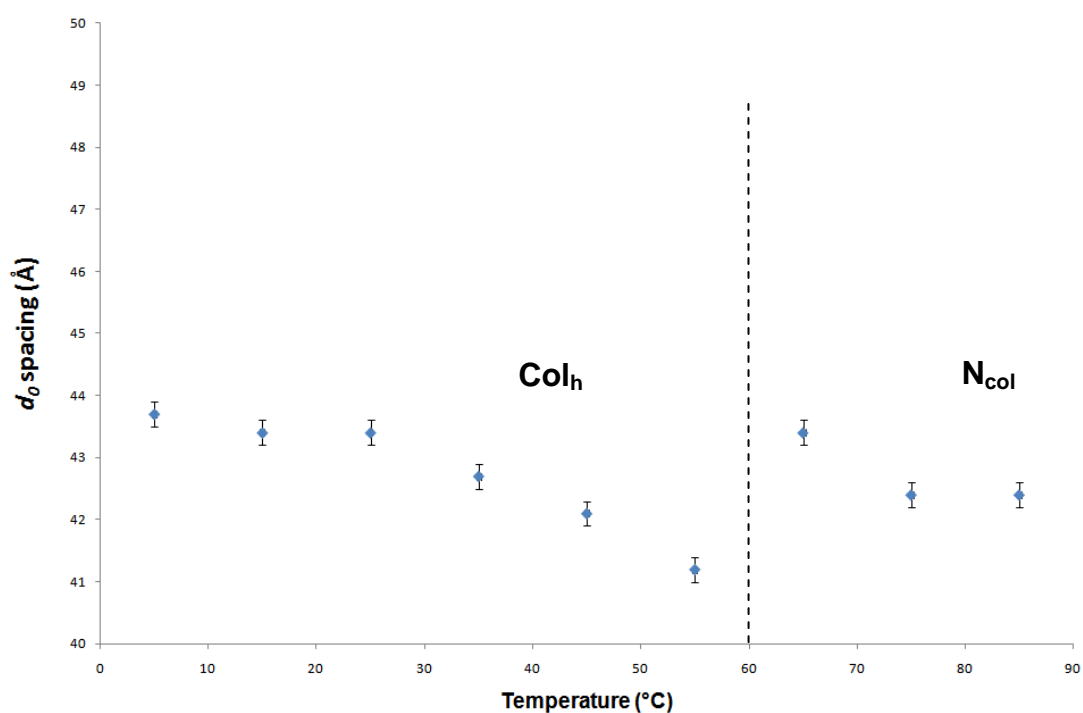
Figure 8.19   Variation of inter-stacking separation (d ±0.2Å) as a function of temperature exhibited by black dye for 27% wt/wt%.

On further dilution and at elevated temperatures the isotropic phase forms, which is accompanied by a complete loss in order of the system.

The interesting results were obtained for 25% wt/wt% when the hexagonal – nematic transition occurred over the range of 25° - 35°C temperatures on heating. However, on cooling this sample from 75°C down to 5°C the hexagonal symmetry did not appear again (Table 8.1, Figures 8.20, 8.21).
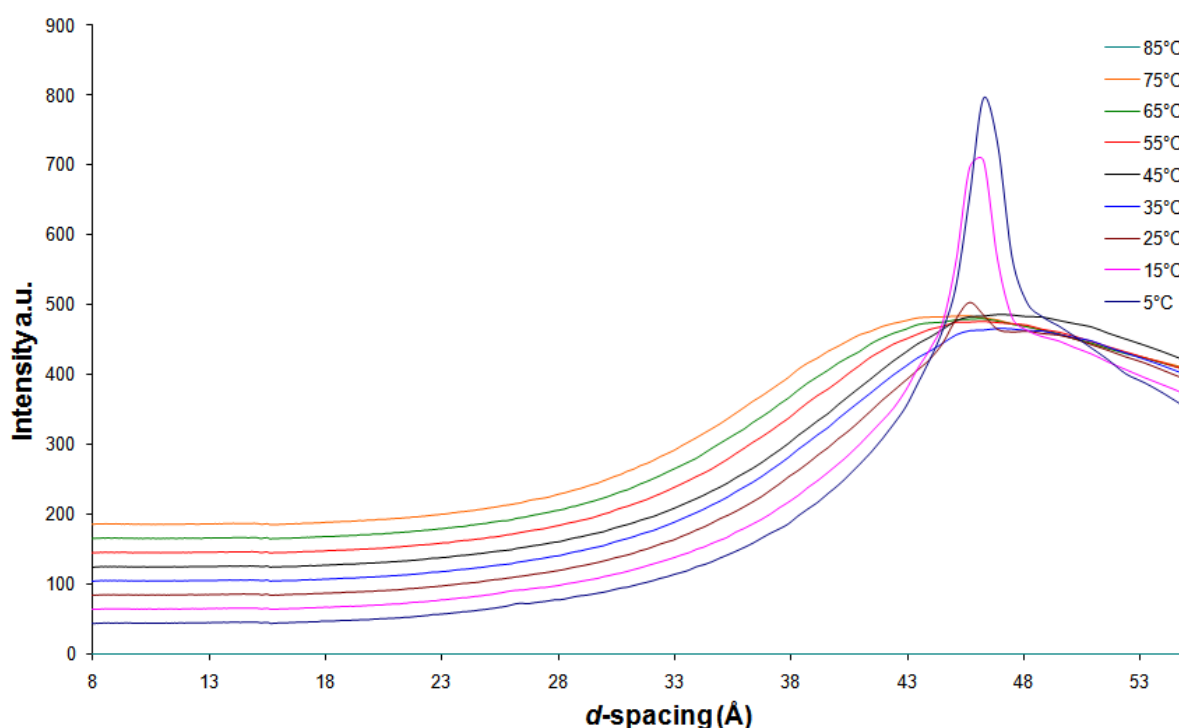
Figure 8.20   **The small – angle X-ray diffraction patterns for 25% wt/wt% black dye on heating Col$_h$ phase (5° - 15°C), Col$_h$ + N$_{col}$ coexisting region (25°C) and N$_{col}$ phase (35° - 85°C).**

.
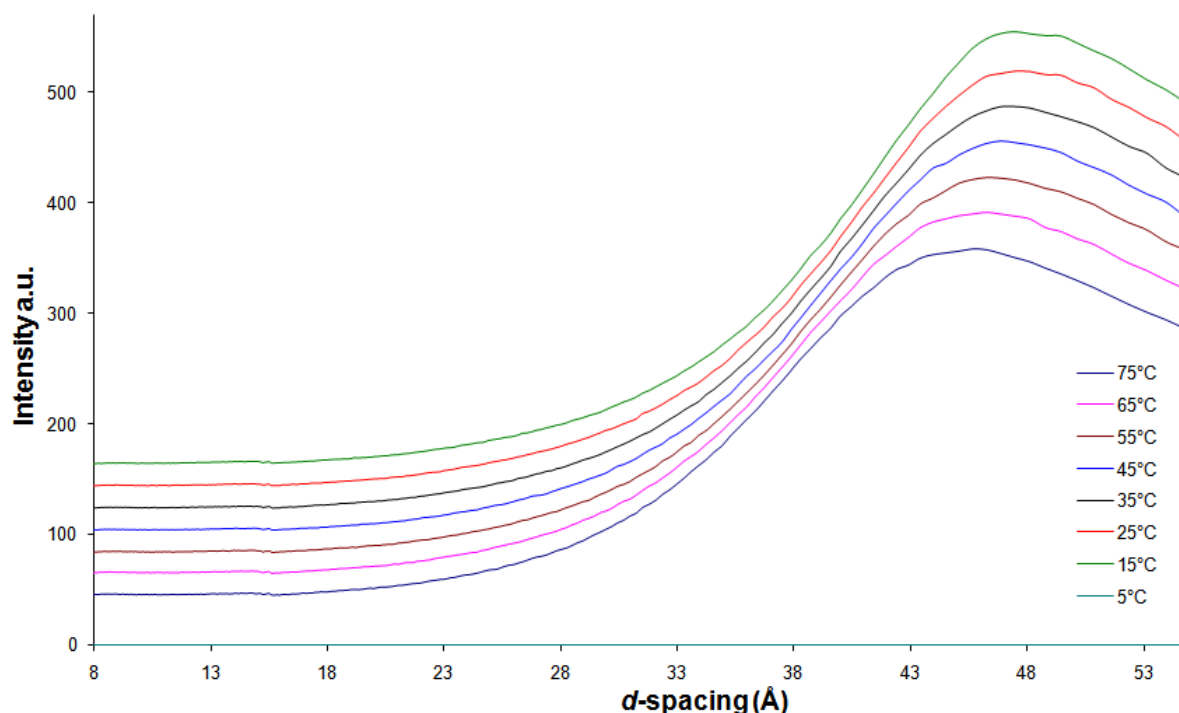
Figure 8.21   **The small – angle X-ray diffraction patterns for 25% wt/wt% black dye on cooling, N_{col} phase was stable over the studied range of temperatures (5°C - 75°C).**

It implies that there is a certain level of hysteresis present and the system is much slower to reorder back into the hexagonal lattice from the nematic – like array. It can also be observed by monitoring the changes in viscosity within the time. A sample exhibiting the hexagonal ordering of aggregates appeared to be viscous if left on the bench for some time after preparation. However, the viscosity changed on shaking resulting in a fluid-like state. It usually took several hours for the mesophase to return to its initial viscosity state. This observation is similar to the one observed by optical microscopy and demonstrates the slow reordering of the aggregates on cooling the sample from the high temperatures. This phenomenon also suggests that the aggregates become smaller in size on agitation of the mesophase, which destabilises the hexagonal phase resulting in the sample looking less viscous. However, when the sample is left for some time the aggregates increase in size and reorder back slowly.

The small – angle X-ray diffraction results can then be employed in conjunction with the density data in order to elucidate the structural parameters of the hexagonal mesophase. The method described in section 7.2 was employed for calculating the diameter of the black dye aggregates. The hydrophilic groups were assumed to be in aqueous solution and in order to subtract these moieties the dye concentrations were multiplied by 0.61 for the whole range

of concentrations studied. The diameters and molecular cross – sectional areas are summarised in Table 8.1. The cross – sectional area calculated was approximately 180 Å, however, due to the complexity of the molecular structure it was difficult to subtract precisely the areas occupied by a solvent along with the hydrophilic moieties. Yet the calculated value of cross – sectional area when compared with the actual area gives a clear indication of the aggregates comprised of unimolecular dye stacks.
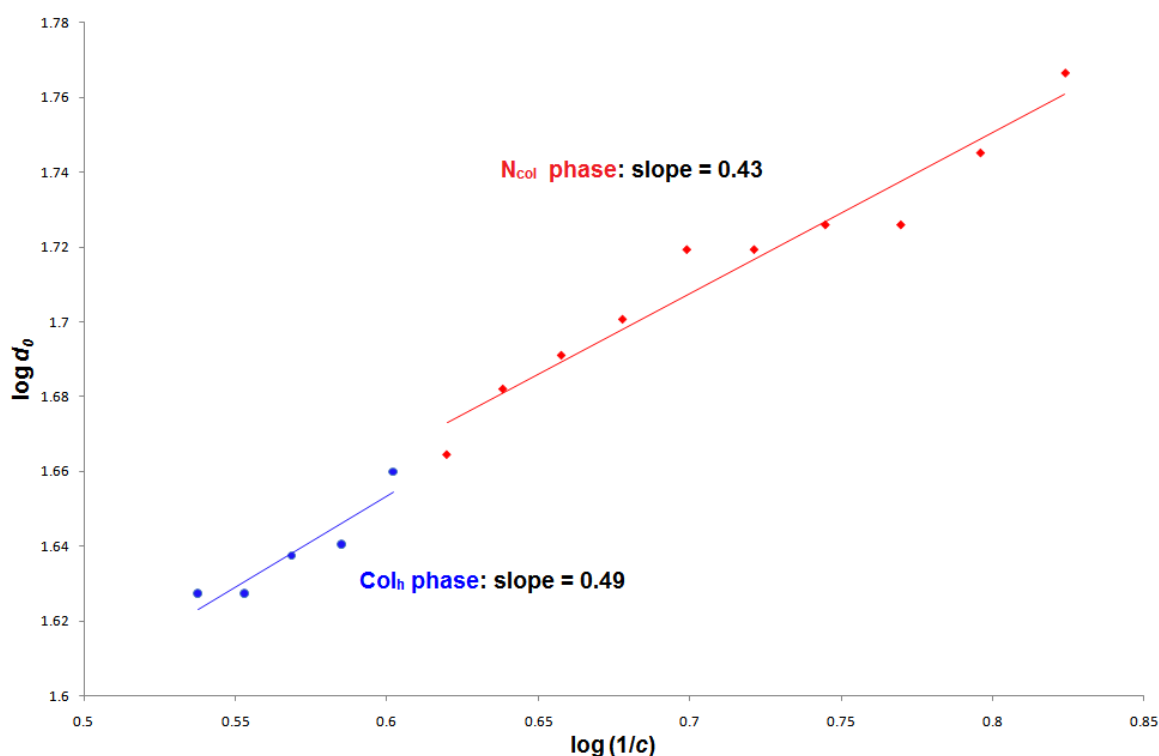
Figure 8.22   **Log d_0 against log (1/c) for black dye.**

Figure 8.22 displays a plot of log d_0 versus log 1/concentration. A straight line in blue colour represents a line of the best fit for the hexagonal mesophase and in red for the nematic one. The experimental data satisfactorily fit these straight lines (correlation coefficient R^2 equal to 0.9 for hexagonal phase and 0.94 for the nematic one). The tangents of the slopes of these straight lines are equal to 0.49 for the columnar hexagonal mesophase and 0.43 for the nematic phase. The gradient for the hexagonal phase is close to the expected value of 0.5 for two – dimensional swelling of hexagonal mesophases. However, for the nematic phase the gradient differs slightly suggesting a relative disorder of the bundles of aggregates within the nematic phase.

These wide – and small – angle X-ray diffraction studies reveal that the shape of the dye molecule plays a significant role in the way the molecules are organised within the stacks. Cu-phthalocyanine dye possesses a circular molecular shape, which gives P-phase behaviour hence the absence of 6.8 Å reflection. However, this reflection was present for the whole range of temperatures and concentrations studied for black dye with its plank-like molecular structure. It suggests that the molecules are packed on the top of each other in a head-to-tail arrangement. A possible configuration for the dimers within the aggregates can be proposed on the basis of further studies by proton nuclear magnetic resonance.

Table 8.1   **Inter-aggregate parameters for black dye for various concentrations and temperatures. Data derived from SAXS XRD.**

					29% wt% black dye							
T°C	**{00l} orders**	d_0	$d_0/\sqrt{3}$	*comms*	**log d_0**	a	ρ_{sol} (g/cm³)	ρ_d (g/cm³)	v_d	φ_{dc}	d_{dc}	S_{dc} (Å²)
5°C	2	42.7	24.7	peak	1.63	49.3	1.146536	1.828523	0.54689	0.11	16.8	149.7
15°C	2	42.4	24.5	peak	1.63	49.0	1.143358	1.814582	0.551091	0.11	16.7	151.4
25°C	2	42.4	24.5	peak	1.63	49.0	1.139197	1.800627	0.555362	0.11	16.8	152.2
35°C	2	42.4	24.5	peak	1.63	49.0	1.134924	1.790496	0.558504	0.11	16.8	152.9
45°C	2	41.8	24.1	peak	1.62	48.3	1.130633	1.784018	0.560532	0.11	16.5	155.7
55°C	2	41.2	23.8	peak	1.61	47.6	1.125907	1.778334	0.562324	0.11	16.3	158.5
65°C	2	40.3	23.2	peak	1.61	46.5	1.120896	1.773932	0.563719	0.11	15.9	162.7
75°C	2	41.8	-	diffuse peak	1.62	-	1.115665	1.770921	0.564678	0.11	-	-
85°C	1	41.8	-	diffuse peak	1.62	-	1.110048	1.768165	0.565558	0.11	-	-
75°C	1	42.1	-	diffuse peak	1.62	-	1.115678	1.770994	0.564655	0.11	-	-
65°C	1	42.7	-	diffuse peak	1.63	-	1.120914	1.774034	0.563687	0.11	-	-
55°C	2	40.6	23.1	peak	1.61	46.9	1.125933	1.778481	0.562278	0.11	16.1	160.9
45°C	2	41.2	23.8	peak	1.61	47.6	1.130658	1.784159	0.560488	0.11	16.3	157.9
35°C	2	41.8	24.1	peak	1.62	48.3	1.134941	1.790592	0.558475	0.11	16.5	155.1
25°C	2	41.8	24.1	peak	1.62	48.3	1.139208	1.800689	0.555343	0.11	16.5	154.4
15°C	2	42.1	24.3	peak	1.62	48.6	1.143372	1.814661	0.551067	0.11	16.6	152.5
5°C	2	42.4	24.5	peak	1.63	49.0	1.146571	1.82872	0.54683	0.11	16.7	150.7

					28% wt% black dye							
T°C	**{00l} orders**	d_0	$d_0/\sqrt{3}$	*comms*	**log d_0**	a	ρ_{sol} (g/cm³)	ρ_d (g/cm³)	v_d	φ_{dc}	d_{dc}	S_{dc} (Å²)
5°C	2	42.7	24.6	peak	1.63	49.3	1.138623	1.811785	0.551942	0.10	16.5	153.3
15°C	2	42.4	24.5	peak	1.63	49.0	1.135255	1.796265	0.556711	0.10	16.5	155.2
25°C	2	42.4	24.5	peak	1.63	49.0	1.130979	1.781212	0.561416	0.10	16.5	156.1
35°C	2	42.4	24.4	peak	1.63	49.0	1.126628	1.77037	0.564854	0.10	16.6	156.8
45°C	2	41.8	24.1	peak	1.62	48.3	1.122350	1.763873	0.566934	0.10	16.3	159.7
55°C	2	41.2	23.5	peak	1.61	47.6	1.117588	1.757936	0.568849	0.10	16.1	162.6
65°C	2	40.3	23.1	peak	1.61	46.5	1.112426	1.752677	0.570556	0.10	15.7	166.9
75°C	2	42.1	-	diffuse peak	1.62	-	1.107155	1.749528	0.571583	0.10	-	-
85°C	1	41.8	-	diffuse peak	1.62	-	1.101372	1.745925	0.572762	0.10	-	-
75°C	1	42.1	-	diffuse peak	1.62	-	1.107171	1.749621	0.571552	0.10	-	-
65°C	1	42.7	-	diffuse peak	1.63	-	1.112447	1.7528	0.570516	0.10	-	-
55°C	2	40.6	23.3	peak	1.61	46.9	1.117599	1.758001	0.568828	0.10	15.8	165.0
45°C	2	41.2	23.8	peak	1.62	47.6	1.122373	1.764008	0.566891	0.10	16.1	162.0
35°C	2	41.8	24.0	peak	1.62	48.3	1.126641	1.770446	0.564829	0.10	16.3	159.0
25°C	2	41.8	24.1	peak	1.62	48.3	1.130993	1.781294	0.56139	0.10	16.3	158.3
15°C	2	42.1	24.2	peak	1.62	48.6	1.135271	1.796359	0.556682	0.10	16.4	156.3
5°C	2	42.4	24.3	peak	1.63	49.0	1.138641	1.81189	0.55191	0.10	16.4	154.4

27% wt% black dye												
$T°C$	$\{00l\}$ orders	d_0	$d_0/\sqrt{3}$	*comms*	log d_0	a	ρ_{sol} (g/cm³)	ρ_d (g/cm³)	v_d	φ_{dc}	d_{dc}	S_{dc} (Å²)
5°C	2	43.7	25.2	peak	1.64	50.5	1.130635	1.793352	0.557615	0.10	16.7	153.6
15°C	2	43.4	25.1	peak	1.64	50.1	1.127644	1.7795787	0.5619308	0.10	16.6	155.4
25°C	2	43.4	24.9	peak	1.64	50.1	1.124202	1.7691074	0.5652568	0.10	16.6	156.1
35°C	2	42.7	24.7	peak	1.63	49.3	1.120875	1.7641929	0.5668314	0.10	16.4	159.1
45°C	2	42.1	24.3	peak	1.62	48.6	1.116688	1.7581497	0.5687798	0.10	16.1	161.9
55°C	2	41.2	24.0	peak	1.61	47.6	1.111827	1.7515593	0.5709199	0.10	15.8	166.2
65°C	1	43.4	-	diffuse peak	1.64	-	1.106480	1.7451726	0.5730092	0.10	-	-
75°C	1	42.4	-	diffuse peak	1.63	-	1.101057	1.741195	0.5743182	0.10	-	-
85°C	1	42.4		diffuse peak	1.63	-	1.094625	1.7337487	0.5767849	0.10	-	-
75°C	1	42.7	-	diffuse peak	1.63	-	1.101103	1.7414743	0.5742261	0.10	-	-
65°C	1	43.7	-	diffuse peak	1.64	-	1.106489	1.7452272	0.5729913	0.10	-	-
55°C	2	44.1	24.0	peak	1.64	50.9	1.111849	1.7516929	0.5708763	0.10	16.9	155.2
45°C	2	41.8	24.1	peak	1.62	48.3	1.116704	1.7582469	0.5687484	0.10	16.0	163.1
35°C	2	42.4	24.5	peak	1.63	49.0	1.120898	1.7643326	0.5667866	0.10	16.3	160.2
25°C	2	42.7	24.7	peak	1.63	49.3	1.124233	1.7692956	0.5651967	0.10	16.4	158.6
15°C	2	43.1	24.8	peak	1.63	49.8	1.127663	1.779694	0.5618943	0.10	16.5	156.5
5°C	2	43.4	24.9	peak	1.64	50.1	1.130657	1.7934856	0.5575735	0.10	16.6	154.7

26% wt% black dye												
$T°C$	$\{00l\}$ orders	d_0	$d_0/\sqrt{3}$	*comms*	log d_0	a	ρ_{sol} (g/cm³)	ρ_d (g/cm³)	v_d	φ_{dc}	d_{dc}	S_{dc} (Å²)
5°C	2	44.1	25.4	peak	1.64	50.9	1.122526	1.7727383	0.5640991	0.10	16.6	156.4
15°C	2	43.7	25.3	peak	1.64	50.5	1.119798	1.7601267	0.5681409	0.10	16.5	158.5
25°C	2	43.7	25.2	peak	1.64	50.5	1.116587	1.7507883	0.5711713	0.10	16.5	159.1
35°C	2	43.4	25.1	peak	1.64	50.1	1.113223	1.7455675	0.5728796	0.10	16.4	160.7
45°C	1	42.7	-	diffuse peak	1.63	-	1.109222	1.7406115	0.5745107	0.10	-	-
55°C	1	41.8	-	diffuse peak	1.62	-	1.104931	1.7375354	0.5755278	0.10	-	-
65°C	1	43.7	-	diffuse peak	1.64	-	1.100475	1.7367188	0.5757985	0.10	-	-
75°C	1	43.7	-	diffuse peak	1.64	-	1.095099	1.7331041	0.5769994	0.10	-	-
85°C	1	42.4	-	diffuse peak	1.63	-	1.088371	1.7237447	0.5801323	0.10	-	-
75°C	1	43.1	-	diffuse peak	1.63	-	1.095123	1.7332554	0.576949	0.10	-	-
65°C	1	43.7	-	diffuse peak	1.64	-	1.100496	1.7368512	0.5757546	0.10	-	-
55°C	1	41.5	-	diffuse peak	1.62	-	1.104978	1.7378318	0.5754297	0.10	-	-
45°C	1	42.4	-	diffuse peak	1.63	-	1.109286	1.7410151	0.5743776	0.10	-	-
35°C	2	43.1	24.6	peak	1.63	49.7	1.113267	1.7458449	0.5727886	0.10	16.7	161.8
25°C	2	43.4	24.8	peak	1.64	50.1	1.116599	1.7508639	0.5711466	0.10	16.4	160.2
15°C	2	42.7	25.1	peak	1.63	49.3	1.119813	1.7602213	0.5681104	0.10	16.1	162.2
5°C	2	43.7	25.2	peak	1.64	50.5	1.122563	1.7729716	0.5640248	0.10	16.4	157.8

25% wt% black dye											
T˚C	**{00l} orders**	**d_0**	**$d_0/\sqrt{3}$**	***comms***	**log d_0**	***a***	**ρ_{sol} (g/cm^3)**	**ρ_d (g/cm^3)**	**v_d**	**φ_{dc}**	**d_{dc}**	**S_{dc} (Å^2)**
5˚C	2	46.2	26.2	peak	1.66	53.3	1.114295	1.7496755	0.5715346	0.09	17.1	153.5
15˚C	2	45.7	26.0	peak	1.66	52.8	1.110859	1.7319515	0.5773834	0.09	17.0	156.1
25˚C	1	45.7	-	diffuse peak	1.66	-	1.106856	1.7171282	0.5823677	0.09	-	-
35˚C	1	46.9	-	diffuse peak	1.67	-	1.102639	1.7062257	0.5860889	0.09	-	-
45˚C	1	46.9	-	diffuse peak	1.67	-	1.098058	1.6974211	0.589129	0.09	-	-
55˚C	1	46.3	-	diffuse peak	1.67	-	1.093479	1.6925142	0.590837	0.09	-	-
65˚C	1	45.7	-	diffuse peak	1.66	-	1.088747	1.6900608	0.5916947	0.09	-	-
75˚C	1	45.1	-	diffuse peak	1.65	-	1.083584	1.6879265	0.5924428	0.09	-	-
85˚C	-	-	-	-	-	-	-	-	-	-	-	-
75˚C	-	-	-	-	-	-	-	-	-	-	-	-
65˚C	1	45.7	-	diffuse peak	1.66	-	1.088761	1.6901526	0.5916626	0.09	-	-
55˚C	1	46.3	-	diffuse peak	1.67	-	1.093492	1.6925995	0.5908072	0.09	-	-
45˚C	1	46.3	-	diffuse peak	1.67	-	1.098074	1.697526	0.5890926	0.09	-	-
35˚C	1	46.9	-	diffuse peak	1.67	-	1.102651	1.7063044	0.5860619	0.09	-	-
25˚C	1	46.9	-	diffuse peak	1.67	-	1.106878	1.7172725	0.5823188	0.09	-	-
15˚C	1	47.5	-	diffuse peak	1.68	-	1.110894	1.732181	0.5773069	0.09	-	-
5˚C	1	47.5	-	diffuse peak	1.68	-	1.114317	1.7498197	0.5714874	0.09	-	-

24% wt% black dye							
T˚C	**{00l} orders**	**d_0**	**log d_0**	**ρ_{sol} (g/cm^3)**	**ρ_d (g/cm^3)**	**v_d**	**φ_{dc}**
5˚C	1	46.2	1.66	1.105804	1.7229148	0.5804117	0.09
15˚C	1	46.2	1.66	1.102592	1.7060184	0.5861601	0.09
25˚C	1	46.2	1.66	1.097975	1.6864692	0.5929548	0.09
35˚C	1	45.7	1.66	1.093233	1.671652	0.5982106	0.09
45˚C	1	45.7	1.66	1.088055	1.6585618	0.602932	0.09
55˚C	1	45.1	1.65	1.082421	1.6464325	0.6073738	0.09
65˚C	1	44.5	1.65	1.076751	1.637684	0.6106184	0.09
75˚C	1	44.5	1.65	1.070820	1.6304528	0.6133266	0.09
85˚C	-	-	-	-	-	-	-
75˚C	-	-	-	-	-	-	-
65˚C	1	45.1	1.65	1.076834	1.6382509	0.6104071	0.09
55˚C	1	45.1	1.65	1.082503	1.6469926	0.6071673	0.09
45˚C	1	46.3	1.67	1.088088	1.6587872	0.6028501	0.09
35˚C	1	46.3	1.67	1.093251	1.6717749	0.5981667	0.09
25˚C	1	46.3	1.67	1.097986	1.6865444	0.5929284	0.09
15˚C	1	46.3	1.67	1.102603	1.7060935	0.5861343	0.09
5˚C	1	46.3	1.67	1.105817	1.7230036	0.5803818	0.09

T°C	{00*l*} orders	d_0	log d_0	ρ_{sol} (g/cm³)	ρ_d (g/cm³)	v_d	φ_{dc}
23% wt% black dye							
5°C	1	46.2	1.66	1.098261	1.7005841	0.5880333	0.09
15°C	1	46.2	1.66	1.095626	1.6871033	0.5927319	0.09
25°C	1	48.1	1.68	1.092483	1.6772996	0.5961964	0.09
35°C	1	48.1	1.68	1.088607	1.6681416	0.5994695	0.09
45°C	1	47.5	1.68	1.084499	1.662275	0.6015852	0.09
55°C	1	46.9	1.67	1.080274	1.6598576	0.6024613	0.09
65°C	1	45.7	1.66	1.076276	1.6628696	0.6013701	0.09
75°C	1	45.1	1.65	1.072148	1.6684232	0.5993683	0.09
85°C	-	-	-	-	-	-	-
75°C	-	-	-	-	-	-	-
65°C	1	45.7	1.68	1.076281	1.6629052	0.6013572	0.09
55°C	1	46.2	1.66	1.080289	1.6599646	0.6024225	0.09
45°C	1	47.5	1.68	1.084523	1.6624461	0.6015233	0.09
35°C	1	48.1	1.68	1.088619	1.6682271	0.5994388	0.09
25°C	1	48.1	1.68	1.092497	1.6773994	0.5961609	0.09
15°C	1	48.1	1.68	1.095644	1.6872316	0.5926869	0.09
5°C	1	48.8	1.69	1.098293	1.7008122	0.5879544	0.09

T°C	{00*l*} orders	d_0	log d_0	ρ_{sol} (g/cm³)	ρ_d (g/cm³)	v_d	φ_{dc}
22% wt% black dye							
5°C	1	50.9	1.71	1.081830	1.667945	0.59954	0.08
15°C	1	50.9	1.71	1.080085	1.660671	0.602166	0.08
25°C	1	50.2	1.70	1.077391	1.653504	0.604776	0.08
35°C	1	49.5	1.69	1.073943	1.646846	0.607221	0.08
45°C	1	48.8	1.69	1.069831	1.646594	0.607314	0.08
55°C	1	48.8	1.69	1.065055	1.652223	0.605245	0.08
65°C	1	46.9	1.67	1.059732	1.655583	0.604017	0.08
75°C	1	45.7	1.66	1.053922	1.665404	0.600455	0.08
85°C	-	-	-	-	-	-	-
75°C	-	-	-	-	-	-	-
65°C	1	46.9	1.67	1.059717	1.65568	0.603981	0.08
55°C	1	47.5	1.68	1.065036	1.65229	0.605221	0.08
45°C	1	48.8	1.69	1.069819	1.646691	0.607279	0.08
35°C	1	49.5	1.69	1.074006	1.64695	0.607183	0.08
25°C	1	49.5	1.69	1.077520	1.6536	0.604741	0.08
15°C	1	50.9	1.71	1.080260	1.660813	0.602115	0.08
5°C	1	50.9	1.71	1.082013	1.668049	0.599503	0.08

				21% wt% black dye			
T°C	{00*l*} orders	d_0	log d_0	ρ_{sol} (g/cm^3)	ρ_d (g/cm^3)	v_d	φ_{dc}
5°C	1	50.9	1.71	1.081830	1.6390428	0.6101122	0.08
15°C	1	50.9	1.71	1.080085	1.6313082	0.6130049	0.08
25°C	1	50.2	1.70	1.077391	1.6242717	0.6156605	0.08
35°C	1	49.5	1.69	1.073943	1.6178697	0.6180967	0.08
45°C	1	48.8	1.69	1.069831	1.6117771	0.6204332	0.08
55°C	1	48.8	1.69	1.065055	1.6052586	0.6229526	0.08
65°C	1	46.9	1.67	1.059732	1.5987037	0.6255068	0.08
75°C	1	45.7	1.66	1.053922	1.5921994	0.628062	0.08
85°C	-	-	-	-	-	-	-
75°C	-	-	-	-	--	-	-
65°C	1	46.9	1.67	1.059717	1.5985866	0.6255526	0.08
55°C	1	47.5	1.68	1.065036	1.6051103	0.6230101	0.08
45°C	1	48.8	1.69	1.069819	1.6116834	0.6204693	0.08
35°C	1	49.5	1.69	1.074006	1.6183616	0.6179089	0.08
25°C	1	49.5	1.69	1.077520	1.6252788	0.6152791	0.08
15°C	1	50.9	1.71	1.080260	1.6326743	0.612492	0.08
5°C	1	50.9	1.71	1.082013	1.6404714	0.6095809	0.08

				20% wt% black dye			
T°C	{00*l*} orders	d_0	log d_0	ρ_{sol} (g/cm^3)	ρ_d (g/cm^3)	v_d	φ_{dc}
5°C	1	53.2	1.73	1.071060	1.667945	0.6318245	0.08
15°C	1	53.2	1.73	1.069396	1.660671	0.6347981	0.08
25°C	1	52.4	1.72	1.066742	1.653504	0.6376143	0.08
35°C	1	52.4	1.72	1.063280	1.646846	0.6403442	0.08
45°C	1	50.9	1.71	1.059129	1.646594	0.6430313	0.08
55°C	1	48.8	1.69	1.054373	1.652223	0.6457113	0.08
65°C	1	47.5	1.68	1.049074	1.655583	0.6484029	0.08
75°C	1	46.9	1.67	1.043273	1.665404	0.6511347	0.08
85°C	-	-	-	-	-	-	-
75°C	-	-	-	-	-	-	-
65°C	1	47.5	1.68	1.049082	1.65568	0.6483754	0.08
55°C	1	48.8	1.69	1.054386	1.65229	0.6456668	0.08
45°C	1	48.8	1.69	1.059143	1.646691	0.6429839	0.08
35°C	1	50.9	1.71	1.063293	1.64695	0.6403005	0.08
25°C	1	51.6	1.71	1.066754	1.6536	0.6375743	0.08
15°C	1	53.2	1.73	1.070774	1.660813	0.630279	0.08
5°C	1	53.2	1.73	1.074458	1.668049	0.620898	0.08

				19% wt% black dye			
T˚C	{00*l*} orders	d_0	log d_0	ρ_{sol} (g/cm^3)	ρ_d (g/cm^3)	v_d	φ_{dc}
5˚C	1	54.0	1.73	1.061407	1.5301021	0.6535512	0.08
15˚C	1	53.2	1.73	1.057532	1.5032664	0.6652181	0.08
25˚C	1	52.4	1.72	1.053570	1.4847652	0.6735072	0.08
35˚C	1	51.6	1.71	1.049953	1.4765484	0.6772551	0.08
45˚C	1	50.9	1.71	1.045841	1.4702166	0.6801719	0.08
55˚C	1	48.8	1.69	1.041515	1.4673705	0.6814912	0.08
65˚C	1	48.1	1.68	1.036405	1.4625046	0.6837585	0.08
75˚C	1	47.5	1.68	1.031343	1.4623704	0.6838213	0.08
85˚C	-	-	-	-	-	-	-
75˚C	-	-	-	-	-	-	-
65˚C	1	47.5	1.68	1.036421	1.4626426	0.683694	0.08
55˚C	1	48.1	1.68	1.041562	1.467776	0.6813029	0.08
45˚C	1	50.2	1.70	1.045861	1.4703892	0.6800921	0.08
35˚C	1	50.9	1.71	1.049987	1.4768418	0.6771206	0.08
25˚C	1	51.6	1.71	1.053591	1.4849464	0.673425	0.08
15˚C	1	52.4	1.72	1.057574	1.5036288	0.6650578	0.08
5˚C	1	53.2	1.73	1.061433	1.5303264	0.6534554	0.08

				18% wt% black dye			
T˚C	{00*l*} orders	d_0	log d_0	ρ_{sol} (g/cm^3)	ρ_d (g/cm^3)	v_d	φ_{dc}
5˚C	1	53.2	1.73	1.051397	1.4683884	0.6810187	0.08
15˚C	1	53.2	1.73	1.047409	1.4390808	0.694888	0.08
25˚C	1	53.2	1.73	1.043398	1.4192197	0.7046125	0.08
35˚C	1	51.6	1.71	1.039182	1.4052585	0.7116128	0.08
45˚C	1	48.1	1.68	1.035196	1.3999348	0.714319	0.08
55˚C	1	46.9	1.67	1.030978	1.3981652	0.715223	0.08
65˚C	1	45.1	1.65	1.026226	1.3965751	0.7160374	0.08
75˚C	1	44.5	1.65	1.021120	1.3963498	0.7161529	0.08
85˚C	-	-	-	-	-	-	-
75˚C	-	-	-	-	-	-	-
65˚C	1	45.1	1.65	1.026251	1.3968028	0.7159207	0.08
55˚C	1	47.5	1.68	1.030997	1.3983383	0.7151345	0.08
45˚C	1	47.5	1.68	1.035217	1.400126	0.7142214	0.08
35˚C	1	49.5	1.69	1.039204	1.4054589	0.7115114	0.08
25˚C	1	50.2	1.70	1.043419	1.4194109	0.7045176	0.08
15˚C	1	50.9	1.71	1.047433	1.4392994	0.6947825	0.08
5˚C	1	51.6	1.71	1.051426	1.4686525	0.6808963	0.08

17% wt% black dye

T°C	**{00*l*} orders**	d_0	**log** d_0	ρ_{sol} (g/cm^3)	ρ_d (g/cm^3)	v_d	φ_{dc}
5°C	1	53.2	1.73	1.041854	1.4039177	0.7122925	0.08
15°C	1	53.2	1.73	1.037846	1.3727441	0.7284679	0.08
25°C	1	53.2	1.73	1.033630	1.3498588	0.7408182	0.08
35°C	1	51.6	1.71	1.029054	1.3317821	0.7508736	0.08
45°C	1	50.2	1.70	1.024315	1.3191087	0.7580877	0.08
55°C	1	48.8	1.69	1.019698	1.3136533	0.7612359	0.08
65°C	1	47.5	1.68	1.014946	1.3122721	0.7620371	0.08
75°C	1	45.5	1.66	1.009883	1.312784	0.7617399	0.08
85°C	-	-	-	-	-	-	-
75°C	-	-	-	-	-	-	-
65°C	1	47.5	1.66	1.014971	1.3125132	0.7618971	0.08
55°C	1	48.1	1.69	1.019703	1.3137015	0.7612079	0.08
45°C	1	50.2	1.70	1.024335	1.3193015	0.7579768	0.08
35°C	1	50.9	1.71	1.029072	1.3319557	0.7507757	0.08
25°C	1	51.6	1.71	1.033658	1.3501288	0.7406701	0.08
15°C	1	52.4	1.72	1.037864	1.3729177	0.7283758	0.08
5°C	1	53.2	1.73	1.041871	1.4040816	0.7122093	0.08

16% wt% black dye

T°C	**{00*l*} orders**	d_0	**log** d_0	ρ_{sol} (g/cm^3)	ρ_d (g/cm^3)	v_d	φ_{dc}
5°C	1	59.4	1.77	1.034533	1.3541546	0.7384681	0.07
15°C	1	58.4	1.77	1.031647	1.3325826	0.7504225	0.07
25°C	1	55.6	1.75	1.028848	1.3229139	0.7559071	0.07
35°C	1	51.5	1.71	1.025985	1.321447	0.7567462	0.07
45°C	1	50.8	1.71	1.023009	1.3262838	0.7539864	0.07
55°C	1	50.8	1.71	1.019860	1.335811	0.7486089	0.07
65°C	1	49.3	1.69	1.016447	1.3483841	0.7416284	0.07
75°C	1	48.0	1.68	1.012776	1.363547	0.7333814	0.07
85°C	1	46.7	1.67	1.008589	1.3782679	0.7255484	0.07
75°C	1	48.0	1.68	1.012799	1.3637827	0.7332547	0.07
65°C	1	49.3	1.69	1.016471	1.34863	0.7414932	0.07
55°C	1	50.0	1.70	1.019883	1.3360466	0.7484769	0.07
45°C	1	50.8	1.71	1.023032	1.3265195	0.7538525	0.07
35°C	1	51.5	1.71	1.025998	1.3215802	0.7566699	0.07
25°C	1	52.3	1.72	1.028869	1.3231291	0.7557842	0.07
15°C	1	54.7	1.74	1.031670	1.3328183	0.7502898	0.07
5°C	1	54.7	1.74	1.034551	1.354339	0.7383676	0.07

15% wt% black dye							
T°C	**{00l} orders**	**d_0**	**log d_0**	**ρ_{sol} (g/cm^3)**	**ρ_d (g/cm^3)**	**v_d**	**φ_{dc}**
5°C	1	61.5	1.79	1.027606	1.3020624	0.7680124	0.07
15°C	1	59.4	1.77	1.025063	1.2828586	0.7795092	0.07
25°C	1	58.4	1.77	1.022392	1.2740813	0.7848793	0.07
35°C	1	51.5	1.71	1.019576	1.2732312	0.7854033	0.07
45°C	1	50.8	1.71	1.016557	1.2781752	0.7823654	0.07
55°C	1	50.8	1.71	1.013250	1.286912	0.7770539	0.07
65°C	1	50.8	1.71	1.009859	1.3009067	0.7686947	0.07
75°C	1	50.0	1.70	1.006333	1.3190457	0.7581239	0.07
85°C	1	50.0	1.70	1.002430	1.3382672	0.7472349	0.07
75°C	1	50.0	1.70	1.006357	1.3193079	0.7579732	0.07
65°C	1	50.0	1.70	1.009883	1.301169	0.7685397	0.07
55°C	1	50.8	1.71	1.013276	1.2871962	0.7768823	0.07
45°C	1	50.8	1.71	1.016593	1.2785687	0.7821246	0.07
35°C	1	51.5	1.71	1.019598	1.2734716	0.785255	0.07
25°C	1	51.5	1.71	1.022412	1.2742998	0.7847447	0.07
15°C	1	59.4	1.77	1.025093	1.2831864	0.77931	0.07
5°C	1	59.4	1.77	1.027633	1.3023574	0.7678384	0.07

8.4 Nuclear Magnetic Resonance Spectroscopy

Nuclear magnetic resonance spectroscopy is a useful tool that utilises the magnetic properties of the nuclei [148-150] to provide information regarding the physical, chemical, electronic and structural properties of the molecules within the liquid crystalline state [87, 151, 152].

The main objective of this research is to explore the molecular structures within the aggregates for the black dye in aqueous solution. Proton NMR (^{1}H NMR) is used so that each proton of the dye molecule can be studied. It is well-known that the size of the aggregates increase as the concentration is raised. As a result, it is anticipated that chemical shifts obtained from the proton spectra will change with concentration [153]. This is due to the ring current effect caused by the electrons circulating within the π-cloud of an aromatic ring, which itself produces a magnetic field. This field opposes the applied field at the centre of the ring, but reinforces it outside of the ring. This makes it possible to investigate the extent to which the protons are in proximity to the π-clouds of the dye molecules above and below them and the possibility of any slip within the aggregates.

A wide range of concentrations (0.01 − 20% wt / wt% black dye) was investigated. The measurements were taken at 25°C and the spectrum of 3% wt/wt% dye is shown in Figure 8.23 as an example. Optical microscopy reveals that black dye exists in the isotropic phase at concentrations lower than 15% wt/wt% dye. However, an analysis of the spectrum of 3% wt/wt% dye proves that even at low dye concentrations the dye exists in an aggregated form.
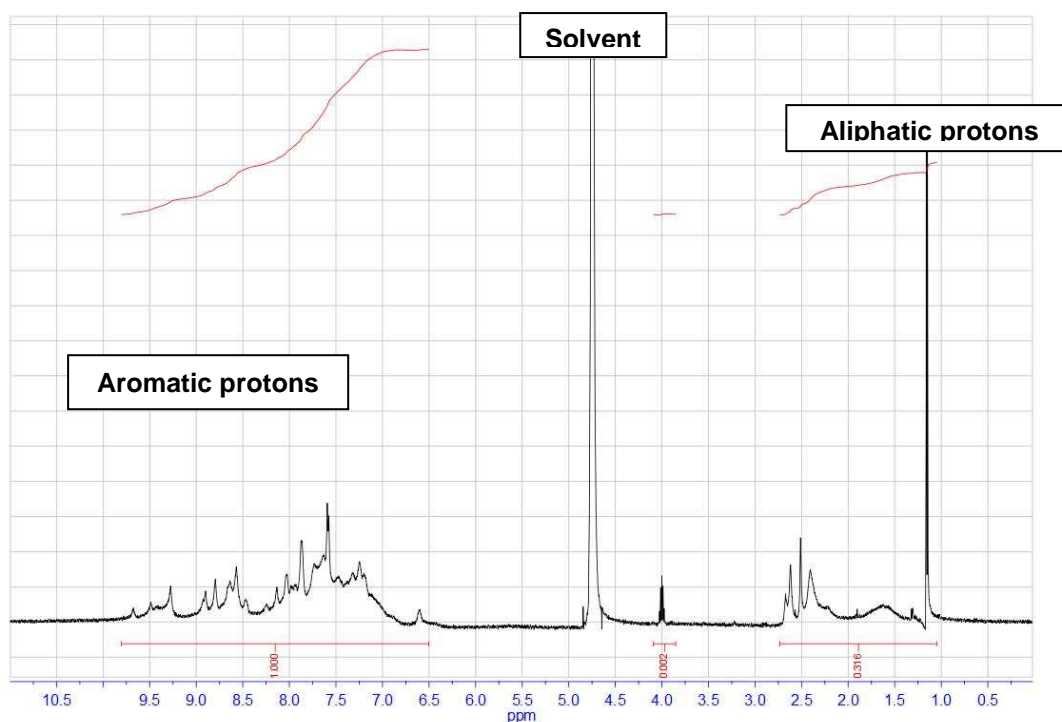
Figure 8.23 **^{1}H NMR spectrum of 3% wt/wt% black dye in D$_2$O solution at 25°C.**

The ^{1}H NMR spectrum of 3% wt/wt% black dye in deuterated water displays line broadening making it difficult to assign each individual peak. However, three distinct groups of peaks can be recognised on this spectrum. The unresolved region in the range of 6.5 – 9.5 ppm corresponds to the aromatic protons of the molecule; the large solvent peak at 4.8 ppm and the remaining unresolved group in the range of 1 – 2.8 ppm arises from aliphatic protons. Unfortunately, the concentrations used for the optical microscopy measurements were too high for NMR to be useful. At high dye concentrations the spectrum is impossible to resolve due to the broad lines produced by the large aggregates (Figure 8.24).
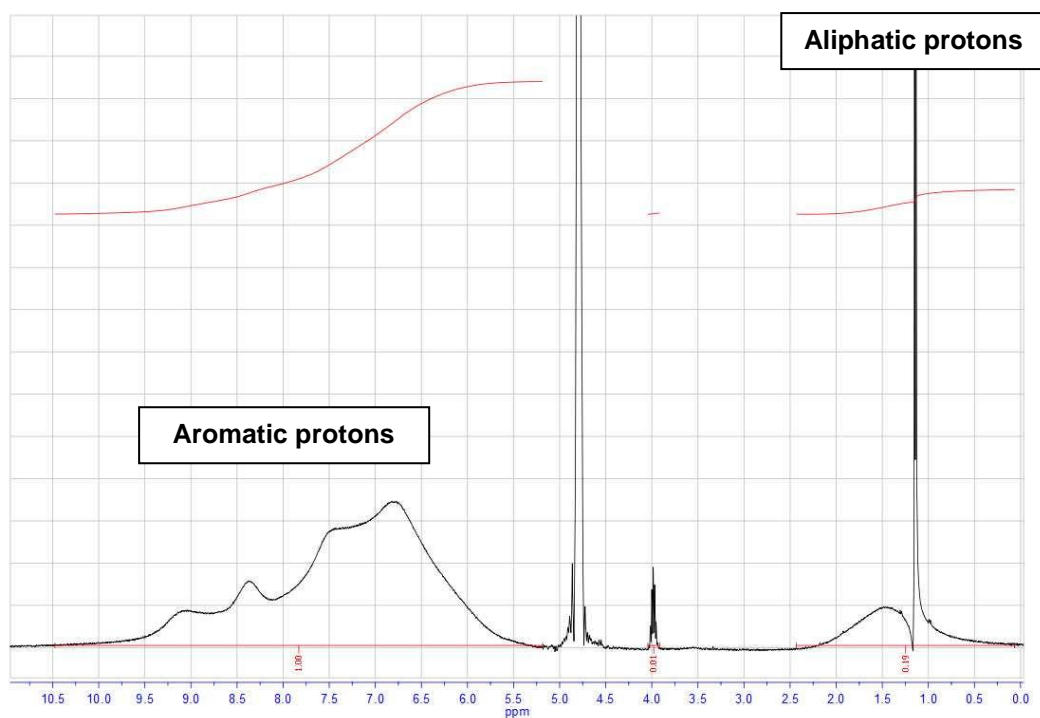
Figure 8.24 ^{1}H NMR spectrum of 15% wt/wt% black dye in D$_2$O solution at 25°C.

At this high concentration the spectrum displays significantly broader and shifted peaks. However, at much lower concentrations the spectra looks improved with regards to resolution (Figure 8.25), although due to the fairly broad signals this spectrum is still difficult to assign with total confidence.
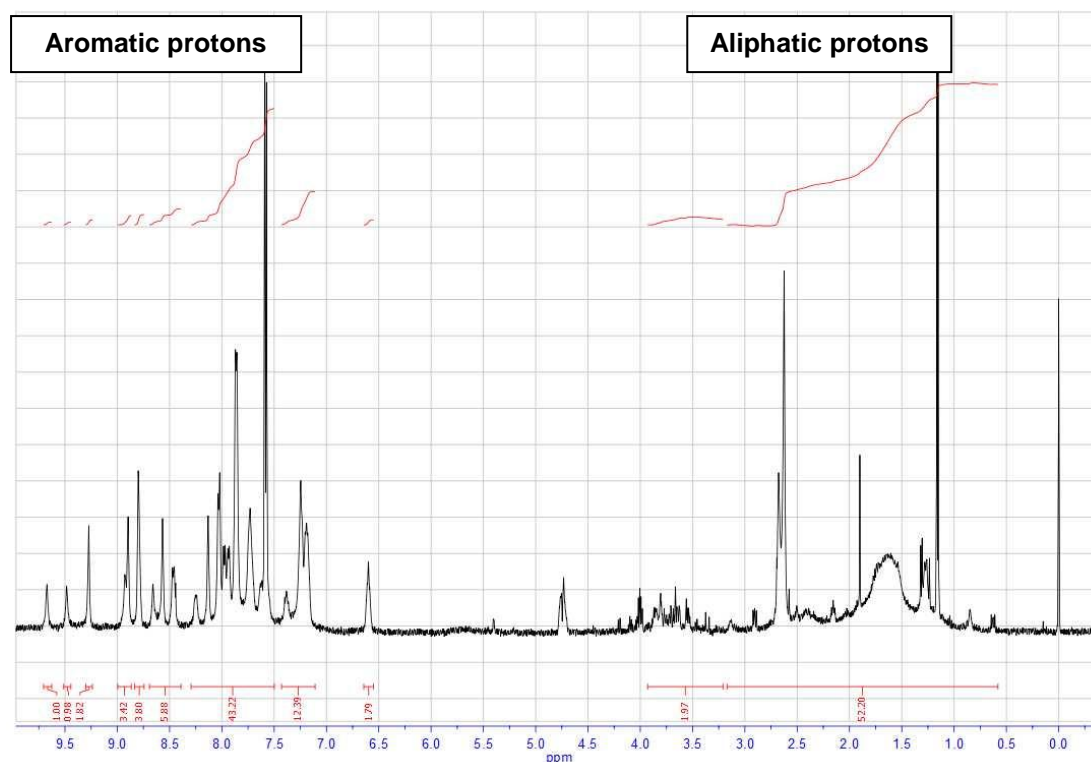
Figure 8.25 ^{1}**H NMR spectrum of 0.07% wt/wt% black dye in D$_2$O solution at 25°C (with subtracted solvent peak).**

As the samples get more concentrated, the width of the peaks become broader. This is mainly due to the increase in size of the aggregates leading to the slowing down of their tumbling motion with respect to the NMR timescale, i.e. dipolar relaxations begin to occur. The increase in dye concentration leads to a downfield shift of all peaks corresponding to the aromatic peak region. The changes in chemical shifts of the peaks with composition indicate the shielding occurring due to the ring anisotropy within the aggregates. It happens because the monomers start joining together forming dimers, trimers and more complicated aggregates with the increase in concentration. Those molecules located in the centre of these complicated stacks will experience the maximum ring current shielding effect from the two molecules either side, whereas the molecules at the ends of the stacks will be affected only by the molecules in the centre. The spectra for low concentrations indicate that there must be a reasonable number of monomeric, dimeric and small size aggregates present in the system as the aggregates keep forming and falling apart, i.e. the exchange between the dye molecules must be very rapid with the respect to the NMR timescale. Thus, the spectrum would give quite high chemical shifts due to the reason that there are more end molecules in the system experiencing minimum or no shielding. As the concentration is raised, the time-averaged

176

spectrum will shift towards the lower chemical shifts. This is due to the formation of large aggregates and, hence, the ratio between the end molecules and the centre ones will be reversible as almost all molecules will be locked up in the centre and experience the maximum shielding from the neighbouring molecules.

The shielding effect can be measured easily from the proton NMR experimental data by calculating the difference in chemical shifts in ppm for the least and the most concentrated samples. The small difference is an indication of the small shielding effect occurring in the system. Thus, it has been suggested that those protons, whose chemical shifts do not change greatly with increasing dye concentration are located outside the core of the stack. Large differences in chemical shifts are mainly due to large shielding effects, hence caused by the ring currents in neighbouring molecules. This suggests that protons with large shifts must be in the core of the stacks. Unfortunately, due to the difficulties in assigning the spectra it was impossible to calculate these values. However it can be seen that the variation of chemical shifts mainly happens for the aromatic protons, however, the chemical shift of the aliphatic region do not change to a great extent. It happens because the aliphatic groups are located in the outer part of the molecule and thus, are less affected by π – shielding.

CHAPTER NINE

9. Conclusions

Chromonic liquid crystals [41] are formed when compounds with disc-like or plank-like molecular shapes are dispersed in water. Even in dilute solution they have a strong tendency to aggregate into stacks, which become ordered to give liquid crystals at higher concentrations. These liquid crystals occur widely in aqueous dispersions of many formulated products such as pharmaceuticals [154] and the dyes used in inkjet printing [21]. The aggregation behaviour of two chromonic commercial dye systems, which are Cu − phthalocyanine dye and the black azo dye, were successfully investigated. Both of these dyes are currently being manufactured on a large scale by Fujifilm Imaging Colorants. Under certain conditions these dyes form chromonic lyotropic liquid crystalline mesophases. The complexity of the dye structures lead to complex phase behaviour of both systems, which gives rise to a series of problems in production/processing and transportation. We undertook a quantitative study to uncover the factors that determine the occurrence and properties of these dyes and this class of mesophase in a combined experimental and theoretical investigation. The results are of the great importance for the ink-jet industry, in which small structural differences often result in unwanted aggregation of the molecules, rendering promising new formulations useless.

The dyes were supplied by Fujifilm Imaging Colorants Ltd. Multiple techniques, such as optical microscopy, NMR (^{1}H), wide- and small − angle X-ray diffraction, UV-vis absorption spectroscopy and electron paramagnetic resonance have been used in order to examine the behaviour of the dyes in the solution and liquid crystalline phases.

The phase diagrams were constructed with the help of polarising optical microscopy. Both dyes exhibited the sequence of phases and temperature changes similar to those previously observed for other chromonic systems [21, 24, 155]. The phase diagrams were overall of the peritectic form. The isotropic, nematic and hexagonal columnar phases were observed at different concentrations and temperatures. The nematic phase was characterised by its schlieren texture, however, the columnar phase possessing the hexagonal symmetry was characterised by its fan − like appearance for both dyes. The transition from nematic to columnar hexagonal phase on a peripheral evaporation appeared to be gradual with no distinct boundary.

Consequently, the UV-vis absorption spectroscopy was used for studying the extent to which aggregation occurred in the Cu – phthalocyanine dye solution with respect to concentration. The shape of the spectra was similar to those observed for other Cu – phthalocyanine dyes with the same chromophore. The dye studied exhibited the decrease in absorption maxima with increasing dye concentration implying the occurrence of aggregation of dye molecules even in very dilute solutions. The H – aggregation with its parallel arrangement of the dye molecules in a nearly vertical stack was confirmed. Furthermore, the experimental results were analysed using the new model proposed by P. J. Camp in which the molar absorption coefficients were fitted not only assuming the monomer – dimer equilibrium operating in the solution, but also considering the formation of trimers and higher aggregates. The impact of changes in dye concentration upon the equilibrium cluster distribution was obtained by utilising the sensitivity of the peak intensities at the absorption maxima.

The wide – angle reflection corresponded to a spacing of 3.5 Å for both dyes, which remained constant for the range temperatures and concentrations studied for Cu – phthalocyanine dye. However it changed slightly for the black dye. An unusual feature of the X-ray diffraction pattern of the mesophases occurred in the form of diffuse reflections at ca. 6.8 Å for the black dye. It was proposed that these arise from "head-to-tail" molecular packing within the stacks.

Small – angle diffraction patterns confirmed the results obtained by optical microscopy and allowed to perform the structural studies on both dyes. The formation of the hexagonal mesophase was confirmed at high concentrations. Quantitative information about the aggregate size and the mesophase structure was obtained by small - angle X-ray diffraction together with density data measured experimentally. The approximate diameter and the cross - section area of the aggregates were calculated from the measured d-spacings in the hexagonal columnar phase, which in comparison with the theoretical cross – sectional area proved packing of the molecules into single molecule columnar aggregates.

Additionally the EPR and ^{1}H NMR methods were employed in order to broaden our understanding about the process of aggregation of the studied dyes. Electron paramagnetic resonance proved the high tendency of Cu – phthalocyanine dye to aggregate in aqueous solution even at the concentration as low as 1.4×10^{-7} M, which came in a good agreement with the UV – vis data. More detailed studies can be performed by this method in order to obtain the information about the kinetics of aggregation along with the magnetic properties of the dye in monomeric, dimeric and aggregated forms. ^{1}H NMR was used in

order to study the state of aggregation of the black dye in solution with respect to variable concentration. The experiment was conducted in dimethyl sulphoxide and deuterated water with the peaks assigned accordingly. However, due to the complexity of the molecule along with the limited time and access to the resource, it is impossible to draw the detailed conclusions regarding the extent to which aggregation occurred over the range of compositions from the proton NMR experimental data we have collected.

These studies have broadened our understanding of the phase behaviour and the aggregation properties of these water soluble commercial dyes. However, there are still the open questions in the behaviour of these systems providing a basis for further work. The first area of interest arising from this research is the effect of changes in the position, nature and number of solubilising groups around the periphery of the dye molecules. We have already performed the studies on Cu – phthalocyanine dye behaviour with two and four solubilising groups present in the molecular structure. However, these studied are incomplete and require further attention in order to draw the adequate conclusions in regards of the phase behaviour.

More X-ray diffraction studies will be useful in order to examine the nematic phase with the samples aligned in the magnetic field. The more detailed work will be interesting in order to study the nematic – hexagonal transition of the black dye. The comparison of this data with the experimental results obtained for Cu – phthalocyanine dye will widen our understanding in the way the molecular structure effects the mesophase formation at high concentrations. Furthermore, it will be interesting to look at the liquid crystal structures relaxation after initial formation (slow relaxation of structures has been observed for other systems, particularly for low dye concentration mesophases) [48].

Other areas of research, which will be of the industrial use and academic interest include the influence of additives and the variation of solvents.

These systems can be modelled using a combination of computer simulation and analytical theory. The application of the computational methods will help to explore the structure and dynamics of the dye aggregates in aqueous solution. These calculations will widen our knowledge on the details of molecular organisation and dynamics of molecules within a chromonic stack [45].

References

1. Herbst, W., Hunger, K., *Industrial Organic Pigments: Production, Properties, Applications.* 1997, Weinheim: VCH. 652.
2. Fryberg, M., *Dyes for Inkjet Printing.* Rev. Prog. Coloration, 2005. **35**: p. 1 - 30.
3. Hatch, M.J., Schultz, M., *Taking Brand Initiative: How Companies can align Strategy, Culture and Identity through Corporate Branding*. 2008, San Francisco: Wiley.
4. http://www.fujifilmimagingcolorants.com. *Fujifilm Imaging Colorants web page*.
5. Bolotin, B.M., Loseva, M. V., *The relationship between the structures of organic compounds and their mesogenic properties*. 1979, Moscow.
6. Tomilin, M.G., *Liquid crystals' interactions with surfaces*. 2001, Saint-Petersburg: Politechnika.
7. Oswald, P., Pieranski, P., *Nematic and Cholesteric Liquid Crystals: concepts and physical properties illustrated by experiments.* Vol. 1. 2005: CRC Press, Taylor and Francis.
8. Gray, G.W., *Chapter 1. Introduction and Historical Development*, in *Handbook of Liquid Crystals. Fundamentals.*, G.J. Demus D., Gray G.W., Spiess H.-W., Vill V.,, Editor. 1998, Wiley-VCH. p. 1 - 17.
9. Lozman, O., *A Brief Introduction to Liquid Crystals*. 2006, FFIC.
10. Lozman, O., *Liquid Crystals and Aggregation. Application to Inkjet and beyond.* 2006, FFIC.
11. http://www.cmns.leeds.ac.uk/discotic.htm. *Discotic Liquid Crystals*.
12. Shibaev, V.P., *Liquid Crystalline Polymers.* Soros Educational Journal, 1997. **6**: p. 40 - 46.
13. Usol'zeva, N.B., *Lyotropic Liquid Crystals: Chemical and Molecular Stuctures.* 1994, IvGU: Ivanovo. p. 220.
14. Mateer, D.L., *The liquid-crystalline behaviour of photographic sensitising dyes.*, in *Department of Chemistry and Applied Chemistry*. 1997, University of Salford: Manchester.
15. Hird, M., *Synthesis of Liquid Crystals*, in *Materials presented at the British Liquid Crystal Society Winter Workshop*. 2006, University of Hull: Hull.
16. Anacker, E.W., Chose, H.M., *Counterions and Micelle Size. II. Light Scattering by Solutions of Cetylpyridinium Salts.* Journal of American Chemical Society, 1968. **90**: p. 3161 - 3166.
17. Mazer, N.A., Benedec, G.B., Carey, M.C., *An Investigation of the Micellar Phase of Dodecyl Sulphate in Aqueous Sodium Chloride Solutions Using Quasielastic Light Scattering Spectroscopy.* Journal of Physical Chemistry, 1976. **80**: p. 1075 - 1085.
18. Reiss - Husson, F., Luzzati, V., *The Structure of the Micellar Solutions of Some Amphiphilic Compounds in Pure Water as Determined by Absolute Small-Angle X-Ray Scattering Techniques.* Journal of Physical Chemistry, 1964. **68**: p. 3504 - 3511.
19. Hayashi, S., Ikeda, S., *Micelle Size and Shape of Sodium Dodecyl Sulphate in Concentrated Sodium Chloride Solutions.* Journal of Physical Chemistry, 1980. **84**: p. 774 - 751.
20. Lydon, J., *Chromonic Mesophases.* Current Opinion in Colloid and Interface Science, 2004. **8**: p. 480 - 490.
21. Horowitz, V.R., Janowitz, L.A., Modic, A.L., Heiney, P.A., Collings, P.J., *Aggregation Behaviour and Chromonic Liquid Crystal Properties of an Anionic Monoazo Dye.* Physical Review, 2005. **72**: p. 041710 - 041710 - 15.

22.   Turner, J.E., Lydon, J.E., *Chromonic Mesomorphism: the Range of Lyotropic Discotic Phases*
Molecular Crystals and Liquid Crystals, 1988. **53**: p. 93 - 99.
23.   Attwood, T.K., Lydon, J.E., *A New Model for the Molecular Arrangements in Chromonic Mesophases.* Molecular Crystals and Liquid Crystals, 1986. **51**: p. 9 - 14.
24.   Lydon, J.E., *Chromonic Liquid Crystal Phases.* Colloid and Interface Science, 1998. **3**: p. 458 - 466.
25.   Sandquist, H., Berichte der Deutschen Chemischen Gesellschaft, 1915. **48**: p. 2054.
26.   Sandquist, H., Kolloid-Zeitschrift, 1916. **19**: p. 113 - 121.
27.   Balaban, I.E., King, H., *Trypanocidal Action and Chemical Constitution.* Journal of Chemical Society, 1927. **1**: p. 3068 - 3097.
28.   Gaubert, P., Comptes - Rendus, 1933. **197**: p. 1436 - 1438.
29.   Scheibe, G., *Die Stereoisomerie Organischer Farbstoffe und ihr Polymerer Farbstoffe*
Angewandte Chemie, 1939. **52**: p. 631.
30.   Jelley, E.E., *Spectral Absorption and Fluorescence of Dyes in the Molecular State.* Nature, 1936. **138**: p. 1009 - 1010.
31.   Lydon, J., *Chromonics.* Handbook of Liquid Crystals, ed. D. Demus, Goodby, J.W., Gray, Spiess, H.-W., Vill, V. Vol. 2 B, Low Molecular Weight Liquid Crystals II. 1998, Weinheim: Wiley - VCH.
32.   Lydon, J., *A Personal History of the Early Days of Chromonics.* Liquid Crystals Today, 2007. **16**(2): p. 13 - 27.
33.   Cox, J.S.G., Woodard, G.D., McCrone, W.C., Journal of Pharmaceutical Society, 1971. **60**: p. 1458 - 1465.
34.   Hartshorne, N.H., Woodard, G.D., *Mesomorphism in the System Disodium Cromoglycate - Water.* Molecular Crystals and Liquid crystals, 1973. **23**: p. 343 - 368.
35.   Lydon, J.E., *New Models for the Mesophases of Disodium Cromoglycate (Intal).* Molecular Crystals and Liquid Crystals, 1980. **64**: p. 19-24.
36.   Goldfarb, D., Luz, Z., Spielberg, N., Zimmerman, H., *Structural and Orientational Characteristics of the Disodium Cromoglycate - Water Mesophases by Deuterium NMR and X-Ray Diffraction.* Molecular Crystals and Liquid Crystals, 1985. **126**: p. 225 - 246.
37.   Attwood, T.K., Lydon, J. E., Jones, F., *The chromonic phases of dyes* Liquid Crystals, 1986. **1**(6): p. 499 - 507.
38.   Vasilevskaya, A.S., Generalova, E.V., Sonin, A.S., *Chromonic mesophases.* Russian Chemical Reviews, 1989. **58**(9): p. 904 - 916.
39.   Attwood, T.K., Lydon J. E., Hall, C.; Tiddy, G. J. T., *The Distinction between Chromonic and Amphiphilic Lyotropic Mesophases.* Liquid Crystals, 1990. **7**(5): p. 657 - 668.
40.   Turner, J.E., *Lyotropic Discotic Dye / Water Systems*, in *Astbury Department of Biophysics*. 1988, University of Leeds: Leeds.
41.   Lydon, J., *Chromonics.* Handbook of Liquid Crystals, ed. G.J. Demus D., Gray G.W., Spiess H.-W., Vill V.,. Vol. 2A. 1998, Weinheim: Wiley-VCH.
42.   Ormerod, A.P., *The Formation of Chromonic Liquid Crystals by Water-soluble Azo-dyes*, in *Division of Chemical Sciences*. 1994, University of Salford: Salford. p. 226.
43.   Ormerod, A.P., *The Influence of Additives on Lyotropic Dye / Water Liquid Crystals*, in *Department of Chemistry and Applied Chemistry*. 1991, University of Salford: Salford.
44.   Edwards, D.J., Jones, J.W., Lozman, O., Ormerod, A.P., Sintyureva, M., Tiddy, G.J.T., *Chromonic Liquid Crystal Formation by Edicol Sunset Yellow.* Journal of Physical Chemistry B, 2008. **112**(46): p. 14628 - 14636.

45. Chami, F., Wilson, M.R., *Molecular Oder in a Chromonic Liquid Crystal: a Molecular Simulation Study of the Anionic Azo Dye Sunset Yellow.* Journal of American Chemical Society, 2010. **132**(22): p. 7794 - 7802.

46. Maiti, P.K., Lansac, Y., Glaser, M.A., Clark, N.A., *Self - Assembly in Lyotropic Chromonic Liquid Crystals.* Condensed Matter, 2001. **1**: p. 1 - 27.

47. Nastishin, Y.A., Liu, H., Shiyanovskii, S.V., Lavrentovich, O.D., Kostko, A.F., Anisimov, M.A., *Pretransitional Fluctuations in the Isotropic Phase of a Lyotropic Chromonic Liquid Crystal.* Physical Review, 2004. **2004**: p. 051706 - 051706 - 9.

48. Henderson, J.R., *Discotic Amphiphiles.* Journal of Chemical Physics, 2000. **113**(14): p. 5965 - 5970.

49. Henderson, J.R., *Physics of Isodesmic Chemical Equilibria in Solution.* Physical Review, 1997. **55**(5): p. 5731 - 5742.

50. Tanford, A., *The Hydrophobic Effect: Formation of Micelles and Biological Membranes*. 1973, New York: Wiley - Interscience. 200.

51. Vikingstad, E., *Partial Molal Volumes and Compressibilities of Micellar Aggregates*, in *Aggregation Processes in Solution*, E. Wyn-Jones, Gormally, J., Editor. 1983, Elsevier Scientific Publishing Company: Amsterdam. p. 100 - 117.

52. Kauzmann, W.J., *Some Factors in the Interpretation of Protein Denaturation*, in *Advances in Protein Chemistry*, C.B. Anfinsen, Editor. 1959, Academic Press Inc.: New York. p. 1 - 63.

53. Sheppard, S.E., Lambert, R.H., Walker, R.D., *Optical Sensitizing of Silver Halides by Dyes III. The Relation of Sensitizing to the Absorption Spectra and Constitution of Dyes.* Journal of Chemical Physics, 1941. **9**: p. 96.

54. Sheppard, S.E., Geddes, A.L., *Effect of Solvents upon the Absorption Spectra of Dyes. V. Water as Solvent: Quantitative Examination of the Diemrization Hypothesis.* Journal of American Chemical Society, 1944. **66**(1): p. 2003 - 2009.

55. Hartshorne, N.H., Woodard, G.D., *Mesomorphism in the System Disodium Cromoglycate - Water.* Molecular Crystals and Liquid Crystals, 1973. **23**(2): p. 343 - 368.

56. Herz, A.H., *Aggregation of Sensitizing Dyes in Solution and their Adsoption on to Silver Halides.* Advances in Colloid and Interface Science, 1977. **8**(1): p. 237 - 298.

57. Hunter, C.A., Sanders, J.K.M., *The Nature of π-π Interactions.* Journal of American Chemical Society, 1990. **112**(14): p. 5525 - 5534.

58. http://herkules.oulu.fi/. *Complexation of N-heteroaromatic Cations with Crown Ethers and Tetraphenylborate*. 2000.

59. Semenov, I.N., Perfilova, I.L, *Chemistry*. 2000, Saint-Petersburg: Himizdat.

60. Israelachvili, J., *Intermolecular and Surface Forces*. 1992, London: Academic Press Limited.

61. Attwood, T.K., Lydon, J. E.,, *Lyotropic Mesophase Formation by Anti-asthmatic Drugs.* Molecular Crystals and Liquid Crystals, 1984. **22**(17): p. 3574 - 3577.

62. Berezin, B.D., *Coordination compounds of porphyrins and phthalocyanines*. 1981, Bath: John Wiley & Sons. 286.

63. Hartshorne, N.H., *Optical Properties of Liquid Crystals.*, in *Liquid Crystals and Plastic Crystals*, G.W. Gray, Winsor, P.A., Editor. 1974, John Wiley and Sons: London.

64. Neubert, M.E., ed. *Characterisation of Mesophase Tyoes and Transitions.* Experimental Studies of Physical Properties and Phase Transitions, ed. S. Kumar. 2001, Cambridge University Press: New York.

65. Gleeson, H., *The Physics of Liquid Crystals*. 2006: Hull.

66.   Hartshorne, N.H., ed. *The Microscopy of Liquid Crystals*. 1974, Microscope Publications Ltd.
: London.
67.   Lydon, J., *Polarised Light Microscopy*, in *British Liquid Crystal Society*. 2006: Hull.
68.   Sackman, H., *Advances in Liquid Crystals*. 1974, London: Academic Press.
69.   Walker, J., *The Analytical Theory of Light*. 2009: BiblioLife. 434.
70.   Landsberg, G.S., *Optics*. 2006, Moscow: Fizmatlit. 847.
71.   Nikon, M. *Introduction to Optical Birefringence*. http://www.microscopyu.com/articles/polarized/birefringenceintro.html].
72.   Hartshorne, N.H., Stuart, A., *Practical Optical Crystallography*. 1971, London: Edward Arnold Ltd. 326.
73.   Gay, P., *An Introduction to Crystal Optics*. 1967, Singapore: Longman. 261.
74.   Dyson, N.A., *X-Rays in Atomic and Nuclear Physics*. Second Edition ed. 1990, Cambridge: Cambridge University Press. 400.
75.   Hull, S., Smith, R.I., David, W.I.F., Hannon, A.C., Mayers, J., Cywinski, R.,, *The POLARIS Powder Diffractometer at ISIS*. Physica B, 1992. **180**: p. 1000 - 1002.
76.   West, A.R., *Solid State Chemistry and its Applications*. 1987, Singapore: John Wiley and Sons Ltd.
77.   Fetisov, G.V., *Synchrotron Radiation for Structural Chemistry*. Fundamental and Applied Physics. 2007, Moscow: FizMatLit. 672.
78.   Ternov, I.M., Mihailin, V.V., *Synchrotron radiation. Theory and experiment*. 1986, Moscow: Energoatomizdat.
79.   Ternov, I.M., Mihailin, V.V., Halilov, V.R., *Synchrotron radiation and it's applications*. 1987, Moscow: Moscow University Press.
80.   Seddon, J., *Structural Studies of Liquid Crystals by X-ray Diffraction*, in *Handbook of Liquid Crystals*, G.J. Demus D., Gray G.W., Spiess H.-W., Vill V.,, Editor. 1998, Wiley - VCH: Cambridge. p. 635 - 669.
81.   Daresbury, L. *http://www.srs.ac.uk/srs/*. 2004.
82.   http://www.esrf.eu/computing/scientific/FIT2D.
83.   Zollinger, H., *Colour Chemistry: Synthesis, Properties and Applications of Organic Dyes and Pigments*. 1991, New York: VCH Publishers. 637.
84.   Rao, C.N.R., *Ultra - Violet and Visible Spectroscopy: Chemical Applications*. 1975, London: Butterworth. 242.
85.   Schoeff, L.E., Williams, R.H., *Principles of Laboratory Instruments*. 1993, St. Louis: Mostby.
86.   Breitmaier, E., Voelter, W., *Carbon - 13 NMR Spectroscopy; High Resolution Methods and Applications in Organic Chemistry and Biochemistry*. 1990, New York: Weinheim
514.
87.   Breitmaier, E., *Structure Elucidation by NMR in Organic Chemistry: a Practical Guide.* 2002, Chichester: Wiley. 270.
88.   Haigh, C.W., Mallion, R.B., *New Tables Of 'Ring Current' Shielding in Proton Magnetic Resonance.* Organic Magnetic Resonance, 1972. **24**: p. 203 - 228.
89.   Martin, N.H., Allen, N.W., Moore, J.C., *An Algorithm for Predicting NMR Shielding of Protons over Substituted Benzene Rings.* Joutnal of Molecular Graphics and Modelling, 2000. **18**(3): p. 242 - 246.
90.   Martin, N.H., Allen, N.W., Moore, J.C., *A Proton NMR Shielding Model for the Face of a Benzene Ring.* Journal od Molecular Structure - Theochem, 1998. **454**(2 - 3): p. 161 - 166.

91. Saika, A., Slichter, C.P., *A Note on the Fluorine Resonance Shifts.* Journal of Chemical Physics, 1954. **22**: p. 26 - 28.

92. Fahey, H.P., Graham, G.C., , *The Proton Magnetic Resonance Spectrum of Phenanthrene.* Journal of Physical Chemistry, 1965. **69**(12): p. 4417 - 4418.

93. Bain, A.D., *Chemical Exchange in NMR.* Progress in Nuclear magnetic Resonance Spectroscopy, 2003. **43**(3 -4): p. 63 - 103.

94. Chen, A.D., Johnson, C.S., Lin, M., Shapiro, M.J., *NOE Pumping: A Novel NMR Technique for Identification of Compounds with Binding Affinity to Macromolecules.* Journal of the American Chemical Society, 1998. **120**(39): p. 10258–10259.

95. Dehner, A., Kessler, H., *Diffusion NMR Spectroscopy: Folding and Aggregation of Domains in p53.* Chembiochem, 2005. **6**: p. 1550 - 1565.

96. Cavanagh, J., *Protein NMR Spectroscopy, Second Edition: Principles and Practice.* 1996, San Diego: Academic Press. 912.

97. McKeown, N.B., *Phthalocyanine Materials: Synthesis, Structure and Function.* 1998, Cambridge: University Press.

98. Dandridge, A.G., Drescher, H.A.E., Thomas, J., *Dyes*, S.D. Ltd., Editor. 1929: Great Britain.

99. Linstead, R.P., *Phthalocyanines. Part I. A New Type of Synthetic Colouring Matter.* Journal of the Chemical Society, 1934: p. 1016-1017.

100. Linstead, R.P., Lowe, A.R., *Phthalocyanines. Part III. Preliminary Experiments on the Penetration of Phthalocyanines from Phthalonitrile.* Journal of the Chemical Society, 1934: p. 1022 - 1027.

101. Linstead, R.P., Lowe, A.R., *Phthalocyanines. Part V. The Molecular Weight of Magnesium Phthalocyanine.* Journal of the Chemical Society, 1934: p. 1031 - 1033.

102. Linstead, R.P., Noble, E.G., Wright, J.M., *Phthalocyanines. Part IX. Derivatives of Thiophene, Thionaphthene, Pyridine and Pyrazine, and a Note of Nomenclature.* Journal of the Chemical Society, 1937: p. 911 - 921.

103. Cronshaw, C.J.T., *Les Phthalocyanines.* Endeavour, 1942. **1**: p. 79 - 83.

104. Leznoff, C.C., Lever, A.B.P., *Phthalocyanines: Properties and Applications.* 1989, New York: VCH Publishers Inc.

105. Mozer, F.H., Thomas, A.L., *The Phthalocyanines.* Vol. 1 and 2. 1983: CRC Press.

106. Slack, N., Chambers, S., Johnston, R., *Operations Management.* 2004, Madrid: Prentice Hall. 794.

107. Hanaki, N., Tateishi, K., Tanaka, S., *Water Soluble Phthalocyanine Compound - Containing Ink for Ink Jetting, Ink Jet Recording Method and Method for Improving Ozone Gas Discoloration of Coloured Image Material*, W.I.P. Organisation, Editor. 2003. p. 1 - 142.

108. Tateishi, K., Tanaka, S., Yabuki, Y., *Dye Mixture and Ink Containing the Same*. 2007, Fujifilm Corporation: USA.

109. Egerton, G.S., Morgan, A.G., *The Photochemistry of Dyes II - Some Aspects of the Fading Process.* Journal of the Society of Dyers and Colourists, 1970. **86**(6): p. 242 - 249.

110. Keuch, P., *Kinetics: Fading of Triphenylmethane Dyes - Pseudo First Order Reaction.* 2004, Regensburg: Didaktik.

111. Brezova, V., Pigosova, J., Havlinova, B., Dvoranova, D., Durovic, M., *EPR Study of Photochemical Transformations of Triarylmethane Dyes.* Dyes and Pigments, 2004. **61**: p. 177 - 198.

112. Coyle, J.D., *Introduction to Organic Photochemistry.* 1986, England: John Wiley and Sons.

113.   Gruen, L.C., *The Aggregation og Copper Phthalocyanine Dyes.* Australian Journal of Chemistry, 1972. **25**: p. 1661 - 1667.

114.   Camp, P.J., Jones, A. C., Neely, R. K., Speirs, N. M., *Aggregation of Copper(II) Tetrasulfonated Phthalocyanine in Aqueous Salt Solutions.* The Journal of Physical Chemistry, 2002. **106**(44): p. 10725 - 10732.

115.   Hussain, S., *Aggregation of Cyan Dye with Fuji additive.* 2006, FFIC: Manchester. p. 1 - 15.

116.   Gourteman, M., *Optical spectra and electronic structure of porphyrins and related macrocycles.*, in *The Porphyrins*, D. Dolphin, Editor. 1977, Academic Press: New York. p. 1-157.

117.   Claessen, G.C., Hahn, U., Torres, T., *Phthalocyanines: from outstanding electronic properties to emerging applications.* The Chemical Record, 2008. **8**: p. 75-97.

118.   Cooper, T.M., Stone M.O., , *Investigation of self-assembly upon formation of an electrostatic complex of congo red and a helical peptide.* Langmuir, 1998. **14**(23): p. 6662 - 6668.

119.   Smith, J.O., Olson D.A., Armitage B.A, *Molecular Recognition of PNA-Containing Hybrids: Spontaneous Assembly of Helical Cyanine Dye Aggregates on PNA Templates.* J. Am. Chem. Soc., 1999. **121**: p. 2686-2695.

120.   Owens, R.W., Smith, D.A., , *STM imaging of cyanine dye J-aggregates formed on carboxyl-terminated self-assembled monolayers* Langmuir, 2000. **16**(2): p. 562-567.

121.   Wright, J.D., *Molecular Crystals.* 1995, Cambridge: Cambridge University Press. 235.

122.   Neumann, B., Pollmann, P., *Effect of pressure on the UV-Vis spectra of Acid Red 266, Benzopurpurine 4B and Congo Red in water and ethane-1,2-diol up to 2400 bar.* Phys. Chem. Chem. Phys., 2001. **3**: p. 4508 - 4514.

123.   Schutte, W.J., Sluytersrehbach, M., Sluyters, J.H., *Aggregation of an octasubstituted phthalocyanine in dodecane solution.* Journal of Physical Chemistry, 1993. **97**: p. 6069 - 6073.

124.   Fujiki, M., Tabei, H., Kurihara, T., *Self-assembling features of soluble nickel phthalocyanines.* Journal of Physical Chemistry, 1988. **9**: p. 1281 - 1285.

125.   Jianbo, L., Zhao, Y., Fushi, Z., Fuqun, Z., Yingwu, T., Xinqi, S., *Dimerisation of Metal-free Sulphonated Phthalocyanines in Aqueous Methanol Solution.* Acta Physico - Chimica Sinica, 1996. **12**(2): p. 163 - 168.

126.   Monahan, A.R., Brado, J.A., DeLuca, A.F., *The Dimerisation of a Copper(II)-Phthalocyanine Dye in Carbon Tetrachloride and Benzene.* The Journal of Physical Chemistry, 1972. **76**(3): p. 446 - 449.

127.   Zhang, X., *Novel Methods for Measurement of Aggregation Constant of Dyes.* Science in China, 1993. **37**(11): p. 1298 - 1305.

128.   Chen, Z., Lohr, A., Saha-Moller, C.R., Wurthner, F., *Self-assembled Pi-stacks of functional dyes in solution: structural and thermodynamnic features.* Chemical Society Reviews, 2008. **38**: p. 564 - 584.

129.   Abkowitz, M., Monahan, A. R., *ESR and Electronic Spectral Investigation of the Self-association of Phthalocyanine Dyes in Solution.* The Journal of Chemical Physics, 1973. **58**(6): p. 2281 - 2287.

130.   Yahiro, H., Kimoto, K., Yamauro, H., Komaguchi, K., Lund, A., *Copper Phthalocyanine Encapsulated into Zeolite-Y with High Si/Al: an EPR Study.* Chemical Physics Letters, 2005. **415**: p. 126 - 130.

131.   Collman, J.P., Elliott, C.M., Halbert, T.R., Tovrog, B.T., *Synthesis and Characterisation of "Face - Face" Porphyrins.* Proc. Natl. Acad. Sci. USA, 1977. **74**(1): p. 18 - 22.

132. Tominaga, T., Toshima, N., *Multi-electron Transfer in Composite Phthlocyanine Thin Films: Structure and Electrochromic Properties.* Polymers for Adavanced Technologies, 1995. **6**: p. 197-203.

133. Kitaigorodskiy, A.I., *Molecular Crystals and Molecules.* Physical Chemistry. Vol. 29. 1973, New York: Avademic Press.

134. Berlepsch, H.V., Bottcher, C., Dahne, L., J. Phys. Chem. B, 2000. **104**.

135. Stroobants, A., Lekkerkerker, H. N. W., Macromolecules, 1986. **19**.

136. Goldfarb, D., Luz, Z., Spielberg, N., Zimmermann, H., *Strutural and Orientational Characteristics of the Disodium / Cromoglycate - Water Mesophases by Deuterium NMR and X-Ray Diffraction.* Molecular Crystals and Liquid Crystals, 1985. **126**(2): p. 225 - 246.

137. Ruslim, C., Matsunaga, D., Hashimoto, M., Tamaki, T., Ichimura, K., *Structural Characteristics of the Chromonic Mesophases of C.I. Direct Blue 67.* Langmuir, 2003. **19**: p. 3686 - 3691.

138. Perahia, D., Wachtel, E.J., Luz, Z., *NMR and X-Ray Studies of the Lyomesophases Formed by some Xantone Derivatives.* Liquid Crystals, 1991. **9**(4): p. 479 - 492.

139. Wieslandera, A., Ulmiusb, J., Göran Lindblomb, G., Fontellb, K., *Water Binding and Phase Structures for Different Acholeplasma Laidlawii Membrane Lipids Studied by Deuteron Nuclear Magnetic Resonance and X-ray Diffraction* Biochimica et Biophysica Acta (BBA) - Biomembranes, 1978. **512**(2): p. 241 - 253.

140. Mariani, P., Mazabard, C., Garbesi, A., Spada, G. P., *A Study of the Structure of the Lyomesophases Formed by the Dinucleoside Phosphate d(GpG). An Approach by X-ray Diffraction and Optical Microscopy.* Journal of American Chemical Society, 1989. **111**(16): p. 6369 - 6373.

141. Marrink, S., Mark, A. E., *Molecular View of Hexagonal Phase Formation in Phospholipid Membranes.* Biophysical Journal, 2004. **87**: p. 3894–3900.

142. De Vries, A., *X-ray Diffraction Studies of the Structure of the Skewed Cybotactic Nematic Phase: a Review of the Literature.* Journal of Molecular Liquids, 1986. **31**: p. 193 - 202.

143. Luzzati, V., *X-ray Diffraction Studies of Lipid-Water Systems.* Biological Membranes, ed. D. Chapman. 1968, London: Academic Press.

144. Robertson, J.M., J. Chem. Soc., 1936: p. 3230.

145. Taguchi, T., Wachi, N., Ogawa, M., *Black Ink and Ink Set for Inkjet Recording.* 2009, Fujifilm Corporation: USA.

146. Edwards, D.J., Ormerod, A.P., Tiddy, G.J.T., Jaber, A.A., Mahendrisingham, A., ed. *Aggregation and Lyotropic Liquid Crystal Formation of Anionic Azodyes for Textile Fibers.* Advances in Color Chemistry. Vol. 4. 1996, Blackie Academic and Professional: Cambridge. 83 - 105.

147. Ionov, A.V., *Colloidno-himicheslie Svoistva Liotropnih Zhidkokristallicheskih Sistem na Osnove Vodorastvorimih Organicheskih Krasiteley*, in *Colloidal Chemistry and Physical - Chemical Mechanics*. 2009, Russian University of Chemical Technologies of D.I. Mendeleev: Moscow. p. 118.

148. Hore, P.J., *Nuclear Magnetic Resonance.* 1995, Oxford: Oxford University Press. 96.

149. Keeler, J., *Understanding NMR Spectroscopy.* 2005, Chichester: Wiley - Blackwell. 476.

150. Macomber, R.S., *A complete Introduction to Modern NMR Spectroscopy.* 1998, New York: Wiley - Blackwell. 400.

151. Aksnes, D.W., Kimtys, *High-field Magnetic Resonance Studies of tert-butanol in Liquid and Solid Phases.* Magnetic Resonance in Chemistry, 1991. **29**(7): p. 698 - 705.

152. Gogoll, A., Tanner, D., *Complete 1H and 13C NMR Spectral Assignment of Venturicidin A by 2D NMR Spectroscopy.* Magnetic Resonance in Chemistry, 1989. **27**(9): p. 863 - 871.

153. Fedorov, L.A., *NMR Spectroscopy of Azo Dyes.* Russian Chemical Reviews, 1988. **57**(10): p. 941 - 955.

154. Mundy, K., Sleep, J.C., Lydon, J.E. , *The Intercalation of Ethidium Bromide in the Chromonic Lyotropic Phases of Drugs and Nucleic Acids* Liquid Crystals, 1995. **19**(1): p. 107 - 112.

155. Park, H.S., *Self-Assembly of Lyotropic Chromonic Liquid Crystals: Effects of Additives and Applications*, in *Department of Chemical Physics*. 2010, Kent State University. p. 166.

Appendix

Chromonic Liquid Crystal Formation by Edicol Sunset Yellow[†]

D. J. Edwards,[||] J. W. Jones,[‡] O. Lozman,[‡] A. P. Ormerod,[⊥] M. Sintyureva,[‡] and G. J. T. Tiddy*,[‡]

School of Chemical Engineering & Analytical Science, University of Manchester, PO Box 88, Manchester, M60 1QD, U.K., and FUJIFILM Imaging Colorants Limited, PO Box 42, Hexagon Tower, Blackley, Manchester, M9 8ZS U.K.

Received: March 31, 2008; Revised Manuscript Received: June 13, 2008

The solution and liquid crystalline phases formed by dissolution of the dye Edicol Sunset Yellow (ESY) in water have been examined using optical microscopy, multinuclear NMR (^{1}H, ^{2}H, ^{13}C, ^{23}Na), and X-ray diffraction. From the solution ^{1}H and ^{13}C spectra (particularly ^{13}C), it is clear that the tautomeric form present in all these phases is the hydrazone, NH, structure, not the usually given azo, OH, form. Two chromonic mesophases occur: a nematic (N) phase at ~30–40 wt % and a hexagonal (M) phase at ~40–45 wt %. X-ray diffraction data show that the aggregates in the mesophases are single molecule stacks, with a typical spacing of ~3.5Å, as expected for these systems. The NMR quadrupole splittings (^{2}H$_2$O, ^{23}Na) are similar to those observed for surfactant lyotropic mesophases, suggesting that there are no water molecules or counter ions that are tightly bound to the ESY aggregates. An unusual feature of the X-ray diffraction pattern of the mesophases is the occurrence of diffuse off-axis reflections at ~6.8Å. It is proposed that these arise from a head-to-tail packing of the molecules within the stacks.

Introduction

Molecular self-assembly to form nanostructures is a highly active research topic with relevance for a wide range of interests, from product formulation to biological cells. Chromonic lyotropic liquid crystals are a particular class of self-assembly systems. They occur when planklike, aromatic compounds (usually ionic) having multiple ring structures containing polar substituents are dispersed in water. Even in dilute solutions, these compounds have a strong tendency to aggregate into stacks; the stacks then become ordered at higher concentrations. Lydon[1,2] has recently reviewed the area, pointing out the large range of possible applications. A much better fundamental understanding of the molecular mechanisms underpinning the aggregation is required for the full potential to be developed. The most well-known system studied to date is disodium chromoglycate (DSCG), an antiasthmatic drug. At room temperature, this forms first an isotropic solution (I), then a nematic (N) phase between ~10 and 20 wt % and a hexagonal (columnar) mesophase (M) at higher concentrations (>20 wt %). Similar behavior is shown by numerous other systems, including cyanine and azo dyes.[1–4]

Edicol Sunset Yellow (ESY, Figure 1) is a food coloring azo dye which also forms the nematic and hexagonal phases in water[5] (possessing specific textures identifiable using polarized light[5–9]), but at much higher concentrations than DSCG (~30–40 and >40 wt % for nematic and hexagonal phases, respectively). Recently, Horowitz et al. reported[5] a phase diagram together with other properties of the Edicol/water system, their emphasis
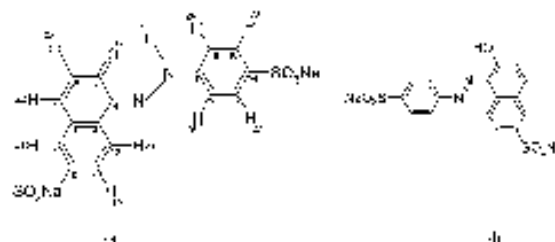
Figure 1. Potential tautomeric structures of ESY: (a) NH form (numbering of atoms is that used for high resolution NMR data; see Table 1) and (b) OH form.

TABLE 1: Conditions for the Preparative HPLC Purification of Edicol Sunset Yellow

Time (mins)	A (%)	B (%)
0	99	1
25	50	50
30	50	50
31	99	1
40	99	1

being on the solution and nematic phases. Their paper[5] gives valuable data on the aggregation mechanisms in solution and on molecular order parameters within the nematic phase. The latter show a remarkably high degree of ordering compared to, for example, surfactant lyotropic mesophases. We have also made studies on this system, looking at both the nematic and hexagonal mesophases. A brief summary of our older results was given several years ago,[9] but we have made further measurements on the system recently. In particular, we address the issue of the molecular and aggregate structures that are present in the three aqueous phases.

Hydroxy-substituted azo dyes contain a labile hydrogen atom that has the potential to exist in either an NH (hydrazone) or OH (azo) form (or varying proportions of both), according to

Chromonic Liquid Crystal Formation by ESY

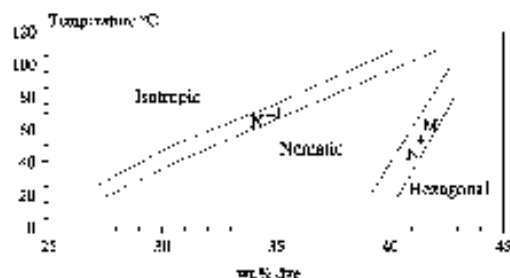*J. Phys. Chem. B, Vol. 112, No. 46, 2008* **14629**

Figure 2. Partial phase diagram of Edicol in aqueous solution.

the other substituents present in the molecule. The two potential structures for Edicol are shown in Figure 1. For hydroxy-azo-naphthalenes, it is generally accepted[10] that the hydrazone form (Figure 1a) is stable, whereas the hydroxyl form is stable for phenyl derivatives. Unfortunately, even with authors who are well aware of this,[9] the Edicol chemical structure is frequently given as the azo form (Figure 1b). Horowitz et al.[5] give this structure only, without discussing this matter. Because of the strong attractive interactions between aggregated dye molecules, it is entirely possible that the form in the stacks differs from the monomers. Here, we first outline recent ^{1}H and ^{13}C high-resolution NMR measurements (particularly ^{13}C) that confirm the hydrazone structure (Figure 1a) for both monomers (low concentrations) and stacks (high concentrations) in the solution phase. In addition, the chemical shift changes with concentration give an indication of the detailed molecular arrangement within the stacks. The data are consistent with a "head-to-tail" organization. We have also employed polarizing optical microscopy to identify the mesophases (nematic, hexagonal) and to construct a phase diagram. Further NMR measurements (^{1}H) on both of the mesophases allow an estimate of molecular ordering from the dipole–dipole splittings. There is a remarkably good agreement with the conclusions of Horowitz et al.[5] where comparisons can be made. From ^{2}H and ^{23}Na NMR quadrupole splittings for sodium ions and water, more information on the molecular interactions within the mesophases can be obtained. Finally, we report additional X-ray diffraction data. In addition to the expected reflections from the organized aggregates and the 3.5 Å reflection from the stacking of aromatic rings, there is an additional reflection at ~6.8 Å that is consistent with a "head-to-tail" organization of molecules within the stacks in all three phases.

Experimental

Materials. Initially, Edicol was obtained from ICI Colors and Fine Chemicals Division and subsequently from Sigma Aldrich. The initial material was purified by dissolution in distilled water to obtain a mesophase, followed by the careful addition of ethanol to form a dye precipitate, which was then recovered by filtering. This was repeated twice more, followed by drying in a vacuum oven to remove residual water and ethanol. The purity of the final solid was verified by elemental analysis and the absence of additional peaks in proton NMR. Toward the end of the project, the material (ex. Sigma) was purified by preparative HPLC using a Waters HPLC system controlled by Empower Pro Waters software (Waters, Milford, MA). This included a Waters 717 Autosampler and a Waters 2996 photodiode array variable wavelength UV detector and employed a Genesis C18 reversed-phase HPLC preparative column (250 mm × 22.5 mm i.d., 15 μm particle size). The solvent system consisted
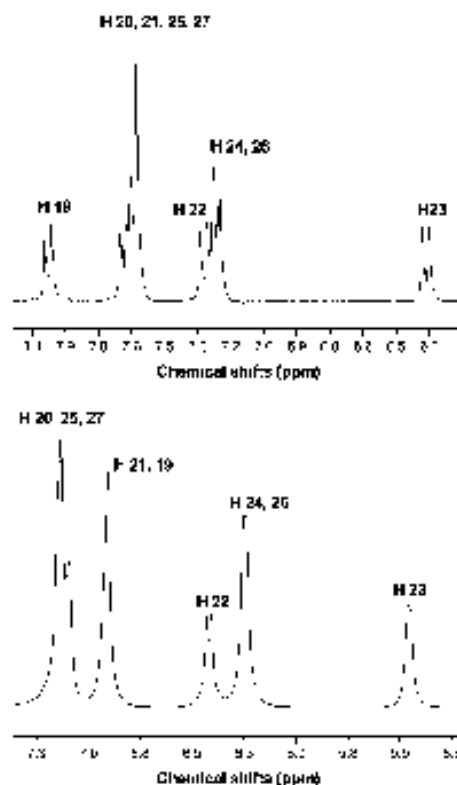

Figure 3. High-resolution NMR spectra (^{1}H) of Edicol in [2]H$_2$O at ambient temperature; upper, 0.5%; lower, 20%.

of 10 mmol of aqueous solution of ammonia acetate (solvent A) and pure acetonitrile (solvent B), which were delivered to the column nonisocratically (Table 1).

A 10% aqueous solution of ESY was injected into the HPLC system and detected by absorbance at 254 nm. Edicol Sunset Yellow was collected manually at 22.5 min with 99.9% purity.

Optical Microscopy. A Carl Zeiss Jena Jenaval polarizing optical microscope and a Linkam TMS90 hot stage were used to conduct the microscopy experiments. The samples were prepared gravimetrically in sealed ampoules and stored in an oven at about 80 °C for at least a day. For the microscopy study, a portion of the sample was placed on a microscope slide with a coverslip placed on top. The edges of the coverslip were then sealed with Araldite to prevent solvent evaporation. The sample was observed during heat/cool cycles using a rate of 5 °C/min, although near the actual transitions, a slower rate of 1 °C/min was used. To avoid difficulties caused by the slow equilibration of compositions in two phase regions, the N/N + I transition point was measured on heating as the temperature at which the isotropic phase began to form, whereas the I/I + N transition was measured on cooling as the temperature at which the nematic phase first appeared. This was repeated a number of times, and the average transition temperature was calculated (error: ± 1 °C). A similar procedure was used for the N/M transition.

NMR Spectroscopy. Measurements were made on a number of high resolution spectrometers, the main instruments being Bruker AC-250, AMX-400, and AV 500 spectrometers and an Inova 400 (IP) spectrometer with either 5 or 10 mm probes. For solution spectra, the samples were placed in conventional
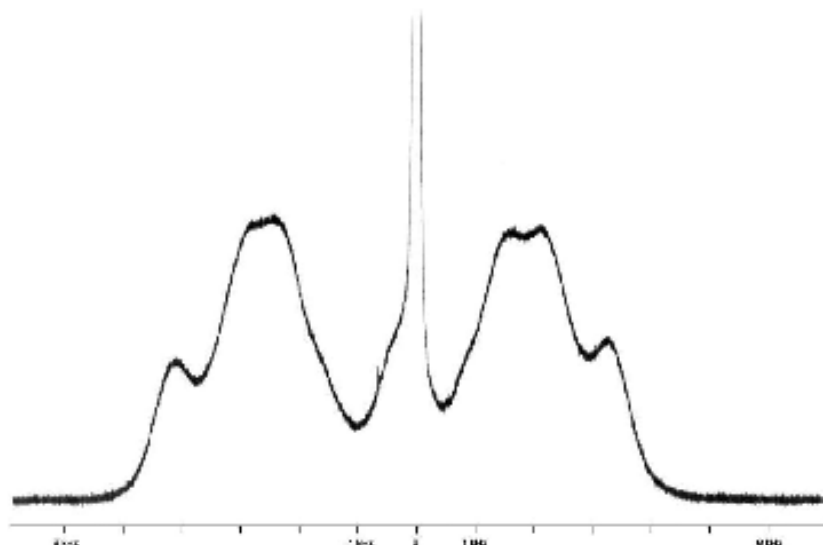
Chromonic Liquid Crystal Formation by ESY

J. Phys. Chem. B, Vol. 112, No. 46, 2008 **14631**

Figure 4. ^{1}H NMR spectrum of Edicol (nematic phase, ambient temperature).

percent. All the samples employed in this study were examined using optical microscopy to verify the phase structures. Calorimetry has also been used to investigate chromonic liquid crystal transitions.[12] However, because the large phase coexistence boundaries and small transition enthalpies (<5%) make it difficult to accurately identify phase transition, it is not our technique of choice.

High-Resolution NMR Studies (^{1}H, ^{13}C) of the Solution Phase. Our initial objective was to establish the tautomeric form present in the solutions. Representative proton spectra at two concentrations in D$_2$O are given in Figure 3. For either nucleus, only a single spectrum is observed over the full range of concentrations examined (0.05−20.00%); hence, the molecular exchange between monomers and aggregates is fast on the NMR time scale (exchange rates >∼10^3 s^{-1}). At the lowest concentrations examined to date (^{1}H, 0.05%; ^{13}C, 1.00%), monomers are present in excess, whereas at 20%, the aggregates are the major species.[5] We are still in the process of obtaining spectra at lower concentrations for both nuclei, but instrument availability has been a limiting factor to date. The resonance assignments are listed in Table 2. The proton spectra are relatively simple, comprising an AA′BB′ pattern (relative intensity, four protons) for the single aromatic ring, a singlet (1 proton) and two AB patterns (each with relative intensities of 2 protons) for the naphthalene ring. The NH undergoes fast exchange with the solvent; hence, it is not observed. Similarly, the carbon-13 spectra are also relatively simple, with most of the assignments being straightforward. An examination of the tautomeric form (Figure 1) shows that the major difference expected between the two is for carbon-5. Kelemen et al.[13] have reported an important study of Raman and NMR spectra in these systems in which model compounds were examined. By comparison with their results, in Figure 1a, carbon-5 is a C=O, with an expected chemical shift of ∼180 ppm, whereas in Figure 1b, it is an aromatic COH, with an expected chemical shift of ∼165 ppm. Clearly, the data in Table 2 show that at both low and high concentrations, the C=O form is present; hence, aggregation does not change the tautomer in this case. [Note that this cannot be assumed to be generally true.]

There is an enormous change in the chemical shifts with concentration for all the peaks, typically ∼0.5−1.5 ppm (Table 2). For conventional organic compounds, changes of ≤0.1 ppm occur. The large changes reflect the well-known influence of aromatic "ring-current" shielding/deshielding because of the aromatic ring-stacking. For all of the ^{1}H and ^{13}C nuclei, the chemical shift changes are to lower values with increasing concentration, indicating that the nuclei are all located in the shielding region of adjacent aromatic groups when aggregates form. With a good estimate of the chemical shift differences between the aggregates and monomers, it should be possible to elucidate the molecular arrangement within the aggregates. Even without the full chemical shift-vs-concentration study, the main changes are apparent. The simplest way to describe the changes is to use a two-state model, with molecules either existing as monomers or aggregates. Within the aggregates, all the molecules are assumed to have the same chemical shifts (δ_a), whether they are located in the center or at the ends of the aggregates. Then the observed chemical shifts (δ_{obs}) are given by

$$\delta_{obs} = p_{mon}\delta_{mon} + p_a\delta_a \qquad (1)$$

where subscripts "mon" and "a" refer to monomers and aggregates, respectively, δ is the chemical shift, and p is the fractional population of the two states ($p_{mon} + p_a = 1.0$).

Unfortunately, we do not yet have data for very low concentrations. Even at the two lowest concentrations measured (0.05 and 0.10%), there is still a small difference between ^{1}H δ_{obs} values (0.05−0.1 ppm); hence, a few aggregates are certainly present at 0.10% and perhaps also at the lowest concentration (the monomer chemical shift is expected to be independent of concentration). For the lowest concentration where ^{13}C δ_{obs} values have been measured (1.0%), there is a very significant fraction of aggregates present. At the two highest concentrations (15.00 and 20.00%), all the chemical shifts are the same within <0.05−0.1 ppm. Thus, at 20%, almost all of the Edicol exists in aggregates. We can obtain a reasonable estimate of the difference between δ_{mon} and δ_a ($\Delta\delta$) if we assume that the ^{1}H δ_{obs} values at 0.05% are for the monomer and the values

14632 *J. Phys. Chem. B, Vol. 112, No. 46, 2008*

Edwards et al.

at 20.00% correspond to the aggregates. Then the experimental data give $^1H \delta_a - \delta_{mon}$ directly, and the $^{13}C \delta_a$ values are also known. The $^{13}C \delta_{mon}$ value can be estimated by taking the differences in δ_{obs} between 1.0% and 20.0% for both ^1H and ^{13}C and scaling up the ^{13}C data using the expression

$$\Delta\delta C = \Delta\delta^H (\text{diff } 1.0\%)^C / (\text{diff } 1.0\%)^H \quad (2)$$

where the superscripts C and H refer to ^{13}C or ^1H nuclei, and diff 1.0% is defined in the Table 2 footnotes. For the two-state model, it is a simple matter to show that at 1.0%,

$$p_a = (\text{diff } 1.0\%)^H / [\Delta\delta^H] = (\text{diff } 1.0\%)^C / [\Delta\delta^C] \quad (3)$$

If the model is valid, then using the $^1H \delta_{obs}$ values, we will calculate the same p_a value, whichever hydrogen is selected. Table 2 shows that this is reasonably valid, but for H_{19} and $H_{25,27}$, the p_a values are larger than for the other hydrogens. Even with this discrepancy, the error in the calculated $\Delta\delta^C$ is likely to be no more than 0.1 ppm.

There is a large variation in the magnitude of $\Delta\delta$ for both ^1H and ^{13}C nuclei. If we assume that "ring-current" shielding is responsible for the changes, then we can determine the molecular organization within the aggregates. Note that nuclei in both of the aromatic rings show the largest $\Delta\delta$ values; hence, it is likely that both rings participate in the stacks, having a coplanar arrangement. If this were not the case, the phenyl ring would fall outside the central core and undergo rotation, and the chemical shift changes would be smaller. Because H_{24} and H_{26} have the second-largest proton $\Delta\delta$ value, both are likely to be in the π-stack core. Thus, they have naphthalene aromatic regions above and below. This is confirmed by the ^{13}C data for C_{11}, showing a $\Delta\delta$ value of a similar magnitude. Similarly, C_3, C_4, and H_{20} of the naphthalene ring are shielded by the phenyl rings. Thus, H_{25} and H_{27} together with C_{13}, C_{14}, and C_{15} from the phenyl ring are outside the core of the π-stacks. Similarly, H_{19}, C_8, and C_9 are also well outside the π-stack core. It is worth noting that most of the atoms close to the sulfonate groups are outside the core. The molecular organization within the aggregates is discussed further below, following the results for mesophase behavior.

We note that the observation of such large changes in the NMR chemical shifts with aggregation offers a simple method to study the influence of numerous third components on the concentration of aggregates. Particularly for water-soluble additives such as urea and electrolytes, which are unlikely to bind preferentially either to monomers or aggregates, any chemical shift changes will be directly related to changes in monomer and aggregate concentrations. This can be confirmed by establishing that the chemical shifts are invariant in the presence of the additive at very low and very high concentrations where one species (monomers or aggregates respectively.) dominates the spectrum.

At the very highest concentrations (>15% Edicol), we observe that the NMR line widths are significantly broadened (~5-10 Hz at 20%). For example, the resonance of H_{23} is broadened into a single peak, losing the structure due to scalar coupling (see Figure 3). Clearly, this arises from increased spin-spin relaxation rates (T_2^{-1}) because of hindered molecular motion from slow rotation of the aggregates. We are currently obtaining additional data for this region, but the line broadening suggests that the correlation time for rod rotation is on the order of 10^{-8} s.

Broad-Line NMR Studies of the Mesophases (^1H). The NMR spectra of crystals and liquid crystals potentially contain

TABLE 4: Water and Sodium Quadrupole Splittings for Edicol

wt % Edicol	temp (°C)	mol ratio Edicol/water	Δ^2H (Hz)	$\Delta^{23}Na$ (kHz)	phase
29.0	25	55.37	362		N
32.0	25	48.06	402	3.25	N
36.0	25	40.21	609	3.73	M
38.0	25	36.90	588	3.78	M
40.00	20	33.93	634		M
	25		625	3.79	M
	30		625		M
	35		625		M
	40		600	3.74	M
	45		600		M
	50		575	3.70	M
	55		563		M
	60		557/500	3.50	N/M
	65		495	3.43	N
	70		490	3.23	N/I (small)

multiple peaks because all the NMR-active nuclei interact with each other through dipole-dipole coupling.[14,15] However, proton NMR spectra of mesophases (prepared with ^2H_2O) usually give a broad, featureless resonance with a half-height width of several kilohertz because the multiple dipole-dipole couplings[14,15] cause overlapping of resonances. In addition, even for simple molecules, the NMR spectra for a normal random "powder" sample are ill-defined because the dipole-dipole couplings are dependent on the angle between the proton-proton vector (r_{ij}) and the NMR magnetic field (θ_{LM}). Within liquid crystals, the intermolecular interactions are averaged to zero by fast molecular motions, but the remaining intramolecular dipole-dipole couplings are sufficient to obscure the individual contributions from specific proton pairs. However, the ESY nematic phase spontaneously orients in the NMR magnet with the liquid crystal axis at right angles to the magnetic field. Oriented samples of the hexagonal phase can also be prepared by slow cooling from the nematic phase. This reorientation is a result of an interaction between the aromatic ring and magnetic field, which is commonplace for thermotropic mesogens possessing aromatic rings. Hence the "powder-orientation" broadening is not present, resulting in narrowing of the resonance lines. In addition, the number of hydrogens in the molecule is small. Thus, the proton spectrum is relatively simple (Figure 4).

The dipole-dipole interaction (D_{ij}) among all the proton pairs (i, j) in the molecule is given by the following equation,[14,15]

$$D_{ij} = [(h\gamma_i\gamma_j)/4\pi^2](3 \cos^2 \theta_{DL} - 1)S_{ij}/2r_{ij}^3 \quad (4)$$

where D_{ij} is the direct coupling between two nuclei, i and j; γ is the magnetogyric ratio ($\gamma_H = 26.75 \times 10^3$ rad G^{-1} s^{-1}); r_{ij} is the vector joining the nuclei, i and j; θ_{DL} is the angle between the magnetic field and the director. $S_{ij} = <3 \cos^2 \theta_{DM} - 1>/2$, where θ_{DM} is the time-averaged angle between the director and the axis, r_{ij}. The term $(3 \cos^2 \theta_{DL} - 1)/2$ describes the dependence of Δ_{HH} on the orientation of the director in the magnetic field. In this case, $\theta_{DM} = \pi/2$. The measured splitting (Δ_{HH}) for two identical nuclei in an oriented sample with the liquid crystal axis at right angles to the magnetic field is given by:

$$\Delta_{HH} = 3|D_{ij}| \quad (5)$$

Because of the r_{ij}^{-3} dependence, the most important contributions to the total Δ_{HH} come from close neighbors. In aromatic C-H groups the dipole couplings between ortho and peri protons dominate the spectrum. For ESY, there are three distinct
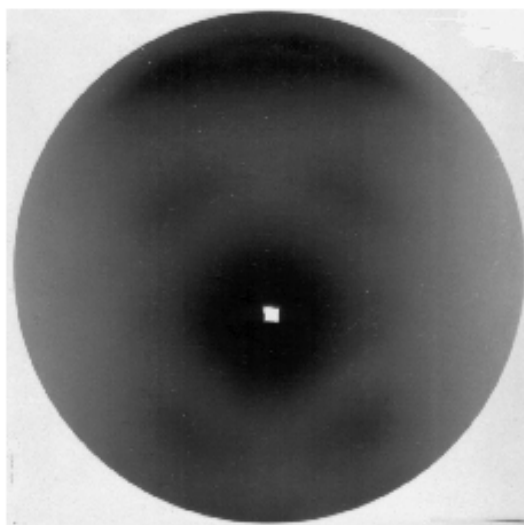
Chromonic Liquid Crystal Formation by ESY

J. Phys. Chem. B, Vol. 112, No. 46, 2008 **14633**

Figure 5. X-ray pattern for 39.6% Edicol at room temperature. The arc at the top is the reflection at 3.34 Å; the off-axis four diffuse spots at 6.5−6.7 Å are clearly visible.

overlapping spectra: one doublet due to H_{24}−H_{25} plus H_{26}−H_{27}, one doublet from H_{19}−H_{20}, and a three-proton spectrum from H_{21}, H_{22}, and H_{23}. Molecular models show that the distances $r_{21,22}$ and $r_{22,23}$ are almost identical (2.44 and 2.48 Å, respectively).[16] Hence, the three-proton spectrum comprises a pair of doublets (H_{21}, H_{23}) and a triplet (H_{22}). The distances $r_{21,22}$ and $r_{22,23}$ are very close to those of the other proton−proton vectors (all in the range 2.44−2.50 Å).[16] It is difficult to assign the doublets to specific groups, since all of them overlap. But the two outer peaks of the 1:2:1 triplet can be clearly distinguished, albeit that they are much less intense than the doublets (Figure 4). Thus, we can determine the sum of the order parameter for $r_{21,22}$ and $r_{22,23}$ ($S_{21,22} + S_{22,23}$). From this we obtain the molecular order parameter, $S_{mol} = (S_{21,22} + S_{22,23})/2$. Since the rings are perpendicular to the stack axis, the stack order parameter (S_s) is given by:

$$-2S_{mol} = S_s \tag{6}$$

Several separate peaks can be discerned in the remaining part of the spectrum. However, the slightly different specific r_{ij} values and the finite spread of chemical shifts make assignments difficult. But an inspection of the other broad peaks in Figure 2 shows that their positions are consistent with similar Δ_{HH} values. Certainly, there are no proton pairs with significantly smaller Δ_{HH} values. Thus, the spectrum shows that the proton pairs in the two aromatic rings have similar Δ_{HH} values; that is, the rings are coplanar. If the phenyl ring underwent independent rotation, then the Δ_{HH} values would be significantly reduced.

Table 3 shows that the order parameter increases with concentration. At ambient temperature, it is only slightly larger in the M phase than for the N phase. This difference between the phases is only a little larger for the temperature scan. Note that the two phase (N + M) samples did not give resolved separate spectra. The two phases were identified by microscopy. Our values of the order parameter can be compared with those of Horowitz et al.[5] We should take into account the difference in concentrations and techniques (Horowitz et al. measured birefringence using a 1.25 m concentration, equivalent to 36.12% in normal water, and ~34% in ^2H_2O).[5] The general agreement

is good, but those of Horowitz et al. are slightly larger than the values reported here. As pointed out in Horowitz et al., the value of the order parameter is large compared to those of thermotropic liquid crystals. This is not surprising, since the packing within stacks is likely to be far more rigid and ordered that that of thermotropic mesophases. The higher values of Horowitz et al. may be related to the use of macroscopic measurement (birefringence), whereas we have a molecular measurement. It is quite likely that the two aromatic rings are not always exactly coplanar and that there is some local molecular mobility/flexibility within the stacks. These factors would result in lower S_{mol} values as measured by NMR. We note that the observation of such a simple ^1H NMR spectrum offers a direct method to study the influence of numerous third components (urea, electrolytes, solutes) on the structure and ordering of the aggregates.

^2H and ^{23}Na Quadrupole Splittings of the Mesophases. For surfactant lyotropic mesophases, studies of NMR quadrupole splittings have been widely used both to study molecular interactions within the mesophases and to determine phase structures.[14,15,17,18] The NMR behavior is similar to that described above for dipole−dipole splittings. Nuclei with a spin quantum number (I) greater than 1/2 have an electric quadrupole moment that interacts with any electric field gradients (efg) at the nucleus. This results in multiple NMR transitions (2I). These are degenerate in isotropic phases, but give multiple lines (2I) for noncubic mesophases. For ^2H_2O in uniaxial mesophases, the separation between the peaks (the quadrupole splitting, Δ^2H_{obs}) is given by

$$\Delta^2H_{obs} = (3/4)E_q S_{OD}[3\cos^2\theta_{LD} - 1] \tag{7}$$

where E_q is the characteristic quadrupole coupling constant and θ_{LD} is the angle between the mesophase director and the external magnetic field. S_{OD} is an order parameter for the nuclear efg, which is given by

$$S_{OD} = \langle 3\cos^2\theta_{DM} - 1\rangle/2 \tag{8}$$

where θ_{DM} is the angle between the efg and the mesophase director and the brackets $\langle\rangle$ indicate a time average. The expressions for sodium quadrupole splittings ($\Delta^{23}Na_{obs}$) are very similar, differing only in that the spin quantum number for ^{23}Na is 3/2, whereas it is 1.0 for ^2H.[17−20]

For surfactant liquid crystals, the behavior of both water and counterion quadruple splittings is usually described using a two-state model that distinguishes between water molecules or ions close to the surfactant aggregates (within ~1−3Å, termed "bound") and those further away (termed "free"). "Free" species are assumed to have zero ordering, as for isotropic solutions. "Bound" species are ordered because the aggregates are ordered. The free and bound species exchange rapidly on the NMR time scale; hence, a single resonance is observed with a Δ value that is proportional to the fraction of bound species (p^b_{water}, p^b_{Na} for water and ions, respectively).

$$\Delta^2H_{obs} = p^b_{water}\Delta^2H^b; \Delta^{23}Na_{obs} = p^b_{Na}\Delta^{23}Na^b \tag{9}$$

where Δ^2H^b and $\Delta^{23}Na^b$ are the quadrupole splittings for bound species.

From surfactant mesophase behavior[17−21] and the studies on chromonic mesophases to date,[22−24] the amount of bound water is expected to vary linearly with solute concentration until the concentration of free water is comparable to the bound fraction. At high concentrations, the values become reasonably constant or even decrease. With sodium sulfate head groups (the closest

14634 *J. Phys. Chem. B, Vol. 112, No. 46, 2008*

Edwards et al.

TABLE 5: The X-ray Spacings at Room Temperature for Various Concentrations of Edicol Sunset Yellow

dye concn % wt/wt	phase	d, spacing, Å (0.4 Å)	ring stacking, Å (0.05 Å)	diffuse reflection, Å (0.2 Å)	column area (Å²)[b]
28.0	I	27.9	3.42	6.7	
29.9	N	25.9	3.36	6.7	
31.5	N	25.5	3.45	6.7	
33.6	N	24.6	3.43		
36.0	N	23.8	3.43		
37.8[a]	N	23.4	3.52	6.4	
39.6[a]	N	22.3	3.34	6.4	
41.5	M	21.3	3.48	6.4	96
43.9	M	20.4	3.45	6.4	94
46.0	M	20.2	3.48	6.4	96

[a] Oriented sample. [b] Calculated according to the method of Luzatti.[26]

structure to the Edicol polar groups for which data are available).[25] there are about 10 bound water molecules per surfactant in the hexagonal phase. In this case, the bound water fraction does not vary strongly with temperature (<100 °C). Thus, we expect deviations from linear behavior above dye/water ratios of ~1:30.

For sodium binding in surfactant mesophases, a much simpler model appears to apply in many cases. Manning has shown that for highly charged aggregates (such as ionic surfactant rod micelles), a process known as "ion condensation" occurs.[26] Here, the counterions "condense" onto the aggregate surface to neutralize most of the charges (typically 70%), with the rest being "free" in solution. Crucially, the bound fraction is independent of surfactant (or dye) concentration and also shows little variation with temperature.

We have measured ^{2}H and ^{23}Na quadrupole splittings, both as functions of composition and temperature (Table 4). The ^{2}H
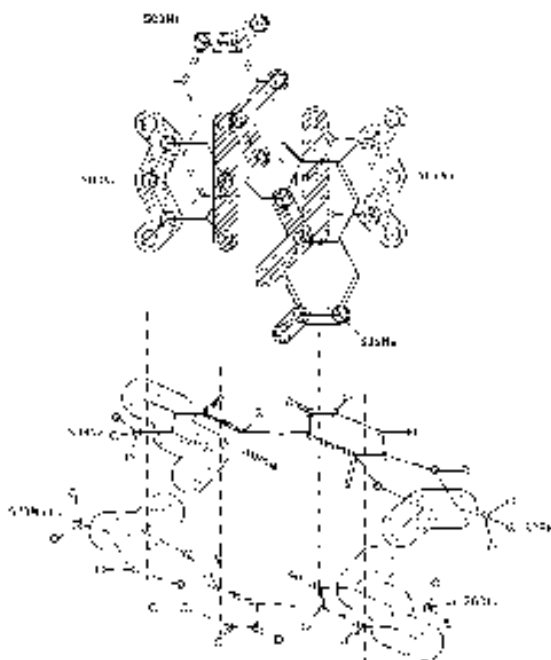

Figure 6. The proposed dimer structure for Edicol, showing both plan (top) and perspective (bottom) views. Highlighted are the high (45° hatched areas) and low (spotted) chemical shifts and also the sulfonate groups.

spectra consist of a single peak for the solution phase, a sharp doublet for the N phase, and a Pake powder pattern for the M phase.[12–14] The latter is transformed into a sharp doublet if the M phase is formed by cooling from the N phase. Overlapping spectra are observed for multiphase samples. The sharp doublets for both the N and M phases indicate that the mesophases are aligned with the director perpendicular to the magnetic field, as expected from other chromonic systems.[22–24] At 25 °C, there is a large initial increase in $\Delta^2 H_{obs}$ with Edicol concentration, but then above ~36%, the values become almost constant. This is very similar to what is observed in surfactant mesophases, suggesting that the water binding is also similar. Only a small decrease with increasing temperature is observed, again similar to surfactant systems. The decrease is similar in magnitude to the decrease in S_{mol} with increasing temperature from the ^{1}H data, indicating that the decrease is due to a reduction in aggregate orientation rather than a decrease in water binding. The similarity of aggregate ordering in the N and M phases is confirmed by the small difference in $\Delta^2 H_{obs}$ for the single sample with coexisting N and M phases. Unlike the case for the ^{1}H spectra, here, the relatively small line widths allow the two spectra to be resolved. Even with the difference in water compositions (and hence, a difference in "free" water concentration), the $\Delta^2 H_{obs}$ values differ by only ~10%. There is a further complication for Edicol that needs to be considered. The labile NH exchanges rapidly with water hydrogens, giving another contribution to $\Delta^2 H_{obs}$. Although the fraction of ^{2}H nuclei in this site is small (<2%), the $\Delta^2 H_{NH}$ value is likely to be large (>1 kHz) and possibly of opposite sign to $\Delta^2 H^b$. This additional complication makes any further analysis of the data reliant on too many variables.

For sodium, all the N and M phase samples give the spectra expected for spin-3/2 nuclei [three peaks with intensities in the ratio 3:4:3; either three sharp peaks for oriented samples (director perpendicular to the magnetic field) or a Pake powder pattern for M samples that are not].[15,18–20] Intensity checks with standard salt solutions demonstrated that all of the sodium ions contribute to the spectrum, rather than some being "tightly bound" to the aggregates and having a spectrum too broad to be observed. The Δ^{23}Na values increase slightly with concentration and also decrease slightly with temperature. These changes are similar to the variations seen in S_{mol}, above, suggesting that small changes in the aggregate ordering are responsible. The absence of a variation with concentration suggests that the "ion condensation" binding model applies, as for surfactant hexagonal phases[19,25] In magnitude the Δ^{23}Na values are less than half those normally observed for surfactant aggregates. We discuss this further below.

X-ray Diffraction Measurements. X-ray diffraction measurements were carried out for a range of compositions at ambient temperature (~24 °C) and for one composition at higher temperatures. Several samples gave patterns indicating that the mesophase director was aligned along the tube axis (see Figure 5); otherwise, there was no preferential alignment direction. The results are given in Table 5. Three distinct contributions to the diffraction patterns were observed. First, there were reflections corresponding to the packing of the aggregates in the range 20–30 Å (not seen in Figure 5 because of intense scattering at the center of the photograph. For the M phase up to four orders of the hexagonal pattern occurred (e.g., d_0 $d_0/\sqrt{3}$, $d_0/2$, $d_0/\sqrt{7}$ at 20.2, 11.6, 10.2, and 7.5 Å for the 46.0% sample), although the higher orders were very weak. For the N and I phases, a single reflection of this type was present. Second, all the samples, including the solution phase, gave a sharp reflection at ~3.4 Å. For oriented samples, this occurred at right angles to the 20–30 Å reflection, as expected for the ring stacking. Finally, most of the samples gave a very diffuse reflection at ~6.5–6.7 Å. This was observed even for the solution phase, although additional experiments are required to investigate the concentration dependence. Remarkably, in the oriented samples, the reflection occurred as four off-axis spots (see Figure 5). Their origin is discussed below. These results are in good agreement with those obtained by Lavrentovich et al.[11]

Following the treatment of Luzzati[27] for surfactant hexagonal phases, we have calculated the column cross-sectional area. Very similar values are obtained for the N and M phases of ~95 Å², close to the area of a single molecule (~97 Å²). Again, this is in good agreement with previous results[5,8,11,28] [In this calculation, we have assumed that the sodium sulfonate groups reside in the aqueous regions (density = 1200 g dm⁻³) and that the aromatic cores (density = 1300 g dm⁻³) contain no water.] Then the column areas for the M phase are 95 Å², which compare well with the area of a single planar Edicol molecule of ~97 Å².

The off-axis diffuse reflection is present in all three phases; hence, it cannot arise from additional ordering from interrod correlations within the mesophases. However, stacking of the molecules in a "head-to-tail" fashion with alternating molecules being rotated by π radians about the column axis would produce a helical structure having a short pitch, which could give rise to the pattern observed.[29–32]

Discussion and Conclusions

First, it is clear that the usual chemical structure given for Edicol (with an OH) is incorrect, the tautomer in solution being the NH form. Considerable information on the structure of the stacks can be derived from the NMR and X-ray data. Figure 6 shows the structure of Edicol with the atoms having the largest and smallest chemical shift changes with concentration. We take the largest changes to correspond to atoms that are located above or below the aromatic cores of neighboring molecules in the stacks. Those with the smallest changes must be located at the edges of their neighbors. Thus, we propose that the arrangement of the molecules is as shown in Figure 6. Note that there is no evidence for any water molecules or counter ions to be bound at specific sites within the stacks. These species interact with the stacks in a manner similar to their behavior in surfactant liquid crystals.

The long-range order within the stacks is much less clear. The M phase has hexagonal symmetry by X-rays and is uniaxial from NMR. But Edicol itself is more rectangular than circular, having an aromatic core of ~14 Å × 8 Å. Thus, it could form a "rectangular" phase with biaxial symmetry, as is seen for some ionic surfactant systems.[4] An important observation is that the

diffuse reflection at ~6.7 Å occurs in the isotropic phase, so the same reflection for the ordered N and M phases is unlikely to arise from interactions between aligned stacks. However, as suggested previously,[9] the off-axis broad spots at 6.4–6.7 Å in the X-ray data could arise from a helical arrangement of dimers within the stacks, where the helix repeat is two molecules. The existence of dimers as a distinct species would have a strong influence on the thermodynamics of self-association, making the assumption of isodesmic association invalid, but this is not necessary for the head-to-tail structure. One consequence of the structure shown in Figure 6 is that the stacks have a much more irregular surface than is the case for surfactant micelles. The water and sodium ions close to the surface (the "bound" species) will experience electric field gradients over a range of angles, rather than just one at 90° to the director. Hence, the quadrupole splittings of Na^+ ions is expected to be smaller than for the surfactant systems, as we observe.

References and Notes

(1) Lydon, J. Chromonic liquid crystal phases. *Curr. Opin. Colloid Interface Sci.* **1998**, *3* (5), 458–466.

(2) Lydon, J. Chromonic mesophases. *Curr. Opin. Colloid Interface Sci.* **2004**, *8* (6), 480–490.

(3) Turner, J. E. PhD Thesis, Leeds University, 1988.

(4) Tiddy, G. J. T.; Hassan, S.; Rowe, W. Surfactants liquid crystals. In *Handbook of Applied Surface and Colloid Chemistry*, Holmberg, K., Ed.:, John Wiley & Sons Ltd, New York, 2002; p 465–504.

(5) Horowitz, V. R.; Janowitz, L. A.; Modic, A. L.; Heiney, P. A.; Collings, P. J. Aggregation behavior and chromonic liquid crystal properties of an anionic monoazo dye. *Phys. Rev. E: Stat. Nonlin. Soft Matter Phys.* **2005**, *72*, 041710.

(6) Jabber, A. A. PhD Thesis, Keele University, 1994.

(7) Ormerod, A. P. MSc and PhD Thesis, Salford University, 1994.

(8) Luoma, R. J. PhD Thesis, Brandeis University, 1995.

(9) Edwards, D. J.; Ormerod, A. P.; Tiddy, G. J. T.; Jaber, A. A.; Mahendrasingham, A. Aggregation and lyotropic liquid crystal formation of anionic azo dyes for textile fibers. *Adv. Color Chem. Ser.* **1996**, *4*, 83–106.

(10) Gordon, P. F.; Gregory, P. *Organic Chemistry in Colour*, Springer Verlag: Berlin, 1983, p 95.

(11) Park, H.-S.; Kang, S. W.; Tortora, L.; Finotello, D.; Kumar, S.; Lavrentovich, O. D. 2008, to be published.

(12) Lee, H.; Labes, M. M. Phase diagram and thermodynamic properties of disodium cromoglycate-water lyomesophases. *Mol. Cryst. Liq. Cryst.* **1983**, *91*, 53–58.

(13) Kelemen, J.; Moss, S.; Sauter, H.; Winkler, T. Azo-hydrazone tautomerism in azo dyes. II. Raman, NMR and mass spectrometric investigations of 1-phenylazo-2-naphthylamine and 1-phenylazo-2-naphthol derivatives. *Dyes Pigments* **1982**, *3* (1), 27–47.

(14) Khetrapal, C. L.; Kunwar, A. C.; Tracey, A. S.; Diehl, P. *NMR Basic Principles and Progress*; Springer Verlag: Berlin, New York, 1975.

(15) Emsley, J. W., Ed. *Nuclear Magnetic Resonance of Liquid Crystals*; Riedel: Hingham, MA, 1985; p 110.

(16) Wilson, M.; Fatima, C. 2008, personal communication.

(17) Kang, C.; Khan, A. Self-assembly in systems of didodecyldimethylammonium surfactants: binary and ternary phase equilibria and phase structures with sulphate, hydroxide, acetate, and chloride counterions. *J. Colloid Interface Sci.* **1993**, *156* (1), 218–228.

(18) Halle, B.; Wennerstroem, H. Interpretation of magnetic resonance data from water nuclei in heterogeneous systems. *J. Chem. Phys.* **1981**, *75*, 1928–1943.

(19) Wennerstrom, H.; Lindman, B.; Lindblom, G.; Tiddy, G. J. T. Ion condensation model and nuclear magnetic resonance studies of counterion binding in lyotropic liquid crystals. *J. Chem. Soc., Faraday Trans. 1* **1979**, *75* (3), 663–668.

(20) Lindblom, G.; Lindman, B.; Tiddy, G. J. T. Ion binding studied using quadrupole splittings of sodium-23(1+) ions in lyotropic liquid crystals. The dependence on surfactant type. *J. Am. Chem. Soc.* **1978**, *100*, 2299–303.

(21) Carvell, M.; Hall, D. G.; Lyle, I. G.; Tiddy, G. J. T. Surfactant-water interactions in lamellar phases. An equilibrium binding description of interbilayer forces. *Faraday Discuss. Chem. Soc.* **1986**, *81* (1), 223–237.

(22) Harrison, W. J.; Mateer, D. L.; Tiddy, G. J. T. Liquid-crystalline J-aggregates formed by aqueous ionic cyanine dyes. *J. Phys. Chem.* **1996**, *100*, 2310–2321.

(23) Harrison, W. J.; Mateer, D. L.; Tiddy, G. J. T. J-aggregates and liquid crystal structures of cyanine dyes. *Faraday Discuss.* **1997**, *104*, 139–154.

(24) Yu, L. J.; Saupe, A. Deuteron resonance of water-d_2 of nematic disodium cromoglycate-water systems. *Mol. Cryst. Liq. Cryst.* **1982**, *80* (1–4), 129–34.

(25) Blackmore, E. S.; Tiddy, G. J. T. Optical microscopy, multi-nuclear NMR deuteron, nitrogen-14 and chlorine-35 X-ray studies of dodecyl- and hexadecyltrimethylammonium chloride/water meso-phases. *Liquid Crystals* **1990**, *8* (1), 131–151.

(26) Manning, G. S. Polyelectrolytes. *Annu. Rev. Phys. Chem.* **1972**, *23*, 117–140.

(27) Luzzati, V. X-ray diffraction studies of lipid-water systems. In *Biological Membranes*; Chapman, D., Ed.; Academic Press: London, 1968; p 71–123.

(28) Prasad, S. K.; Nair, G. G.; Hegde, G.; Jayalakshmi, V. Evidence of wormlike micellar behavior in chromonic liquid crystals: rheological, X-ray, and dielectric studies. *J. Phys. Chem. B* **2007**, *111*, 9741–0746.

(29) Franklin, R. E.; Gosling, R. G. Molecular configuration in sodium thymonucleate. *Nature (London, U.K.)* **1953**, *171*, 740–741.

(30) Watson, J. D.; Crick, F. H. C. Molecular structure of nucleic acids. A structure for deoxyribose nucleic acid. *Nature (London, U.K.)* **1953**, *171*, 737–738.

(31) Wilkins, M. H. F.; Stokes, A. R.; Wilson, H. R. Molecular structure of deoxypentose nucleic acids. *Nature (London, U.K.)* **1953**, *171*, 738–740.

(32) Holmes, K. C.; Blow, D. M. *The Use of X-ray Diffraction in the Study of Protein and Nucleic Acid Structure* Interscience Publishers: New York, 1966; p 239.